Characterizing the Influence of the Textile-Sensor Interface on Stitched Sensor Performance

A Thesis
SUBMITTED TO THE FACULTY OF
UNIVERSITY OF MINNESOTA
BY

ELLEN DUPLER

IN PARTIAL FULFILLMENT OF THE REQUIREMENTS
FOR THE DEGREE OF
MASTER OF SCIENCE

Advisors: Dr. Lucy Dunne, Dr. Sarah Swisher

July 2019

Acknowledgements

I would like to give thanks to all of the fellow co-researchers, advisors, and friends who have helped educate me or merely mentally support me throughout this work.

- Lucy Dunne, for being an advisor and taking a chance on me - for welcoming me into the Wearable Technology Lab
- Sarah Swisher, for being an advisor and reaching out to me before I even started to give me the "insider baseball rules" on graduate school, as well as believing I could compete a degree in electrical engineering
- Lana Yarosh, for being an advisor and giving me confidence in my work within the computer-human interaction field
- Pete Marchetto, for being an advisor, being so supportive of my ideas and helping me understand different strain measurement techniques and equipment
- Andrew Thomas, for helping me with the impedance measurements of my strain sensors
- Kevin Eschen, for helping me setup the Digital Image Correlation (DIC) to attempt measuring strain in these textile and stitch sensors
- Yuhang Sun, Zack Levonian, and William Lane who have helped me learn and interpret my model/machine learning results
- To the Emerging Technologies Research Collaboratory (prev. Wearable Research Collaboratory) members and Professor Ann Hill Duin for helping support my work and making me feel so welcome in the University research community
- To my lab mates and Dr. Brad Holschuh who mentally or technically supported me with this research: Nika Gagliardi, Heidi Woelfle, Simon Ozbek, Esther Foo, Alireza Golgouneh and everyone else at the Wearable Technology Lab
- To my friends who helped me take the leap to graduate school in the first place: Michelle Weaver (née Marval), Ian MacDonald, Katrina DeSantis, Molly Callahan, Kyle DiRenzo, and Steven Griffith
- To my undergraduate professors who gave me the courage to go to graduate school: Katsuyo Thornton, Max Shtein, and Richard Robertson
- For my family, my partner Wade Larson, and Wade's family, who have given me endless support throughout my graduate degree and beyond
-

Abstract

Textile-based strain sensors are first defined with examples of various sensing mechanisms and applications, focusing on on-body smart garments for biomonitoring. A current lack of research in the textile substrate influence on sensor performance is noted, with a thesis investigation outlined to highlight key variables that may be important for successful sensor design. Two conductive thread stitch-based strain sensors are chosen for the textile-based strain sensors and two fabric substrates (2-way and 4-way stretch) are used to investigate their influence on sensor performance. Part 1 investigates if fabric strain properties change due to the attachment of sensors and how the sensor performance changes due to fabric choice and attachment angle. Part 2 uses the recommendations for textile choice, stitch geometry of the sensor, and sensor placement based on Part 1 results to create a 3-sensor, 60° strain rosette. Between the two versions of rosettes fabricated, the 4-way fabric and chainstitch geometry, the strain rosette is proven to improve the overall sensor performance in predicting force, displacement, and force direction. This rosette is characterized and using machine learning model algorithms, model-fitted for future garment based strain sensing applications.

Table of Contents

Table of Tables

Table of Figures

1. Introduction

The human body exhibits a remarkable amount of dimensional change during daily activities. Information about how the body moves and extends is studied in the fields of medicine, kinesiology, apparel, human factors and more. This information can be quantitatively measured using mechanical or vision tools, or through the use of novel on-body strain sensors. When a strain sensor is exposed to an applied force something about it changes. The detection and measurement of this change can then be used to infer something about the applied force. Once known, other operations can be triggered or used for a variety of wearable technology or health monitoring applications. Wearable technology in this context is defined as any computing tool that uses the human body as a support environment (Gemperle, Kasabach, Stivoric, Bauer & Martin, 1998).

Traditional thin film strain measuring devices such as extensometer and load cells are well suited for industrial purposes but rendered inapplicable for the dynamic surfaces of soft goods, apparel, and the human body. The closest commercial options are the flexible thin film strain sensor or optical tracking, such as digital image correlation (DIC). Even with being flexible and potentially somewhat stretchable, these strain sensors are hard pressed to extend or twist like human skin and are physically limited to sense strains at a much smaller strain range (0-10%) than experienced on the skin (up to ~50%)(Kirk & Ibrahim, 1966). For biomonitoring purposes and medical products that bridge the gap between traditional electronics and the human body, such as exoskeletons and prostheses, new feedback strain sensors that bridge this gap must be developed. Many strain sensing technologies are been pursued in research for these types of applications, with some finding success in particular applications, but many have been found lacking for the desired smart wearable systems that require ambulatory biomechanical monitoring. In addition to achieving electrical sensor accuracy and reliability within the specifications of human movement, wearable strain sensing needs to consider both electrical performance and human factors within the use environment. A failure in meeting these requirements will result in low adoption and low impact. Strain sensing technologies that cause discomfort, are too fragile for the environment, or lack in accuracy will disappoint users.

There are many reasons why pursuing textile-based strain sensing technologies is a promising avenue. Textile fabrics have a number of favorable characteristics when compared to rigid or flexible substrates made from either metal or plastic for strain sensing on the human body. The human skin itself undergoes strain caused by the manipulation of muscle, bone and tissue. Textiles can be very durable for this repeated stretching, compression and twisting of the body. Their range for elastic deformation can be larger than other substrates and can conform, or drape, over complex 3D shapes. Placed on a person or animal, textiles are comfortable because of their surface characteristics, material properties, and porosity. Textiles can be washed or subjected to any number of surface treatments to improve waterproofing or self-cleaning, to make ideal long-term wearable sensors for health monitoring. Composite functional textiles can be formed by incorporating fibers of different materials in a nonwoven web or extruded/twisted into yarn for knitting or weaving. The textile structure, based on the web, knit, or weave pattern, can be designed to give preferential deformation directions. To make a sensor, one can view the entire textile structure as part of the sensor design or use its components: fiber, yarn, matrix, thread, etc. Yarns or conductive threads can be made into a strain sensor and incorporated in knits, woven fabrics or as stitches. Stitched strain sensors on knitted textile substrates are the focus of this thesis work.

User comfort and ease of integration into smart garments and soft goods are both improved with textile-based strain sensors, but there are a couple downsides. Regardless of the sensor mechanism, as a strain sensor, it must be inherently influenced by the textile substrate's anisotropic stretch properties (nonwovens can be made with isotropic properties but are usually not stretchable enough to be considered for form-fitting stretch garments). Measuring in-plane strain comprehensively is difficult because textiles typically bend and fold before compressing. Even with an applied tensile force, the textile knit structure is a network, displacing that force in complex ways that makes modeling near impossible with conventional means. With these limitations in mind, much of the research on textile-based strain sensors still fail to address the impact of these system variables in reporting sensor performance; however there are a few studies that corroborate an influence of sensor response due to fabric substrate choice (Gioberto, 2015; Gioberto & Dunne, 2013) or fabric behavior (Harms, Amft & Tröster, 2010). Rather, characterization of promising sensors lack rigor in reporting the influence of these factors on the ultimate sensor response, making the repeatability of these studies difficult. Instead of black boxing

these effects, we should explore this space and understand how textile properties affect an integrated strain sensor. Strain sensing theory and fiber/yarn/textile mechanics are large academic fields in their own right, so I did not set out to provide a comprehensive understanding with this thesis. Rather, I designed a set of experiments to highlight certain factors that impact strain sensor performance because it uses a textile substrate rather than a substrate with more isotropic properties. Through this investigation, many common sense choices are justified, but new insights are also brought to light.

After reviewing the available sensor mechanisms for textile strain sensing outlined in Chapter 2, I was drawn to use a conductive stitched sensor in two geometries (coverstitch and chainstitch) for sensor testing, and representative 2-way (one-directional) and 4-way (bi-directional) stretch textiles as substrates. Typically, 4-way knits are used for skin-tight garments to provide garment mobility and comfort around joints like the knees and shoulders that need to accommodate bi-directional movement, but 2-way knits could also be used in areas where only one direction of stretch is significant (such as the lower back during flexion).

Gioberto and Dunne (2012, 2016) introduced a garment-integrated strain sensor that is stitched onto a textile substrate and operates via a variable conductive path principle. The basic premise of floating a looped conductive thread on one side of the textile in a stitch geometry using a sewing machine to create a "stitched stretch sensor" is the foundation for their jointly filed US Patent US9322121B2 (2016). The sensor mechanism involves relating a change in conductive path to a force or elongation of the textile substrate. As the textile stretches, the contact points of the looped conductive thread shift and the resistance changes. There are multiple stitch types that fulfill the geometric requirements and only a few have been researched as promising repeatable sensors (i.e. the overlock stitch, bottom and top 2-needle coverstitch). Previous work has characterized the overall theory for certain stitch geometries, as well as its performance as an in-plane stretch sensor (Gioberto, Compton, Dunne, 2016), an out-of-plane bend sensor (Gioberto, Coughlin, Bibeau, Dunne, 2013), and a normal force sensor (Berglund, 2016); minor investigations have looked into the impact of the textile substrate on performance (Gioberto & Dunne, 2013). This thesis uses the current best-performance stitch sensor, the 2-needle bottom coverstitch, and also introduces a new stitch geometry, the chainstitch, which hasn't been studied before but outperforms the coverstitch as a

strain rosette sensor (Fig 1). Understanding the impact of the textile-sensor interface on the sensor performance composing the bulk of this study, with the aim of improving the commercial viability and robustness of this sensor in a variety of applications, using a variety of different substrates.
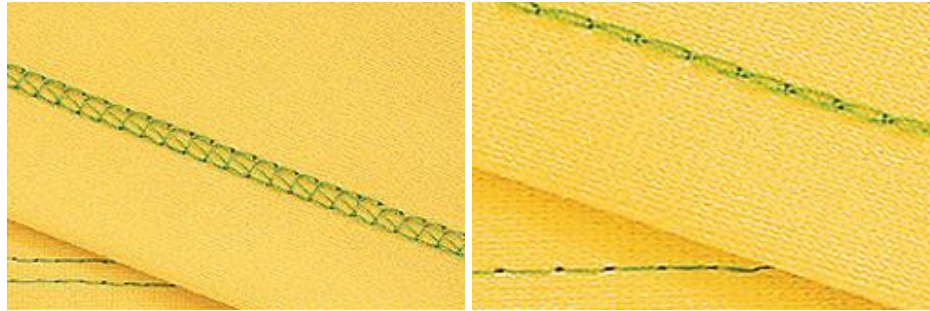
Figure 1. (Left) Coverstitch geometry, previously characterized (Right) Chainstitch geometry, operating with the same piezo-resistive behavior, characterized here [Image Credit: Sewingmachineplus]

Because the stitch repetitively secures itself to the fabric *without* restricting its stretch, it's likely that the fabric's mechanical properties will influence the stitched stretch sensor performance, making it an ideal sensor to use for this study.

Three main research questions guided the first part of this investigation (Fig 2). The first focused on characterizing how much force is required to stretch a 4-way and 2-way textile substrate a fixed distance, and seeing if the stitched sensor constricted this movement in any way. The 4-way stretch knit (stretch in vertical and horizontal directions) is used for maximum comfort in a garment and ideally the sensor minimally constrains the textile elongation. Also, the entire range of deformation forces should be easily overcome by the users for the garment to not constrain the user's movement, meaning that only the amount of displacement dominates sensor response. The second question set out to assess whether the sensor responds differently to the angle it was stitched into the textile, with respect to the knit structure. If so, this would affect garment construction or characterization of biasing the sensor data because the response would be different depending on the angle it was sewn into the textile. The third question focused on understanding how the sensor response varies as the angle of applied force changes (relative to the sensor direction). This force would have decreasing principal tensile component (inline) and increasing perpendicular tensile components (perpendicular to the sensor) and potentially higher shear tensile components. Since the knit is a network of

interlocked loops instead of a homogenous material, this force undergoes a transformation that is complex to model. Using the results of

Using the findings of this characterization and subsequent design recommendations, the second part of this investigation created a practical example on improved strain sensing used a 3-sensor strain rosette pattern. This rosette can detect with high accuracy the force direction of a uniaxial strain, as well as the force and displacement using a machine learning model fit.

RQ 1A
How much does the direction of stretch influence the amount of tensile force required?

RQ 1B
Does the stitched sensor constrain the fabric, increasing the amount of force required?

RQ2
Stretching inline with the sensor, will the angle it was stitched at influence its performance?

RQ3
Stretching at an angle 0<x<90 to the sensor, how does the sensor performance change?

RQ4
Can a strain gauge rosette be successfully designed to infer 2D-plane strains on a textile?

Figure 2. An overview of research questions within this thesis

The experimental design and results are discussed for each of these questions in Chapters 3 and 4, respectively, before an overall conclusion is reached. In Chapter 3 these results include comparing key mechanical and sensor performance between different sensor fabrication choices: knit substrate characteristics, stitch angle relative to the knit, and angle of applied force. Design implications are given for certain use cases of wearable strain sensing and a recommendation for a specific knit, sensor geometry, and sensor placement is identified and implemented to create and evaluate a 2-D strain rosette (Chapter 4).

2. Background

The choices for wearable biomechanical strain sensing can be seen as lying on a line scale. On one end, there are strain sensing mechanisms that require a controlled

setting and the use of additional equipment like cameras and complex data acquisition systems. On the other end, there are other strain sensors adhered to the skin and appropriate for only short periods of time. In between these two extremes are sensors that are developed using textiles as a layer or substrate to take advantage of the comfort benefits of textiles for longer-term sensing. Garments act as a second skin around the human body and offers a great opportunity to house biomechanical sensors; however, how a textile deforms under applied force adds additional complexity to strain sensing behavior in 2D plane, let alone on the 3D surfaces on the human body. In this thesis, I focus on textile-based strain sensing to further sensor development by uncovering key textile-sensor behaviors.

Biomechanical movement can be captured through multiple methods, but only a few allow sensing in ambulatory applications without extensive amount of support equipment. Originally, visual assessments of humans performing motions were made either in person or through video recordings by trained personnel. The use of goniometers for measuring joint angles is a standard clinical practice due to their easy use within the setting, but capture only 2D angular information. A more sophisticated 3D analysis can be made through motion capture systems (Vicon, OptiTrack, Qualisys) with markers on palpated body landmarks. A system records marker positions and converts them into a digital 3D space. Both of these options require user/patient attendants, use of equipment in closed controlled environments, and trained clinicians or technicians to who interpret data accordingly. Some systems have reduced the need for optical markers for better usability (CATRASYS, Microsoft's Kinect™) and have shown some success in tracking biomechanical motion of walking (Gómez, Castejón, García-Prada, Carbone, & Ceccarelli, 2016). However, because the data acquisition is done optically, anything obstructing the line-of-sight (including other body parts) limits data capture and analysis; additionally, this analysis is made for a fixed data-collection in a single session, whereas longer-term continuous motion monitoring would afford more realistic understanding of biomechanical movement.

For these reasons, Inertial Monitoring Units (IMUs) have been explored. These areas electronic modules that include a 3-axis accelerometer, 3-axis gyroscope, and sometimes a 3-axis magnetometer, prove useful in providing positional and motion information. Once secured to the body or limb of interest, the sensor information can

measure data on site to be analyzed by a computer program via wireless communication. The freedom to remotely capture biomechanics motion is now available for wearable applications but the IMU is still a rigid printed circuit board (PCB), a rigid technology that uses hard, inflexible and uncomfortable materials to make up its sensor package. Integrating multiple IMU point sensors into a garment meant to be continuously worn is a workaround for a dynamically moving human body, but not the ideal solution. The IMU is also a point sensor, limiting its ability to provide detail on large sections of the human body (ex. limbs, torso, head). Herein lies the opportunity to supplement or even replace IMUs with fully textile-integrated and distributed sensors that can span the entire garment without reducing comfort.

Key steps to successful sensor-textile design include understanding the advantages and limitations of the underlying textile dynamics (focusing on knits), potential sensor mechanisms, and their context suitability specific on-body sensing applications. We begin this study of the textile-sensor interface with an overview of knit structure and mechanics.

2.1 Knit Mechanics

Typically for clothing design, the end use application drives the textile choice. For wearable sensing, the garment or textile should easily conform around the human body and be easy to doff and don. The human body also moves and changes shape with movement, elongating and contracting due to the movement of bone, muscle and tissues. We desire the garment to not impede mobility, so that means the garment must be well fitted with sufficient ease or utilize elastic fabrics. Stretch fabrics (knits) are perfect for areas of the body that go through extreme dimensional change, like joints often a good choice, while remaining close-fitting and comfortable. Additionally, elastic knits include elastane (Spandex™ or Lycra™) fibers which improve the textile's materials to allow recovery to the original dimension after being stretched, making them worthy contenders for textile-based sensor designs.

Knit mechanics is a large body of research, so only key background information is presented here. Knit fabrics are made by interlocking looped yarns, and are divided mainly into two groups of loop designs: weft knits have the yarns looped horizontally to form consecutive rows, and whereas warp knits have the yarns looped in the vertical direction

(Fig 3). The horizontal direction is called the course, or the cross-wise direction, and the vertical direction is called the wale or length-wise direction. Different stitch patterns are used to create a knit textile, and with the four most popular being: the knit stitch, the purl stitch, the missed-stitch, and the tuck stitch (Fig 3).
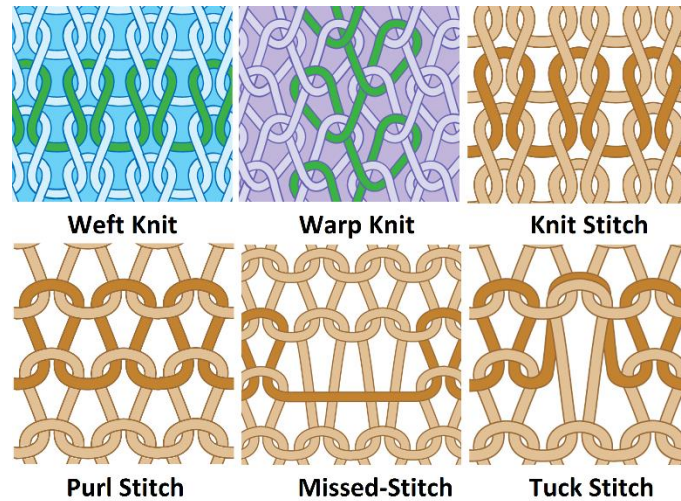
Figure 3. Knit classifiers [Image credit: Threadmagazine.com]

Describing knit mechanics begins with the yarn. The characteristics of yarn as twisted fibers have a number of variables that affect the textile's mechanical properties: material composition, fiber density, yarn twists, etc. Even with simple axial forces applied, yarn deformation is more complicated than just fiber extension in one direction; as a helix of intertwining strands, an axial force also results in torsional and bending forces inside the yarn. Even with complex behavior, mechanical properties can still be characterized at the fiber and yarn level.

Next, the characteristics of the knit structure affect textile mechanics, like the number of loops and spacing, which some say is more influential on the knit mechanics than the yarn themselves. Popper (1966) proposed a theoretical explanation for biaxial knit deformation that suggests at relatively low forces, knit fabric mechanical properties are dependent solely on the geometry, not on fiber properties. The looped structure, influenced by the yarn geometry, has a certain number of courses and wales in a specific area. As the knit is deformed, the spaces get smaller and yarns slide past each other at their loop crossing points. Only then, after a certain amount of force, do the yarns themselves deform and stretch. Popper (1966) postulates that the primary mechanism of

applied forces affects the yarn loops, first by straightening the curved yarns and then deforming further by yarn stretching.

As Senthilkumar and Anbumani (2014) summarize, most textiles have nonlinear deformation behavior with the presence of viscoelasticity and that elastic fabrics especially should be studied for their dynamic elastic behavior. Both knit directions, coursewise and walewise, were studied as well as increasing extensions from 20-50% at a controlled strain rate using an Instron® strain tester. Stress and strain were calculated, and the dynamic work recovery (ratio of the area under the loading curve and unloading curve) and the hysteresis were compared for each test condition. Testing both a cotton knit and a cotton/Spandex knit, their results showed a greater knit loop density due to the elastane material. The stress at a given extension was also lower in the cotton/Spandex knit and higher work recovery (less energy loss, Fig 4). As the extension range increased, so did the initial slope of the hysteresis curve. This means that as fabricated, the elastane material holds the knit structure in a slight compressive state under no external strain, allowing for larger strains to result in lower fabric stress. As the strain range increases, the hysteresis behavior changes slightly but still remains present as an inherent property of the knit structure and fiber materials used. These results corroborate elastic knits suitability for textile-based sensors and also the need to mechanically characterize their unique behavior when selecting one for a sensor design. Trends do exist and can be revealed through controlled strain testing, even with fabrics, but their limitations (such as hysteresis) should be accepted. Even though, the variability and breadth of fabrics begets a complexity in mechanical modeling that makes generalizable findings difficult.
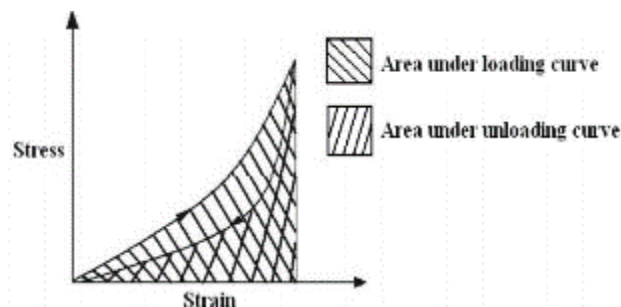
Figure 4. Relationship of dynamic work recovery with stress (strain) (Senthilkumar and Anbumani, 2014)

In summary, modeling knit mechanics has been attempted many times, and many acknowledge that a theoretical model can work up to a certain point of yarn loop spacing,

before more complicated strain behavior begins. Restricting sensors that are applied to knits within this regime (as long as the strain regime is appropriate to the actual application) allows the sensor design to avoid these extra strain behavior complications (Fig 5).
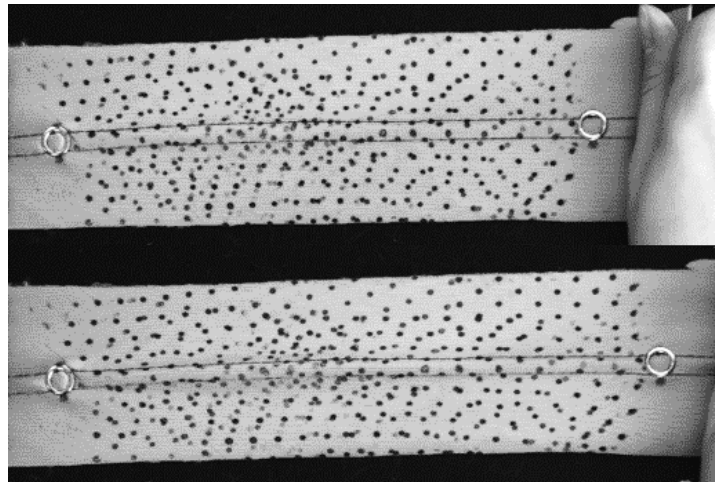
Figure 5. Stretching a knit fabric uniaxially (30% strain)

As a result of these complexities, most research groups studying wearable strain sensors tend to select a single applicable textile substrate (woven, nonwoven, or knit) and characterize the sensor as a part of this larger system. Studying sensor variability on multiple textile substrates is rarely if ever done. Without performing these studies, it is unknown whether that particular sensor is undesirably sensitive to the underlying textile structure.

2.2 Defining a Textile-based Strain Sensor

Generally speaking for a textile-based strain sensor, a textile-based strain sensor uses a textile substrate (as opposed to any other material like plastic films or rubber, metal, ceramic, etc.) to which the sensor attaches. Alternatively, the sensor is made an intrinsic part or the entirety of the textile structure. The physical structure of the textile and the bonding mechanism for the strain sensor can differ greatly among designs. Some choose to bond the sensor directly to a textile substrate through adhesion, stitching, coating or printing; others choose to incorporate the sensor into the textile design itself, as a strip within a woven or knitted, a yarn in a knit, or incorporated in the matrix of a nonwoven. An alternative to either option is to create a textile where the entirety becomes the sensor through coating or making all yarns part of the sensor.

As to whether "textile-based" is correctly applied, the field varies on defining the levels of integrating electronics and textiles. Bosowski, Hoerr, Mecnika, and Jockenhövel (2015) described three levels of integrating electronic components into textiles (Fig 6). Modifying current garments to accommodate electronics is referred to as textile-adapted (e.g. adding heated panels as a layer and pockets to house batteries for a heated garment). Integrating electronics onto textile through interconnection is referred to as textile-integrated. A complete integration would then constitute designing the sensing mechanism within the yarn or textile structure itself. Alternatively, Kaushik et al. (2015) classifies only two levels: classical (embedding electronics into the textile, fixing it as a characteristic of the whole system), and integrated (integrating into the textile, minimizing any separation between what is electronic and what is the textile). Although the classifications may differ, a distinct difference between the two latter levels is a general ability to easily remove the sensor or sensing mechanism from the textile.
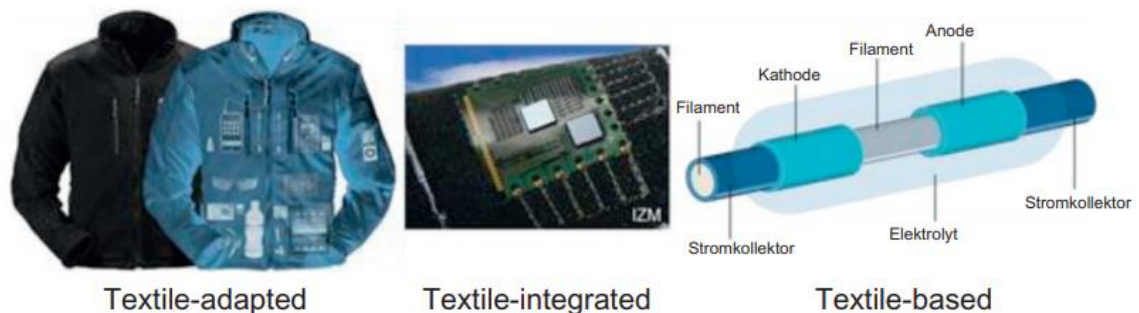
Figure 6. Different levels of sensor and textile sensing systems, as defined by Bosowski et al. (2015)

For our purposes, I have chosen to use "textile-based" in its more classical meaning, to indicate the sensor has been attached to a textile substrate in some way that makes separation difficult. The fabrication of textile-based strain sensors can be generalized as follows (Fig 7). Although the variety of sensor technologies makes it difficult to describe an overarching fabrication sequence, it usually begins by selecting the sensor mechanism. The sensor itself is fabricated prior to attachment to the textile or at the same time, in which the specific fabrication steps depends on the sensor mechanism. Afterwards, the secondary processes of attaching contacts, electrical traces, and often protective or insulation layers are completed. Similar to any electrical device, the sensor+textile system is then characterized for quality or performance before collecting its necessary strain measurements in a given application.
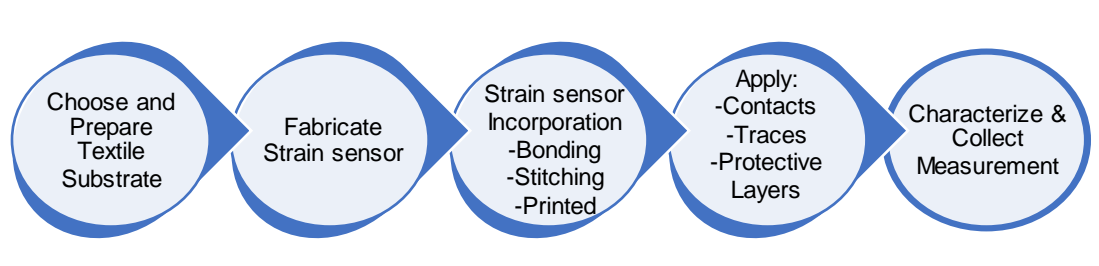
Figure 7. Typical Textile-based Strain Sensor Fabrication Sequence

To sense strain, an applied force changes a particular quality of the sensor in a way that is measurable. This happens in one of three system states (where the ideal strain sensor would operate in the second regime).

1. Applied force < the force to deform the sensor
   - The force is stored as potential energy but too low to obtain a strain reading

2. Applied force > the force to deform the sensor, AND
   Applied force < the force to deform the sensor <u>permanently</u>
   - The force causes elastic deformation able to be translated to a strain reading, and the sensor returns to its original state once the force is removed

3. Applied force > the force to deform the sensor <u>permanently</u>
   - The force causes elastic deformation able to be translated to a strain reading, but the sensor does not return to its original state once the force is removed (also includes the phenomenon of viscoelastic response)

A strain sensor operates on the principle of Hooke's law. Take any material and apply a force, F, upon an area, A, and a resultant stress, σ, is induced inside that material. If the stress exceeds a body's inertial forces, the body will move, otherwise it will stay motionless and that stress will reside inside the body as potential energy. For a small *rigid* body with a force spread across the body with equal magnitude,

$$\sigma = \frac{F}{A}$$

This stress is then related to strain through a material property value, E, called the modulus of elasticity or elastic modulus,

$$\sigma = E \cdot \varepsilon$$

Therefore, the relationship of force to strain is,

$$\varepsilon = \frac{F}{E \cdot A}$$

Most textiles used for garments or soft goods, however, are made from knit or woven threads and not a solid material, so an adaption to Hooke's law is made. With testing yarns, linear density is used as the area term and related to a new stress term called "tenacity" or specific stress. For full knit textiles, both area and the modulus of elasticity are near impossible to exactly determine, so these variables are often estimated through the areal density or empirically determined from the specific test setup. The key physical understanding remains, that the force can be related to the experienced strain in a proportional manner.

2.3 Examples & Applications of Textile-based Strain Sensors

Even within the scope of textile-based strain sensors, there are many different sensing modalities and designs. Each has advantages and disadvantages for the designer to consider. This section is devoted to providing an overview of the sensing modality and examples that have been used.

Indirect methods are limited in realizing true smart garments, but they have a history of providing accurate biomechanical strain measurements are often used to compare novel designs against as a gold standard. Optical sensing uses the modulation of light due to mechanical motion to sense strain and has shown some success in wearable strain sensing research. In the electronics field, many passive strain sensors are developed on the principle that a change in the applied force will change the sensor's electrical impedance (resistance, capacitance, and inductance). This development has been paralleled in the textile-sensor field as well.

2.3.1 Indirect Strain Sensing

Motion capture software setups (Vicon, CATRASYS, Kinect™, OptiTrack, Qualisys) with and without optical markers placed along the human body have seen some commercial success and is often used as a benchmark for testing other textile-based strain sensors for their validity. These systems require a lot of investment and trained personnel, even though the usability of these systems are improving.

Digital Image Correlation (DIC) is an alternative, requiring less equipment and capital but is restricted to capturing a much smaller area. It's typically used for rigid or planar surfaces, but this method has shown some success in generating strain mapping data on curved surfaces on the body and on fabrics (Obropta, 2015; Farajikhah, Madanipour, Saharkhiz & Latifi, 2012; Takasaki, 1970). Precision textile printing techniques are used to create the Moiré patterns, although tolerances in the printed pattern will limit strain measurement resolution. As the textile is subjected to displacement, curvature, strain or rotation, the pattern shifts and an optical system documents and measures the offset to calculate an estimated strain. These indirect methods are limited for tracking 3D deformation, where the optical system has limited depth profiling, but it does benefit from not restricting movement with any additional electronic components (which might potentially interfere with the measurand).

Instead of relying on an optical tracking system, another indirect method which is a one-time, destructive measurement method is the brittle-coating technique that uses another material known to crack or craze at certain stresses. By coating the textile material of interest and subjecting it to stresses, the visual examination of the cracks or crazing can be compared against the reference to infer the strain or stress distribution (Crow & Dewar, 1984). This method destroys the brittle-coating, is limited in strain range (often much less than desired for wearable sensing), and is not applicable to repeated cycles of testing.

While indirect methods are great for not influencing body movements by placing any extra restrictive elements on the user, it places the burden of computing entire in external equipment. Optical systems require accurate visual measurements that match what is happening on the body. Indirect methods like these are of limited relevance for longer-term measurements in real-world, ambulatory applications. Other sensing technologies are better suited to these situations.

2.3.2 Optical Strain Sensing

Various optical fiber sensors have been implemented for strain sensing by affixing to or weaving within textiles. Polymer optical fiber (POF) sensors are made with a polymer coating and cladding in which the light travels through the core from the light source to the

light detector. As the POF sensor is bent or strained, the transmitted light changes and is measured via the light detector. Light intensity changes due to either of two reasons: a change in bending radius (bending-based) or a change in the birefringent core (Fiber Bragg Grating). The bending-based method tends to have lower sensitivity, but is easier to integrate.

The advantages of the POF sensors are their biocompatibility, lower electrical shock risk (no electricity is conducted along the length of the sensor), insusceptibility to electromagnetic fields, small size, flexibility, and light weight). They have the ability to sense changes over long distances at the speed of light without severe signal loss. As sensors, they have high sensitivity and linearity. An early successful commercial example was the DataGlove™ that used POFs along the fingers to measure finger joint motion (Fig 8, Left), used for both clinical joint assessments and virtual reality applications (Zimmerman, Lanier, Blanchard, Bryson & Harvill, 1986). Other uses have been found in respiratory monitoring of anaesthetized patients in the MRI environment, in which any metal or conductive parts would cause safety concerns or potentially disturb the imaging process. Narbonneau et al. (2010) used two different optical sensors (macro-bending-based and Fiber Bragg Grating (FBG)-based) stitched onto the fabric that were made into an upper body harness. The macro-bend sensor was stitched in a large serpentine geometry with 10 loops and reported to have a high stability in sensitivity (variation < 10%) when elongated between 2-15% (Fig 8, Center, Right). For the FBG sensor 12cm long, they reported a gauge sensitivity of 0.32nm/% elongation leading to 0.1% measurement accuracy for elongations between 0-3% which was stated realistic for the application (Narbonneau et al., 2010).

Figure 8. (Left) DataGlove by VPL (Zimmerman et al., 1986) (Center) POF sensor embedded into elastic stretch band (Narbonneau et al., 2010) (Right) Respiratory sensing harness for the MRI (Narbonneau et al., 2010)

Zheng et al. (2014) also demonstrated the use of a similar serpentine POF sensor onto a chest belt to measure human respiration in MRI conditions wherein the sensors were characterized to have a repeatable strain range up to 21%, sensitivity ~3, hysteresis under 4%, and repeatability under 3%. Dunne (2007, 2010) explored the comfort/accuracy trade-offs of using these sensors in situations with higher human activity and movement, which would introduce high motion artifacts. Dunne (2007) found that added garment ease didn't negatively impact the sensor signal in areas of the body that didn't undergo significant motion or additional outside forces. When flexion testing on the knee, the POF sensor showed signal deterioration as it moved away from the body with a ~75% increase in noise and ~75% signal amplitude reduction.

The disadvantages of the POF sensor include its difficulty in manufacturing or fabrication with a garment or textile, as well as custom fitting lengths to match application needs or body lengths. As an optical sensor it requires a light generator and detector, which results in additional bulk and cannot be placed in areas of the body that induce a very tight bend radius (like the back of the knee). For smaller form factors and distributed sensing, passive strain sensors should be considered.

2.3.3 Capacitive Strain Sensing

Capacitive sensing requires two conductive materials separated by a deformable insulator. Many approaches have been investigated using this principle: capacitive fibers, flexible capacitive sensors attached to textiles, or using a textile as either the conductor or insulator layer. Google's Project Jacquard is a well-known example of a commercially successful capacitive-sensing textile.

Capacitive strain sensors can be made very small to very large, depending on the measurand area of interest and can be more sensitive than other sensor technologies. If a textile is placed in between, the porosity or density of the fabric would change its dielectric value as it was deformed. Guaranteeing this contact and consistent spacing with the textile inner layer is difficult as the sensors age with repeated mechanical stress. Many commercial strain sensors utilize capacitive sensing and encapsulate the sensing materials with a protective coating such as silicone. The compromise of comfort is outweighed by the reliability of the sensor. Stretchsense® offers one such sensor, shown

in Figure 9, Left, that has a typical sensitivity of 5.30 pF/mm for a 7cm sensing length (Stretchsense, 2019).
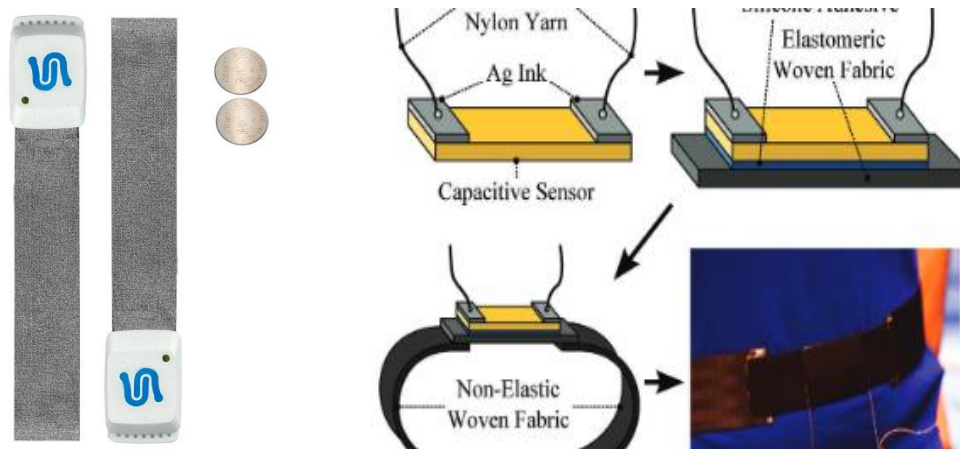
Figure 9. Left) StretchSense ® stretch sensor (StretchSense, 2019) (Right) Capacitive soft sensor (Atalay et al, 2017)

Atalay et al, (2017) developed a microstructured metal film capacitive-based soft strain sensor (Fig 9, Right). The substrate of the sensor is a silicone elastomer that's surface microstructured through a laser treatment while it is under a biaxial prestrain. An adhesion layer of aluminum and then silver is sputter deposited onto both sides of the elastomer. The prestrain is then removed and the sensors are cut into their final shape. The sensor is then glued to a fabric substrate with silicone rubber adhesive before being characterized. The microstructuring and prestrain processes helped this sensor remain sensitive up to 85% strain, with a GF of 0.90.

Maiolino, Maggiali, Cannata, Metta, and Natale (2013) created another soft capacitive sensor, choosing a 3D air mesh fabric dielectric layer and a grounded conductive Lycra placed over a flexible printed circuit board (FPCB) wrapped over the body of interest. They found that the 3D air mesh fabric improved mechanical integrity and contact with conductive layers over time, compared to the previously used silicone foam. To compensate for thermal drift they also embedded pressure-insensitive capacitors into the layout. The characterization showed two different linear regions when determining sensitivity, as they defined was the change in capacitance over the change in applied pressure: a sensitivity of 2.50 fF/kPa in the range of 2-45 kPa and 0.86 fF/kPa in the range of 65-160 kPa. The hysteresis was also fairly low, the maximum difference between cycles corresponding to ~29 kPa or 9.1 fF, or ~5% of the whole sensing range ($\Delta C = 0-200$ fF).

However, the FPCB limits comfort and doesn't accommodate the large strains often present in wearable garments.

The advantages of capacitive sensing is the high sensitivity to low forces with good signal resolution, low cost, flexibility, suitable form factor for wearable sensing, and relatively easy fabrication. The downsides are that measuring capacitive is difficult compared to resistance and its sensitivity to environmental conditions, like heat and humidity, affects performance. Capacitive sensors also require AC power to function, which may increase the electronics and overall complexity of the wearable system.

2.3.4 Piezoelectric Strain Sensing

Piezoelectric materials have a specific dipole molecular property that generates an electric field when strained, but requires a current collector that measures this property. The use of piezoelectric materials for textile-based strain sensors is an uncommon method due to the difficulty in designing this system for flexible sensor measurement, although it has been attempted at the research level. One group has developed a system to create stretchable piezoelectric P(VDF-TrFE) fiber bundles through an electrospinning process and serrated collector to align and separate bundles. The ends of the fiber bundle could then be coated with a conductive contact material, such as aluminum, and made into a sensor. Affixed to tissue tape as a substrate, these bundles were stretched along a human bicep and subjected to a number of stretching, contraction and rotation movements. Although more work is needed to improve the robustness of the sensor system for handling, this sensor was able to produce repeatable, sensitive enough signals for arm movements (Hsu, Chan & Tang, 2017).

2.3.5 Piezoresistive Strain Sensing

Piezoresistive materials have been widely used for fabricating flexible sensors. As force is applied, these materials experience a change in electrical resistivity. A conductive material is required that has a nominal resistance much greater than that of the contacts and traces. To meet the basic requirement, this resistance must change as the conductive material is strained. To meet flexibility requirements, nanomaterials with piezoresistive properties has been commonly used as a coating or seed layer on yarns or textiles.

Carbon-based nanomaterials are commonly used, due to their mechanical robustness and good conductivity. Lee, Lee, Kim, Kim, and Kim (2016), used a hybrid ZnO nanowire (NW)/reduced graphene oxide (rGO) layer coating on top of a polyethylene terephthalate (PET) to create a piezoresistive strain sensor. The PET textile was oxygen plasma-treated to make the textile surface more hydrophobic (more compatible), before the rGO layer was spray-coated onto the textile to provide the initial conductive network and contact electrodes. Zinc oxide NW were grown on top to serve as the piezoresistive material before adding a layer of PDMS. The same process was repeated on a PET film substrate. Both the textile-based and film-based sensors were subjected to the same bending strain experiments. The resulting gauge factor (GF) of the textile-based, ~7.64, was found to be higher than that of the film-based, 4.57, which they attributed to the textile's superior deformability under high bending radii.

Ren, Wang, Zhang, Carey, Chen, Yin, and Torrisi (2017) took a similar approach to create an rGO cotton-based conductive textile to use as a bending strain sensor (Fig 10, Left). The cotton fabric was impregnated with a graphene oxide through water dispersion and vacuum filtration, then thermally reduced using a hot press method. A 3cm by 1cm conductive fabric sensor was subjected to tensile and compressive bending strains, generating a resistance change of +906% and -131%, respectively.
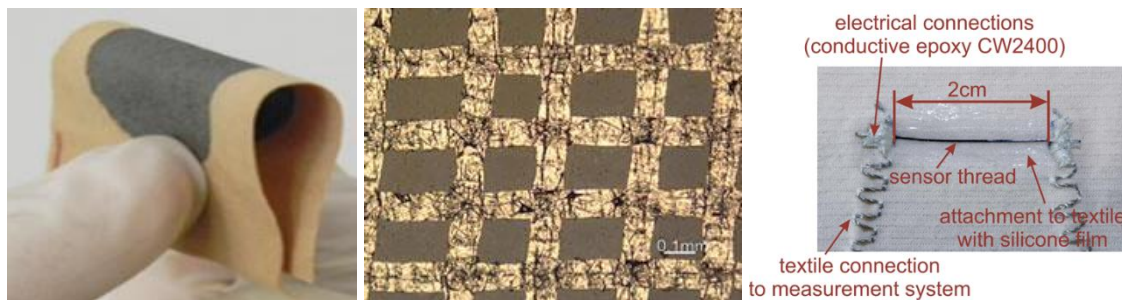
Figure 10. Textile-based strain sensors made with: (Left) printed graphene conductive ink on cotton fabric (Ren et al., 2017) (Center) Thin film copper/graphene mesh (Wang et al., 2014) (Right) Extruded polymer/carbon black fiber (Mattmann, Tröster & Clemens, 2008)

Another strategy is to use a pseudo-piezoresistance effect by changing the circuit path through deformation. One way this can be accomplished on the nano or micro-scale is through cracks or voids of a conductive material. Generally, carbon nanostructures are used with reduced graphene oxide to create this conductive network, and detailed strain response characterization has been done on these materials (Li, 2015; Benchirouf, Müller & Kanoun, 2016). Carbon-based materials have a reputation of non-toxicity (outside the

body applications), mechanical durability and acceptable conductivity. This method has been explored as a coating on top of textiles, made into a textile itself, and as a fiber. These conductive nanocomposites can be encapsulated in a polymer matrix to allow stretching and flexing, such as polydimethylsiloxane (PDMS), polyvinyl alcohol (PVA) and epoxy (Castano & Flatau, 2014). Wang et al. (2014) created a graphene woven fabric with high sensitivity (Fig 10, Center). As the sensor is stretched, microcracks expand and increase the resistance. Their testing showed the graphene woven fabric showed GF of 35 under 0.2% strain, 10^3 for strains 2-6%, and 10^6 for higher strains.

One group (Mattmann, Tröster, & Clemens, 2008) created an extruded piezoresistive polymer/carbon black composite fiber of a specific wt% to optimize both conductivity and stretchability. To create the sensor, it was laid on top of two different textiles and connected to conductive thread with conductive epoxy (Fig 10, Right). The fiber was then covered in silicone to protect and bond it to the textile substrate. Their results found this sensor did not have a significant difference in measurement based on the textile, with a sensitivity of 250 Ω/% strain and a GF of ~20 for a 2cm sensor length.

Another way to accomplish piezoresistance on the macro scale is to create a circuit pattern that changes due to deformation. Weaving or stitching conductive yarns to a textile are two such methods. The stitching method especially has the advantage of manufacturing ease, because the design of the sensor and textile integration is simple. One downside to sensors based on conductive coated threads is that the conductive material coating can deteriorate due to the sewing process (Tao et al., 2017). The main culprits are the friction of the thread removing parts of the coatings due to the necessary tension of the thread in the sewing machine, and the normal rubbing (and washing) during sensor operation. For normal threads and yarns, thread lubricants, wax or coatings can reduce the friction caused by the sewing machine but could reduce the overall conductivity if used with conductive threads.

Gioberto and Dunne (2012) introduced a conductive stitched sensor that uses its looped geometry to generate a piezoresistive response when stretched (Fig 11, Left). Easily sewn onto any textile substrate that allows some stretch, this strain sensor is the quickest to fabricate with an obtrusive form factor that is comfortable for the user. The bottom-cover stitch geometry using a Shieldex silver-coated 235/34 dtex 4-ply thread

showed a sensitivity of 5.5Ω/in for a 25% elongation and 16.8Ω/in for a 50% elongation (Gioberto, Compton, & Dunne, 2016). Their testing showed the 3in sensor having a GF of ~1.74.
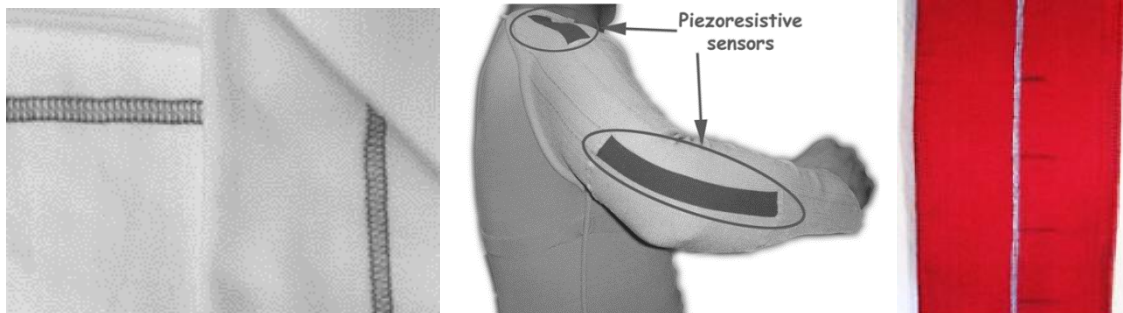
Figure 11. Different conductive circuit patterns: (Left) coverstitch with conductive thread (Gioberto & Dunne, 2012) (Center) knit section with conductive yarn and Lycra coated with carbon-filled rubber (Paradiso, Loriga & Taccini, 2005) (Right) Elastomeric tape strain sensor, made with conductively woven yarns (Kannaian et al., 2015)

Paradiso, Loriga, and Taccini (2005) showed that a carbon-loaded rubber-coated Lycra fabric and conductive yarn (Europea PAC 250 dtx/1) could also be used a piezoresistive strain fabric sensor (Fig 11, Center). They noted that the piezoresistivity depended on the contact between the yarn loops and conductivity of the yarn itself, but that the sensor increased in resistance linearly with strain up to 50% strain in the course direction with a GF of ~0.4, but only up to 20% in the wale direction with a GF of ~4 (resistance still increased but at a decreasing rate).

Kannaian, Naveen, Muthukumar, and Thilagavathi (2015) fabricated a 25cm strip of woven elastomeric textile tape with a conductive center stripe to create a strain sensor (Fig 11, Right). They investigated both weave structure and conductive thread per dent on their influence on the sensor's gauge factor. Their results indicated that higher conductive thread per dent (6) and increased interlacement in the weave structure increased the sensor's GF (~1.64). The tension weight of the weave also played a role, where they suggested that there is an optimal value for the particular interlacements in the weave. This is another example for how the textile structure affects the sensor performance.

Piezoresistive sensors are easier to measure, tend to use simpler circuitry, and come in slim, flexible and often extensible form factors that suit wearable sensing. There are many designs due to the fairly simple modality of changing resistance based on

mechanical forces. Depending on the design, fabrication can be low cost and easy like with the stitched sensors, or more time intensive like with the conductive nanoparticle coatings. Because many piezoresistive sensors are based on conductive coatings, some designs suffer from deterioration as the sensor is used and causes a sensor drift over time or limits the overall sensor lifetime. They can also be less sensitive to forces compared to capacitive sensors, but piezoresistive sensors can be sensitive to large strain ranges to match that of the human body.

2.3.6 Desirable Qualities

The majority of sensors are passive or active electrical sensors, so many of the desirable qualities for a textile-based strain sensor can be presented as follows (Fig 12). The signal-to-noise ratio must be adequate, as well as the sampling frequency (meeting Nyquist's requirement). The sensor itself should be repeatable with high accuracy and precision given the strain range of the application. It should be affected as little as possible by external factors like temperature changes, humidity, presence of static electricity, or sensor placement.

Detection system:
Measures strain sensor's changed property, calculates strain value

- Adequate sensor resolution (analog-to-digital)
- Compatible with flexible conductive traces to sensor contacts on textile

Strain sensor:
Converts strain to a measurable property

- Repeatable
- Appropriate sensitivity for sensing application
- Little environmental influence (temperature and humidity)
- Low internal noise

Flexible substrate:
Detects strain over area of interest

- Good contact from flexible substrate to body of interest
- Good contact of the strain sensor to the flexible substrate

Figure 12. Representation for a textile-based strain sensor measurement system, with desired variables

The scope of this thesis is reduced to look at only sensors that can be attached to a textile substrate, in which the sensor integration may affect performance due to the textile substrate's nature. For these cases, the qualities of textile-based strain sensor are based on a number of design decisions:

- The textile must be applicable for wearable applications like limb joint movement

- ○ Comfortable and biocompatible
- ○ Capable of stretching as needed for movement (4-way or 2-way stretch)
- ○ Typical of readily available close-fitting underwear or sportswear garments
- The sensor must be easy to integrate into the textile
  - ○ Sewn, physically attached or screen printed onto the textile
  - ○ Not limiting the textile's applicability (such as severely limiting stretch or rendering it biocompatible)
- The sensor should have some proven reliability with the amount of textile deformation and speed of deformation that occurs in worn clothing during normal human activities (stretching, walking)
  - ○ Previous research has shown it works within body elongations (e.g. 50% strain at the elbow per Kirk & Ibrihim, 1966)
  - ○ Not overly influenced by fabrication, especially variability between samples individual sensors or between sample groups

Ultimately, the sensor selection process resulted in selecting a conductive thread stitch-based strain sensor which is a specialty of my current research lab. The advantage of easily modifying stitch geometry and placement onto textile substrates, method of attachment to the textile, and previously demonstrated success meant this sensor suited the thesis investigation.

2.4 Stitched Stretch Sensor Prior Work

The stitched stretch sensor is made from a conductive thread stitched in a looped, serpentine geometry and held in place by one or more non-conductive threads for a specific stitch pattern (US Patent No. US9322121B2, 2016). This conductive thread is typically a synthetic fiber coated with a conductive material like silver with a flexible core and durable coating to allow the thread to be run through a sewing machine. A significant advantage of this sensor is its simple fabrication. Conductive coated thread (ex: Lamé Lifesaver, Shieldex® Silver-plated twisted yarn) is loaded into a standard industrial coverstitch sewing machine that can float looper threads on top and/or bottom of the fabric.

As sewn with a coverstitch sewing machine, the two top needles are threaded with the non-conductive thread and create a parallel row that secures the bottom conductive thread turned in a serpentine manner (Fig 13). Using the same machine, by removing the

top right needle and thread, the chainstitch geometry is achieved. When the stitched sensor is sewn onto a stretchy knit textile, the sensor is free to change its dimensions along with the textile and is very unobtrusive. As the textile is stretched and relaxed, the geometric change causes the electrical resistance to change, in a piezoresistive manner.

The "stitched stretch sensor" has been previously characterized as a strain sensor, a bend sensor and a normal (out-of-plane) force, showing that it has varying sensor response due to each of these interactions. Previous publications have reported sensor performance for the 2-thread top and bottom coverstitch geometry in varying widths, the ISO #406 stitch class, as well as the 4-thread overlock geometry (using a serger machine), the ISO #514 stitch class (Gioberto & Dunne, 2012, 2014; Gioberto, Compton & Dunne, 2016). These looped stitch geometries are shown in Figure 13. In the 2-thread bottom coverstitch, it was shown to have a repeatable linear response with cyclical strain, appropriate using in garments made for wearable sensing applications.

Figure 13. (Top left to bottom right) The chainstitch; narrow two thread bottom coverstitch; regular 2-thread bottom coverstitch; 3-thread bottom coverstitch

2.4.1 As a Stretch Sensor

A comparison study of the stitch sensor performance was conducted between the top and bottom coverstitch geometries and the overlock stitch geometry (Gioberto, Compton, Dunne, 2016). It showed that the bottom coverstitch sensor decreased linearly in resistance as stretched, while the top coverstitch increased linearly in resistance at a smaller amplitude. The overlock sensor had a sharper increase and plateau for the same extension range, resulting in an overall smaller amplitude and narrow range of elongation. All three sensor response curves are shown in Figure 14, with the bottom coverstitch

performing the best as a repeatable linear sensor over the entire elongation range of 0-50%. This study also compared the sensor performance with respect to conductive thread ply. Different ply silver-coated nylon conductive threads were tested from Shieldex, with the 4-ply 235/35 dtex and 5-ply custom-fabricated outperforming the 2-ply 177/17 dtex 2-ply thread.
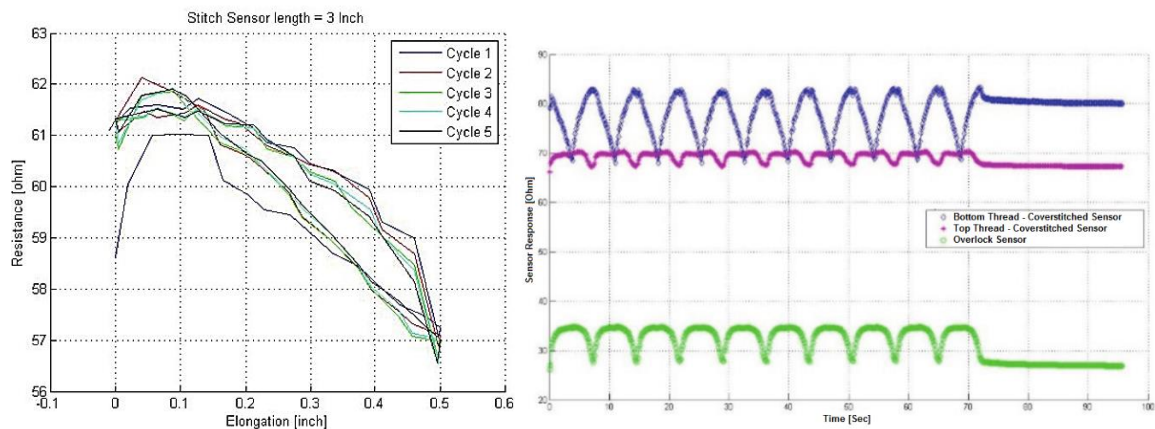
Figure 14. (Left) Typical bottom coverstitch linear sensor response with elongation. (Right) The sensor response of the bottom coverstitch (top), overlock (middle), top coverstitch (bottom) with cycling of elongation and relaxation (Gioberto, Compton, Dunne, 2016)

2.4.2 As a Bend Sensor

Gioberto, Coughlin, Bibeau, and Dunne (2013) also investigated the stitched sensor's potential for of the coverstitched sensor detecting bends or garment folding, useful for predicting garment fit or activity-recognition. Sewing stitched sensors into a pair of jeans along the dorsal and lateral lengths near the knee along with Vicon motion capture markers as a baseline, the resistance was measured both with an animatronic running mannequin and with human trials. The peak-to-peak resistance response was mapped onto the Vicon estimated joint angle and correlation coefficient values were calculated as 0.80 (dorsal sensor) and 0.78 (lateral sensor) (Fig 15). The range of peak-to-peak response for a nominal resistance of 55Ω dorsal sensor and 74Ω for the lateral sensor were -60% and -8%. In the human trials, the dorsal sensor had a higher correlation coefficient value for knee bend motions (0.88) and lower for the sit/stand (0.75) and squat (0.78). The lateral sensors had correlation coefficient values of 0.85, 0.88, and 0.89, respectively.
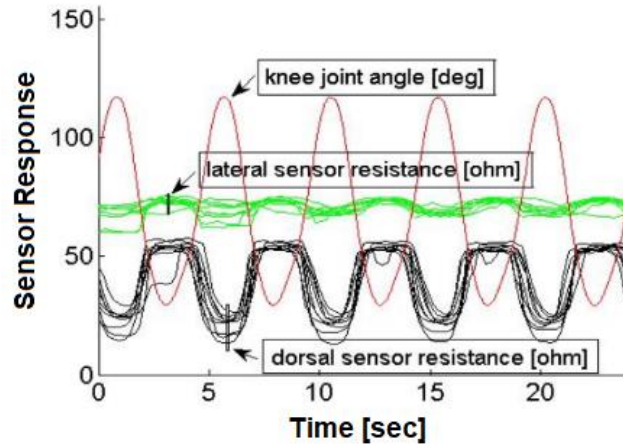
Figure 15. Stitched Sensor Performance tracking Joint Angle of the knee in the animatronic mannequin testing (Gioberto, Coughlin, Bibeau, Dunne, 2013)

The coverstitched stretch sensor was further characterized as a bend sensor in Instron tensile bench testing. The folding induces more electrical contact points with the conductive twisted yarn, thus decreasing resistance. With insulation that protects against the portions of the sensor from shorting with itself in extreme bends, the overall sensor sensitivity and average peak-to-peak response decreased while increasing the linearity of the response (Table 1).

Table 1. Selection of Characterized Bend Sensor Results from (Gioberto, Dunne, 2014)

Samples		Baseline (Ω/in)	Sensitivity (Ω/in)	Avg Peak to Peak (Ω)	Linearity (Bending) (Ω/bend length)
Stiff Denim Substrate	**Insulated**	73	2.19	3.14	0.98
	Un-Insulated	41	12.11	18.71	0.66
Least Stiff Denim Substrate	**Insulated**	63	1.55	2.39	0.98
	Un-Insulated	41	11.78	17.79	0.67

2.4.3 As a Normal Force Sensor

Berglund (2016) compared a commercial 4.4in long flex sensor (Spectra Symbol, Salt Lake City, UT) and a bottom coverstitch stitch sensor for which better sensed out-of-plane normal forces. The coverstitch sensor was sewn on an elastomeric knit using the Shieldex 4-ply 235/35 dtex thread was conducted. Both commercial and stitched sensors were attached to a ½-1in thick compressible layer (polyurethane batting or polyester foam) in either a curved or flat form factor, meant to simulate typical skin surface curvatures. An Instron tensile tester was used to apply a controlled rate of compression to a maximum 1in depression at the sensor into the compressible layer (Fig 16).
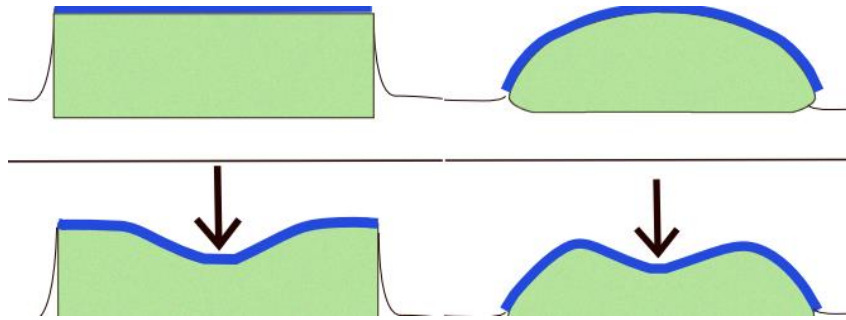
Figure 16. Normal force compressing of a bottom coverstitch stitch sensor (Berglund, 2016)

The average R^2 values of the linear sensor response with measured force were compared between compressible layer materials, surface geometry, and sensors. Although there was a visible response with the cycling (Fig 17), the linear fit still had moderate R^2 values of ~0.68, with the polyurethane/flex sensor combination having the smallest R^2 value (0.11) to polyester foam/flex sensor having the greatest (0.75). Over all the test conditions, the coverstitched sensor had higher R^2 values in most conditions compared to the commercial flex sensor and had a greater sensor recovery as the force decreased on the latter half of the cycle. Different lengths and two coverstitch stitch widths were also fabricated for comparison: 3/16in (narrow) and 1/4in (normal). There was no clear relationship of increased repeatability or greater sensor response with increased sensor length, and there was similar sensor linearity with either stitch widths (Berglund, 2016).
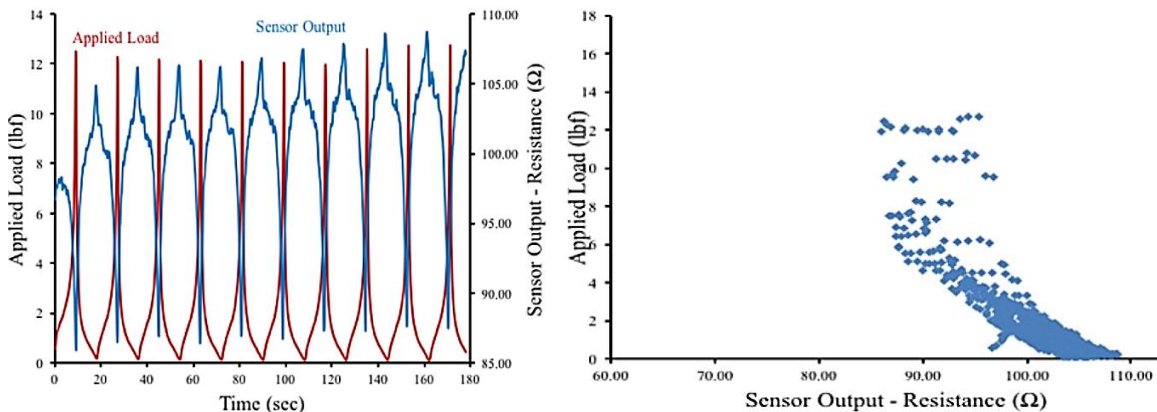
Figure 17. (Left) Cyclical sensor response from a bottom-coverstitch on foam, given a normal compressive force (Right) Plotting the applied force given the sensor output (Berglund, 2016)

Berglund, Foo, Holschuh, and Dunne (2017) furthered this work by reporting the sensor performance of the bottom coverstitch sensor layered with silicone substrates

(Shore values 10 and 50) to sense normal forces. Due to the curved sensor response, they chose a 3rd order polynomial fit, which is different than other model fits for this sensor. They found that the layered assembly method, which involved a textile substrate embedded in silicone, translated to a large sensor performance difference when compared to the sensor direct stitched to already cured silicone (Fig 18). Here is another example of how the sensor performs differently due to textile substrate conditions; Figure 18 shows a much smaller peak to peak response that saturates much earlier for the textile-embedded stitch sensor.
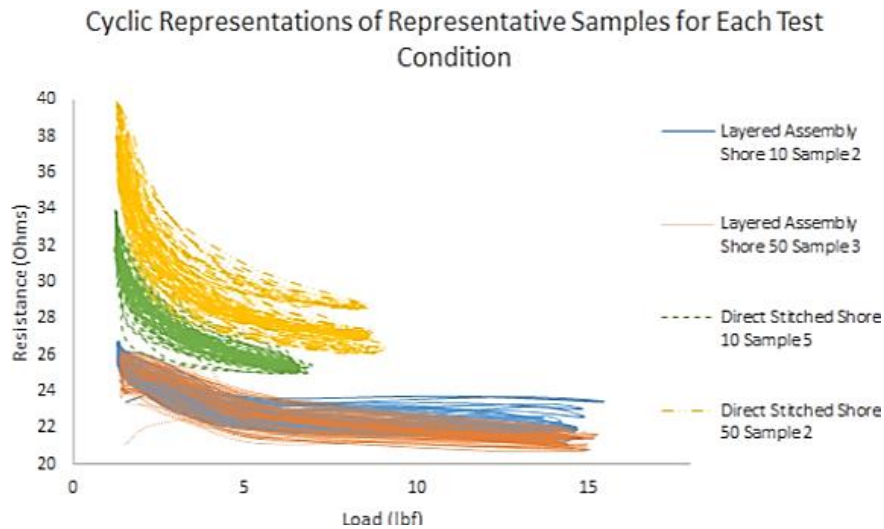
Figure 18. Comparing different assembly methods and Silicone Shore value substrates in the layered stitch normal force sensor (Berglund et al., 2017)

2.4.4 Preliminary Pilots on Knit Structure Effects

The 514 four-thread overlock stitch geometry was also characterized as a stretch sensor (Gioberto & Dunne, 2013) on multiple elastic fabric substrates. An Instron tensile tester was used to control elongation and a digital multimeter (DMM) to record sensor resistance. Interestingly, this stitch geometry has a repeatable nonlinear sensor response, as shown in Figure 19, with a linear region between 18-29% strain (depending on the fabric substrate). Additionally, the normalized peak-to-peak resistance differs depending on the fabric substrate and is highest for the elastomeric fabrics, but is relatively small between 2-14Ω. This supports the influence of the substrate choice on sensor performance.
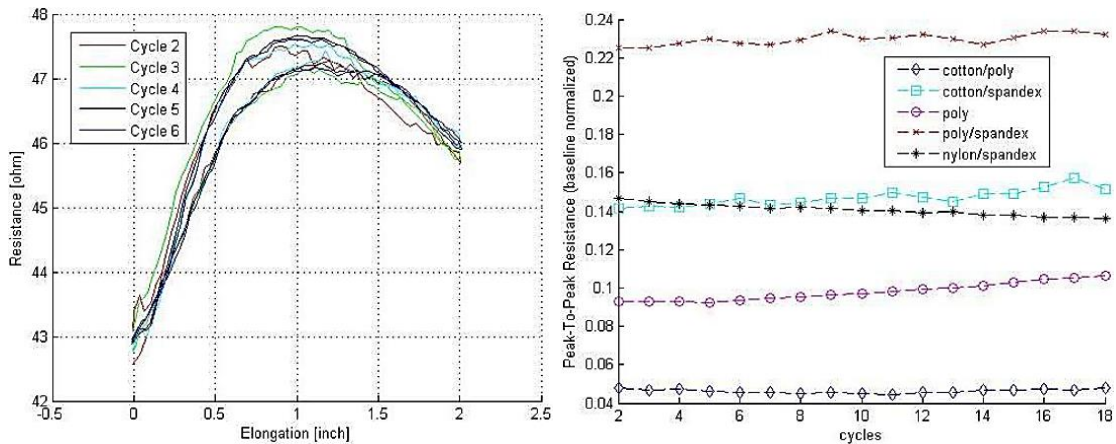
Figure 19. (Left) Sensor Resistance given Elongation of the overlock stitch sensor on a cotton/spandex substrate (Right) Normalized Peak-to-Peak Resistance for different fabric substrates (Gioberto & Dunne, 2013)

As the previous work indicates, the fabric substrate already showed it had influence in the sensor sensitivity. However, all prior work has been done with the sensor stitched in the direction of maximum extension and the load applied in line with that direction. Preliminary benchtop tests were completed to investigate whether the sensor response would vary upon different sensor placements when stretched the same distance by hand. Resistance of the sensor was calculated by an Arduino microcontroller measuring a voltage divider analog input, normalized and plotted. Only one specimen per sample group was tested, each a 5in polyester/spandex 4-way knit square with a sewn coverstitch sensor (Fig 20, Left). Both the crosswise (course) and lengthwise (wale) directions were similar in elongation when tested by hand, but it was confirmed the preferential stretch direction was the cross-wise or "horizontal" direction (Sample 2). The 45° bias direction was designated the diagonal (Sample 1).
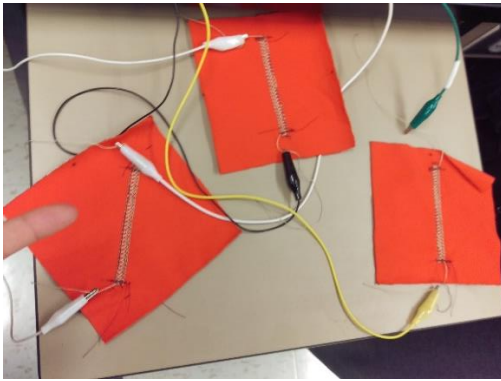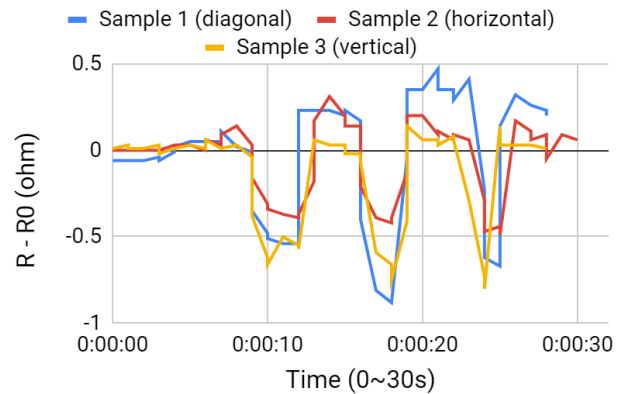
Figure 20. (Left) Initial benchtop test setup with 3.5in sensors stitched at the vertical (0°), diagonal (45°), and horizontal (90°) directions on the knit (Right) normalized resistance change measured via an Arduino voltage divider breadboard

The sensor responds to stretching with a negative change in resistance (seen as the three dips in Figure 20, Right), although a positive change in resistance after each dip indicates a dynamic baseline drift. This drift seems to be largest for the diagonal sample and then the horizontal sample. The amplitude of resistance change when stretched is similar in magnitude between the vertical and diagonal samples but smaller for the horizontal sample. These results lends credence to this thesis work, revealing a change in sensor performance depending on the sensor placement.

2.4.5 Characterizing Impedance of the Coverstitch Sensor

Due to the sensors' planar looped structure, there was interest in seeing whether it had any impedance properties other than resistance. An important electrical property of some coiled electrical conductors is inductance, in which a magnetic flux is produced proportional to the amount of current passed through the conductor. The coverstitched sensor takes the form of a planar coil in air (also called a hollow core or free air). This property would have not been important in previous characterization or applications because this sensor had been exclusively used with direct current; however, future AC applications would need to know this property so an impedance test was conducted.

Two coverstitch sensor specimens in the coverstitch geometry were made using different 4-way knit fabric cut into 5x5in squares. These knits had slightly different fabric content (teal knit was a polyester/elastomer blend, gold knit was a nylon/elastomer blend), which influenced their maximum extension and recovery abilities but both had bidirectional

stretch. The resistance of both coverstitch sensor specimens in the relaxed position was 20-21Ω. When stretched ~3cm (40% strain) the sensor resistance decreased to 17-18Ω. Using a benchtop impedance meter, an AC frequency range of 1 kHz - 1MHz was scanned, taking 5 impedance measurements at increasing intervals of 111 kHz. The scan was first tested in the relaxed position, then repeated in the stretched position to see if the geometric change of the looped conductive thread would present different results for two trials each specimen. The measured impedance at each tested frequency was averaged and then plotted against a log of frequency. An example of one trial is shown in Figure 21 (The remainder can be found in Appendix A). Both fabrics and trials had similar results.
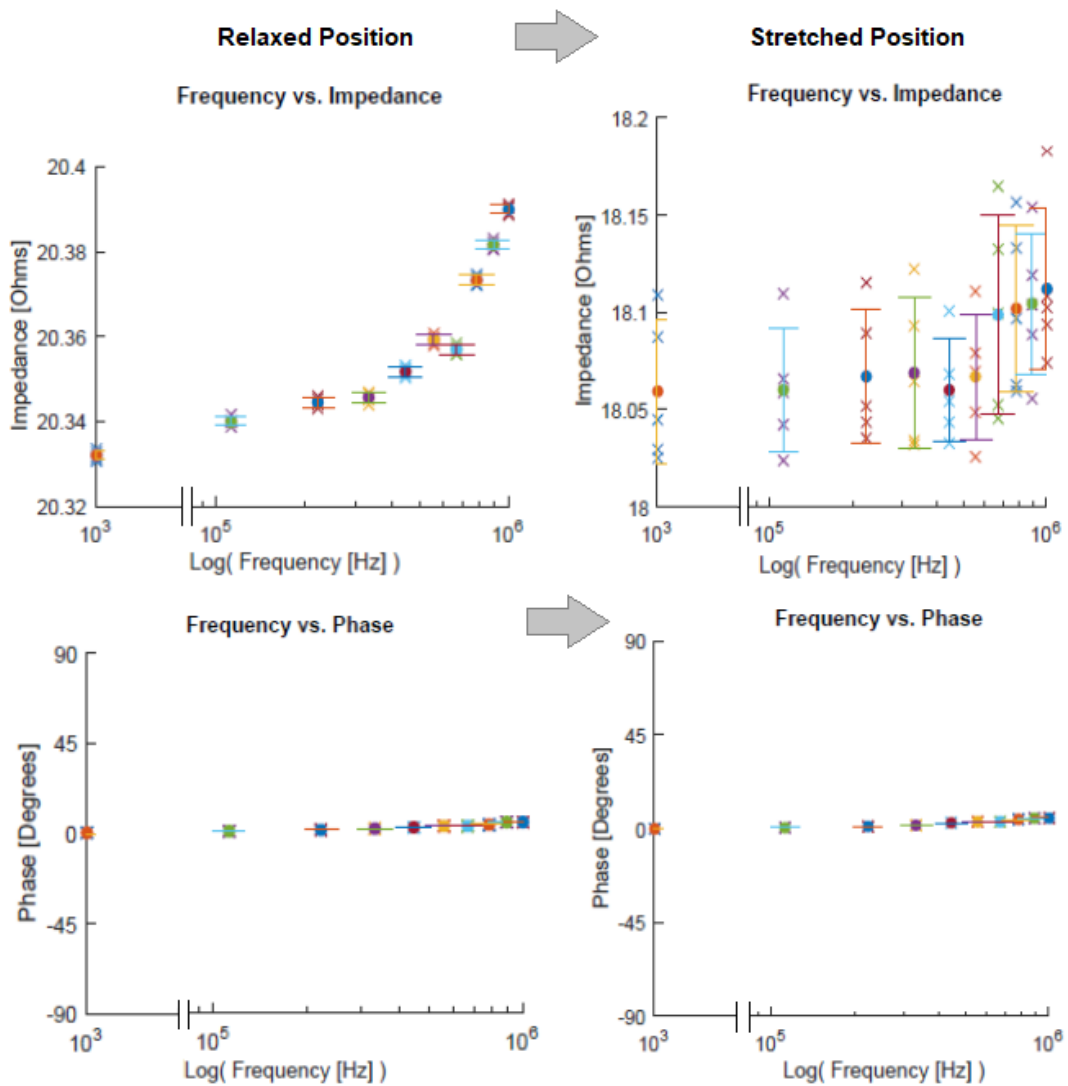
Figure 21. (Top Left) Impedance Measurements (1 kHz-1MHz) 4-way polyester/spandex knit coverstitch sensor in relaxed position, (Top Right) impedance in stretched position, (Bottom Left) Phase Angle in relaxed position (Bottom Right) Phase Angle in stretched position

Figure 21 (top row) shows close to zero complex components to the impedance for the coverstitch sensor, indicating resistance behavior in alternating current. This seems to be the case for both the relaxed or stretched position in this frequency range, with a change of ~0.7Ω due to increasing frequency in the relaxed position and 0.15Ω in the stretched. The phase angle remains near 0°. This disproves the idea that the looped structure in the stitched sensor could present inductive properties in the frequency range of 1 kHz to 1MHz. To note, there was a limitation to the testing procedure, as the impedance was not characterized while the sensor was being stretched, just in the two static positions. Also, only the coverstitch geometry was considered, so this characterization could be different for other stitch geometries. However, if this geometry didn't produce any significant deviations from purely resistive behavior, it is unlikely that other looped geometries will act differently.

3. Part 1 - Characterizing the Influence of Sensor-Knit Placement and Strain Direction

In this chapter, the first three research questions are explored (Fig 2). The knit mechanical behavior of the chosen knit substrates are characterized both with and without the presence of the stitched sensors and the results are compared in section 3.1. Then the sensor performance is characterized for five different sensor placements with inline (section 3.2) and offset forces (section 3.3). While each section describes the methods and results for that particular characterization, the chapter concludes with a discussion about design implications for regarding the sensor-textile interface.

3.1 Sensor-Knit Mechanical Behavior

The textile-based strain sensor is subject to two effects: how the strain translates through the textile substrate, and if that translation is modified through the fabrication of the sensor. The angle between the applied force and direction of the loops in the knit structure affect how much force is required to stretch the knit. Intuitively, we can often sense the difference in elasticity when we stretch a knitted textile in multiple directions. The names 4-way and 2-way stretch reflect how similar or different the "stretchiness" can be. This stiffness can also change as a function of distance due to the knit loop structure, so the first investigation looks at a specified strain range and the linearity/nonlinearity of

the mechanical response for each knit textile. To do this, non-destructive tensile testing measures the force and displacement simultaneously, which are then used to calculate the modulus of elasticity, E.

Additionally, to attach these stitched sensors, a sewing needle pushes through the textile from top to bottom and affixes the lockstitch top thread(s), while the bottom looper performs the work of creating the looped geometry. The act of stitching has the potential to either increase flexibility or constrain it, so we cannot assume one or the other for every stitch geometry and textile substrate. Stitch geometry can greatly affect how much it constrains the stretch of the textile, while the act of creating space in the textile affords increased flexibility and drape. (An easily envisioned example is how a normal lockstitch geometry can constrain a stretchy textile in the stitch direction, compared to the zigzag stitch.)

How these two structures interact is the focus of the first research question.

RQ 1A: How much does the direction of stretch influence the amount of tensile force required?

RQ 1B: Does the stitched sensor constrain the fabric's mechanical properties, increasing the amount of force required to deform it?

If indeed there was a noticeable change in the elastic modulus due to the presence of the stitched sensor, this could be considered as a bias error if the change is consistent as a factor, or noise if the error is random.

3.1.1 Specimen Fabrication

To serve as the textile substrate, two knit fabrics were selected. The first is a 4-way stretch double knit ("scuba knit") fabric, believed to be ~93% polyester/7% Spandex blend (the exact make-up unknown). The second is a 100% polyester 2-way interlock Ponte knit fabric (2-way knits don't usually have elastomeric content, because there would be some amount of lengthwise stretch then.) Both of these are typical for skin-tight garments like athleisure wear and undergarments. The double knit structure in both and the addition of Spandex (only in the 4-way stretch) affords the knit extra stretch for a wide

strain testing range and stability to completely recover when the textile is stretched and relaxed. The designation of 4-way means the fabric stretches in both the vertical and horizontal directions, whereas a 2-way stretches only in one direction, often in the horizontal (crosswise) direction.

Specimen preparation began with cutting the knit fabric into 5in/12.7cm squares, which was selected because it easily accommodated a stitch sensor at least 7cm long. The 7cm length of sensor was selected due to being in the range of similar commercial sensors. For each specimen group, three samples were made for redundancy and fabrication variability due to the sewing and placement processes.

Fabric was cut and specimens grouped using recommendations specified in ASTM D4964: Standard Test Method for Tension and Elongation of Elastic Fabrics (Constant-Rate-of-Extension Type Tensile Testing Machine):

- Fabric was not used <5.5in from the selvage edges (<10% of fabric width, either 45in or 54in)
- Specimens for each sample group were selected randomly from the mixed pile of diagonally-spaced cut fabric, to avoid specimens that were cut from the same area of the fabric (allowing knit manufacturing variability to be included in the results)

To serve as a reference point for all samples, the stiffest direction (lengthwise/wales for both knit fabrics) was given the reference 0° and angles of the knit structure were set with respect to this direction. The stretch factor is the amount of stretch per inch when knit is stretched to its maximum (without buckling), and generally ranges from 18-100% for stretch knits. The recovery factor is the behavior of the knit to return to original shape when relaxed from stretching, measured as the ratio of the original length and recovered length. Measuring the stretch and recovery factor by hand and with a ruler using a handbook method (Joseph-Armstrong, 2010) gave the following stretch and recovery estimations. The preferential stretch direction, in the crosswise/courses direction, was then given the reference of 90° for fabrication.

- 4-way (red): no discernible difference in elongation* between 0° and 90° = 63% elongation with full recovery

- 2-way (blue): 0° = lengthwise 6% elongation, 90° = crosswise 50% elongation, both with near full recovery

*Because the 4-way fabric was difficult to discern the stiffest direction by hand, force-strain measurements, taken with an Instron 3365 tensile tester, were used to confirm the crosswise direction was the preferential stretch direction.

Although great care was taken to cut parallel to the warp and weft, there inevitably was some variation in the knit structure as cut so that some specimens had a small angle (and not perfectly 0°) as the vertical reference axis.

Two stitch geometries were selected, based on previous research and pilot testing. The bottom coverstitch ISO #406 and chainstitch ISO #401 can be seen in Figure 22. The coverstitch had been used in previous publications as a recommended strain sensor with published sensor results, but pilot testing showed a significant sensor sensitivity of offset forces that offers challenges when desiring to have specific sensor behavior depending on the angle of force applied with respect to the sensor axis. Other stitch geometries were explored, settling on the chainstitch due to its unique one-thread width while keeping a looped conductive structure that stretches as the fabric is stitched.
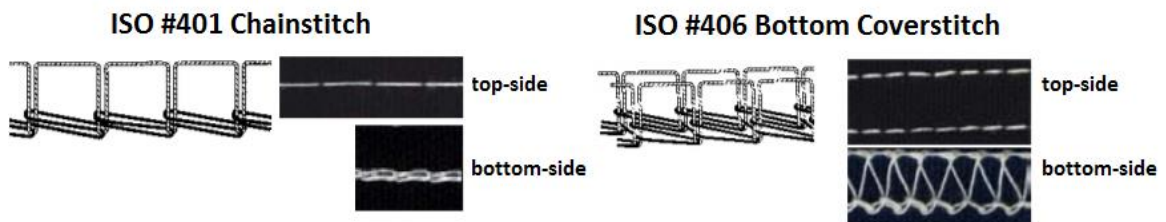
Figure 22. Stitch geometries used for testing (Left) ISO #401 Chainstitch, (Right) ISO #406 Bottom Coverstitch

To answer the research questions, certain angles needed to be studied to understand their resulting effect on knit mechanics and sensor performance. The knit is assumed to be symmetric, so only the range of angles between 0°-90° were studied. Five angles were selected: 0°, 30°, 45°, 60°, and 90°. The combination of stitch geometry, textile substrate, and stitched angle resulted in 22 total sample groups with 3 samples tested per group (66 total specimens), as summarized in Table 2.

Table 2. Summary of Sample Groups (3 Specimens per Sample Group)

Substrate	4-way knit											2-way knit										
Stitch Geometry	Fabric Only	Coverstitch					Chainstitch					Fabric Only	Coverstitch					Chainstitch				
Stitched Angle (°)	n/a	0	30	45	60	90	0	30	45	60	90	n/a	0	30	45	60	90	0	30	45	60	90

Fabric was cut and then marked with the 0° reference point. The angle for each specimen group was also marked (Fig 23). The stitched sensor was then sewn onto the fabric along these reference marks. An industrial coverstitch machine (Juki MF-7723 high-speed, flat-bed) was used for both stitched sensors. The conductive thread used was Shieldex® Conductive Twisted Yarn Silver Plated Nylon 66 Yarn 235/34 dtex 4-ply (bottom looper thread) and the non-conductive thread (top thread) was a typical cotton/polyester sewing thread. This thread was selected due to recommendation from research conducted by Gioberto and Dunne (2016) of sensor performance and low error, ease of sewing, and flexibility. This thread, shown in Figure 24, is 99% silver plated with a linear resistance of <50Ω/m (and average of 20-35Ω/m was measured with a digital multimeter during sensor fabrication).
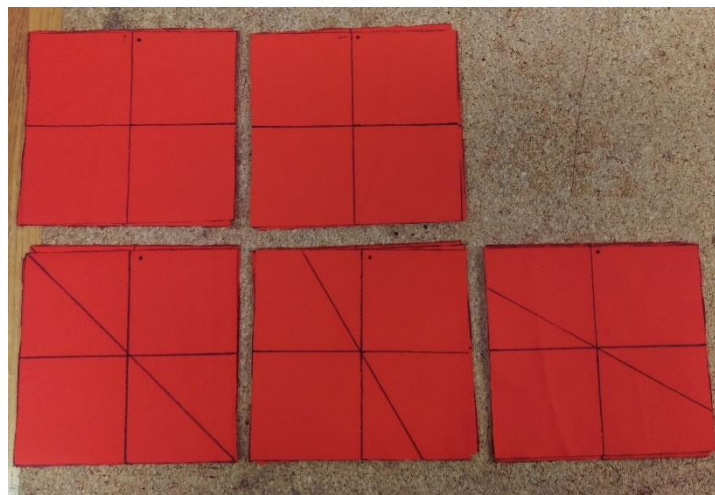
Figure 23. Cut Fabric Samples with line marks to indicate stitch angles

Cross section views of nylon fiber showing silver deposits
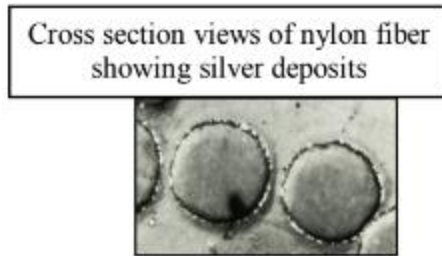
Figure 24. Shieldex® Conductive Twisted Yarn Silver Plated Nylon 66 Yarn [Image Credit: VTT/Shieldex Trading USA]

From the center point, 3.5cm was measured in both directions to mark the end points for a 7cm stitch length and then a male-sided metal gripper snap was attached to create an electrode for the sensor. A finished sample consisted of a 12.7cm (5in) square of fabric with a ~7cm long sensor and two male metal gripper snaps were pressed onto both ends of the sensor (Fig 25).
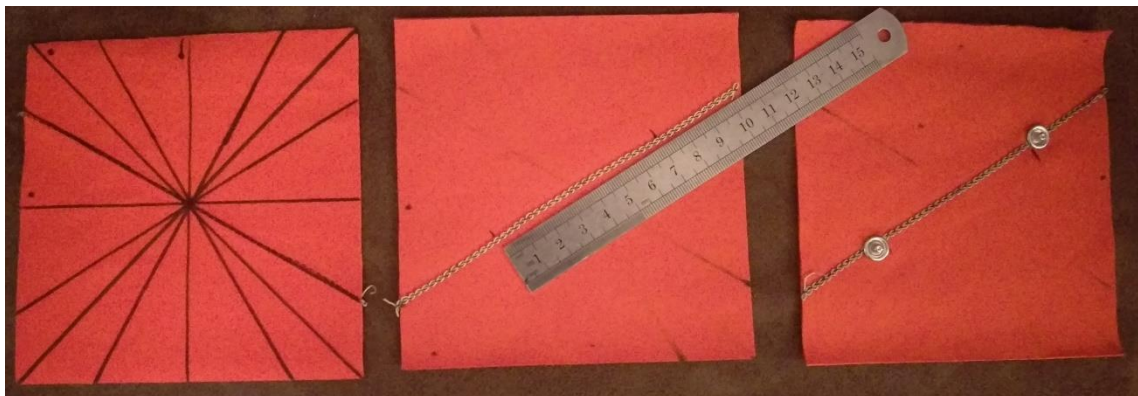
Figure 25. Sample Fabrication Process

During the sensor sewing process, it was noted that the 4-way fabric, which was thicker, did have a tendency to lie flatter than the 2-way fabric. The coverstitched sensors sewed on the 2-way fabric showed some puckering (Fig 26). However, this is an effect of using the same sewing machine tension parameters in an attempt to decrease stitch sensor variability.
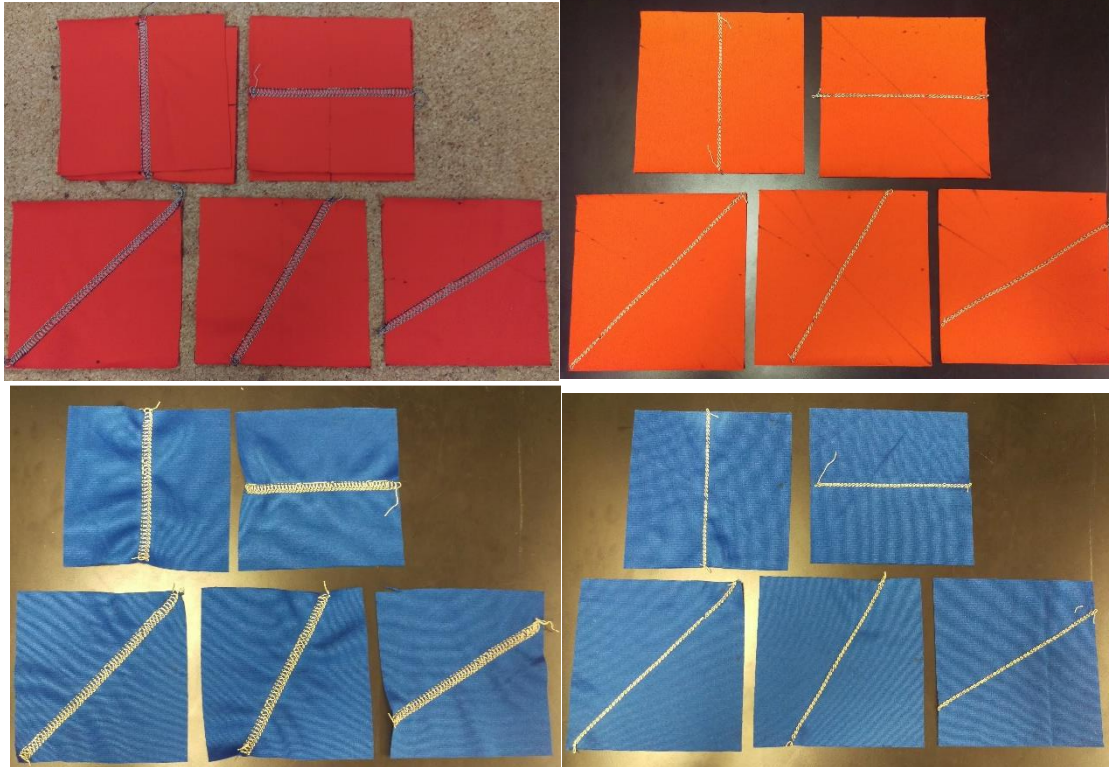
Figure 26. Stitch Sensors sewn at different angles to the referenced 0° (Stiffest Direction) (Top) 4-way knit (Bottom) 2-way knit

The average resistance values of each finished specimen were measured with a hand hand multimeter (Fluke® 101 Basic Digital Multimeter), then the resistances of the 3 specimens per sample group were averaged, as shown in Table 3.

Table 3. Average Nominal Resistances of Samples (3 Specimens per Sample Group)

Average Resistance (Ω)					
Sample Group	Degree from 0° (Stiffest Direction)				
4-way knit	**0°**	**30°**	**45°**	**60°**	**90°**
Coverstitch	10.5	8.8	12	10.8	12.1
Chainstitch	9.7	11.6	11.1	11.9	10.9
2-way knit					
Coverstitch	7.9	8.6	8	6.6	7.9
Chainstitch	7.8	7.6	7.6	7.7	7.3

3.1.2 Methods

There are multiple ways to evaluate the mechanical performance, from industry standards to research methods proposed in literature. ASTM D4964 is an industrial test method for characterizing elongation properties of wide elastic fabrics like stretch knits. It recommends standard tensile test equipment (like the Instron®), specimen preparation

and certain test parameters to achieve repeatable and reliable test results. The prior work by Gioberto et al. (2012, 2016) describes a test setup with the Instron and a multimeter to measure similar electromechanical sensor properties as this thesis, and the work done by Senthilkumar and Anbumani (2014) measured similar mechanical properties. These test methods aided in the development of the methods used herein (Table 4). Finally, additional pilot studies I performed helped finalize details, such as the snaps used for electrical leads, the selected strain speed, and test condition order.

Table 4. Applicable Published Test Methods

Test Method Source:	ASTM D4964	Conductive Stitched Sensor Published Methods (Gioberto et al., 2012, 2016)	Elastic Recovery of Elastic Knits (Senthilkumar & Anbumani, 2014)
Tensile Tester	Constant rate of elongation	Constant rate of elongation	Constant rate of elongation
Strain rate & Strain range	300-500mm/min, 30%, 50%, 70% or as agreed upon	63.5mm/min, 25%, 35%, 50%	500mm/min, 20%, 30%, 40%, 50%
# Specimens	5	1+	10
# Strain Cycles	3 cycles	5-20 cycles	10 cycles
Equipment & Measurement Sampling Frequency	Constant rate of extension (CRE) type tensile testing machine (use ASTM D1775 if using a constant rate of load (CRL))	BK-Precision 2831E Digital Multimeter measuring Resistance of Sensor (3.3Hz), Instron tensile tester(10Hz)	Instron tensile tester
Specimen attachment method	Looped specimen stretching over two prongs attached to test grips of tensile tester	Grab method of clamping two sides of fabric in the test grips of tensile tester	Per ASTM D4964 looped specimen over grips
Other	Recommend room temp 21°C, 65% RH, elongation calculated from the third cycle, points of measurement taken from loading (outgoing) cycle only	Measurement leads attached after grips, all data has to remove constant bias	Measured average wales and courses per cm, avg loop length, fabric areal density, thickness

An Instron 3365 test machine equipped with Bluehill 3 software was used to conduct all of the tensile test measurements. This is standard equipment used for general materials and textile tensile testing because it produces a constant rate of elongation, controlling either displacement or force while continuously measuring the other. All tensile testing (and fabric sample conditioning) occurred in an indoor lab space with temperatures in the general range of 20-23C, humidity 16-24%.

Specimens were cut in square shapes instead of a looped sample (prescribed in ASTM D4964) and tested in the grab test method in order to be more in common with test methods common to textile-based sensor prototypes in research, due to its greater applicability to real-use situations. Only 3 specimens per sample group were used instead of 5 to reduce testing time without sacrificing specimen variability. No greater than 100N force was used during testing to lower risk of fabric failure, and the default measurement sampling rate was used (0.02s = 50Hz). The loading/unloading crosshead speed was 200 mm/min, which was selected as a comfortable speed for collecting repeatable data with the Instron and within the recommended range based on Table 4. The strain range of ~30% (2cm of a 7cm sensor = 29%) was also selected as a comparable range to other studies and industry standards, and because it was it was the upper range of possible extension (under 100N) for the 2-way knit's stiffest direction.

Due to the test condition order, each specimen would be placed in the tester and run through multiple force placements. To reduce the risk of anchoring effects, the first cycle of data was discarded. Then the measurement data taken from an average of three subsequent cycles (unless explicitly mentioned differently, then only the last cycle).

Samples of the fabric alone and with a stitched sensor were stretched with the Instron tensile tester. The force required to achieve the same elongation distance of 2cm was recorded. If more force was required to stretch the fabric, this resulted in a higher elastic modulus value and indicate a stiffer direction.

A precycle, then 3 cycles of stretching/relaxing were conducted for each uniaxial force direction: 0°, 30°, 45°, 60°, 90° for both the 4-way and 2-way knit fabrics. The tests were repeated with fabric specimens with stitched sensors aligned to the same force directions. The Instron tensile tester collected cycle identification, force (N), and displacement (mm) raw data.

The physical properties of the textile and sewn sensor are captured by the force range and the elastic modulus. The **force range, ΔF**, is defined as the amount of force required to elongate to the maximum displacement. Due to the knit structure, the fabric stiffness (and therefore the force range) may change with force angle.

$$\Delta F = F_{max} - F_{min}$$

The raw force data was smoothed with a moving average (window of 5). The maximum and minimum forces were captured for each specimen in the sample group as well as for each cycle. These were averaged to become the force range for each sample group.

The **elastic modulus, E,** is calculated from the primarily linear relationship between the stress and strain of the elongated sensor and fabric. This is captured first as force and displacement measurements and then multiplied by a factor that includes the specimen and sensor physical dimensions (Fig 27). We can relate the force F with E as,

$$F = EA\varepsilon$$

where strain ε is the displacement divided by the original length, area A of the fabric in between the clamps, and E is the elastic modulus. By graphing Force(strain) the slope of a linear fit is EA, so to just get the elastic modulus, we divide by the area.
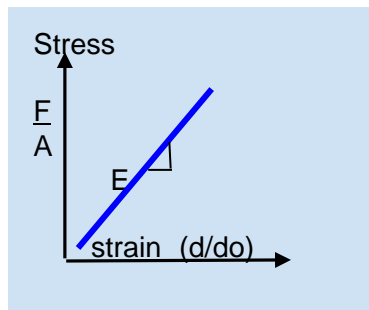
Figure 27. Converting force(displacement) measurements into stress(strain) to calculate the elastic modulus

A linear fit of the form $y = mx + b$ is generated from the force(displacement) data and then the slope m needs to be multiplied by a factor that includes the sensor length and the area that the tensile force is applied to.

$$E = slope\ of\ stress/strain;\ \frac{\frac{F}{A}}{\frac{d}{d_o}} = \frac{d_o}{A} \cdot \frac{F}{d} = \frac{d_o}{A} \cdot m$$

(Written in other forms, $= .00712N/mm = 7.12kPa = 0.00712MPa$)

In this case, A is the area between the tensile tester grips, assuming uniform stress and that the stress is limited to this area. Unfortunately this is only an approximation and limitation to the calculations, since the grip test method allows fabric to exist beyond the

width of the grips. Force vs displacement plots were graphed as a linear function, then fit to a linear model to generate the slope value, m, and converted to the elastic modulus with the factor:

$$\frac{d_o}{A} = \frac{70mm}{3500mm^2}$$

The sensor length for all specimens are 70mm long and the Instron tensile tester grips are 5cm wide to give an estimated area of 3500mm². In this case, the 1cm diameter snap is not counted as part of the strain area, nor was the additional fabric beyond the width of the grips. For example, if the calculated m slope was 0.356N/mm, then the linear fit slope (of the form $y = mx + b$) would be used to calculate the elastic modulus as,

$$E = slope\ of\ stress/strain$$

$$= \frac{\frac{F}{A}}{\frac{d}{d_o}} = \frac{F}{d} \cdot \frac{d_o}{A} = 0.356 \frac{N}{mm} \cdot \frac{70mm}{3500mm^2} = 0.00712 \frac{N}{mm} \cdot \left(\frac{1000^2 mm}{1m^2}\right) = 7120Pa$$

(Written in other forms, $E = .00712N/mm = 7.12kPa = 0.00712MPa$)

The *linearity error (R²)* measures how well the data fit the linear relationship (i.e. slope) of stress as strain increases. A R^2 closer to 1 means that that percentage of total variation present in the data is around the average and accommodated by the model. The quality of fit can be represented by the *root-mean-square error (RMSE)*, calculated by averaging the differences predicted with the linear fit and the actual data. RMSE values closer to 0 means the fit standard error is very good and the model is well fit to the data. For these purposes, only the elongation portions of the curves are fitted to a linear function, so only actual data from this is considered in the RMSE. Both R^2 and RMSE was calculated and reported with the results.

3.1.3 Results & Discussion

Reviewing the fabric-only mechanics first, we can see differences in the force range, linearity, and hysteresis characteristics between the 4-way and 2-way knits. The force range decreases from the stiffest direction (0°) to the least stiff direction (90°) as expected, but it decreases differently for each knit (Fig 28). Not surprisingly, the 4-way knit shows similar stiffness in all directions, with a very slight decrease overall from 0°-90°. Interestingly, the 2-way knit shows a nonlinear, almost exponential decrease from 0°-90° with much larger initial forces, varying from a maximum of 4.2N to a maximum of 85.6N

depending on the force direction. This baseline is necessary to compare the influence of the stitched sensor later.
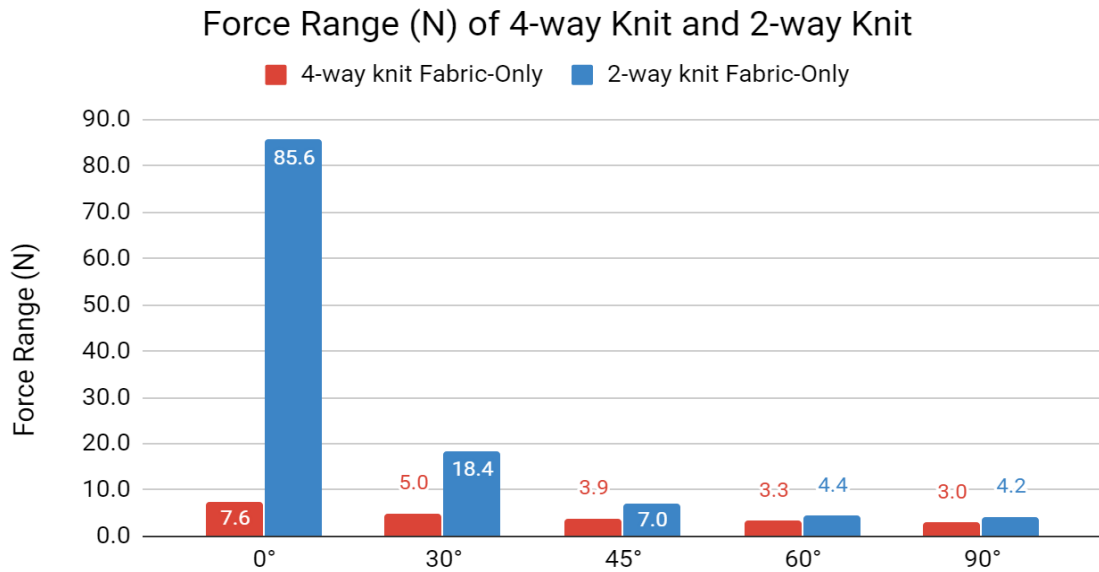
Figure 28. Force Range for both 4-way and 2-way knits as the force direction changes 0°-90°

The fabric's stiffness, varied by knit type and force direction, seems to have a large impact on linearity for the 2-way fabric (Fig 29, Left). The stiffest directions in the 2-way fabric show more exponential behavior of force(displacement) than linear. This trend is seen until the force direction angle approaches 90°, where the force becomes more linear with elongation (Fig 29, Right).
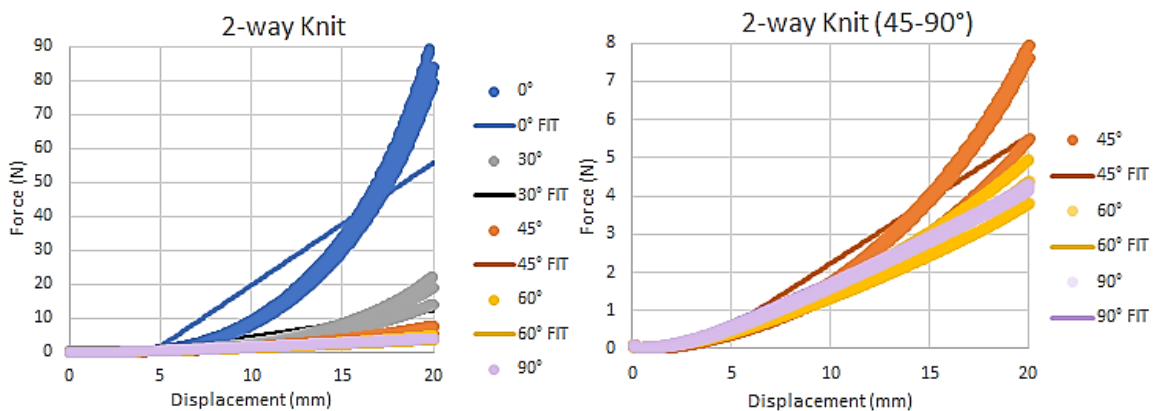
Figure 29. Loading Curves for the 2-way Knit (Left) for all force directions, (Right) for force directions 45°, 60°, and 90°

The full cycle of a typical graph for the 2-way knits are seen shown in the top two graphs in Figure 30 (elongation curve is the left-most line and relaxation curves is the right-most line). Only the averaged sample elongation data is shown in the bottom two graphs in Figure 30. (Note: more plots for the other sample groups can be found in Appendix B). The best fit linear fit is calculated using the elongation-only data and shown in the red line in each graph. At 0°, the tensile force approaches 90N curving throughout, while at 90°, the tensile force linearly increases to 4N.
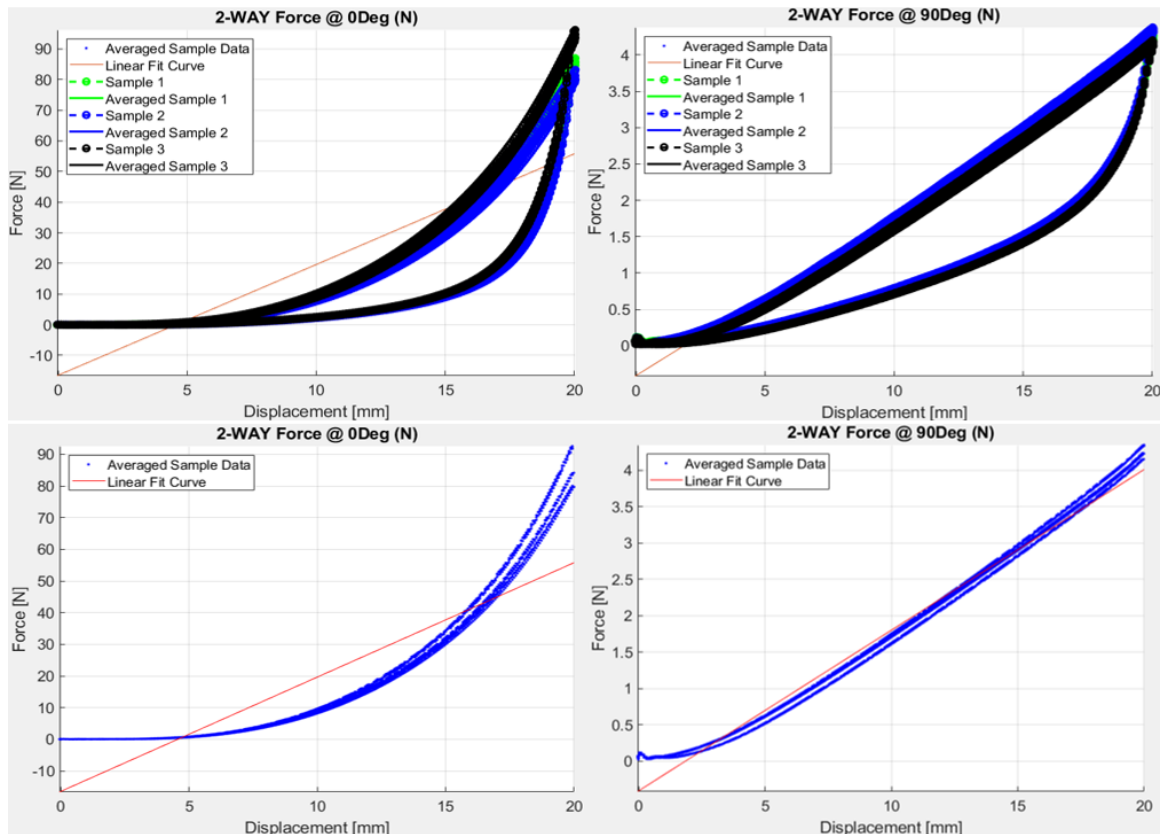
Figure 30. Tensile behavior for the stiffest and least stiff directions of the 2-way knit

Comparatively, the 4-way knit has more similar force ranges from stiffest to least stiff (7.6N at 0°, 3.0N at 90°) (Fig 31). For this fabric, the same influence of stiffness on linearity cannot be seen (Fig 32). Overall, the linearity is much better in the 4-way knit for all force directions than the 2-way (which looks linear only after 60°).
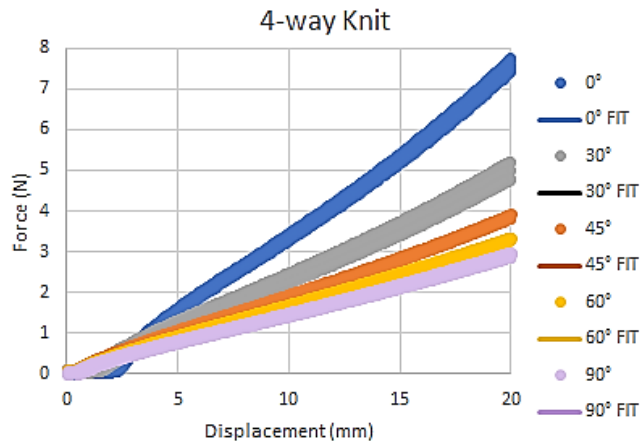
Figure 31. Loading Curves for the 4-way Knit for all force directions
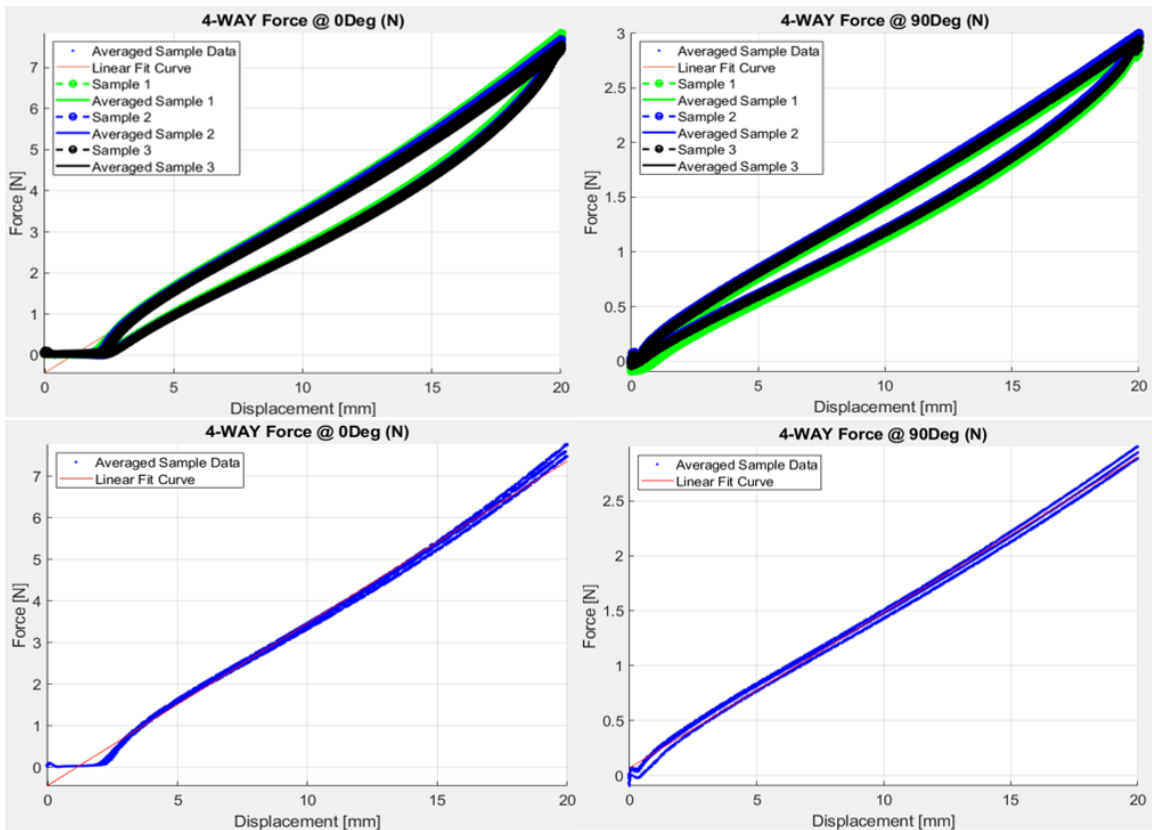
Figure 32. Tensile behavior for the stiffest and least stiff directions of the 4-way knit

Figures 30 and 32 also showcase the different hysteresis loops between the two knits. Regardless of force direction, the hysteresis loop of the 2-way knit is larger than the 4-way knit. The cyclic behavior is repeatable in both knit types and shows little difference between the three specimens in each sample group, each cycling three times. The size of this hysteresis loop is important when using measurements from the entire cycle; however,

it is less so when only analyzing and taking data only from the elongation curve (like in this study).

Next, fabric mechanics were compared with the presence of each stitch geometry. Prior research stated the linear response of the stitched sensor. It would be expected that the 4-way stitched samples would have a similar linear response as the 4-way knit. However, the 2-way knit didn't have a linear response for force applied in the 0°-45°, so it is interesting to see whether the response is any more linear. The force range was calculated for each sample group and compiled in Figure 33 for the 4-way knit and Figure 34 for the 2-way knit.

Force Range (N) of 4-way Knit with and without Sensors

■ 4-way knit Fabric-Only   ■ 4-way knit Coverstitch   ■ 4-way knit Chainstitch
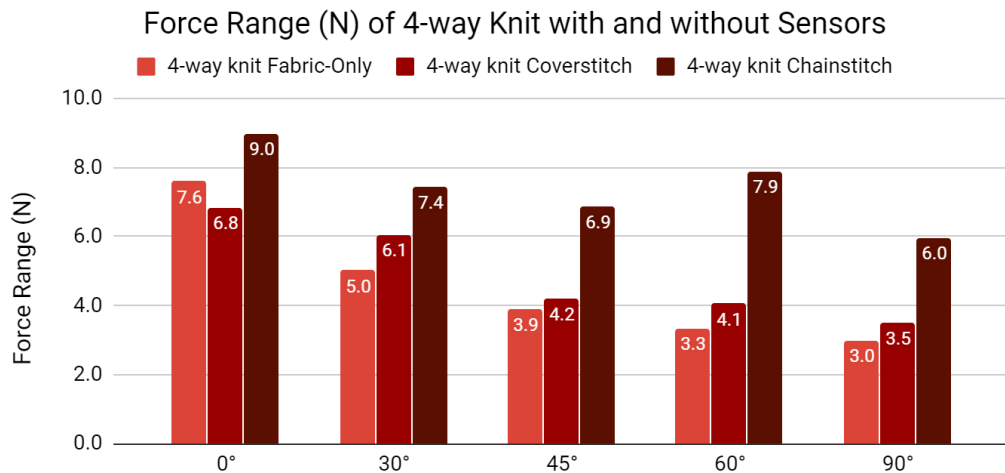
Figure 33. Comparing the Force Range for 4-way Knit with and without Sensors

Force Range (N) of 2-way Knit with and without Sensors

■ 2-way knit Fabric-Only   ■ 2-way knit Coverstitch   ■ 2-way Chainstitch
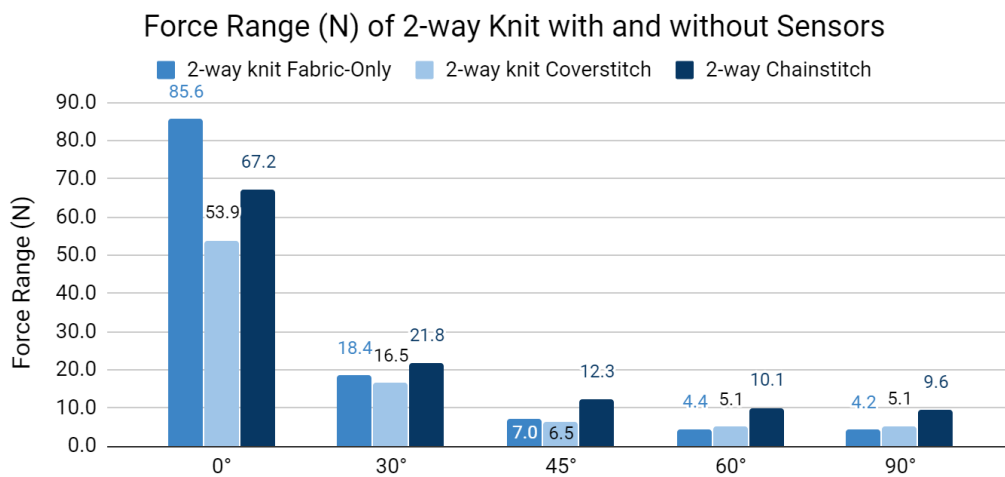
Figure 34. Comparing the Force Range for 2-way Knit with and without Sensors

Across all sample groups except the 2-way knit in the 0°, the chainstitch sensor geometry increased the apparent stiffness. Since this stitch geometry has a straight lockstitch-like attachment to the fabric, this is not surprising that the elongation is resisted by the stitch. The coverstitch geometry has a zigzag attachment which stretches easier. Looking more closely at individual force responses for each of the sensor groups, it's revealed that the chainstitch follows the fabric's linear response until strains of ~21% (or a displacement of 15mm) as seen in Figure 35. Conversely, the coverstitched sensor shows little interference with the general linear behavior of the textile's intrinsic stretchy directions, and at most, shows a slight increase in stiffness. The idea that the stiffness may be decreased because of slight non-destructive puncturing of the fabric substrate by the stitch sensor during fabrication does not seem to be present, although it could be overridden by the other effects mentioned.
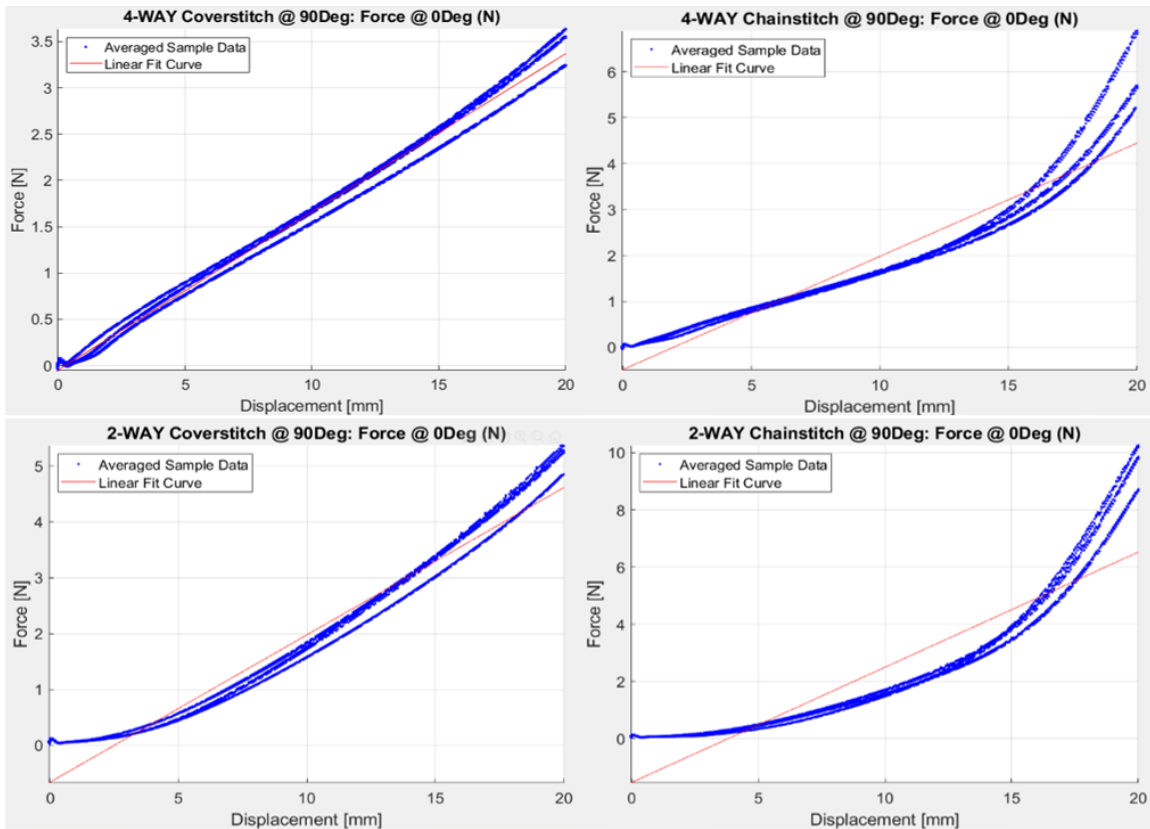
Figure 35. Force response for knits with stitched sensors (Left) coverstitch geometry (Right) chainstitch geometry (Top) 4-way knit (Bottom) 2-way knit

Focusing on the 90° force direction, Figure 36 shows the apparent stiffness changing with the knit fabric type and stitch geometry. Of all the sample groups, the 2way

fabric and chainstitch sample groups begets less consistent linear force responses compared to the 4way fabric and coverstitch sample groups.
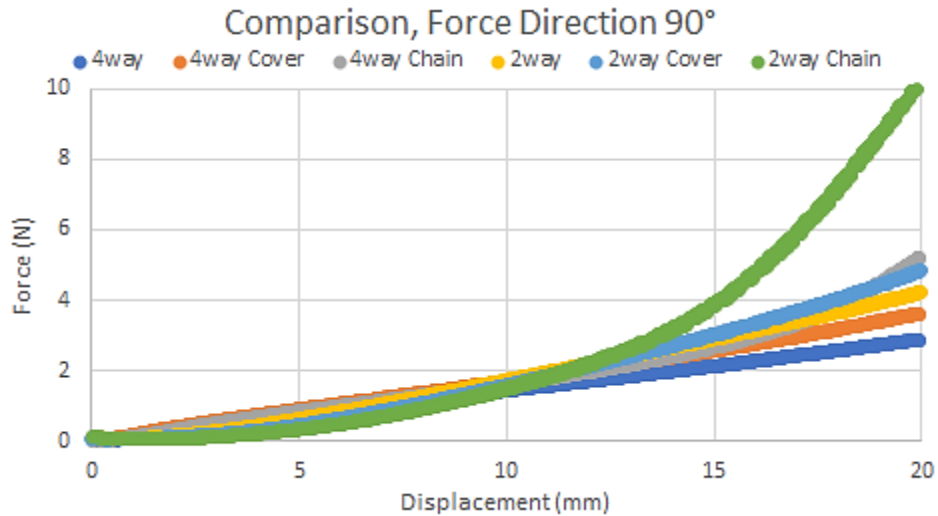
Figure 36. Comparing knit fabric type and stitch geometry variables when force applied in the 90°

The elastic modulus was also calculated. Because this is a linear fit calculation, the linearity error R^2 and average RMSE were also calculated and is higher in the less linear responses of some sample groups (i.e. the 2-way knit and chainstitch groups as previously mentioned). Table 6 shows all the calculated values for the fabric only sample groups, and the rest can be viewed in Appendix B. From these data, Table 5 shows the pertinent data needed for comparing the elastic modulus values with and without the sensors for each knit.

Table 5. Analysis of Fabric-Only Elastic Modulus

Sample Group	Calculations E (N/mm)	Degree from 0°				
		0°	**30°**	**45°**	**60°**	**90°**
4-way knit Fabric-Only	E(0°)	**0.007789**	**0.0049502**	**0.003719**	**0.0031802**	**0.0028262**
	% of E(0°)	100%	64%	48%	41%	36%
	Fit Line R^2	1.00	0.99	1.00	1.00	1.00
	Avg Fit Line RMSE	0.0029	0.0023	0.00090	0.00069	0.0008
2-way knit Fabric-Only	E(0°)	**0.07222**	**0.015566**	**0.0066762**	**0.0044484**	**0.0044188**
	% of E(0°)	100%	22%	9%	6%	6%
	Fit Line R^2	0.80	0.79	0.89	0.95	0.99
	Avg Fit Line RMSE	0.21	0.046	0.014	0.0060	0.0029

Table 6. Comparing the Elastic Modulus with and without Stitched Sensors

Sample Group	Calculations E (N/mm)	Degree from 0°				
		0°	30°	45°	60°	90°
4-way Fabric-Only	E(0°)	0.007789	0.0049502	0.003719	0.0031802	0.0028262
2-way Fabric-Only	E(0°)	0.07222	0.015566	0.0066762	0.0044484	0.0044188
4-way Coverstitch	% of fabric only E(0°)	92%	124%	115%	126%	121%
4-way Chainstitch		112%	136%	162%	204%	175%
2-way Coverstitch		61%	88%	91%	113%	119%
2-way Chainstitch		77%	114%	149%	188%	183%
Color guide:		+/- 0-20%	+/- 21-40%	+/- 41-61%	+/- 61-80%	+/- 81-100%

This comparison is near identical to what has been previously discussed for the force ranges, since the slopes have just been multiplied by a factor to get these values. When given an error percentage, the chainstitch sample groups have the largest difference from the fabric. In the scenario where the fabric elastic modulus in known, this comparison shows whether further testing with the sensor itself should be done. In other words, if using the fabric modulus as an approximation then the approximation would be the least accurate for the chainstitch sensor groups (+/-100%) and most accurate for the coverstitch sensor groups (+/-40%). This highlights the importance of this investigation and influence of both fabric choice and sensor stitch geometry on estimating real forces.

3.2 Sensor Performance with Inline Forces

Knowing that there are differences in both force range and stiffness (i.e. elastic modulus) based on the direction of force pulled, the next question is related to the sensor performance.

If the knit is stretchy enough, the human body can easily stretch it enough to perform movements, so slight differences in force depending on sensor placement can be overcome. For example, when bending into the squat position with the pants fixed at the waistband and ankles, the muscles still accomplish the same extension (in this case, we are neglecting any additional tendencies for the material to slide instead of stretch due to the stiffness increase in certain directions). So given the same displacement, does the sensor performance change due how it's placed with respect to the knit structure?

The knit structure is shown to exhibit different force ranges when stretched in different directions. If the sensor performs differently depending on the angle it was

stitched into the fabric, then either or both of two things are happening: 1-the force is propagating through the knit in a degree-specific manner, or 2-the knit structure and stitched sensor stitch points are affecting how much force is experienced by the stitched sensor. Ideally, the sensor performance will not differ much.

RQ2: When force is applied inline with the sensor, will the angle the sensor is stitched relative to the knit structure influence its performance?

3.2.1 Methods

To answer this question, for all stitched sample groups, force was applied in the same direction as the stitch sensor. Because the sensors are stitched with different angles with respect to the knit textile, the sensor performance can be compared to determine if certain stitched angles affect the sensor performance, given the same displacement. The same samples for the previous study were used.

An additional transducer in the Instron 3365 tester was setup to measure voltage, precise to 0.0001V. The stitched stretch sensor mechanism creates a change in resistance, so a Wheatstone bridge circuit was constructed with 3 other reference resistors of comparable resistance (10Ω+/-5%, 1W). The voltage divider was also considered, but the Wheatstone bridge is more accurate at small voltage changes and more common in industry specifically for strain sensors.

A supply voltage of 5V was used, provided by a microcontroller board. The bridge voltage was measured by an extra Instron transducer, setup for measuring voltage. This allowed for simultaneous measurement data of force, displacement, time, and voltage readings. To calculate the resistance, the Wheatstone bridge resistance calculation was used, which can be simplified because of the same value for the reference resistance:

$$R_x = \frac{R_2 V_s - (R_1 + R_2)V_B}{R_1 V_s + (R_1 + R_2)V_B} R_3$$

$$when \; R_1 = R_2 = R_3, then \quad R_x = \frac{R^2 V_s + 2R^3 V_B}{R V_s - 2R V_B} = \frac{R + 2R(V_B/V_s)}{1 - 2(V_B/V_s)}$$

For this comparison coverstitch and chainstitch sensors were stitched along the directions of 0°, 30°, 45°, 60°, and 90° with respect to the knit's stiffest direction (0°) as summarized in 3.1. Because the Instron grips are metallic, fabric covers were sewn to fit on the grippers and provide electrical isolation and prevent any sensor resistance interference. To ensure a tight grip and prevent any fabric slipping, the Instron pneumatic grips were set at 80psi. This high pressure was required only elongating the stiffest 2-way knit directions (a setting of 50psi would be sufficient for any 4-way knit only testing)

The sensor response was characterized with 3-cycles of 20cm elongation at a strain rate of 50mm/min, corresponding to the strain range of 0-29%. The elongation data from all three cycles was smoothed with a moving average (window of 5) and then aggregated together to generate a linear best fit. This resulting analysis used the following to compare the following sensor performance variables between sample groups:

Regarding the electrical properties, the stitched sensor exhibits piezoresistive behavior but the resistance is not directly measured in data acquisition. It is calculated from a measured voltage, here through a Wheatstone bridge circuit. The sensor response is measured by the bridge voltage and needs to be calculated using the value of the reference resistor values. The voltage at zero extension is used to calculate the nominal resistance and changes with varying extension. The maximum change from nominal resistance is considered the peak-to-peak change. This maximum was averaged for each specimen (S1, S2, S3) in the sample group to calculate an **Average Peak-to-Peak Change in Resistance**, $\overline{\Delta R}$

$$\overline{Peak\ to\ Peak\ \Delta R} =$$

$$= \frac{\left(R_{S1,d=max} - R_{S1,d=0}\right) + \left(R_{S2,d=max} - R_{S2,d=0}\right) + \left(R_{S3,d=max} - R_{S3,d=0}\right)}{3}$$

Sometimes the average peak-to-peak change is resistance is called the *sensor response* or *resistance range.* This is helpful in comparing a sensor's performance in different conditions or different sensors in the same condition, either in absolute terms (Ω) or normalized (%).

The ratio of the normalized change in the sensor response over the normalized strain is called the *sensitivity* or **gauge factor (GF)**. For stitched strain sensors, the resistance changes with tensile strain, $R(\varepsilon)$, so the gauge factor can be calculated as follows:

$$Gauge\ Factor = \frac{\Delta R/R}{\Delta L/L}$$

The GF is calculated using uniaxial strain inline with the sensor axis, generating a plot of normalized change in length ($\Delta L/L$) on the x-axis and normalized change in resistance on the y-axis. A linear fit is generated and the slope (rise/run) represents the GF. This value is typically around 2 for most metals and traditional strain sensors and varies for other soft sensors. High sensitivity is often a trade-off with a larger sensing range (% strain).

To have good force directional accuracy, the sensor would ideally ignore forces in all directions other than its main orientation. In reality, for a reasonable value of resistance change, the sensor has a minimum thickness that can be affected by offset forces. Sometimes, the sensor geometry is manipulated to encourage directional sensitivity. An example of this is to use a tight rectangular zigzag pattern where small portions of the conductor are perpendicular to the main sensing direction. Sensitivity to offset forces introduces another variable, called the **transverse sensitivity factor**, K_t.

$$K_T = \frac{Gauge\ factor\ (transverse\ direction)}{Gauge\ factor\ (axial\ direction)}$$

The transverse sensitivity factor was also calculated in a similar manner to the GF, except the uniaxial tensile force is applied in-plane and perpendicular to the sensor axis. (As will be explained below, this definition has been redefined from measuring perpendicular 90° to measuring 60°.)

Sensor **linearity (R^2)** characterizes the linear relationship (i.e. slope) of strain with change in sensor response for the loading cycle only. This is pertinent to linear sensor responses, as opposed to other response curves like exponential, logarithmic etc. The conductive stitched sensors are classified as linear sensors, so nonlinear behavior can be

indicative of non-negligible variable effects, large hysteresis, large degrees of error, or permanent deformation. It has been proposed that there is a trade-off in having high sensitivity or high linearity (Amjadi, Kyung, Park & Sitti, 2016). The closer linearity is to 1.0, the more linear the sensor data.

The **_root-mean-square error (RMSE)_**, desired to be close to 0, was calculated for the linear fit of sensor response.

The **_dynamic baseline drift_** describes how much the sensor response at zero extension drifts over consecutive cycling and was calculated over the 3 consecutive cycles. The recovery behavior of both the sensor and fabric substrate influences this value, which is desired to be as close to zero as possible.

Calculating the **_average hysteresis error_** uses data from the entire cycle (both elongation and relaxation curves). To convey a practical meaning, the hysteresis error was calculated by finding the maximum difference between the curves for every displacement value (Fig 37).

$$for\ all\ x\ in\ the\ dataset\ 0 < x_i < d_{max}: find\ \{x_i, y_{iE}\}\ and\ \{x_i, y_{iR}\}$$

$$Hysteresis\ Error = \frac{|Y_{iR} - Y_{iE}|}{|Y_{d=20} - Y_{d=0}|} \times 100\%$$
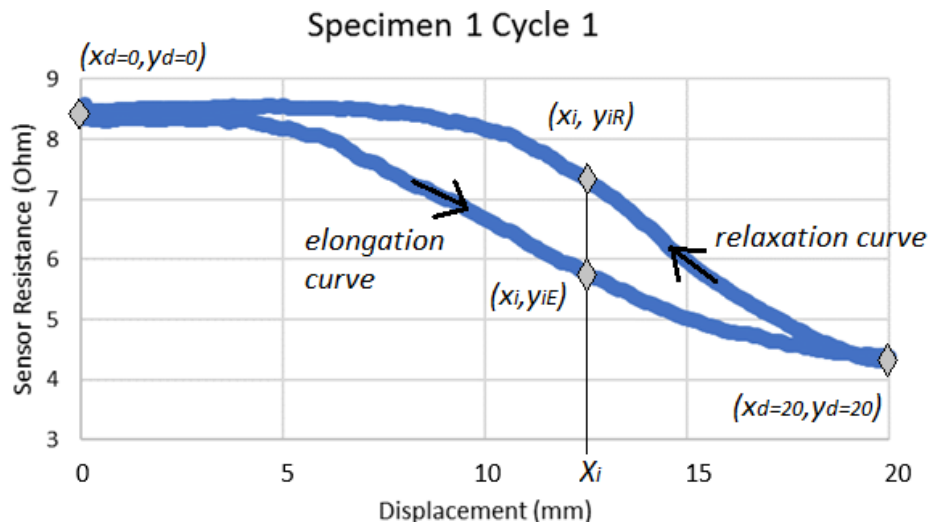
Figure 37. Definition of points used in the Hysteresis Error calculation

To simplify the calculation for each sample group, only the data from the third cycle for each specimen is used to report average hysteresis error per sample group. Depending on the context, the hysteresis error is reported as either a value (ohms for resistance) or as a percentage (normalized to the entire range ΔR).

$$Hysteresis\ Error =$$

$$= \frac{Hysteresis\ Error_{S1} + Hysteresis\ Error_{S2} + Hysteresis\ Error_{S3}}{3}$$

In reality, the applied force is not the only thing that will change the sensor's resistance. Increasing the strain rate may change the sensor response by increasing the viscoelastic mechanical properties. (Human motion around 1Hz would translate to a comparable strain rate of 2*2cm/s=2400mm/min, higher than the 200mm/min strain rate used in this study.) Temperature, humidity, water content % within the textile and/or conductive yarns can also affect the sensor measurements. Generally, the error due to the temperature coefficient of resistance effect should be minimal in the temperature range of the application, which for wearable applications may range from -30-45C. However, the water content could affect both mechanical and electrical behavior. The effect of these variables were not studied in this thesis investigation.

In summary, the following variables were reported:
- Peak-to-Peak change in Resistance (Ω) : $\Delta R = |R_{d=max=20mm} - R_{d=0}|$
- Gauge Factor : $\dfrac{\Delta R/R}{\Delta L/L}$
- Transverse Sensitivity : $Transverse\ Gauge\ Factor\ (Force\ @\ 60°)$
- Linearity, given by the linear regression coefficient of determination: R^2
- RMSE (Ω)
- Dynamic Baseline Drift (Ω): $R_{d=0,third\ cycle} - R_{d=0,first\ cycle}$
- Hysteresis Error (%): $Hysteresis\ \% = \left|\dfrac{Y_2 - Y_1}{X_2 - X_1}\right| \cdot 100\%$

3.2.2 Results & Discussion

The sensor performance is captured first as a change of bridge voltage. Each sensor as fabricated has some variation in nominal resistance, so to compare between specimens and between sample groups the nominal resistance (R(d=0)) baseline is removed to get a graph that shows only the change in resistance (Fig 38). The sensor decreases resistance as it elongates, so the change is negative with the elongation data being the leftmost curve and relaxation data being the rightmost curve. The elongation data was then partitioned and smoothed with a moving average (window of 5; elongation portion of the curve shown by the bold lines in Figure 38 (left). The average peak-to-peak resistance change was calculated and then the resistance was normalized with the nominal resistance to be plotted against the normalized strain. A linear regression fit was calculated, where the slope value represents the gauge factor/sensitivity.
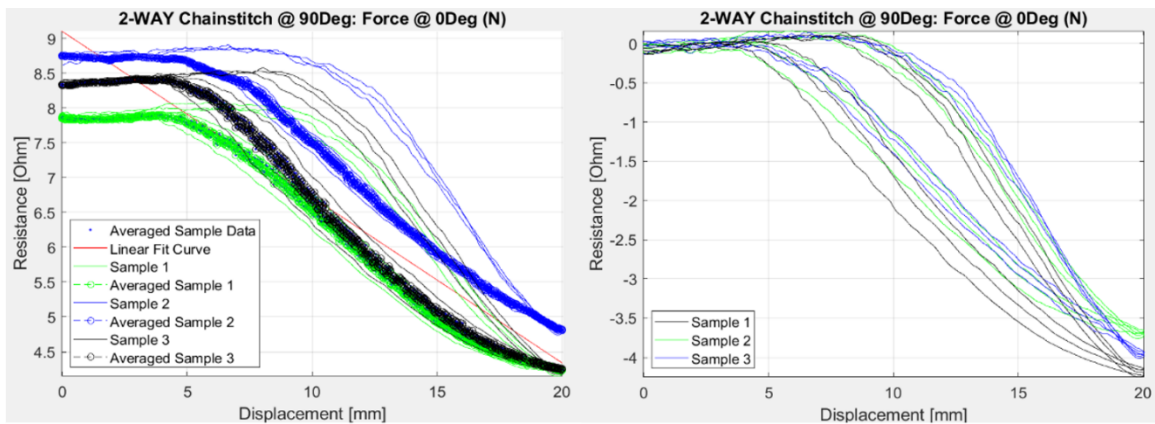
Figure 38. (Left) Data of actual resistance (Right) Data of offset resistance

First the nominal resistance and the peak-to-peak change were summarized for comparison across all the sample groups (Table 7). The goal is to verify whether the sensor performance is affected by sensor placement. Overall, the change in resistance was approximately 28% of nominal for the coverstitch geometry and approximately 46% of nominal for the chainstitch geometry. The stitched angle did not seem to matter greatly for the 4-way knit coverstitch or 2-way knit chainstitch groups, staying within 10% of the response shown by the 0° reference. The stitched angle did result in variation for the 4-way knit chainstitch and 2-way knit coverstitch groups, where ~20% variation of the response shown by the 0° reference was observed. These results could be viewed as a characteristic response given by the sensor orientation. Otherwise, the percentage change was relatively similar for each angle within a sample group.

Table 7. Comparison of Resistance Peak-to-Peak change (Ω)

Sample Group	Calculations	Degree from 0°				
		0°	30°	45°	60°	90°
4-way knit Coverstitch	Avg Nominal Resistance (Ω)	13.58	11.98	13.99	12.87	14.15
	Avg Peak-to-Peak Δ	3.95	3.44	3.68	3.61	4.02
	Δ/Nominal	29%	29%	26%	28%	28%
	% of Δ/Nominal(0°)	**100%**	**99%**	**90%**	**96%**	**98%**
4-way knit Chainstitch	Avg Nominal Resistance (Ω)	9.06	8.98	9.16	8.06	9.40
	Avg Peak-to-Peak Δ	3.75	4.05	4.29	2.77	4.26
	Δ/Nominal	41%	45%	47%	34%	45%
	% of Δ/Nominal(0°)	**100%**	**109%**	**113%**	**83%**	**110%**
2-way knit Coverstitch	Avg Nominal Resistance (Ω)	11.26	9.80	12.60	13.26	12.44
	Avg Peak-to-Peak Δ	3.17	3.41	2.84	3.07	3.14
	Δ/Nominal	28%	35%	23%	23%	25%
	% of Δ/Nominal(0°)	**100%**	**123%**	**80%**	**82%**	**90%**
2-way knit Chainstitch	Avg Nominal Resistance (Ω)	8.23	8.67	8.77	8.58	8.36
	Avg Peak-to-Peak Δ	3.88	4.42	4.42	4.12	3.94
	Δ/Nominal	47%	51%	50%	48%	47%
	% of Δ/Nominal(0°)	**100%**	**108%**	**107%**	**102%**	**100%**
Color guide:		*+/- 0-5%*	*+/- 6-10%*	*+/- 11-15%*	*+/- 16-20%*	*+/- 21-25%*

First, the overall trend of knit choice and stitch geometry was analyzed by averaging all of the individual sensor placement angles, as shown in Table 8. The stitch geometry seems to affect the gauge factor stronger than the fabric choice. The same goes for R^2, hysteresis error, and K_T. A distinct trend is more difficult to see with the RMSE, except that the chainstitch geometry seems to have higher values. The KT is distinctly different for each group.

Table 8. Average Sensor Performance

Sample Group	Averaged Values across all stitched angles					
	Gauge Factor	R^2	Avg RMSE (Ω)	Hysteresis Error (Ω) / (%)	Baseline Drift (Ω)	K_T
4-way knit Coverstitch	-1.12	0.971	0.0142	0.46 / 11.2	-0.422	42%
4-way knit Chainstitch	-1.97	0.965	0.0281	1.46 / 35.8	0.013	10%
2-way knit Coverstitch	-1.01	0.926	0.0206	0.42 / 13.0	-0.053	80%
2-way knit Chainstitch	-2.24	0.942	0.0428	1.60 / 38.0	0.067	5%

Table 9. Sensor Performance Summary Table

Sample Group	Calculations	Degree from 0° of Knit the Sensor was Stitched				
		0°	30°	45°	60°	90°
4-way knit Coverstitch	**Sensitivity/GF**	**-1.15**	**-1.09**	**-1.05**	**-1.14**	**-1.16**
	% of GF(0°)	100%	95%	91%	99%	101%
	Fit Line R²	*0.956*	*0.966*	*0.973*	*0.976*	*0.983*
	Fit Line Avg RMSE (Ω)	*0.0184*	*0.0146*	*0.0134*	*0.0132*	*0.0114*
	Hysteresis Error (Ω)	*0.81*	*0.46*	*0.36*	*0.29*	*0.35*
	Baseline Drift (Ω)	*-0.513*	*-0.088*	*-0.060*	*-0.043*	*-0.0474*
	Transverse** GF	-0.090	-0.548	-0.545	-0.574	-0.616
	Trans sensitivity factor, K_T	*8%*	*50%*	*52%*	*50%*	*53%*
4-way knit Chainstitch	**Sensitivity/GF**	**-1.76**	**-2.00**	**-2.05**	**-2.06**	**-1.96**
	% of GF(0°)	100%	114%	117%	117%	112%
	Fit Line R²	*0.945*	*0.977*	*0.973*	*0.969*	*0.960*
	Fit Line Avg RMSE (Ω)	*0.0316*	*0.0237*	*0.0264*	*0.0285*	*0.0303*
	Hysteresis Error (Ω)	*1.29*	*1.64*	*1.51*	*1.35*	*1.49*
	Baseline Drift (Ω)	*-0.089*	*-0.023*	*-0.050*	*-0.045*	*-0.0179*
	Transverse** GF	-0.081	-0.303	-0.189	-0.193	-0.207
	K_T	5%	15%	9%	9%	11%
2-way knit Coverstitch	**Sensitivity/GF**	**-1.13**	**-1.07**	**-0.93**	**-0.92**	**-1.01**
	% of GF(0°)	100%	95%	82%	82%	89%
	Fit Line R²	*0.949*	*0.964*	*0.887*	*0.951*	*0.879*
	Fit Line Avg RMSE (Ω)	*0.0202*	*0.0157*	*0.0245*	*0.0146*	*0.0278*
	Hysteresis Error (Ω)	*0.28*	*0.43*	*0.52*	*0.44*	*0.44*
	Baseline Drift (Ω)	*-0.131*	*0.116*	*0.112*	*-0.005*	*-0.0234*
	Transverse** GF	-0.765	-0.707	-0.768	-0.816	-1.006
	K_T	68%	66%	83%	88%	100%
2-way knit Chainstitch	**Sensitivity/GF**	**-2.20**	**-2.37**	**-2.31**	**-2.21**	**-2.14**
	% of GF(0°)	100%	108%	105%	100%	97%
	Fit Line R²	*0.933*	*0.954*	*0.948*	*0.934*	*0.941*
	Fit Line Avg RMSE (Ω)	*0.0455*	*0.0402*	*0.0414*	*0.0454*	*0.0413*
	Hysteresis Error (Ω)	*1.62*	*1.84*	*1.73*	*1.65*	*1.17*
	Baseline Drift (Ω)	*0.041*	*-0.058*	*-0.082*	*-0.039*	*-0.0297*
	*Transverse** GF*	*-0.016*	*-0.083*	*-0.149*	*-0.072*	*-0.283*
	K_T	1%	3%	6%	3%	13%
GF Color guide:		*+/- 0-5%*	*+/- 6-10%*	*+/- 11-15%*	*+/- 16-20%*	*+/- 21-25%*
Transverse GF Color guide:		*+/- 0-10%*	*+/- 11-20%*	*+/- 21-40%*	*+/- 41-60%*	*+/- 61-100%*

**Transverse sensitivity was not found to be the least 90° from sensor axis, rather commonly at 60° to stitch angle.

Next, the other sensor performance metrics were measured and compared between sample groups in Table 9. This shows some interesting relationships, which are

discussed by each variable. (The transverse sensitivity factor, K_T, is shown in Table 9 but was actually computed using the results from the next section. To provide a complete analysis, they were added to this table, but more discussion can be found in the next section on why an offset force of 60° was used instead of the more traditional 90° to calculate transverse sensitivity.)

Regarding the gauge factor (GF), the chainstitch geometry showed approximately twice the value than the coverstitch (-2 compared to -1) (Fig 39). Interestingly, although it was clear that the fabric stiffness varied depending on the angle, it doesn't show an influence of fabric stiffness on increasing or decreasing the GF. The 2-way knit chainstitched sample group shows the highest GF (-2.24) and the 2-way knit coverstitched sample group shows the least (-1.01). As a reference, a GF of +/-2 is acceptance for many strain sensors. Looking only at this value, any of the sample groups have potential for strain rosette design although the chainstitch sensor geometry has much lower transverse GF and subsequent transverse sensitivity factor, K_t.
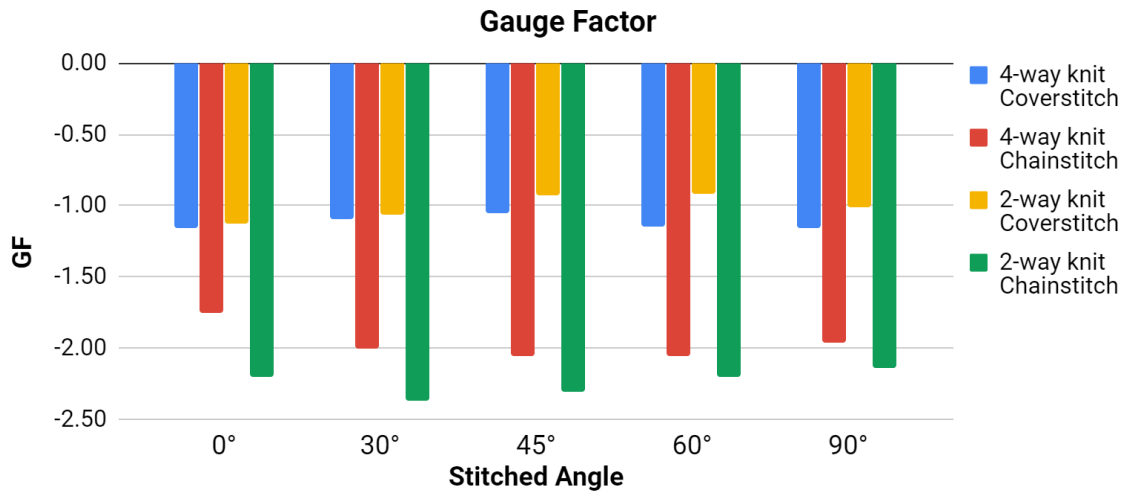
Figure 39. Gauge Factor (Force applied inline)

Digging deeper into this effect further, the Resistance(Displacement) graphs show a loss of linearity at the lower and higher strain bounds with the chainstitch geometry compared to the coverstitch (Fig 40). The biggest takeaway is that the stiffer the knit-sensor combination, the less linear sensor behavior and reduction of sensing region (Fig 41). This shows up with its larger Fit Line RSME values, Hysteresis Errors and lower R^2 values. The implication of this is to match the sensing range with the application and

optimize linear response. A basic recommendation would be to avoid the 2-way chainstitch group since it is stiff both in fabric and in sensor geometry.
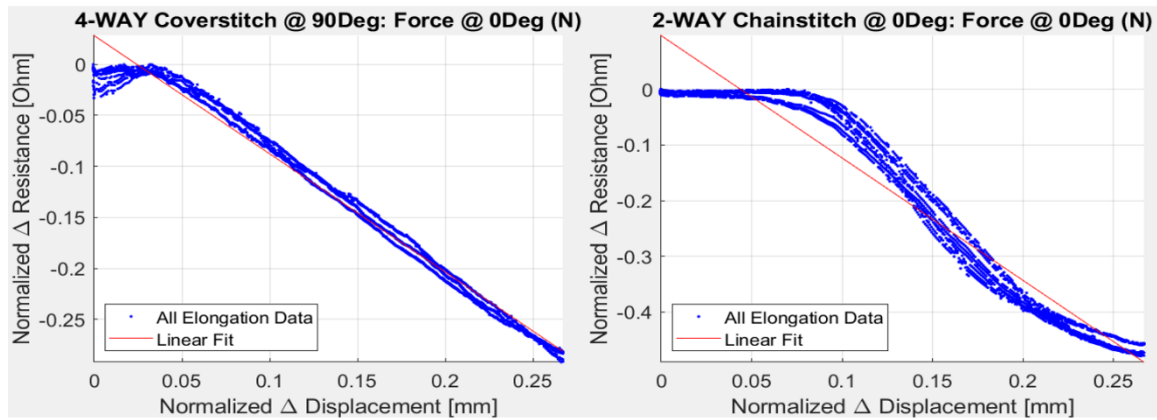
Figure 40. Comparing Sensor Performance between the stiffest stitch geometry and stiffest textile with the least
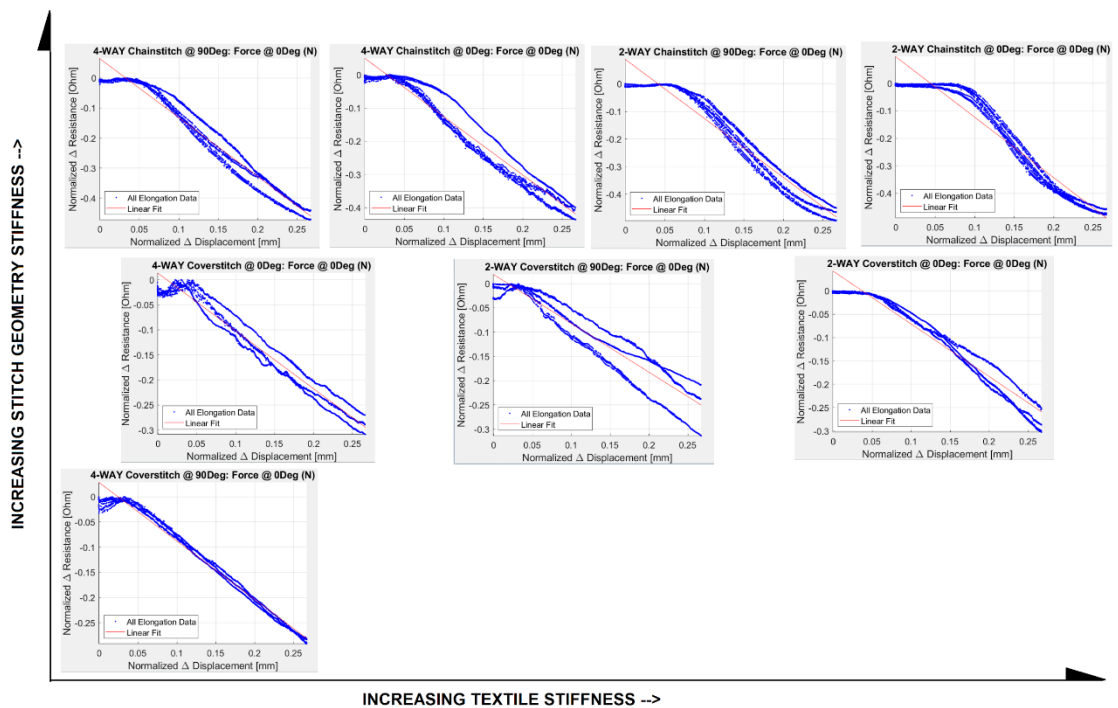
Figure 41. Loose relationship of sensor response with increasing stitch and fabric stiffness variables

Looking closer at the linearity of sensor response shows that all of the sample groups perform similarly except for the 2-way knit chainstitch (Fig 42). Regarding RMSE, the 4-way knit coverstitch has the least error while the 2-way knit chainstitch has the most, although all groups are performing fairly with errors less than 0.05Ω (Fig 43). The RMSE

is representing the "goodness of fit" so with this low error throughout all the groups, it means that the linear model is predicting the sensor response well.

Figure 42. Comparing Linearity Error
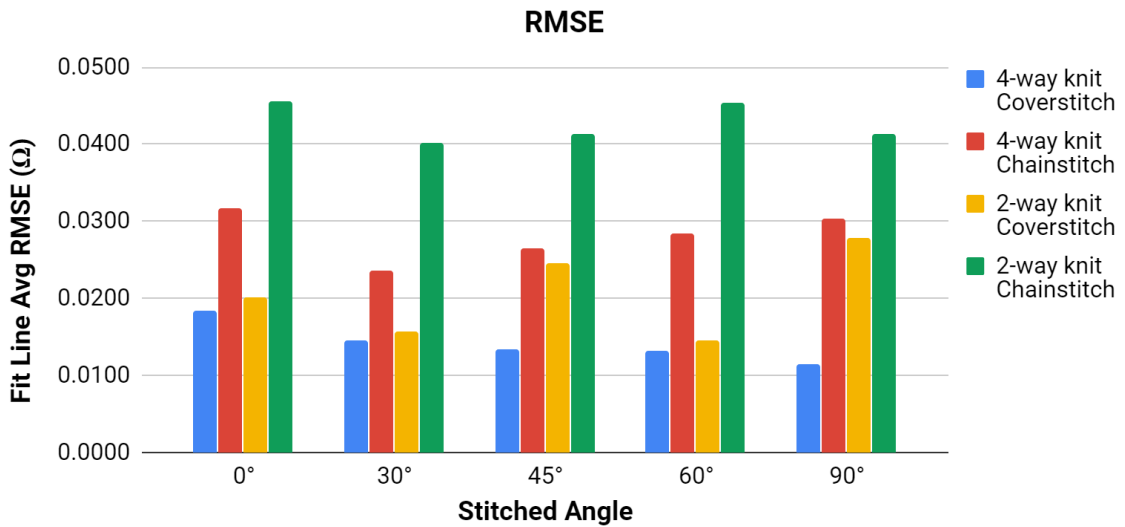
Figure 43. Comparing linear fit "goodness of fit" RMSE

The baseline drift is low for most of the groups, with the highest drifts seen in the stiffest directions (Fig 44). The 4-way knit coverstitch has an especially high drift in the 0° which is not expected. It would not have been surprising to see larger drifts in the 2-way knit stiffer directions, but it is not trending uniformly. Most baseline drifts are in the negative direction (the same direction as elongation) and can be attributed to the imperfect stretch recovery of the fabric in progressive cycling.
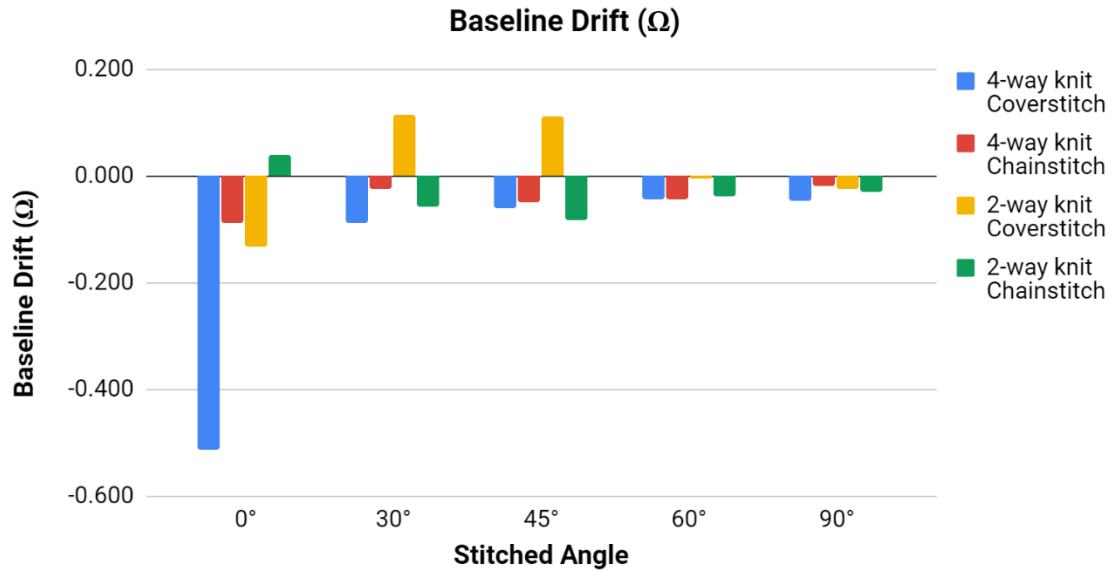
Figure 44. Comparing Baseline Drift

As previously seen in the force(displacement) data, the chainstitch geometry has a larger hysteresis error (Fig 45). Surprisingly, the influence of 2-way knit stiffer directions does not seem to add any additional hysteresis error.

Figure 45. Comparing Hysteresis Error

3.3 Sensor Performance with Offset Forces

Now that the sensor response is fully characterized when the force is applied inline with the sensor, it's important to understand how the sensor responds as the force is

applied at increasing angles from the sensor axis. This response translates to the transverse sensitivity property of any strain sensor, which is desirable low. If the transverse sensitivity is high, then the sensor is unable to distinguish between force directions and is more applicable for more simple binary force detection - whether a force is applied or not. In other words, if the transverse sensitivity is low, then both the force and force direction could be identified separately. This is why the traditional strain rosette design works only if the sensor has low transverse sensitivity.

RQ3: Stretching at an angle 0<x<90 to the sensor, how does the sensor performance change?

3.3.1 Methods

To answer this question, for all stitched sample groups, force was applied in different directions and the sensors for each sample group were measured using the Instron tensile tester with all of the same testing parameters. Similar to selecting the stitch angle variables, the range of interest in a symmetric knit is 0°-90°. Now *with respect to the stitched sensor*, force was applied in five directions: 0°, 30°, 45°, 60°, and 90°. A text matrix for one sample group is shown in Table 10, which is repeated for the other sample groups (i.e. 2-way Coverstitch, 4-way Chainstitch, and 2-way Chainstitch). The same samples and Instron test procedures mentioned before were used.

Table 10. Test Matrix for the 4-way knit Coverstitch Groups (similar for the 2-way knit & Chainstitch groups)

Substrate	4-way knit																			
Stitch Geometry	Coverstitch																			
Stitched Angle (°)	0				30				45				60				90			
Force Direction Angle (°)	30	45	60	90	30	45	60	90	30	45	60	90	30	45	60	90	30	45	60	90

Inserting the specimen into the Instron tester dictated the force direction. A protractor was used to mark the angles to which to align the Instron test grips. The setup for two of the test conditions are shown in Figure 46.

Figure 46. (Left) Test setup for 2-way 30° chainstitch with force applied at 60° (Right) 2-way 30° chainstitch with force applied at 90°

The gauge force, R^2, RMSE, and hysteresis error were calculated in the same manner as before. Based on the gauge force values from each of the offset force directions, the direction used to calculate transverse sensitivity was decided and also included in the results.

3.3.2 Results & Discussion

Calculated values for each sample group were compiled for each stitch angle parameter (0°, 30°, 45°, 60°, 90°). The results for 0° Stitch Angle sample groups are presented in Table 11 and show the full analysis of gauge factor, linearity and error values. (The full results for the rest of the Stitch Angles 30°, 45°, 60°, and 90° can be found in Appendix D.) The 0° column in Table 11 represents sensor response when the force is applied inline with the sensor, which is stitched at 0° in this case. Then the 30°-90° columns represent the sensor performance as the force angle increases from 30° to 90° from the sensor (perpendicular).

Table 11. Gauge Factor, Linearity and Error Values for the Stitched Angle 0° sample groups, when the Force Direction Angle changes from 0°-90°

Sample Group	Calculations	Force Direction (Degree from Stitch Axis)				
		0°	30°	45°	60°	90°
4-way knit Coverstitch 0°	GF	-1.1538	-0.71597	-0.49399	-0.089615	-0.70656
	% of GF(0°)	100%	62%	43%	8%	61%
	Fit Line R²	0.956	0.958	0.851	0.685	0.866
	Fit Line Avg RMSE (Ω)	0.018	0.011	0.015	0.014	0.021
	Hysteresis Error (Ω)	0.81	0.35	0.63	0.55	0.50
4-way knit Chainstitch 0°	GF	-1.7554	-0.78811	-0.23292	-0.080503	-0.22008
	% of GF(0°)	100%	45%	13%	5%	13%
	Fit Line R²	0.945	0.774	0.640	0.662	0.595
	Fit Line Avg RMSE (Ω)	0.032	0.031	0.013	0.004	0.013
	Hysteresis Error (Ω)	1.29	0.46	0.16	0.14	0.16
2-way knit Coverstitch 0°	GF	-1.1293	-0.80841	-0.73199	-0.76455	-0.91222
	% of GF(0°)	100%	72%	65%	68%	81%
	Fit Line R²	0.949	0.973	0.915	0.953	0.948
	Fit Line Avg RMSE (Ω)	0.020	0.010	0.017	0.013	0.017
	Hysteresis Error (Ω)	0.28	0.30	0.24	0.24	0.47
2-way knit Chainstitch 0°	GF	-2.1973	-1.025	0.019658	-0.016448	-0.024615
	% of GF(0°)	100%	47%	-1%	1%	1%
	Fit Line R²	0.933	0.810	0.142	0.035	0.076
	Fit Line Avg RMSE (Ω)	0.046	0.038	0.004	0.006	0.007
	Hysteresis Error (Ω)	1.62	0.39	0.10	0.11	0.14
% of GF(0°) Color guide:		0-10%	11-20%	21-40%	41-60%	61-100%

Similar to the previous section, each of the variables are discussed individually to see the trends or effects of the textile substrate, sensor stitch geometry, or sensor placement. A comparison of the gauge factor progression all sample groups and force direction angles are shown in Table 12.

Sample Group		Calculations	Force Direction (Degree from Stitch Axis)				
			0°	30°	45°	60°	90°
4-way knit Coverstitch	0°	GF	-1.1538	-0.71597	-0.49399	-0.089615	-0.70656
		% of GF(0°)	100%	62%	43%	8%	61%
	30°	GF	-1.0946	-0.6801	-0.4981	-0.54821	-0.68969
		% of GF(0°)	100%	62%	46%	50%	63%
	45°	GF	-1.0544	-0.83621	-0.5947	-0.54466	-0.55551
		% of GF(0°)	100%	79%	56%	52%	53%
	60°	GF	-1.143	-0.86337	-0.63305	-0.57436	-0.60921
		% of GF(0°)	100%	76%	55%	50%	53%
	90°	GF	-1.1601	-0.94217	-0.74592	-0.61632	-0.64227
		% of GF(0°)	100%	81%	64%	53%	55%
4-way knit Chainstitch	0°	GF	-1.7554	-0.78811	-0.23292	-0.080503	-0.22008
		% of GF(0°)	100%	45%	13%	5%	13%
	30°	GF	-2.0033	-1.4659	-0.67142	-0.30334	-0.13559
		% of GF(0°)	100%	73%	34%	15%	7%
	45°	GF	-2.0526	-1.501	-0.57711	-0.18911	-0.21722
		% of GF(0°)	100%	73%	28%	9%	11%
	60°	GF	-2.0567	-1.3337	-0.64921	-0.19339	-0.13488
		% of GF(0°)	100%	65%	32%	9%	7%
	90°	GF	-1.9624	-1.3346	-0.72945	-0.2066	-0.1607
		% of GF(0°)	100%	68%	37%	11%	8%
2-way knit Coverstitch	0°	GF	-1.1293	-0.80841	-0.73199	-0.76455	-0.91222
		% of GF(0°)	100%	72%	65%	68%	81%
	30°	GF	-1.0672	-0.89907	-0.71471	-0.70667	-0.94836
		% of GF(0°)	100%	84%	67%	66%	89%
	45°	GF	-0.93021	-0.85151	-0.68566	-0.76769	-0.90801
		% of GF(0°)	100%	92%	74%	83%	98%
	60°	GF	-0.92177	-0.78347	-0.71639	-0.81569	-1.0269
		% of GF(0°)	100%	85%	78%	88%	111%
	90°	GF	-1.0085	-0.77428	-0.79663	-1.0056	-1.2591
		% of GF(0°)	100%	77%	79%	100%	125%
2-way knit Chainstitch	0°	GF	-2.1973	-1.025	0.019658	-0.016448	-0.024615
		% of GF(0°)	100%	47%	-1%	1%	1%
	30°	GF	-2.3718	-1.8578	-0.84607	-0.082691	-0.58647
		% of GF(0°)	100%	78%	36%	3%	25%
	45°	GF	-2.3064	-1.6553	-0.43243	-0.14931	-0.81941
		% of GF(0°)	100%	72%	19%	6%	36%
	60°	GF	-2.2067	-1.5778	-0.37818	-0.07245	-0.7569
		% of GF(0°)	100%	72%	17%	3%	34%
	90°	GF	-2.1375	-1.6898	-0.94156	-0.28301	-0.74615
		% of GF(0°)	100%	79%	44%	13%	35%
% of GF(0°) Color guide:			0-10%	11-20%	21-40%	41-60%	61-100%

As the angle of force direction increases, the gauge force is expected to decrease. Just looking at the normalized resistance vs strain, it can be seen that the coverstitch responds similarly to offset forces (Fig 47, Left) whereas the chainstitch sensor shows distinct slopes depending on the force angle (Fig 47, Right).
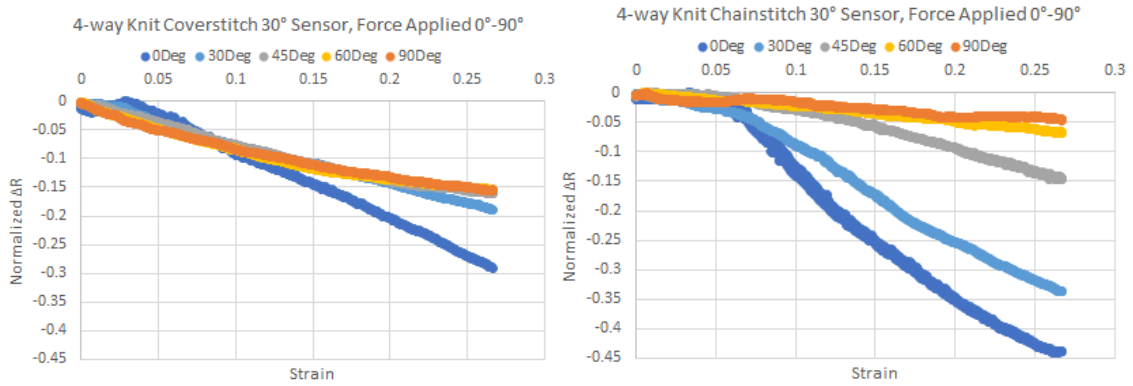
Figure 47. Normalized Δ Resistance vs Strain for (Left) 4-way 30° Coverstitch (Right) 4-way 30° Chainstitch

Plotting the fraction of GF(0°) of all sample groups reveals that a decreasing trend is not always seen, and that the minimum values are not always seen for 90°. As Figure 48 shows, there is still 50+% sensitivity seen for forces applied 30° from the sensor (first column) and decreases thereafter except for the 2-way coverstitched sample groups. This group seems to have an opposite trend, potentially due to unequal stiffness causing increased sensor response when the fabric is pulled in the less-stiff fabric directions. However, the decrease is non-uniform; the coverstitched sensor groups still maintain 30+% sensitivity and relatively uniform for all offset forces except in the 4-way Coverstitch @0° group. The chainstitched sensor groups have a more marked decrease, often falling to near 0 in the 60° force direction. Of these, the 4-way chainstitch groups are more consistent in this trend over the 2-way chainstitch groups.
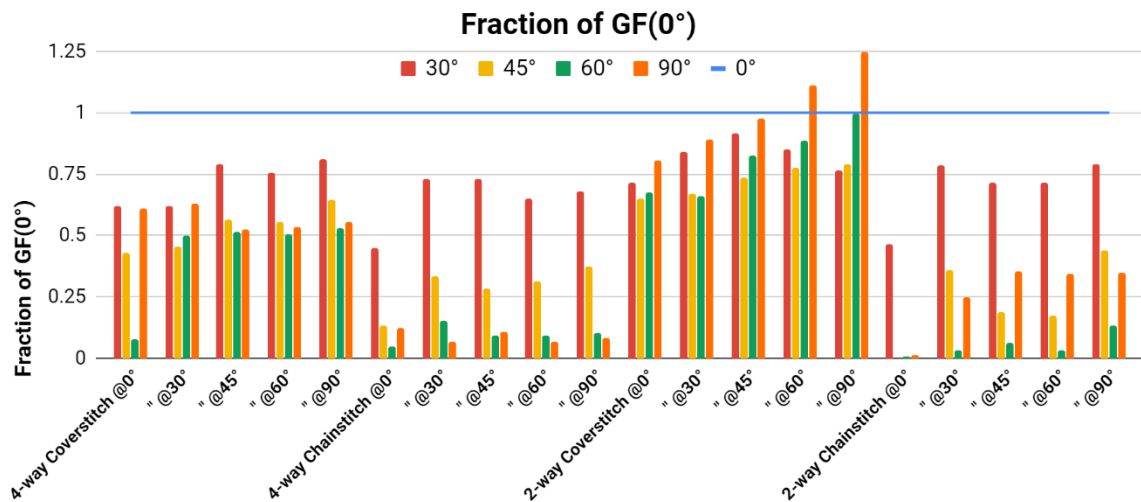

Figure 48. Comparison of Sensor Gauge Factors as Force Direction changes from 0°-90°

Between the sensor geometries the coverstitch is wider than the chainstitch, which is likely causing the higher overall sensitivities in the coverstitch sample groups compared to the chainstitch sample groups. The 90° force may be widening the stitched sensor, inducing a greater sensor response than an offset force of 60°. The combination of fabric and sensor geometry that seems most responsive to offset forces is the 2-way coverstitch @90°, followed by the rest of the 2-way coverstitch groups. These sensor groups seem relatively symmetric in their response, regardless of force direction applied. The combination least responsive to offset forces is the 2-way chainstitch @0°, then the 4-way chainstitch @0°. Using the values from the 60° force the transverse sensitivity for each sample group was computed and shown in Figure 49.
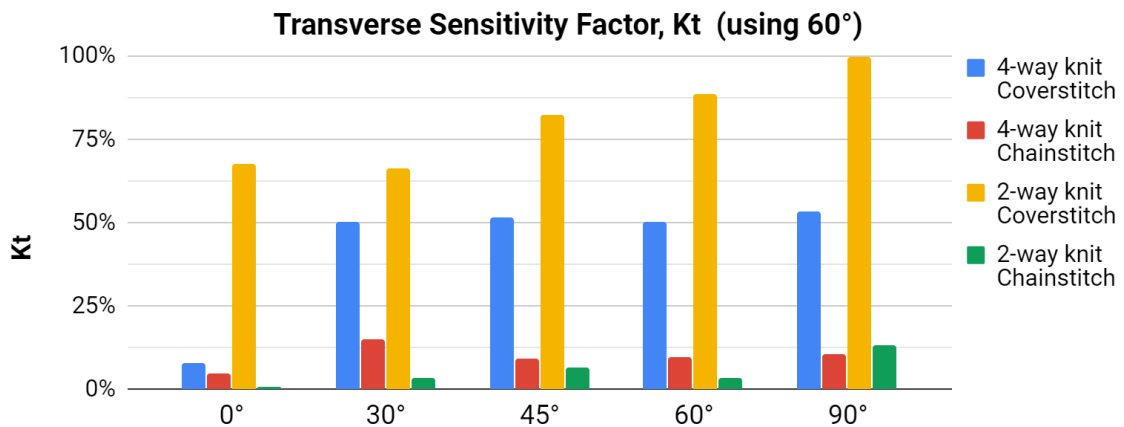

Figure 49. Transverse Sensitivity Factor using the GF_Force@60°/GF_Force@0°

Regarding linearity, the linearity of sensor response decreases as the offset force angle increases from in line to perpendicular (Fig 50). In general, reviewing the linearity for the sensor response due to offset forces is not important, unless an application deemed it useful (ex: used a single coverstitch to detect forces applied in any direction.) In this case, the coverstitch groups do have acceptable R^2 values across the spectrum. The coverstitch geometry has low transverse sensitivity, so the ΔR data of offset forces are scattered around ΔR=0 rather than a linear decrease.
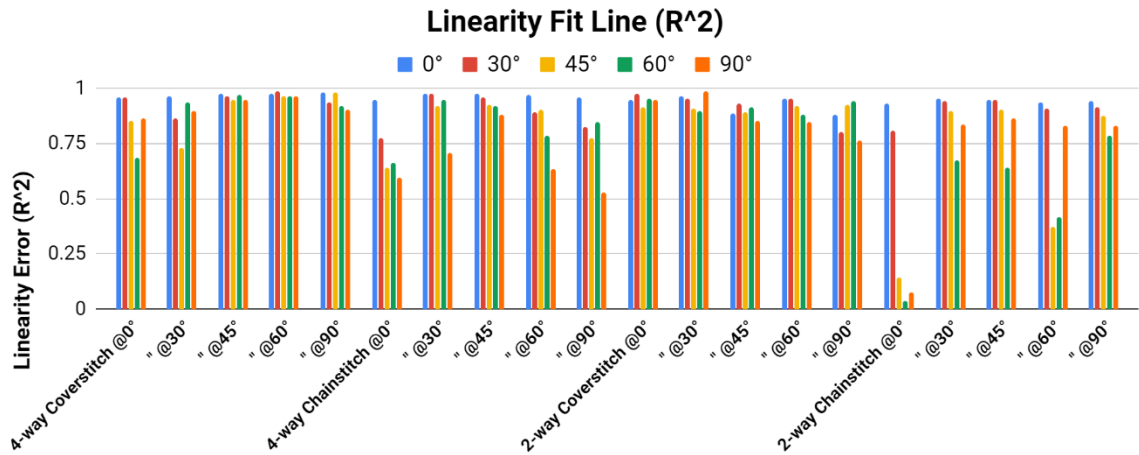
Figure 50. Linearity Error (R2)

The RMSE are related to the R^2 values, where the uniform scattering of data near zero causes high error due to low linearity in the model fit. The RMSE of force applied inline (0°) is the most important for all the sensor groups, so it is not an issue that there are large RMSE errors for some of the sample groups (Fig 51).
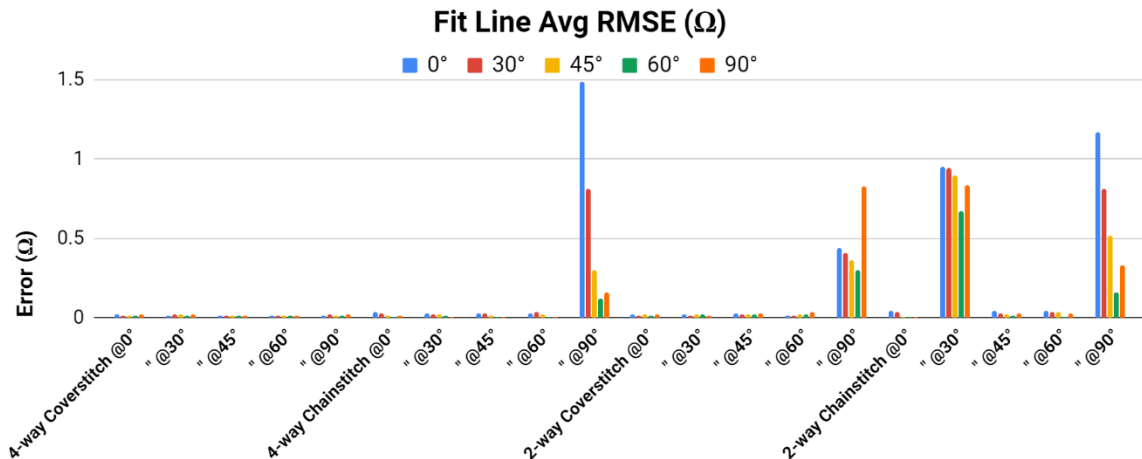

Figure 51. Average RMSE

The 0° direction seems to have the highest dynamic baseline drift. This is interesting to note because the coverstitch sensor groups have a similar sensor response, yet have lower baseline drifts when the force is offset (Fig 52).
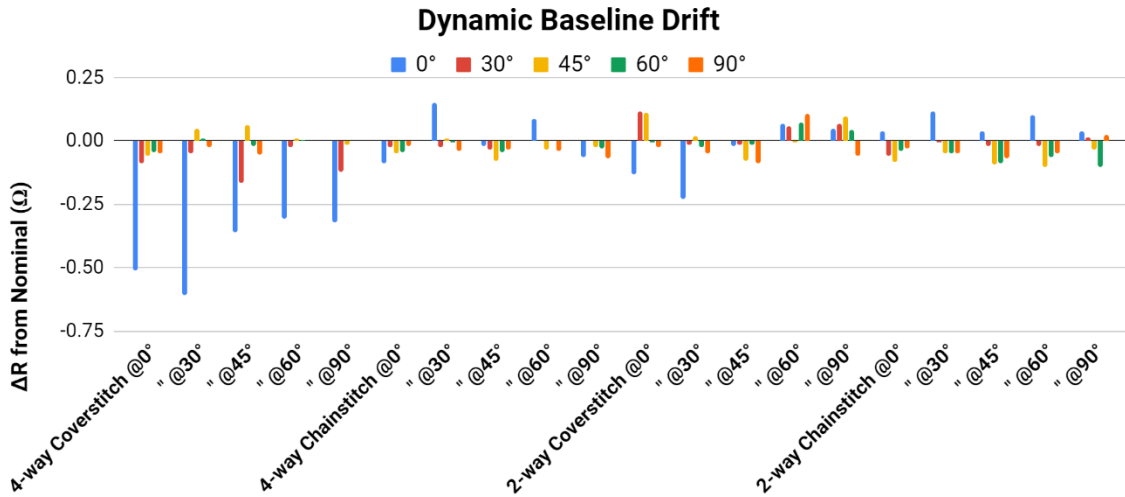
68

Figure 52. Dynamic Baseline Drift

The hysteresis error continues to be higher for the chainstitch sensor geometry sample groups for all offset forces and for all of sensor groups when the force applied in the 0° and 30° (with the 0° usually having the higher values) (Fig 53). The 2-way chainstitch group has the most, followed by the 4-way chainstitch, 4-way coverstitch and then the 2-way coverstitch. Additionally, the chainstitch groups have more variable hysteresis errors whereas the coverstitch groups are more consistent. Across the offset force angles, it cannot be said that a particular offset force (30°-90°) or knit choice increased or decreased hysteresis error, rather it is dictated by the sensor geometry choice and resulting sensor response (ΔR).

The way this error value is calculated captures this and other variables that make it difficult to split into errors that are acceptable (applied as a bias) vs noise. Therefore, using a different error calculation would be more reasonable for including into the decision matrix for sensor placement optimization.
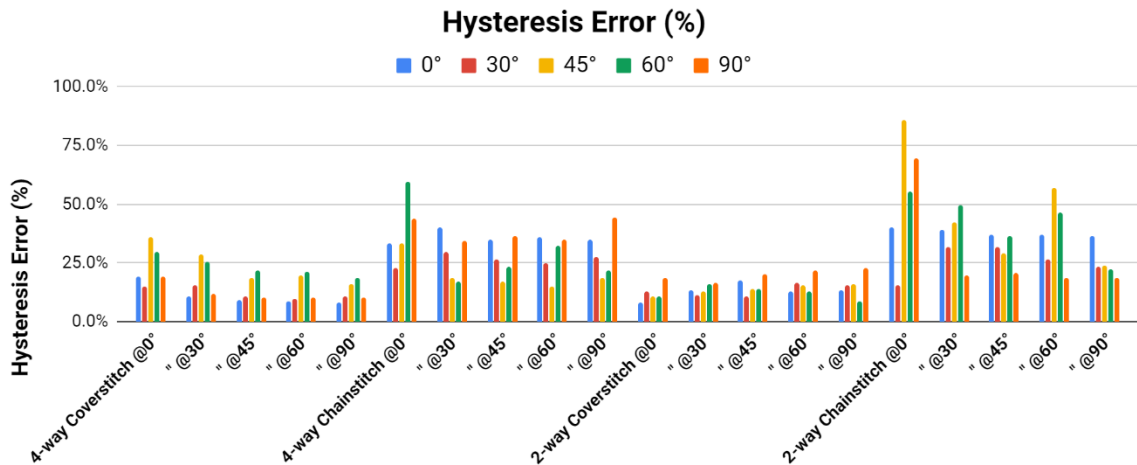
Figure 53. Hysteresis Error

3.4 Discussion

The results of each of the tensile tests presented in this chapter have lent insights in understanding the impact of sensor design and force direction angle on sensor performance. In this section, overarching themes in the data are discussed. Compiling results in Table 13 allows for a summary comparison of both the mechanical and electrical characteristics for these stitched strain sensors.

Table 13. Summary of Sample Analysis

Sample Group	Stitched Angle (°)	Elastic Modulus, E (Pa)	% of Fabric Only E	Avg Nominal Resistance (Ω)	Avg Peak-to-Peak Δ/ Nominal at 29% strain	Gauge Factor	Linearity Error (R²)	Fit Line Avg RMSE (Ω)	Hysteresis Error (Ω)	Transverse Sensitivity Factor, K_T	Baseline Drift (Ω)
4-way knit Coverstitch	0	0.00713	92%	10.5	29%	-1.15	0.956	0.0184	19%	8%	-0.51
	30	0.00613	124%	8.8	29%	-1.09	0.966	0.0146	11%	50%	-0.61
	45	0.00427	115%	12	26%	-1.05	0.973	0.0134	9%	52%	-0.36
	60	0.00399	126%	10.8	28%	-1.14	0.976	0.0132	9%	50%	-0.31
	90	0.00342	121%	12.1	28%	-1.16	0.983	0.0114	8%	53%	-0.32
4-way knit Chainstitch	0	0.00876	112%	9.7	41%	-1.76	0.945	0.0316	33%	5%	-0.09
	30	0.00676	136%	11.6	45%	-2	0.977	0.0237	40%	15%	0.15
	45	0.00601	162%	11.1	47%	-2.05	0.973	0.0264	35%	9%	-0.02
	60	0.00650	204%	11.9	34%	-2.06	0.969	0.0285	36%	9%	0.09
	90	0.00494	175%	10.9	45%	-1.96	0.96	0.0303	35%	11%	-0.07
2-way knit Coverstitch	0	0.04432	61%	7.9	28%	-1.13	0.949	0.0202	8%	68%	-0.13
	30	0.01374	88%	8.6	35%	-1.07	0.964	0.0157	13%	66%	-0.23
	45	0.00607	91%	8	23%	-0.93	0.887	0.0245	18%	83%	-0.02
	60	0.00502	113%	6.6	23%	-0.92	0.951	0.0146	13%	88%	0.07
	90	0.00528	119%	7.9	25%	-1.01	0.879	0.0278	13%	100%	0.05
2-way knit Chainstitch	0	0.05525	77%	7.8	47%	-2.2	0.933	0.0455	40%	1%	0.04
	30	0.01774	114%	7.6	51%	-2.37	0.954	0.0402	39%	3%	0.12
	45	0.00996	149%	7.6	50%	-2.31	0.948	0.0414	37%	6%	0.04
	60	0.00837	188%	7.7	48%	-2.21	0.934	0.0454	37%	3%	0.10
	90	0.00807	183%	7.3	47%	-2.14	0.941	0.0413	37%	13%	0.04

The 4-way knit substrate provided more consistent sensor responses, regardless of the sensor placement or stitch geometry. The 2-way knit horizontal direction is much stretchier than the vertical direction, inducing mechanical behavior that is more exponential. Although the sensor performance was more tempered in matching the mechanical behavior (i.e. it was more linear), at the extreme ends of the tested strain range it still had more error. This resulted in a smaller range of acceptable strain sensing. It was initially thought that the 2-way knit would help limit the sensor response in the stiffer directions and help with force directionality sensing, but for wearable sensing, the force ranges needed to stretch the 2-way knit in the 0°-45° range is larger than acceptable for the application. In summary, 4-way knits are recommended as suitable textile substrates for wearable strain sensing because they offer the most flexibility for sensor placement. Only a representative double knit was tested here, but it is believed that similar commercial 4-way stretch knits would show the same general mechanical behavior. There may easily be applications where 2-way knits are preferred or needed, so placing stitched sensors on only the stretchiest directions is recommended. Alternatively, additional testing to verify a repeatable exponential sensor response may be more applicable.

The knit structure has a symmetric structure that has its stretchiest directions in the horizontal (typically) and diagonal/bias direction. For both knit and sensor geometries tested, lower transverse sensitivity values were seen when the force direction was angled 60° from the lengthwise/wale direction. This is different from traditional strain sensors on isotropic substrates, where the lowest transverse sensitivity is perpendicular from the longest strain sensor dimension.

Relatedly, the chainstitch sensor was much less sensitive to offset forces that the chainstitch sensor. This can be generalized by the difference in the sensor geometry and the area used for attaching the sensor to the textile substrate. This sensitivity to offset forces is explained due to the coverstitch having more width and a larger area of attachment. It would be interesting to repeat this study with other manufactured sensors with different attachment means to confirm the geometry of sensor attachment influences offset force sensitivity. A design implication from this is to adapt the attachment based on the desired sensor behavior; if higher sensitivity is preferred, make the sensor attachment size larger (wider stitch), and if lower sensitivity is preferred, decrease the sensor attachment as much as possible (narrow stitch).

Although the chainstitch sensor had a higher GF than the coverstitch sensor, one disadvantage was the linearity errors at the extreme ends of the tested strain range. This limits the overall accuracy of the model fit. The lockstitch-like stitch geometry also limits the extensibility of the sensor, so it seems to agree with the standard trade-off of strain range and sensitivity.

The dynamic baseline drift seemed to be greatest with the 4-way coverstitch and comparable for the other three groups. This drift is undesirable, yet seems to be an inherent part of textile-based sensors. That this value is higher for a single group indicates that both sensor geometry and fabric recovery play a part in creating this drift. Future work could investigate permutations of this sensor design to find optimal stitch geometries to reduce this drift even further, perhaps by narrowing the coverstitch width or altering the spacing within the loops in the stitch. Other knit fabrics could be selected for the recovery properties (how fast they return to original position). Also, using the same stitch and changing the strain speed could reveal whether the knit choice has a larger effect on this drift value than sensor geometry.

These design implications are all useful for proposing a practical application for these stitched sensors - creating a strain rosette to distinguish the direction of an applied force.

4. Part 2 - Stitched Strain Sensor Rosette

As mentioned before, a challenge that many strain sensors face is to distinguish forces from specific directions (i.e. inline forces from angled in-plane forces and out of plane forces). A traditional approach to this problem is to add additional sensors, but the question remains as to which and where. Strain rosette patterns are a useful design technique that arranges two or more sensors to predict the direction of an in-plane force (Fig 54).
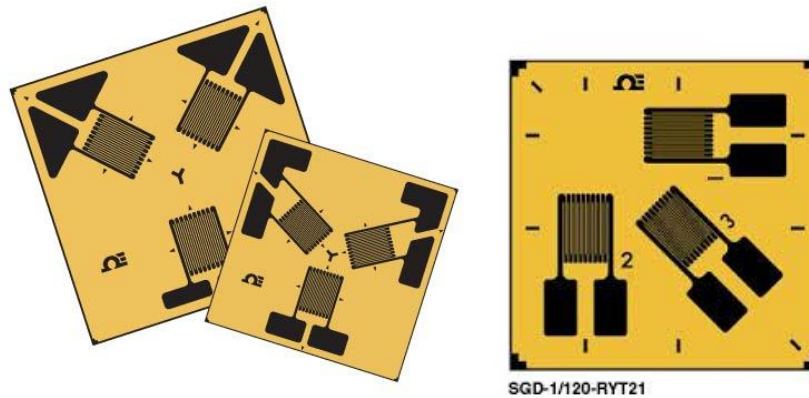
SGD-1/120-RYT21

Figure 54. Strain Rosette Pattern Examples [Image Credit: Omega]

Part 1 characterized the sensor design parameters that can influence stitched strain sensor performance and error. Selecting the most applicable stitched sensor geometries, knit substrates, and placements from those studied in Part 1 to create a strain rosette is the focus of Part 2. In creating a stitched strain rosette, being able to distinguish the direction of in-plane forces should be conceivable.

This is one application of the findings from Part 1. In this section, the primary aim was to validate that differential sensor responses are observed within the rosette structure as strain direction changes, as predicted by the findings of Part 1. Toward this aim, two potential strain rosette designs (one using a chainstitch structure and one using a coverstitch structure) were fabricated and tested using test methods similar to Part 1. Sensor responses were compared quantitatively to confirm differential responses according to strain direction. Finally, to demonstrate a predictive model proof-of-concept, Matlab machine learning modules were used to create example models that predict the force direction, amount of force, and displacement. Different machine learning algorithms were trained and then compared to find the best accuracy for each model (Fig 55). Although developing machine learning algorithms for the strain rosette were not the main focus of the thesis, this investigation is included to demonstrate how the rosette might be used in practice.

Figure 55. Schematic of using the measurements of the 2D Strain Rosette to predict Force Direction, Displacement, and Force

4.1 Strain Rosette Performance

After fabricating the rosette, similar Instron tensile testing is performed to characterize the rosette's mechanical and electrical response. The results of the force range and change in resistance for the 3-sensor rosette are shown and compared to their solo performance (i.e. single sensor per knit).

4.1.1 Specimen Design & Fabrication

Reviewing the discussion for Chapter 3 and the summary Table 13, the 4-way knit fabric was selected for its consistent sensor responses regardless of sensor placement. This is important since the rosette needs to have at least two sensors positioned at different angles. Both the coverstitch and chainstitch sensor geometries seem plausible for making good rosette designs. The coverstitch had higher R^2, lower RMSE and greater linear behavior for the entire strain range. The coverstitch had a higher GF and lower K_T but larger errors.

The resulting combinations used for rosette design were 4-way coverstitch and 4-way chainstitch. Three specimens for each sample group fabricated. Three sensors were stitched in the knit directions (with reference to the lengthwise/wales direction 0°) all crossing at the center of the 5in knit square; Sensor 1 at 30°, Sensor 2 at 90°, and Sensor 3 at 150° (Fig 56). To electrically isolate each sensor, a small piece of Melco™ Iron-on Seam Tape was adhered to the underlying sensor at the center point. Other elastic polymer seam tapes were pilot tested but did not succeed in electrically isolating the sensors. This tape is made of EVA (ethylene-vinyl acetate copolymer) film, is elastic, and

is typically used to create a waterproof seal on seams for outdoor gear and neoprene wetsuits.

Figure 56. (Left) 4-way Coverstitch Rosette (Right) 4-way Chainstitch Rosette

The average linear length and resistance for each of the three sensors per rosette was recorded and shown in Table 14.

Table 14. Average Length and Resistance for Rosette Sensors

Sample	Average Sensor Length (mm)			Average Resistance (Ω)		
4-way knit	Sensor 1: 30°	Sensor 2: 90°	Sensor 3: 150°	Sensor 1: 30°	Sensor 2: 90°	Sensor 3: 150°
Coverstitch Rosette	6.5	6.6	6.8	8.5	12.1	9.5
Chainstitch Rosette	6.8	6.8	7	6.3	6.3	5.9

4.1.2 Methods

The same test methods used in the prior section were used for this evaluation. To generate sensor data, the rosette designs were stretched in the Instron at a controlled rate of elongation (200mm/min) from 0-20mm, for a maximum strain of ~30%. The same Wheatstone bridge circuit with a voltage supply of 5V and reference resistors of 10Ω were used with the Instron transducer to capture voltage measurements concurrently with force and displacement measurements.

With this design and knit structure, the mechanical behavior should be symmetric from 0-180°, so 6 force direction angles were chosen from this range: 0°, 30°, 60°, 90°, 120°, and 150°. The intervals of 30° was selected to capture at least data from at least

one angle in between the 60° spacing of the sensors. Table 15 shows how the test matrix broke down for the 2 sample groups resulting in 12 total test conditions.

Table 15. Rosette Sample Test Matrix (3 Specimens per Sample Group)

Substrate	4-way knit											
Stitch Geometry	Coverstitch						Chainstitch					
Stitched Angle (°)	30, 90, 150						30, 90, 150					
Applied Force Angles (°)	0	30	60	90	120	150	0	30	45	60	90	150

The Instron tester had a limitation of only one available transducer for voltage measurements, so each test condition began first by loading the specimen into the clamps with leads attached to sensor 1. Three cycles of elongation were performed and data were saved for sensor 1. Then leaving the specimen clamped, the leads were attached to sensor 2 and the test was restarted (Fig 57). Finally, the leads are switched to sensor 3 and the test restarted. In this way, the voltage for each sensor was recorded for each test condition. Once each sensor was measured for the particular force angle, the specimen was then unclamped and rotated to the next force angle. The same procedure of elongating and relaxing the specimen 3 cycles (after throwing out the data from the precycle) was performed. After the testing for one specimen is complete, the second and third specimens were tested. The data from all three cycles' elongation curves and from each of the three specimens were used for data analysis, after performing the standard moving average filter (window of 5).
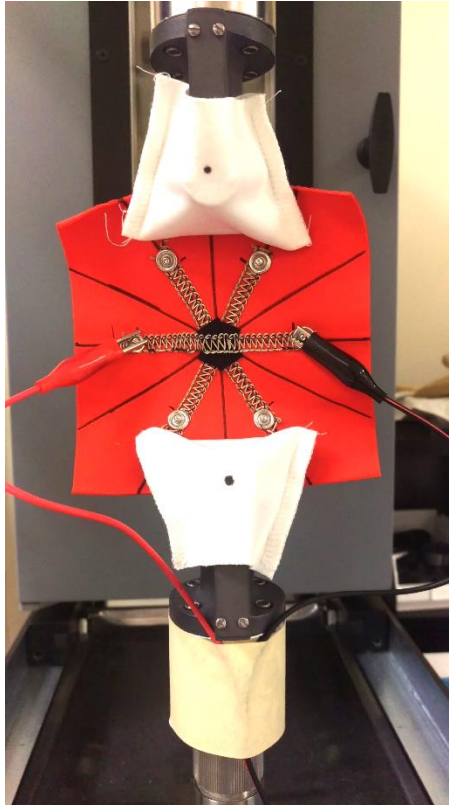
Figure 57. Instron Test Setup for Force @ 0°, recording Sensor 2 (90°) response for the Coverstitch Rosette

To assess the rosette performance for each stitch type and validate its behavior as predicted by the previous characterization experiments, range for force and resistance was calculated for each sensor in each strain direction. It was possible that the force range would be slightly different for the rosette structure, due to the presence of three sensors instead of just one sewn into the fabric. The expected behavior for the rosette was that the sensor data would show a larger sensor response (Average Peak-to-Peak Change in Resistance) when the force angle was in line with the sensor.

4.1.3 Results & Discussion

To characterize rosette performance, force and resistance ranges were calculated for each sensor in each force direction condition (Table 16). The limitation of only testing one sensor at a time was thought to cause some variability in the applied force each time; however, the average of force ranges recording during each test session showed little standard deviation (0.5-2.7%) and provides evidence that this experimental setup limitation has little effect on the results. The Force Range seen in both sensor geometries is fairly similar for each direction, with the highest seen in 0° and 30°/150° directions,

matching the trend behavior of the fabric's own mechanical behavior. However, the force range seen for the rosette does differ when compared to that experienced in a specimen with only one sensor and matches more the fabric-only behavior (Table 17). If this holds up to additional testing to confirm, this is an advantage of the rosette over single sensors in lessening the need for characterizing the sensor+fabric system and relying more on the fabric properties to estimate force.

Table 16. Sensor Response for both Rosette Designs

Force Direction	Calculations	4way Chainstitch Rosette			4way Coverstitch Rosette		
		Sensor 1: 30°	Sensor 2: 90°	Sensor 3: 150°	Sensor 1: 30°	Sensor 2: 90°	Sensor 3: 150°
0°	*Avg Δ Force (N)*	7.49 +/- 0.17			7.87 +/- 0.08		
	Δ Resistance (Ω)	2.25	0.15	0.28	1.94	2.33	1.76
30°	*Avg Δ Force (N)*	6.74 +/- 0.12			5.90 +/- 0.09		
	Δ Resistance (Ω)	**3.28**	0.68	0.45	1.96	1.47	1.95
60°	*Avg Δ Force (N)*	3.84 +/- 0.04			4.03 +/- 0.04		
	Δ Resistance (Ω)	2.37	2.38	0.77	2.18	2.50	2.43
90°	*Avg Δ Force (N)*	3.84 +/- 0.06			3.63 +/- 0.06		
	Δ Resistance (Ω)	0.51	**3.26**	0.50	1.12	2.80	2.54
120°	*Avg Δ Force (N)*	3.61 +/- 0.02			3.84 +/- 0.05		
	Δ Resistance (Ω)	0.65	2.20	1.73	1.13	2.19	2.68
150°	*Avg Δ Force (N)*	5.59 +/- 0.14			5.90 +/- 0.16		
	Δ Resistance (Ω)	0.61	0.49	**2.73**	3.43	1.70	3.00

Table 17. Comparing Force Ranges for Fabric Only, Fabric with 1 Sensor, Fabric with 3 Sensors (Rosette)

Force Range (N) = Fmax - Fmin					
Sample	Degree from 0° (Stiffest Direction)				
	0°	30°	45°	60°	90°
4-way knit Fabric-Only	7.6	5.0	3.9	3.3	3.0
4-way knit Single Coverstitch Sensor	6.8	6.1	4.2	4.1	3.5
4-way knit Single Chainstitch Sensor	9.0	7.4	6.9	7.9	6.0
4-way knit Coverstitch Rosette	7.9	5.9/3.8	n/a	4.0/5.9	3.6
4-way knit Chainstitch Rosette	7.5	6.7/3.6	n/a	3.8/5.6	3.8

Importantly, the magnitude of each sensor's response (Δ Resistance) increases as the force direction aligns with the sensor and decreases as the force direction becomes perpendicular to the sensor for the chainstitch geometry (Fig 58). This is evident in the peaks are seen at each force angle that matches the sensor's stitched angle (30°, 90°, 150°). **These results are key to successfully proving the rosette design for predicting force direction is possible with these stitched sensors using the chainstitch geometry on a 4-way knit substrate.**
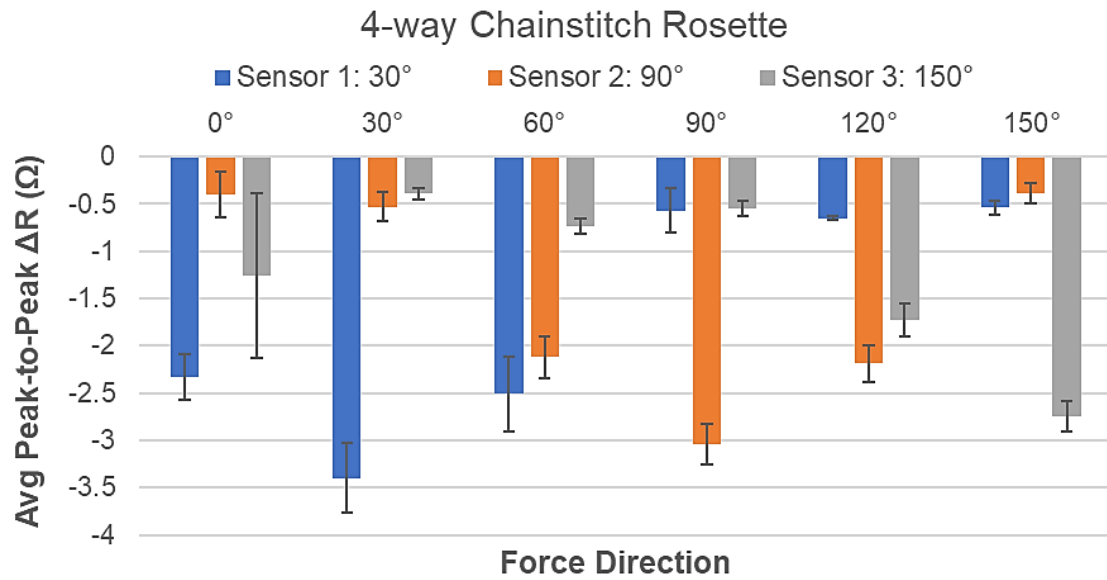
Figure 58. 4-way Chainstitch Rosette Sensor Response

Unfortunately the same successful trends is not seen with the sensor response of the coverstitch rosette (Fig 59). Although the coverstitch had better linearity and lower RMSE and hysteresis errors as a single sensor, these indicators for accuracy did not prove to be sufficient for clearly delineating the force direction with multiple sensors. Sensors 2 and 3 do have peak values at their respective stitch angles (90° and 150°), but their response overlaps with the error bars of other angles. Sensor 1 has even worse accuracy with having its larger response at 150° rather than at 30° (testing was repeated to confirm this unusual behavior). The width of the sensor, previously used to explain the sensor's higher transverse sensitivity, seems to magnify its response. Considering all three sensors, the lower transverse sensitivity of the coverstitch geometry seems to have caused overlapping sensor responses, making it difficult to parse force direction accurately as a rosette.
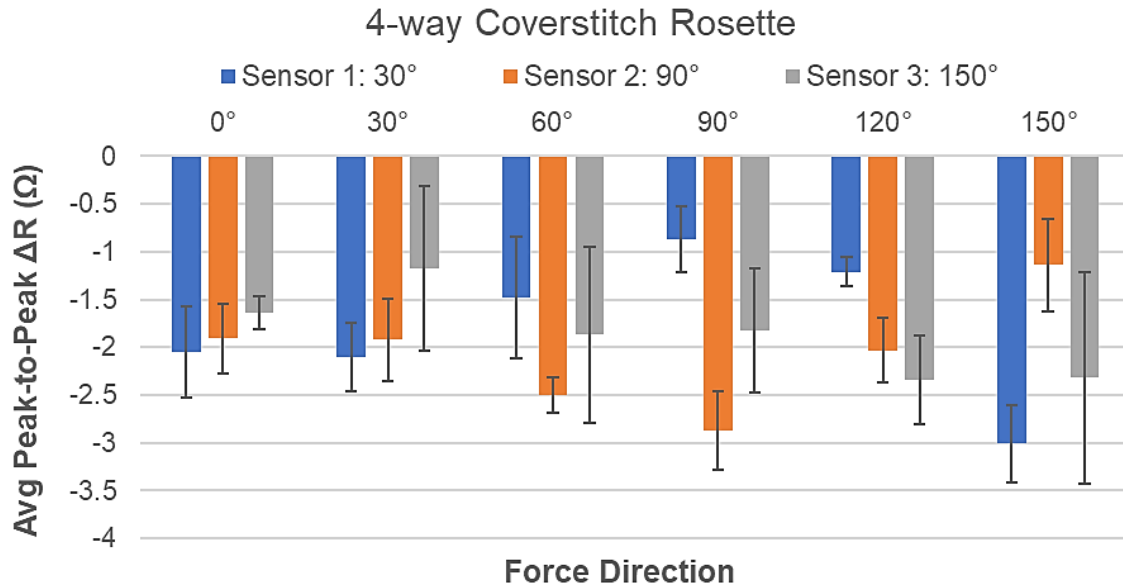
Figure 59. 4-way Chainstitch Rosette Sensor Response

4.2 Modelling the Strain Rosette Performance

For real-world usage, it's reasonable to connect the previously-described characterization work with how a strain rosette would be used in a wearable application. In an ambulatory smart garment application, only the sensor resistance variables would be captured. From this information, in a rosette arrangement an array of sensors could be used to determine the force direction, force magnitude, and displacement. Characterization of the rosette requires the creation of a function or model to map the sensor data to desired real-world variables. For this section, only the chainstitch rosette results were used because they were successful in delineating the force direction and distinct results for the force range.

Linear regression worked well for a single sensor, but due to multiple sensors and force directions present in the data, the overall response become nonlinear (Fig 60). This ruled out multivariable linear regression (although it was attempted to see if the model could predict any of the three variables with accuracy).
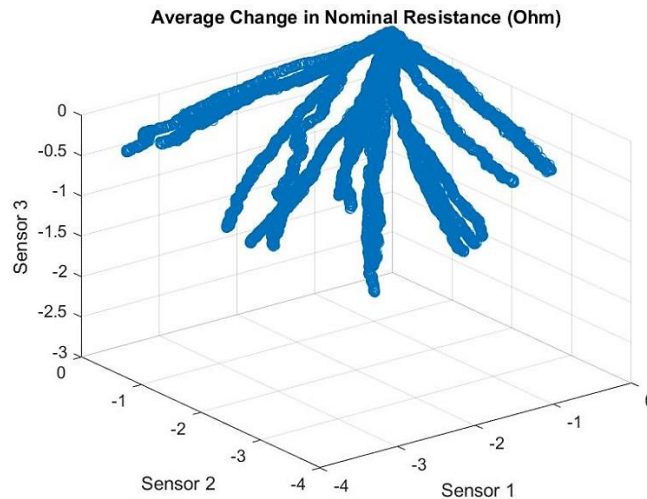
Figure 60. Change in Resistance in 3D for Sensor 1, Sensor 2, and Sensor 3 (0-30% strain) for all Force Directions

Instead, two machine learning approaches were assessed to determine which would be best suited to these data: decision trees and neural networks. Tools within the model fitting modules in Matlab were used: the Statistics and Machine Learning Toolbox and the Deep Learning Toolbox (MATLAB, Release 2018a).

Model fitting begins with visualizing the data, "cleaning" it, and classifying the relationship (or categorizing the problem). Matlab was used for this purpose to verify expected relationships, such as individual sensor's linear response to force or displacement for a given force direction.

Because the variables of resistance, force, and displacement can be labeled, this indicates a supervised learning problem. Decision tree models, which work well for either regression or classification problems were investigated, as well as neural network models. The relationship between variables determines whether regression or classification is appropriate. Regression models work well for predicting a numerical value, whereas Classification models work well for variables that are groups or classes.

The sensor resistance changes proportionally with the force and displacement so regression tree learning models should work well for predicting force and displacement. Classification decision trees are better suited for predicting the force direction from the 3 sensors' resistance, because the direction doesn't have a proportional relationship with sensor resistance like the other two physical measurements.

82

Neural networks are also plausible models to investigate for this problem. Although they are sometimes less preferred because they are harder to interpret and verify why they are accurate, they are successful in many applications previously un-modelable. These models were trained to see if they resulted in higher accuracy over the decision trees. Additionally, since the rate of change for the sensor response could be a good indicator of force direction (instead of treating it as only a classification problem), the neural networks offered a time-dependent option to explore.

4.2.1 Methods

After Instron testing, the data needed to be organized into predictor-output tables to feed into Matlab tools. To represent sensor resistance, either the change in resistance or the normalized resistance could have been used. For this analysis, I chose the change in resistance (0 to -5Ω). As before, data from only the elongation part of the cycle was used. The resistance data was then smoothed with a moving average (window of 5). Due to the three separate tests required to capture all three sensor data, the force and displacement was time-aligned before averaging.

Three tables were created, all with the first three columns as the three sensor resistances and the fourth column as the response variable (displacement, force, or force direction) (Fig 61). Because the force direction is known for each test, this column was manually filled in with the classifier.

	3-variable vector "sensors"		1-variable target
Sensor30	**Sensor90**	**Sensor150**	**Displacement**
-0.0056103	-0.1346361	-0.1722752	-0.0357
0	-0.1360038	-0.1553841	-0.0355667
-0.0077394	-0.1582375	-0.1613239	-0.0352
-0.0119293	-0.1332787	-0.1857849	-0.0144333
-0.0014758	-0.1581023	-0.1865989	-0.0144
-0.009308	-0.1579741	-0.1863289	-0.0138333
-0.0103561	-0.1332802	-0.2024034	-0.0078333

Figure 61. Organizing Data for Matlab model fitting tools

In total, Table 18 shows the layout of variables for model fitting as well as the models attempted for each variable. Specifically, the "Regression Learner", "Classification Learner", "Neural Net Fitting", "Neural Net Pattern Recognition", and "Neural Net Time Series" Matlab tools were used. Within the "Regression Learner" and "Classification Learner" were the decision tree, Gaussian SVM, and weighted nearest neighbor KNN models. Using the Matlab app wizard menus, all default values were initially chosen for the particular menu. For the regression learning, a cross-validation on folds (5 folds) was used to prevent model over-fitting. For the neural networks, the default split of data was used: 70% training, 15% testing, 15% validation.

Table 18. Variables for Model Fitting & Attempted Models

Predicting Elongation		Predicting Force		Predicting Force Direction	
Input Dimensions/ Predictors	Output/ Response	Input Dimensions/ Predictors	Output/ Response	Input Dimensions/ Predictors	Output/ Response
Sensor 1 Resistance	Displacement	Sensor 1 Resistance	Force	Sensor 1 Resistance	Force Direction
Sensor 2 Resistance		Sensor 2 Resistance		Sensor 2 Resistance	
Sensor 3 Resistance		Sensor 3 Resistance		Sensor 3 Resistance	
Models Attempted: ● Decision Trees ● Ensemble Bagged Trees ● Fine Gaussian SVM ● Neural Net Fitting		Models Attempted: ● Decision Trees ● Ensemble Bagged Trees ● Neural Net Fitting		Models Attempted: ● Decision Trees ● Ensemble Bagged Trees ● Weighted Nearest Neighbors KNN ● Neural Pattern Recognition ● Neural Time Series	

4.2.2 Results & Discussion

The amount of data from the chainstitch data was large enough for model-fitting (in total~16,300 data points). Each variable was plotted against another to verify relationships and find any new correlations between the measured variables. A selection are shown in Figure 62, and the remainder can be seen in the Appendix E. The expected linear relationship for force(displacement) was seen, as well as the stepwise lines of varying amplitude (representing the force range) for the force direction(sensor resistance) plot. The presence of distinct lines in the scatterplot of Resistance(S1, S2, S3) boded well for a decision tree model being able to predict with high accuracy. (If the data was more of a scatterplot cloud, this would have been much more difficult for a decision tree to predict with any high accuracy). No new correlations were found.
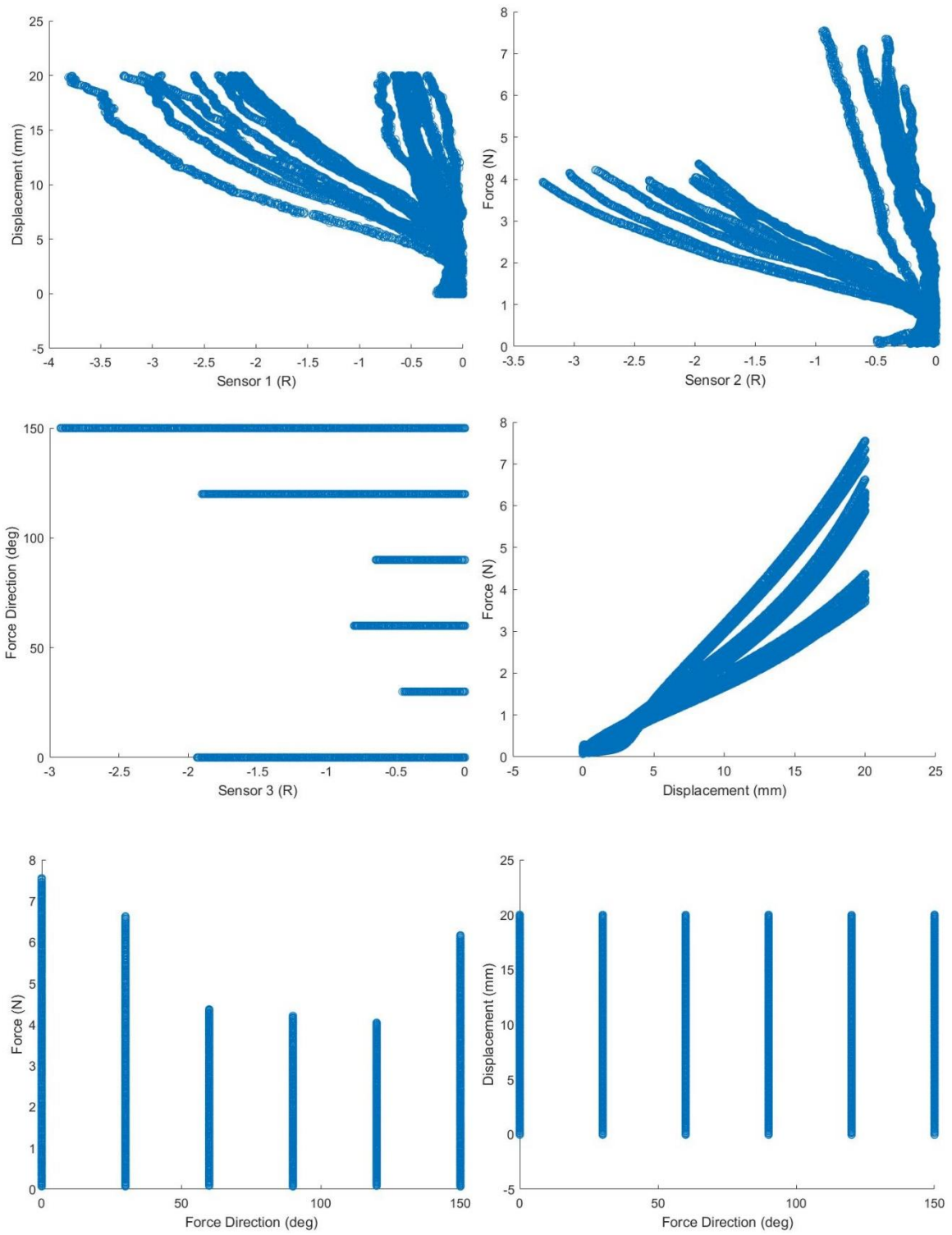
Figure 62. Graphing variables to visualize relationships

Once the data tables were prepared, the various learning models were trained and the performance metrics for each were compared against each other. The results for the Displacement and Force models are summarized in Table 19, and in Table 20 for Force Direction. For the regression learning problems of predicting force and displacement, the R^2 value (close to 1) and the RMSE error (close to 0) were compared, and for the classifier problem of predicting force direction, the accuracy value is given in percentages (%). In this evaluation, only these performance metrics were compared, not the model speed (critical for real-time applications) nor memory requirements or computational overhead (critical for embedded systems). This would be important for business applications, but beyond the scope for the current work. Only default parameters for each of the models, unless marked with an asterisk. (Default values were only tweaked for the model with the highest performance in that group in order to further reduce error.)

Table 19. Comparing Different Model Performances for Displacement & Force Predictors

Predictor:	Displacement (mm)				Force (N)	
Model:	Regression Tree (Fine)	Ensemble Regression Bagged Tree	Gaussian SVM (Fine)	Neural Net Fitting (Levenberg-Marquardt)	Ensemble Regression Bagged Tree	Neural Net Fitting (Levenberg-Marquardt)
Parameters:	Cross-validation folds: 5, Leaf Size: 4	Cross-validation folds: 5, Leaf Size: 1, # of Learners: 40	Cross-validation folds: 5, Kernel scale: 0.43	70% training, 15% Validation, 15% Testing, 10 neural nodes	Cross-validation folds: 5, Leaf Size: 1, # of Learners: 65	70% training, 15% Validation, 15% Testing, 10 neural nodes
Performance Values:	R^2=0.98, RMSE: 0.73992	R^2 = 0.99, RMSE: 0.61976	R^2 = 0.97, RMSE: 0.94094	Testing R^2 = 0.985, RMSE: 1.002	R^2 = 0.99, RMSE: 0.13428	Testing R^2 = 0.99, RMSE: 0.00531

Table 20. Comparing Different Model Performances for Force Direction Predictor

Predictor:	Force Direction (°)			
Model:	Weighted Nearest Neighbors KNN	Ensemble Bagged Trees	Neural Pattern Recognition	Neural Time Series
Parameters:	Cross-validation folds: 5, # of neighbors: 10	Cross-validation folds: 5, # of Learners: 30	70% training, 15% Validation, 15% Testing, 10 neural nodes	70% training, 15% Validation, 15% Testing, 10 neural nodes, delay: 10
Performance Values:	Accuracy = 91.5%	Accuracy = 91.7%	% Error - 19%, CE - 8.23	R - 0.999927, MSE - 0.378

Each model shows respectable accuracy, validating these parameters (force, displacement, and force direction) can be modelled from the collected rosette sensor data.

The best performing model for predicting displacement was the ensemble regression tree (Bagged Tree) with a R^2=0.99 and RMSE=0.62, although the regular regression tree (Fine) was a close second. For this model, the default values for minimum leaf size and number of learners were decreased and increased, respectively, to increase the flexibility of the model and generate a lower error. Also, due to their nature of preventing overfitting, the bagged tree ensemble model is preferred over single decision trees. The best model for predicting force is a closer race; both the ensemble regression tree and neural net fitting models had a R2=0.99 but the neural net has a smaller RMSE=0.00531. Either would be sufficient, but only the performance graphs are shown here for the neural net. The force direction was a classifying problem, so the best performing model was also the ensemble regression tree (Bagged Tree) with an accuracy of 91.7% and a close second was the weighted nearest neighbors KNN model. Again, the default values were changed to increase the flexibility and lower error. Each of these best performing models are discussed further.

Regarding displacement, the lack of a strong sensor response from elongations between 0-6mm presents the majority of large errors in the model fit (Fig 63). There are a few outliers present at 10mm, 12mm and 18-20mm in both the positive and negative directions. Overall the model predictions for look accurate only after elongations of 6mm. Near zero, the errors are biased in the negative direction and then in the positive direction, predicting a lower displacement that is what is actually occurring. This matches the experimental data, where the elongation is stretching the fabric and knit loop structures before starting to strain the knit enough to generate a sensor response.
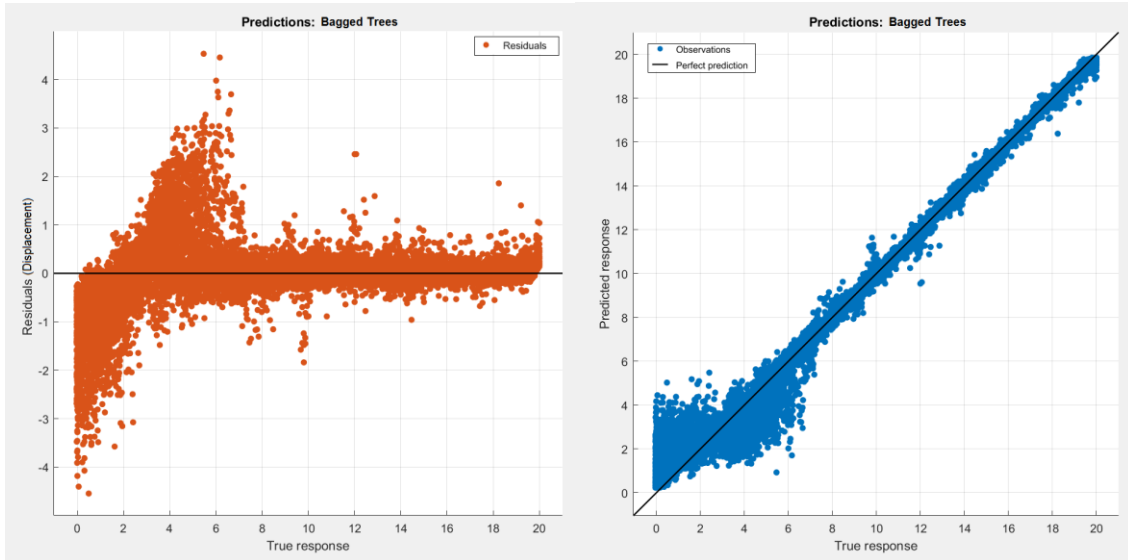
Figure 63. Ensemble Bagged Tree Model performance for predicting Displacement

Just to see if one sensor is contributing more error than the others, each sensor's contribution to the errors was observed (Fig 64). This also could be a consequence of the fabrication, since the center points of first two sensors that were fabricated (Sensor 1-30°, Sensor 3-150°) were fixed with the Melco tape for electrical isolation reasons. However, it doesn't look like there is any visible increase or decrease of residuals for these two sensors compared to Sensor 2. It does look like Sensor 1 has slightly less variability in residuals after -0.5Ω compared to the others, but not in a major way.
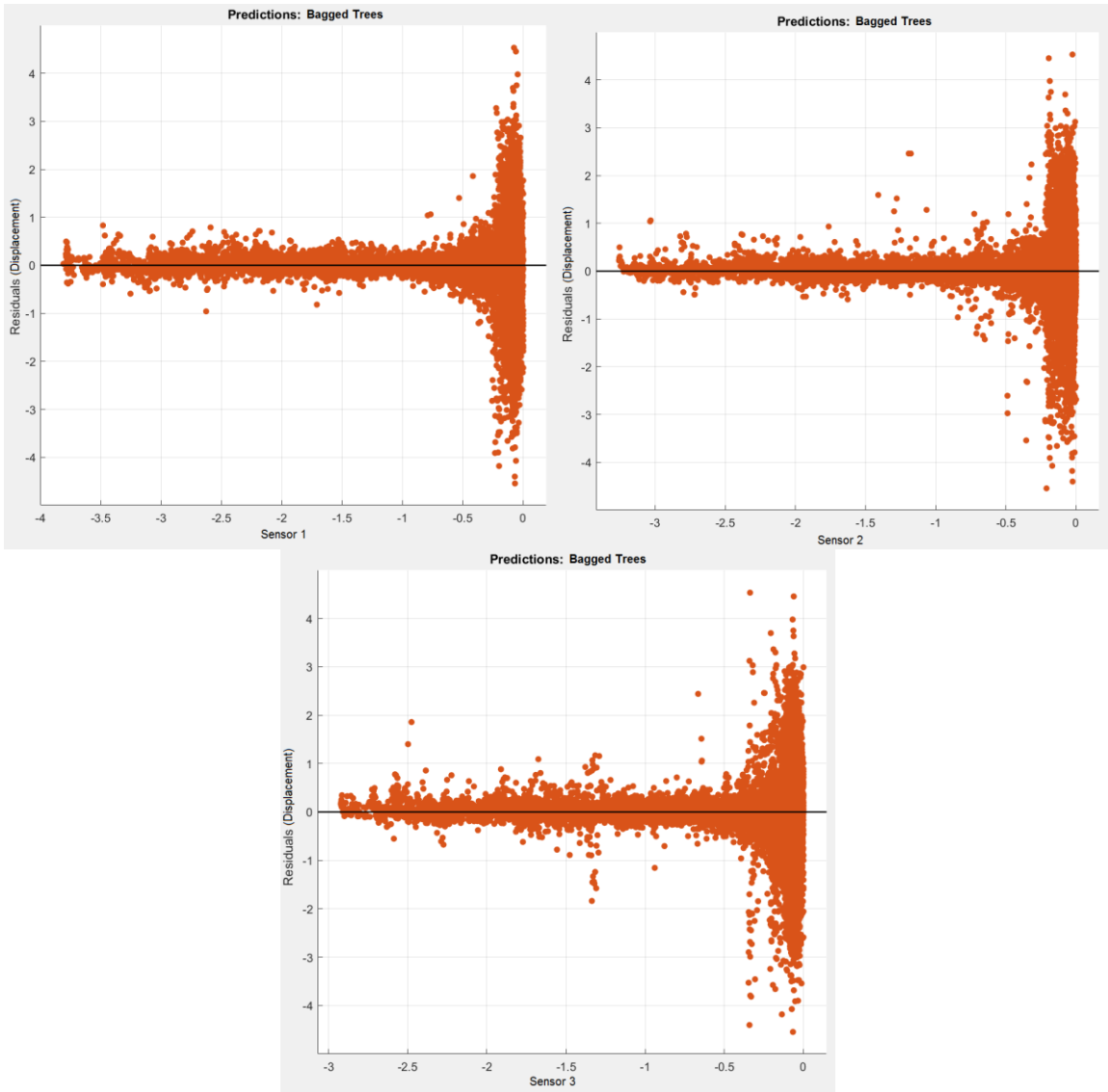
Figure 64. Each sensor's contribution to error in the Ensemble Bagged Tree Model performance for predicting Displacement

Regarding Force, the Error Histogram shows the errors are evenly distributed around the average of zero error, not biased in either direction (Fig 65).
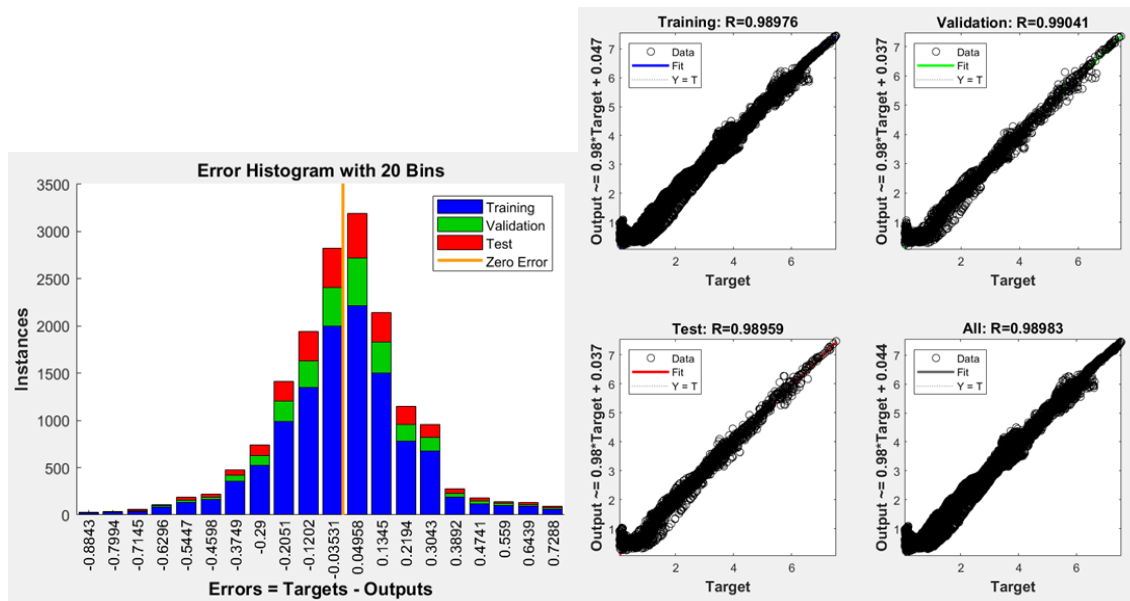
Figure 65. Neural Net Fitting Model performance for predicting Force

Regarding force direction, the variables are usually plotted against each other with a color coding to visualize if there are certain predictors that separate classes well. As Figure 66 shows, the Sensors 1 and 2 show good distinctions between the 0°, 30°, and 60° but is not good at distinguishing 90°, 120° (where they overlap), and 150° (where there is little response). Conversely, Sensors 1 and 3 can distinguish most of the classes except for 90°. This is interesting, because it prompts the question whether three sensors and if only two sensors (placed 45° apart) would be sufficient for 360° force direction detection with high enough accuracy. Overall good distinction between at least two sensors for all classes can be seen, except when the range of resistances is between 0 to approximately -0.7Ω. In this range, all of the sensors are mildly activated and it is not clear which force direction to classify. The parallel coordinates plot shows the mean of each predictor at zero and scales by standard deviation. A larger separation shows stronger ability to distinguish classes which closer separations or overlapping indicates a lesser degree.
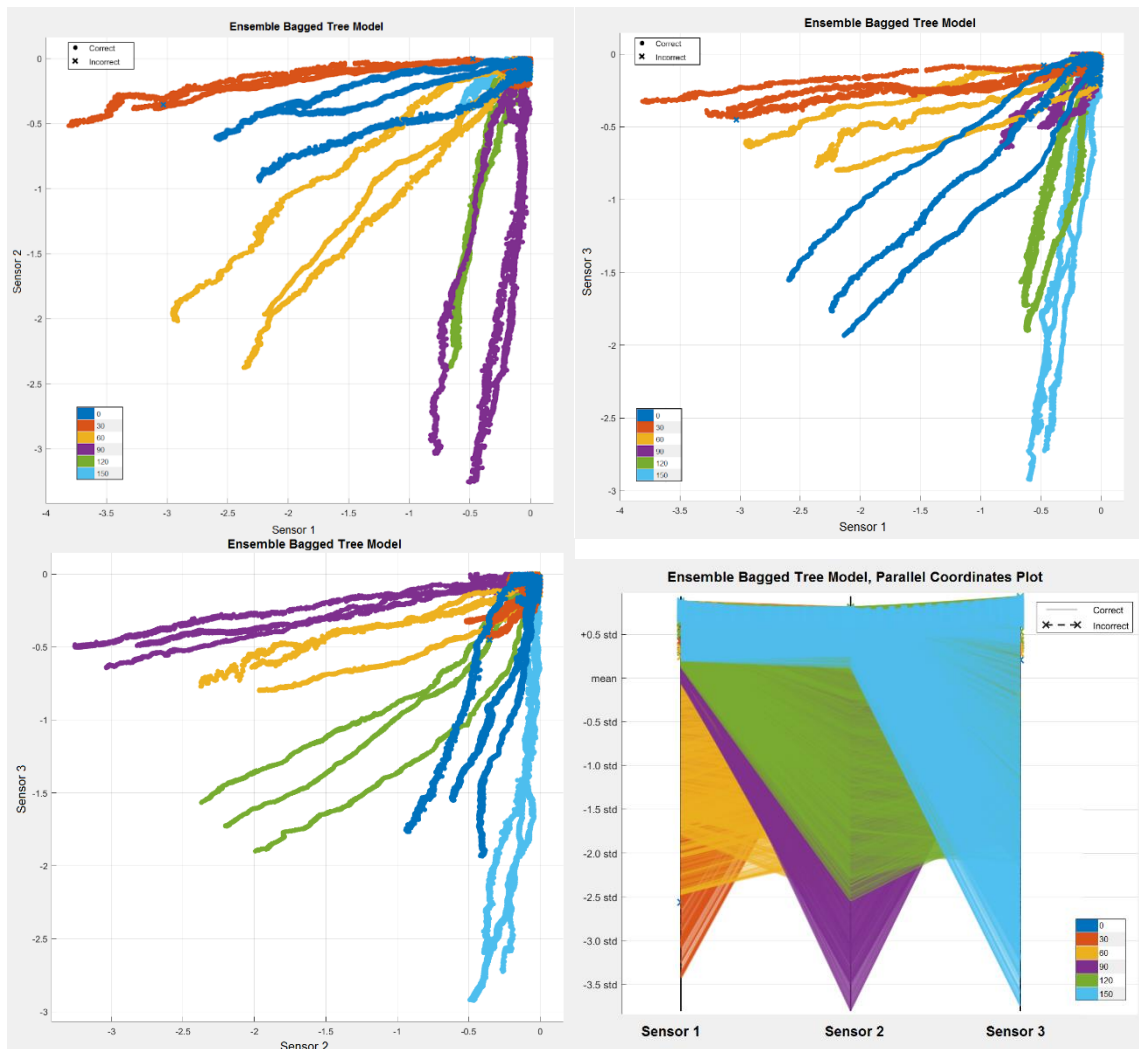
Figure 66. Ensemble Bagged Tree Model performance for predicting Force Direction

The confusion matrix shows how accurate each class was classified by the model (Fig 67). All classes had similar performance, with 91-95% positively predicted values which is high accuracy. Because the sensors don't respond until an elongation 6mm or beyond occurs, the predictability in this regime is understandably inaccurate. If the input data was restricted to only beyond a minimum threshold (corresponding to the 0-6mm elongation threshold), the accuracy of the model would likely increase further.
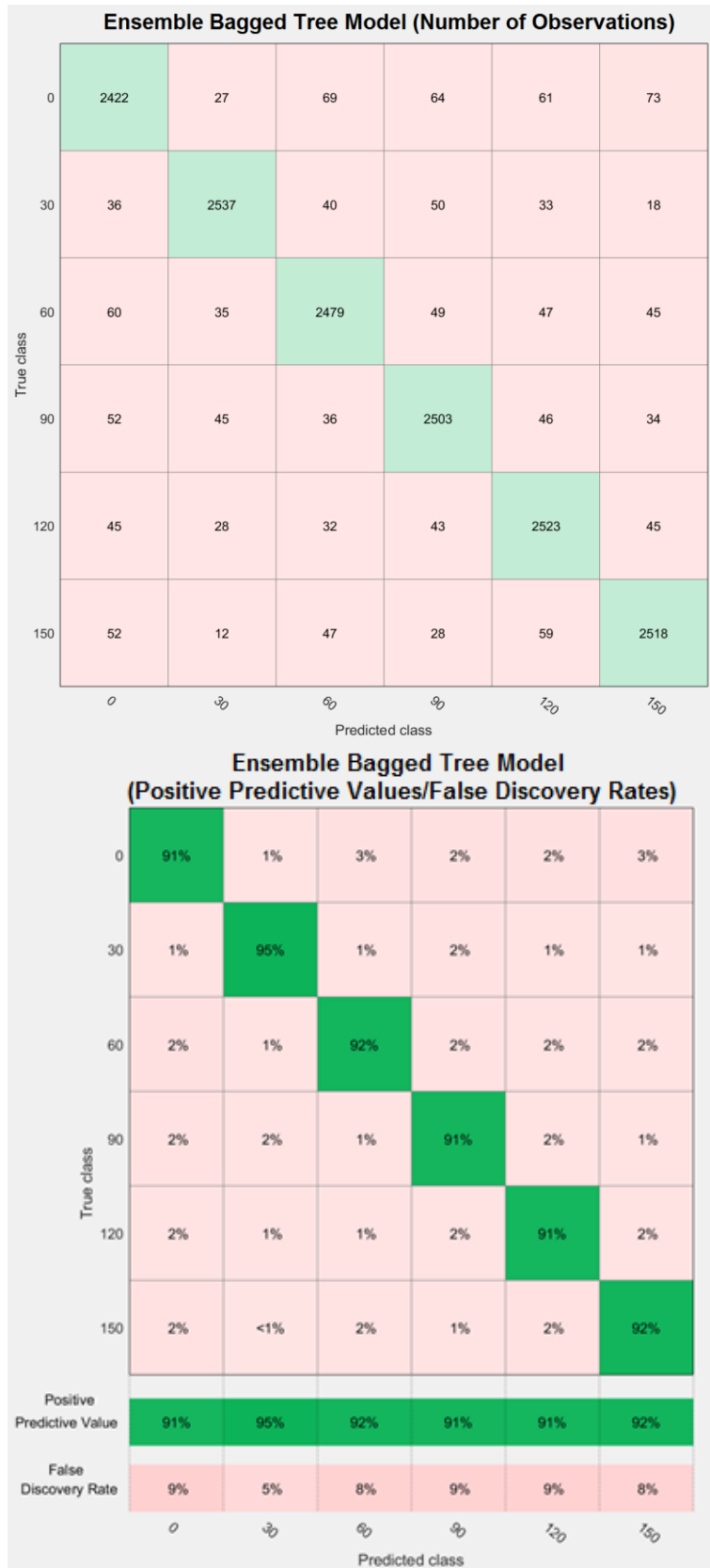
Figure 67. Neural Net Fitting Model performance for predicting Force Direction

Each model was saved as a Matlab script in preparation for running new data and future testing with a prototype garment. One garment example is to have a couple of rosette sensors sewn into a pair of leggings, where it should be able to distinguish the elongation and force direction (Fig 68). This type of information would be useful for diagnosing the degree of Valgus knee/hip rotation or for monitoring degree of muscle mobility in an ACL or hip replacement rehabilitation scenario. Paired with a smartphone application, it could be used to encourage strengthening exercises or encourage the correct form of stretching/squatting (by setting bounds of force direction through a calibration sequence).

Figure 68. Proposed Valgus-detection or Range-of-Motion Tracker application for Rosette Sensors in Leggings [Image Credit: Shein]

4.3 Discussion

Two stitched sensor rosettes were designed based on the results of Part 1, and the chainstitch geometry proved to be successful in distinguishing the force direction. Additionally, the mechanical behavior for the multi-sensor assembly proved to closer match that of the fabric itself when compared with the mechanical behavior of a single-sensor assembly. This is a helpful improvement in reducing the impact of sensor fabrication and should be tested in the future to verify this observation for other rosette designs. The rosette sensor data was further proved to be sufficient in creating accurate

models that predict the force, displacement, and force direction from the resistance readings alone. This finding increases the robustness of this sensor for future garment applications requiring strain sensing capabilities.

5. Conclusion

This investigation characterized the impacts of fabric substrate stretch properties and stitch geometry on a conductive stitched strain sensor. This gap in current wearable sensors is one barrier to fully realizing commercial sensors that do not require extensive characterization and calibration procedures. Algorithms that help smooth noisy data and normalize measurements to nominal data are still highly useful, but key design choices in fabricating a stitched strain sensor can reduce error and improve the analysis of predicted force, elongation, and force direction.

The conductive stitched strain sensor was previously determined to have a linear response but the testing herein showcased how the linear response could become non-linear and even exponential depending on the fabric knit substrate selection. The stiffer directions of the 2-way knit were too exponential in nature that a linear fit is no longer recommended; this is not to say that this combination is unusable. If the application required sensing forces of a higher range >50N, then a stiffer knit fabric is recommended. Potential future testing could confirm whether 2-way knits consistently produce exponential sensor responses and exponential models could be used for these applications. The 4-way knit was easier to compare sensors stitched at various angles without adding some bias because of the angle it was stitched into the knit structure. (To note, the elastic content (Lycra™, Spandex™, etc.) of the 4-way knit afforded repeatable and would be considered to be a prerequisite to selecting appropriate fabric substrates to use with these sensors). Ultimately, for most applications like wearable garments, an elastic 4-way knit fabric with relatively similar mechanical behavior in the 0° and 90° directions would be highly recommended for these sensors.

Using 7cm sensors, strain up to 30% was applied by a tensile tester. Analysis of the sensor response showed that a change in resistance began ~5mm (7%) until the final strain and ended again at ~5mm. Without initially stretched in pretension, these sensors are rated at detected strains 5+%. Additional testing could confirm the upper limit, but the

sensor proved repeatable to 30% strain. The normalized peak-to-peak ΔR was higher for the chainstitch geometry (~46%) than the coverstitch (~27%), resulting in a higher GF.

Two stitch geometries were used: the bottom coverstitch that had previously published success at strain sensing, and the chainstitch that had never been characterized before. Both were successful at strain sensing, with some tendencies that were different between them. The coverstitch geometry proved to be much more sensitive to offset forces than the chainstitch geometry. The high transverse sensitivity factor, K_T, for the coverstitch geometry indicates that even a single sensor would be sufficient at sensing in-plane forces applied in any direction but would be terrible at distinguishing the direction of force applied. This is opposite for the chainstitch sensor, where one or a combination of sensors set in a 60° rosette pattern can successfully delineate force direction. Interestingly, combining three sensors allowed the experienced force range to closer match that of the fabric itself when compared to a single sensor on the fabric. This is more useful when trying to use the fabric mechanical properties to infer the magnitude of force that is elongating the sensor.

The advantages of the coverstitch geometry are a greater sensitivity to offset forces, higher linearity R^2, lower RMSE, and smaller hysteresis error. The advantages of the chainstitch geometry include a greater GF, lower sensitivity to offset forces, and lower baseline drift. For detecting the presence of 2-D plane forces/strains, a single coverstitch sensor stitched along the 4-way knits least stiff direction (90°) would be recommended. For distinguishing individual force directions, a 60° rosette pattern of 3 chainstitch sensors along the 30°, 90°, and 150° on a 4-way knit would be recommended.

The knit textile nature adds complexity to optimize wearable sensing performance, and understanding the effects can lead to wearable sensing insights. The burden of additional characterization is outweighed by the promise of enhancing sensor performance and reducing error, which are two hurdles in realizing commercial success in wearable technology that requires soft strain sensing. The strain rosette is one design option used in traditional strain sensing that shows promise translating to wearable soft sensors. Depending on the application and sensing mechanism, I believe this investigation aids future wearable sensor designers with understanding the interface of textile and sensor mechanics and can be repeated with little alteration for other promising sensors.

References

ASTM International. (2016). *ASTM D 4964: Standard Test Method for Tension and Elongation of Elastic Fabrics (Constant-Rate-of-Extension Type Tensile Testing Machine).* West Conshohocken, PA; ASTM International.

Amjadi, M., Kyung, K., Park, I., & Sitti, M. (2016*).* Stretchable, Skin-Mountable, and Wearable Strain Sensors and Their Potential Applications: A Review. *Advanced Functional Materials, 26*(11), pp.1678-1698.

Atalay, Ozgur, Atalay, Asli, Gafford, Joshua, Wang, Hongqiang, Wood, Robert, & Walsh, Conor. (2017). A Highly Stretchable Capacitive-Based Strain Sensor Based on Metal Deposition and Laser Rastering. *Advanced Materials Technologies, 2*(9), N/a.

Benchirouf, A., Müller, C., & Kanoun, O. (2016). Electromechanical Behavior of Chemically Reduced Graphene Oxide and Multi-walled Carbon Nanotube Hybrid Material. *Nanoscale Research Letters, 11*(1), pp.1-7.

Berglund, M. (2016). *Development of Form-Fitted Body-Worn Force Sensors for Space and Terrestrial Applications*. Master's Thesis. University of Minnesota.

Berglund, M., Foo, E., Dunne, L., & Holschuh, B. (2017).Development of Elastomer-Strain Gauge Composite for On-Body Dynamic Force Measurement. *Proceedings of the 47th Intl. Conf on Environmental Systems,* 2017-239.

Bosowski, P., Hoerr, M., Mecnika, V., Gries, T., & Jockenhövel, S. (2015). Chapter 4. Design and manufacture of textile-based sensors. In *Electronic Textiles: Smart Fabrics and Wearable Technology* (pp. 75-107). Elsevier.

Castano, L., & Flatau, A. (2014). Smart fabric sensors and e-textile technologies: A review. *Smart Materials and Structures, 23*(5), 27.

Crow, R. & Dewar, M. 1984. *Measurement of Stress in Clothing: A Literature Review and Methods Selected.* Defense Research Establishment Ottawa, Canada. Technical Note 84-10.

ISO, (1991). ISO 4915:1991 *Textiles – Stitch Types – Classification and terminology*. Geneva, Switzerland: ISO.

Dunne, L., & Gioberto, G. (2016). *US Patent No. US9322121B2*. Retrieved from https://patents.google.com/patent/US9322121B2/en

Dunne, L. (2010). Optical Bend Sensing for Wearable Goniometry: Exploring the Comfort/Accuracy Tradeoff. *Research Journal of Textile and Apparel, 14*(4), 73-80.

Farajikhah, Madanipour, Saharkhiz, & Latifi. (2012). Shadow Moiré aided 3-D reconstruction of fabric drape. *Fibers and Polymers, 13*(7), 928-935.

Gioberto, G. (2015). *Measuring Joint Movement Through Garment-Integrated Wearable Sensing.* PhD Thesis. University of Minnesota.

Gioberto, G., & Dunne, L. (2012). Theory and characterization of a top-thread coverstitched stretch sensor. *2012 IEEE International Conference on Systems, Man, and Cybernetics (SMC).* 3275-3280.

Gioberto, G., & Dunne, L. (2013). Overlock-stitched stretch sensors: Characterization and effect of fabric property. *Journal of Textile and Apparel, Technology and Management. 8(*3).

Gioberto, G. & Dunne, L. (2014). Garment-Integrated Bend Sensor. *Electronics, 3*(4), 564-581.

Gioberto, G., Compton, C., & Dunne, L. (2016). Machine-Stitched E-textile Stretch Sensors. *Sensors & Transducers, 202*(7), 25-37.

Gioberto, G., Coughlin, J., Bibeau, K., & Dunne, L. (2013). Detecting bends and fabric folds using stitched sensors. *Proceedings of the 2013 International Symposium on Wearable Computers*, 53-56.

Gemperle, F., Kasabach, C., Stivoric, J., Bauer, M., & Martin, R. "Design for Wearability," *Digest of Papers. 2nd International Symposium on Wearable Computers*, 19-20 Oct. 1998, Pittsburgh, PA, USA

Gómez, Castejón, García-Prada, Carbone, & Ceccarelli. (2016). Analysis and Comparison of Motion Capture Systems for Human Walking. *Experimental Techniques, 40*(2), 875-883.

Harms, H., Amft, O., & Tröster, G. (2010). Estimating Posture-Recognition Performance in Sensing Garments Using Geometric Wrinkle Modeling. *IEEE Transactions on Information Technology in Biomedicine, 14*(6), 1436-1445.

Hsu, Y. H., Chan, C. C., & Tang, W. (2017). Alignment of Multiple Electrospun Piezoelectric Fiber Bundles Across Serrated Gaps at an Incline: A Method to Generate Textile Strain Sensors. *Scientific Reports, 7*(1).

Joseph-Armstrong, H. (2010). *Patternmaking for fashion design* (5th Ed.). Upper Saddle River, N.J.: Pearson Education/Prentice Hall.

Kannaian, T., Naveen, V., Muthukumar, S., & Thilagavathi, N. (2015). Experimental Investigations of Woven Textile Tape as Strain Sensor. *Journal of The Institution of Engineers (India): Series E, 96*(2), pp.125-130.

Kaushik, V., Lee, J., Hong, J., Lee, S., Lee, S., Seo, J., . . . Lee, T. (2015). Textile-Based Electronic Components for Energy Applications: Principles, Problems, and Perspective. *Nanomaterials, 5*(3), 1493-1531.

Kirk, W., & Ibrahim, S. (1966). Fundamental Relationship of Fabric Extensibility to Anthropometric Requirements and Garment Performance. *Textile Research Journal, 36*(1), 37-47.

Lee, T., Lee, W., Kim, S., Kim, J., & Kim, B. (2016). Flexible Textile Strain Wireless Sensor Functionalized with Hybrid Carbon Nanomaterials Supported ZnO Nanowires with Controlled Aspect Ratio. *Advanced Functional Materials, 26*(34), 6206-6214.

Li X. (2015) Strain Sensors of Graphene Woven Fabrics. In: Synthesis, Properties and Application of Graphene Woven Fabrics. *Springer Theses (Recognizing Outstanding Ph.D. Research).* Springer, Berlin, Heidelberg.

Maiolino, Maggiali, Cannata, Metta, & Natale. (2013). A Flexible and Robust Large Scale Capacitive Tactile System for Robots. *Sensors Journal, IEEE, 13*(10), pp.3910-3917.

MATLAB & Statistics and Machine Learning Toolbox, Deep Learning Toolbox Release 2018a, The MathWorks, Inc., Natick, Massachusetts, United States

Mattmann, C., Tröster, G., & Clemens, F. (2008). Sensor for measuring strain in textile. *Sensors, 8*(6), pp.3719-3732.

Narbonneau, F., De Jonckheere, J., Jeanne, M., Kinet, D., Witt, J….R. Logier (2010). OFSETH: optical technologies embedded in smart medical textile for continuous monitoring of respiratory

motions under magnetic resonance imaging. *Proc. Biophotonics: Photonic Solutions for Better Health Care II; 77151*(D).

Obropta, E., & Newman, D. (2015). A comparison of human skin strain fields of the elbow joint for mechanical counter pressure space suit development. *Aerospace Conference, 2015. IEEE, 1*(9).

Paradiso, R., Loriga, G., & Taccini, N. (2005). A wearable health care system based on knitted integrated sensors. *IEEE Transactions on Information Technology in Biomedicine, 9*(3), 337-344.

Ren, Wang, Zhang, Carey, Chen, Yin, & Torrisi. (2017). Environmentally-friendly conductive cotton fabric as flexible strain sensor based on hot press reduced graphene oxide. *Carbon, 111*, pp.622-630.

Roy, S., Inamdar, M., & Bhaumik, S. (2016) Review of Exoskeleton Hand Exercisers for Paralyzed patient. *2nd Research Summit on Computer, Electronics and Electrical Engineering NIT Arunachal Pradesh* 3rd -4th June 2016, pp 35-44

Senthilkumar & Anbumani (2014). Dynamic Elastic Behavior of Cotton and Cotton / Spandex Knitted Fabrics. *Journal of Engineered Fibers and Fabrics. 9*(1)

Stretchsense ® Datasheet. 2019. Retrieved from https://www.stretchsense.com/wp-content/uploads/2019/03/SSD18-Datasheet.pdf

Takasaki, H. (1973). Moiré topography. *Applied Optics,* 9(6), 1467-72.

Tao, X. H., Koncar, V. L., Huang, T. C., Shen, C. T., Ko, Y., & Jou, G. (2017). How to make reliable, washable, and wearable textronic devices. *Sensors (Switzerland), 17*(4), p.673.

Wang, Yan, Wang, Li, Yang, Tingting, Li, Xiao, Zang, Xiaobei, Zhu, Miao, . . . Zhu, Hongwei. (2014). Wearable and Highly Sensitive Graphene Strain Sensors for Human Motion Monitoring. *Advanced Functional Materials*, *24*(29), pp.4666-4670.

Zhang, H. (2015). Flexible textile-based strain sensor induced by contacts. *Measurement Science and Technology*, 26(10), p.105102.

Zheng, W., Tao, X., Zhu, B., Wang, G., & Hui, C. (2014). Fabrication and evaluation of a notched polymer optical fiber fabric strain sensor and its application in human respiration monitoring. *Textile Research Journal*, *84*(17), pp.1791-1802.

Zimmerman, T., Lanier, J., Blanchard, C., Bryson, S. & Harvill, Y. (1986). A hand gesture interface device. *SIGCHI Bulletin*, *18*(4), pp. 189–192.

Appendices
Appendix A: Impedance Characterization of the Coverstitch Stitch Sensor

The results for the impedance test is summarized in Table A1 and shown in the Figures A1-A8. Two 4-way knits were used, a teal poly/spandex blend and a gold nylon/spandex blend and a single coverstitch sensor was tested per specimen. The same coverstitch sensor was tested twice, designating the first time as "Trial 1" and the second time as "Trial 2".

Table A1. Coverstitch Sensor on 4-way Knits Impedance Characterization: Average Impedance and Phase Angle

Samples		Calculations	Frequency (Hz)									
			1000	112000	223000	334000	445000	556000	667000	778000	889000	1000000
			Relaxed Position									
Teal Poly/ Spandex 4-way Knit Coverstitch	Trial 1	Avg Impedance (Ω)	20.33	20.34	20.34	20.35	20.35	20.36	20.36	20.37	20.38	20.39
		Avg Phase Angle (°)	0.005863	0.5827	1.169	1.627	2.341	2.925	3.249	3.896	4.670	4.865
	Trial 2	Avg Impedance (Ω)	20.65	20.65	20.66	20.66	20.66	20.67	20.66	20.68	20.68	20.69
		Avg Phase Angle (°)	0.005874	0.5718	1.147	1.597	2.298	2.872	3.190	3.828	4.589	4.782
Gold Nylon/ Spandex 4-way Knit Coverstitch	Trial 1	Avg Impedance (Ω)	20.99	21.05	21.11	21.09	21.09	21.08	21.06	21.05	21.03	21.03
		Avg Phase Angle (°)	0.003879	0.2072	0.2139	-0.0761	-0.1897	-0.2725	-0.3241	-0.4215	-0.5384	-0.5739
	Trial 2	Avg Impedance (Ω)	21.05	21.08	21.08	21.07	21.07	21.05	21.04	21.02	20.99	20.99
		Avg Phase Angle (°)	0.002040	-0.03470	-0.1003	-0.1434	-0.2131	-0.2704	-0.3072	-0.3834	-0.4891	-0.5166
			Stretched Position									
Teal Poly/ Spandex 4-way Knit Coverstitch	Trial 1	Avg Impedance (Ω)	18.06	18.06	18.07	18.07	18.06	18.07	18.10	18.10	18.10	18.11
		Avg Phase Angle (°)	0.007397	0.6415	1.289	1.793	2.578	3.228	3.577	4.295	5.146	5.361
	Trial 2	Avg Impedance (Ω)	18.81	18.82	18.83	18.85	18.85	18.86	18.85	18.87	18.88	18.90
		Avg Phase Angle (°)	0.003339	0.6516	1.309	1.822	2.624	3.281	3.645	4.371	5.238	5.472
Gold Nylon/ Spandex 4-way Knit Coverstitch	Trial 1	Avg Impedance (Ω)	17.32	17.31	17.31	17.33	17.31	17.29	17.29	17.30	17.26	17.23
		Avg Phase Angle (°)	0.000687	-0.09425	-0.1864	-0.2592	-0.3644	-0.4563	-0.5096	-0.6228	-0.7896	-0.8405
	Trial 2	Avg Impedance (Ω)	17.01	17.03	17.03	17.03	17.00	17.00	16.94	16.92	16.91	16.91
		Avg Phase Angle (°)	-0.002394	-0.08651	-0.2045	-0.2853	-0.4279	-0.5433	-0.6129	-0.7474	-0.9271	-0.9699
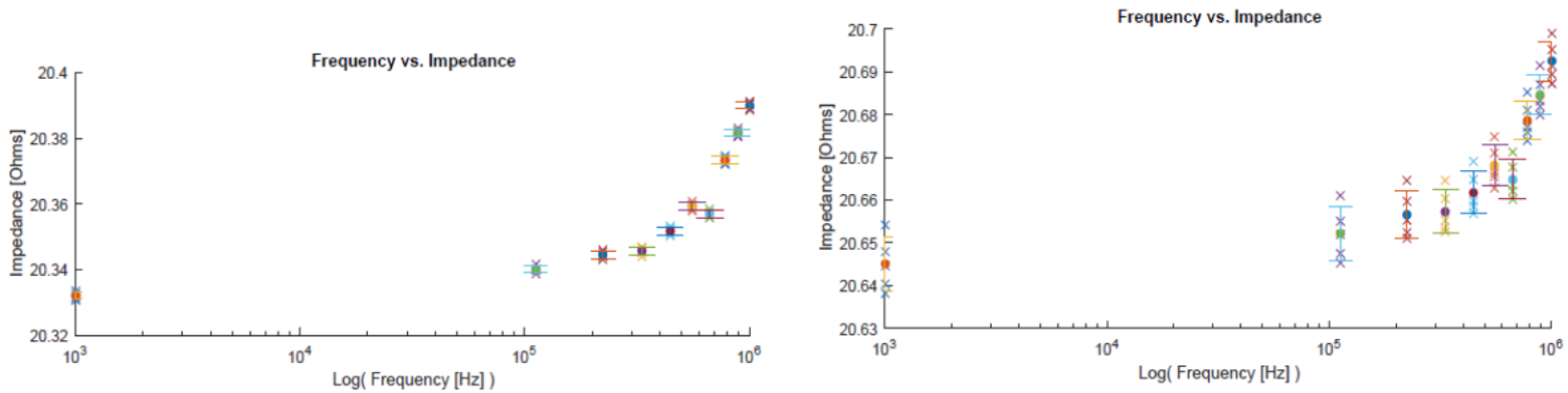
Figure A1. Teal Polyester/Spandex 4-way Knit Coverstitch Impedance in <u>Relaxed</u> Position (Left) Trial 1 (Right) Trial 2
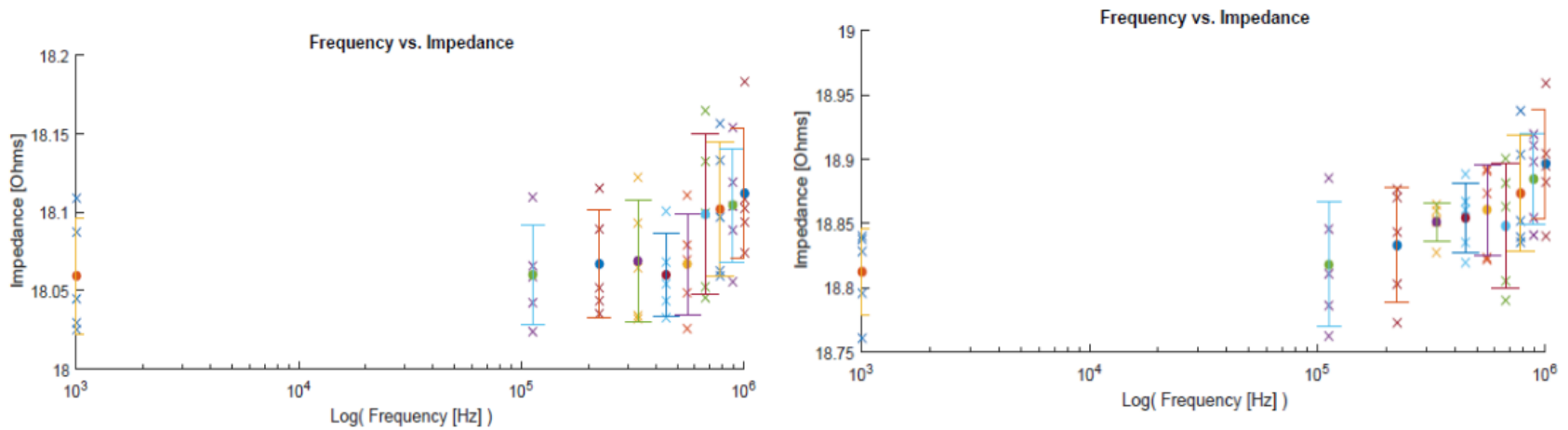

Figure A2. Teal Polyester/Spandex 4-way Knit Coverstitch Impedance in <u>Stretched</u> Position (Left) Trial 1 (Right) Trial 2
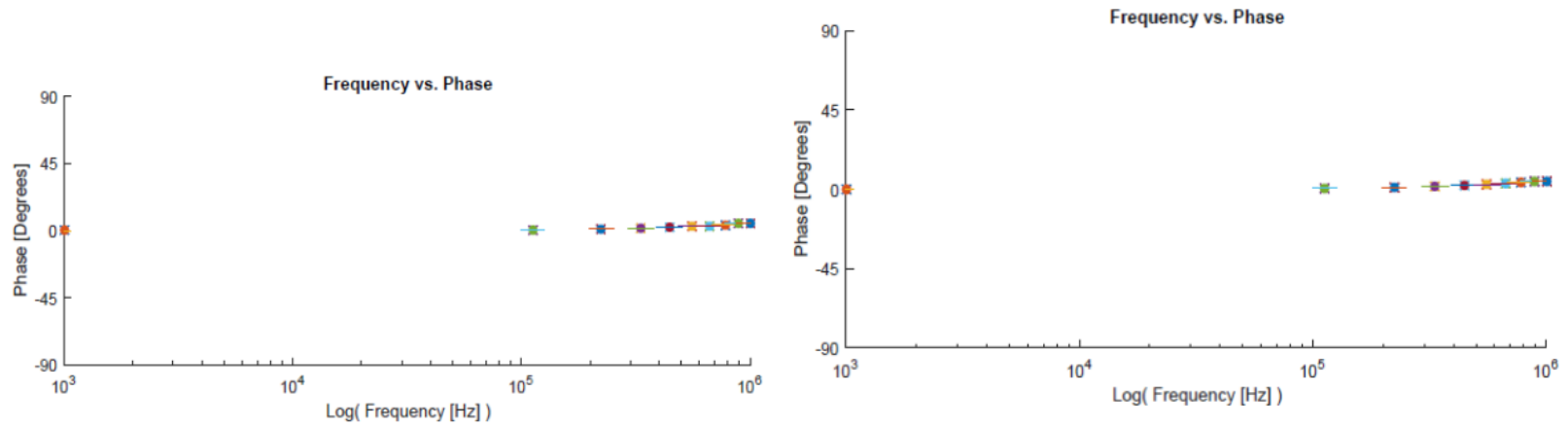
Figure A3. Teal Polyester/Spandex 4-way Knit Coverstitch Phase Angle in <u>Relaxed</u> Position (Left) Trial 1 (Right) Trial 2
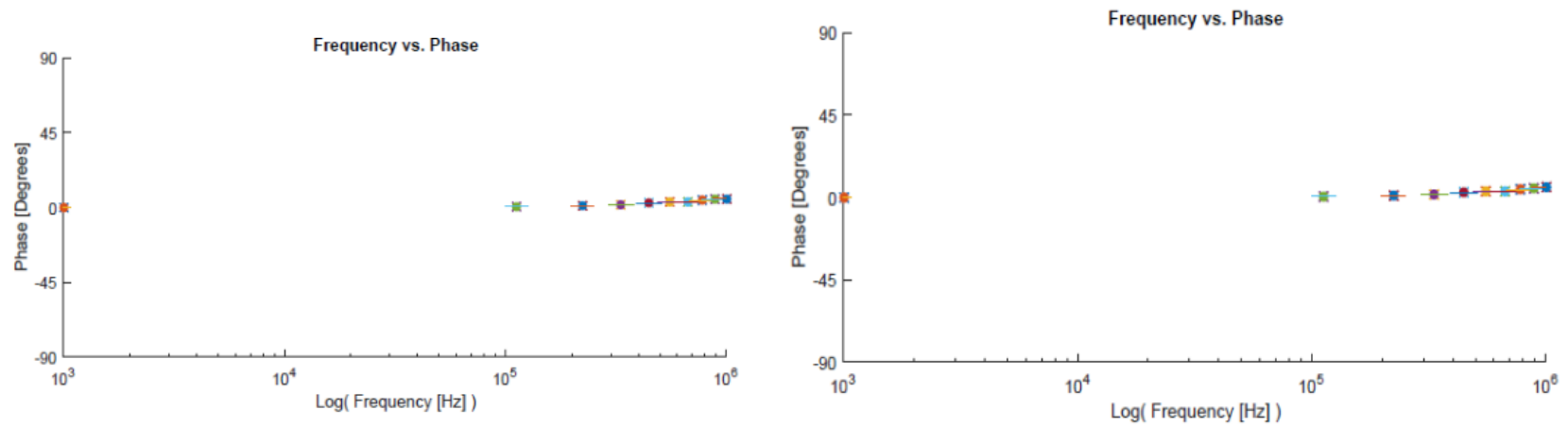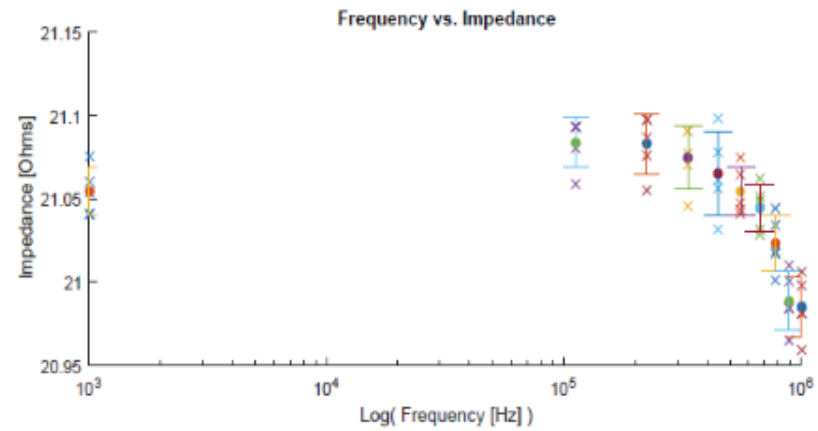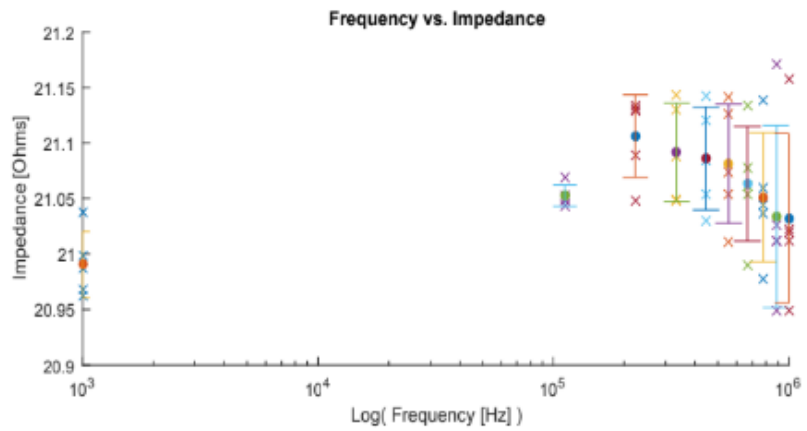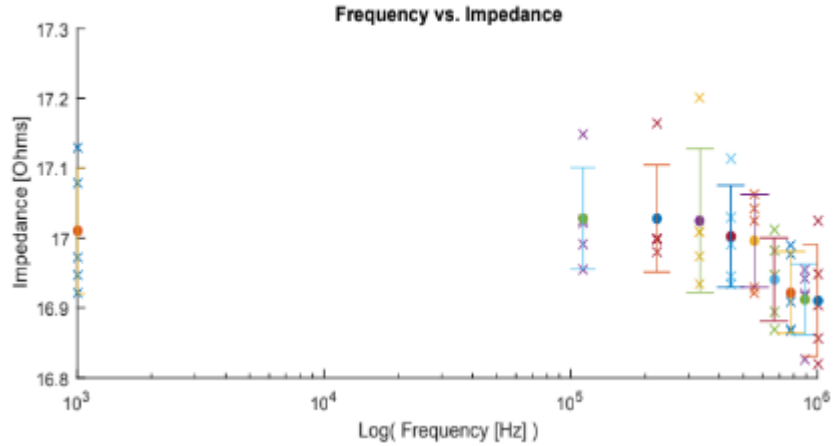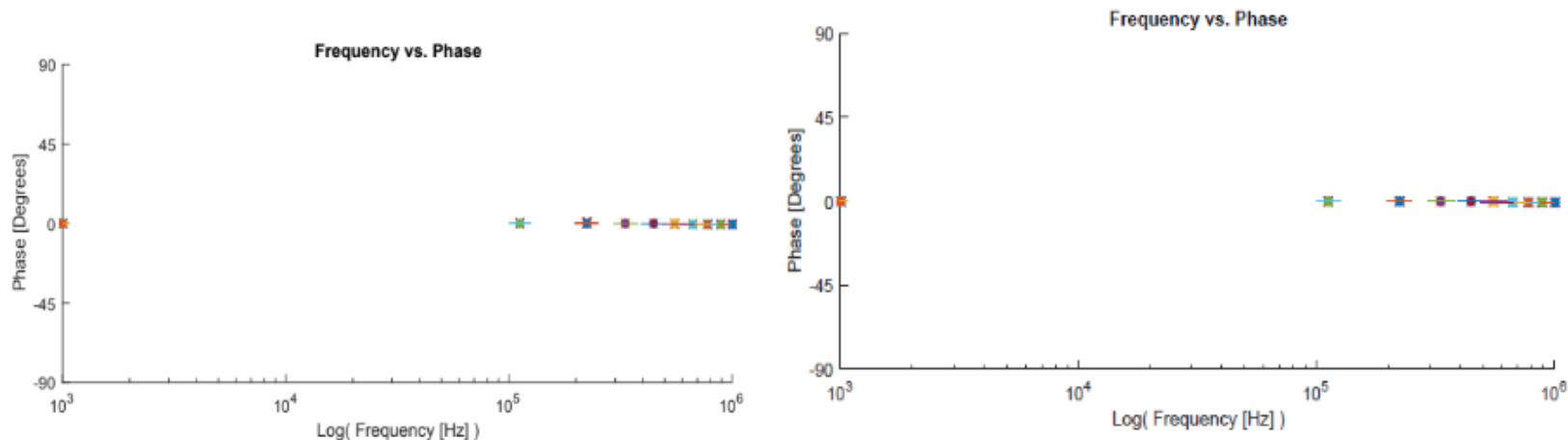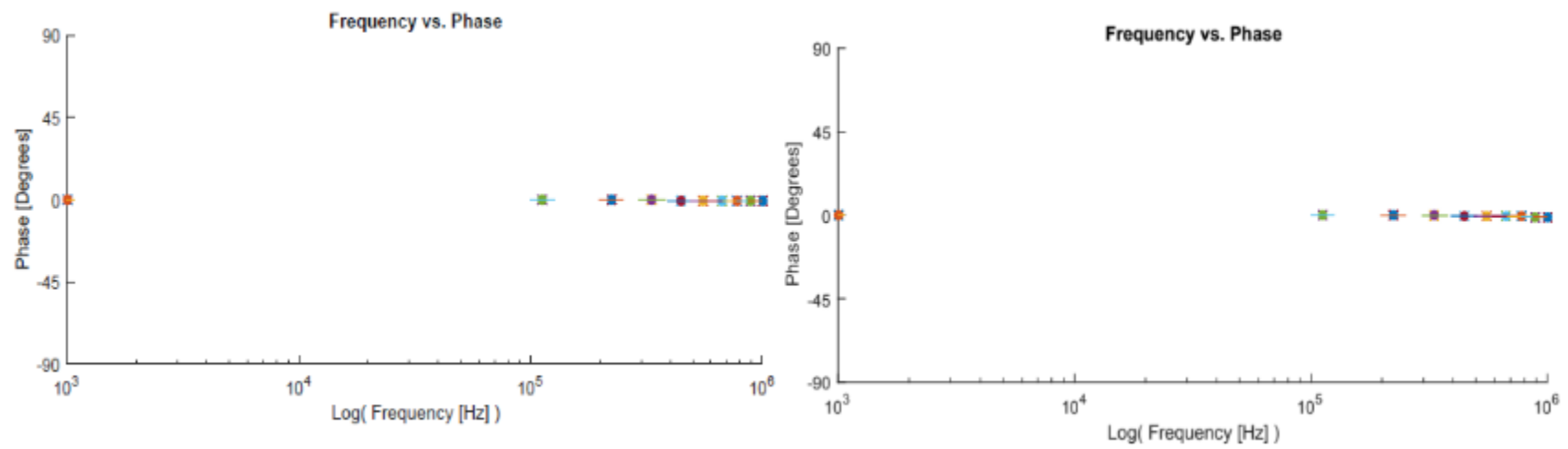

Figure A4. Teal Polyester/Spandex 4-way Knit Coverstitch Phase Angle in <u>Stretched</u> Position (Left) Trial 1 (Right) Trial 2

Figure A5. Gold Nylon/Spandex 4-way Knit Coverstitch Impedance in <u>Relaxed</u> Position (Left) Trial 1 (Right) Trial 2
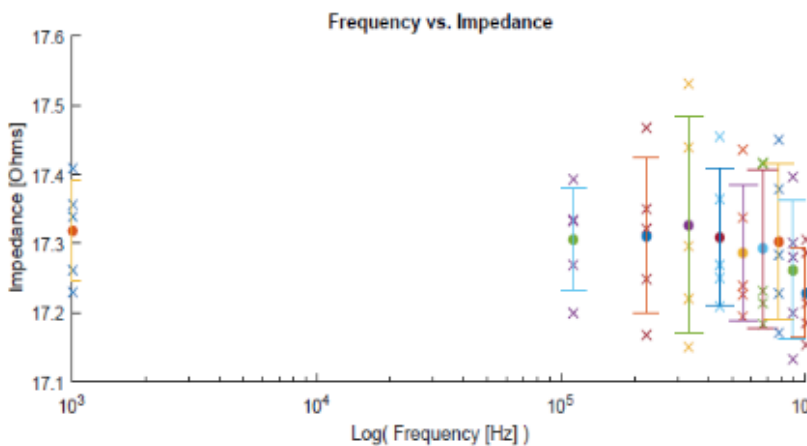
Figure A6. Gold Nylon/Spandex 4-way Knit Coverstitch Impedance in <u>Stretched</u> Position (Left) Trial 1 (Right) Trial 2

Figure A7. Gold Nylon/Spandex 4-way Knit Coverstitch Phase Angle in <u>Relaxed</u> Position (Left) Trial 1 (Right) Trial 2

Figure A8. Gold Nylon/Spandex 4-way Knit Coverstitch Phase Angle in <u>Stretched</u> Position (Left) Trial 1 (Right) Trial 2

Appendix B: Sensor-Knit Mechanical Behavior

Individual Force (Displacement) graphs for each sample group tested are provided in Figures B1-B60. First the 2-way fabric only is presented (Figs B1-10), then the 2-way fabric with the coverstitch (Figs B11-20) and Chainstitch (Figs B21-30) sensors, then the 4-way fabric only (Figs B31-40), and finally the 4-way fabric with the coverstitch (Figs B41-50) and Chainstitch sensors (Figs B51-60). The stitch sensor degrees in the figure titles refer to the angle from 0° (stiffest direction/lengthwise/wale knit direction) that the stitched sensor was sewn onto the knit fabric. The force degrees in the figure titles refer to the angle from the stitched sensor. This section only shows the setup of the force pulled in the same direction as the sensor, when the sensor was present.

These graphs are included to show the variety of exponential to linear mechanical behavior exhibited, depending on the fabric used, sensor placement, and the stitched sensor geometry.
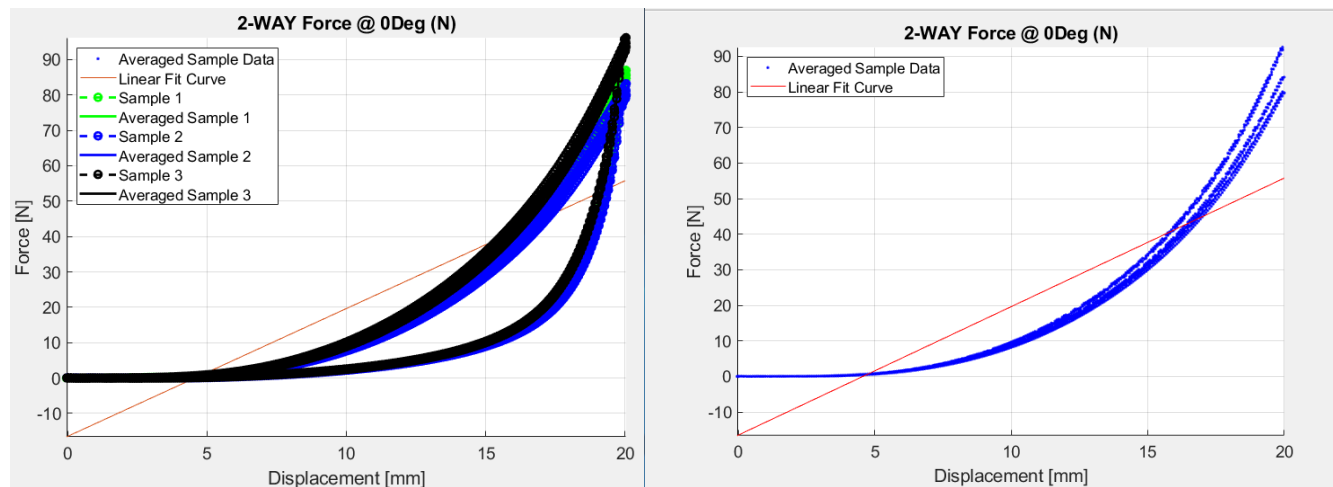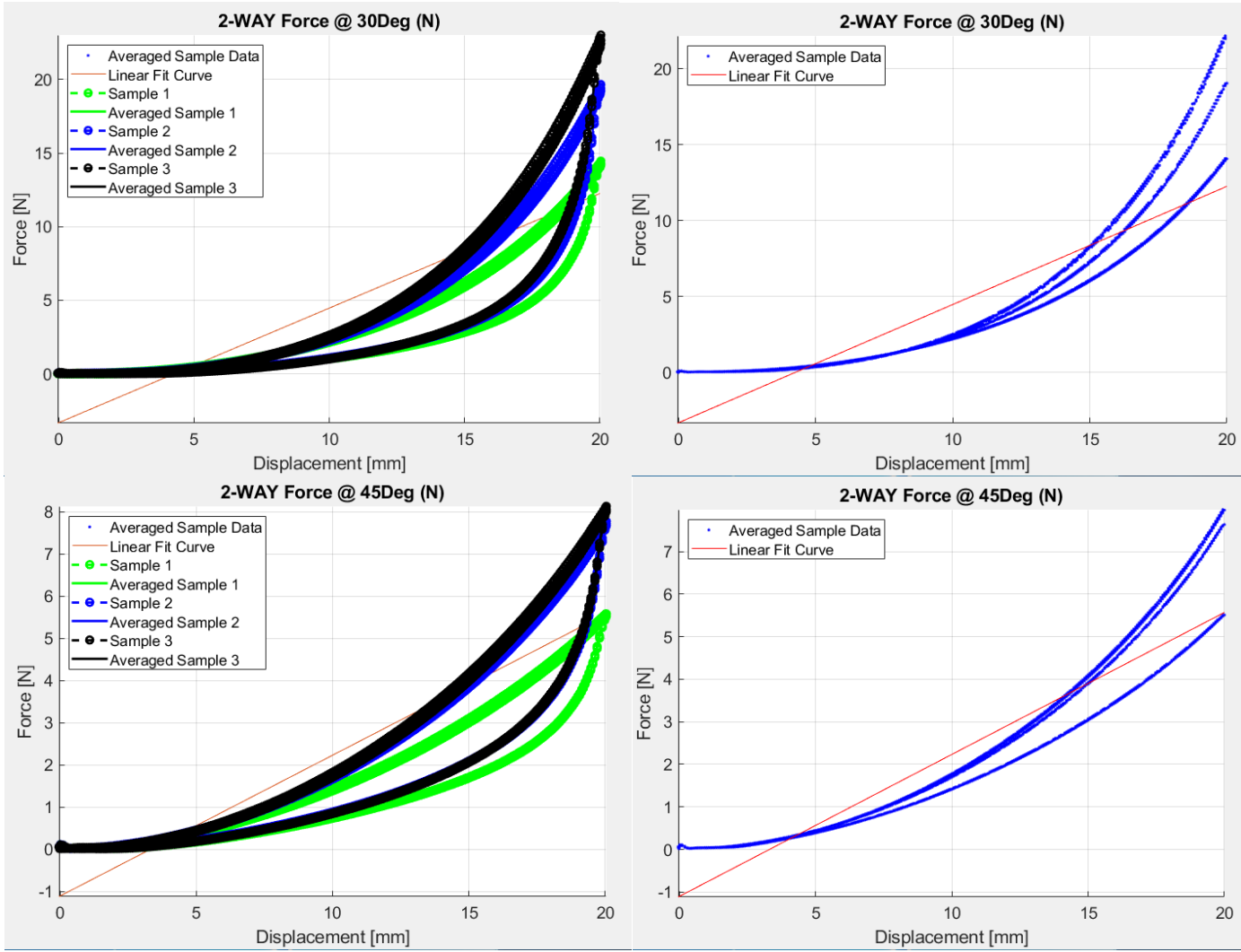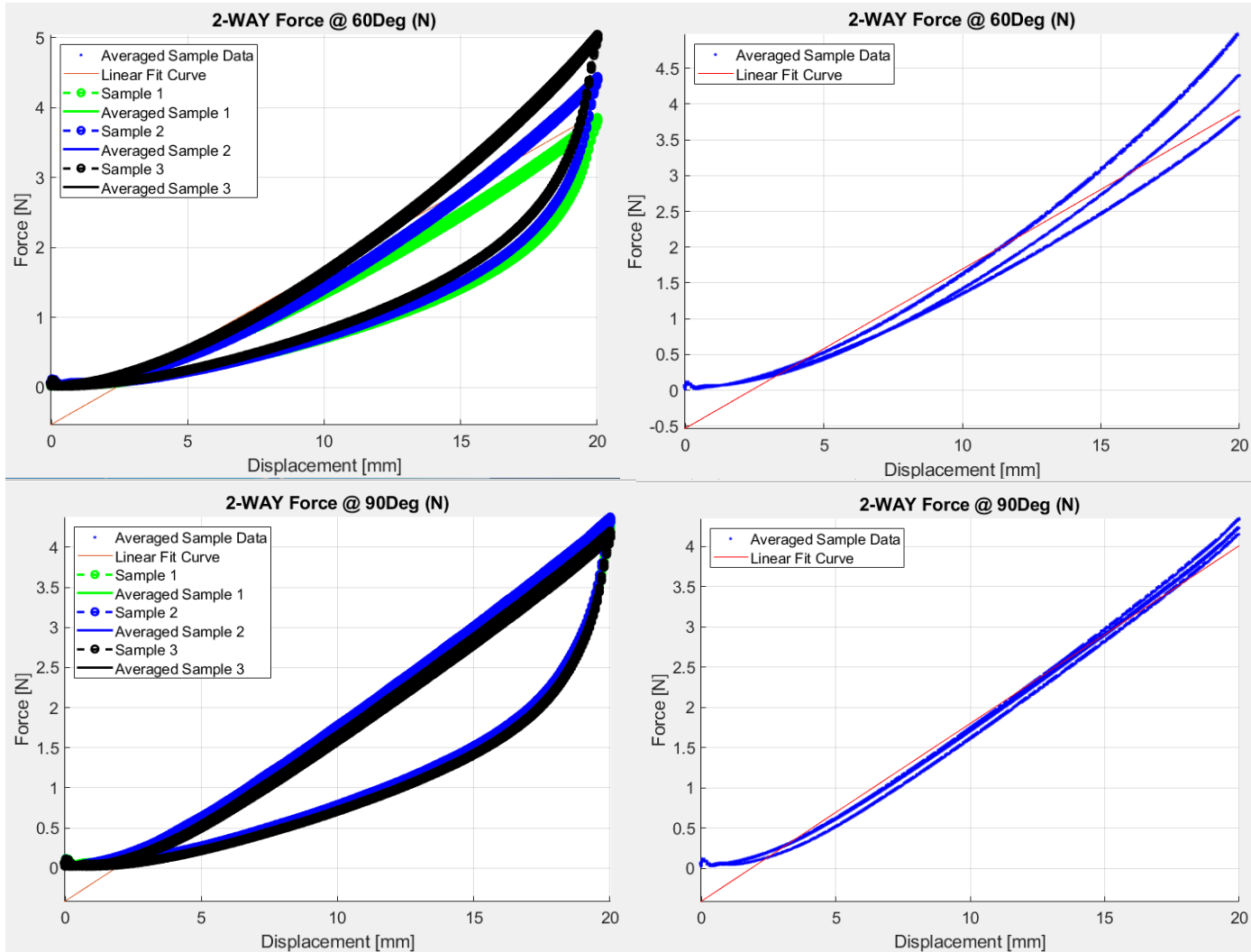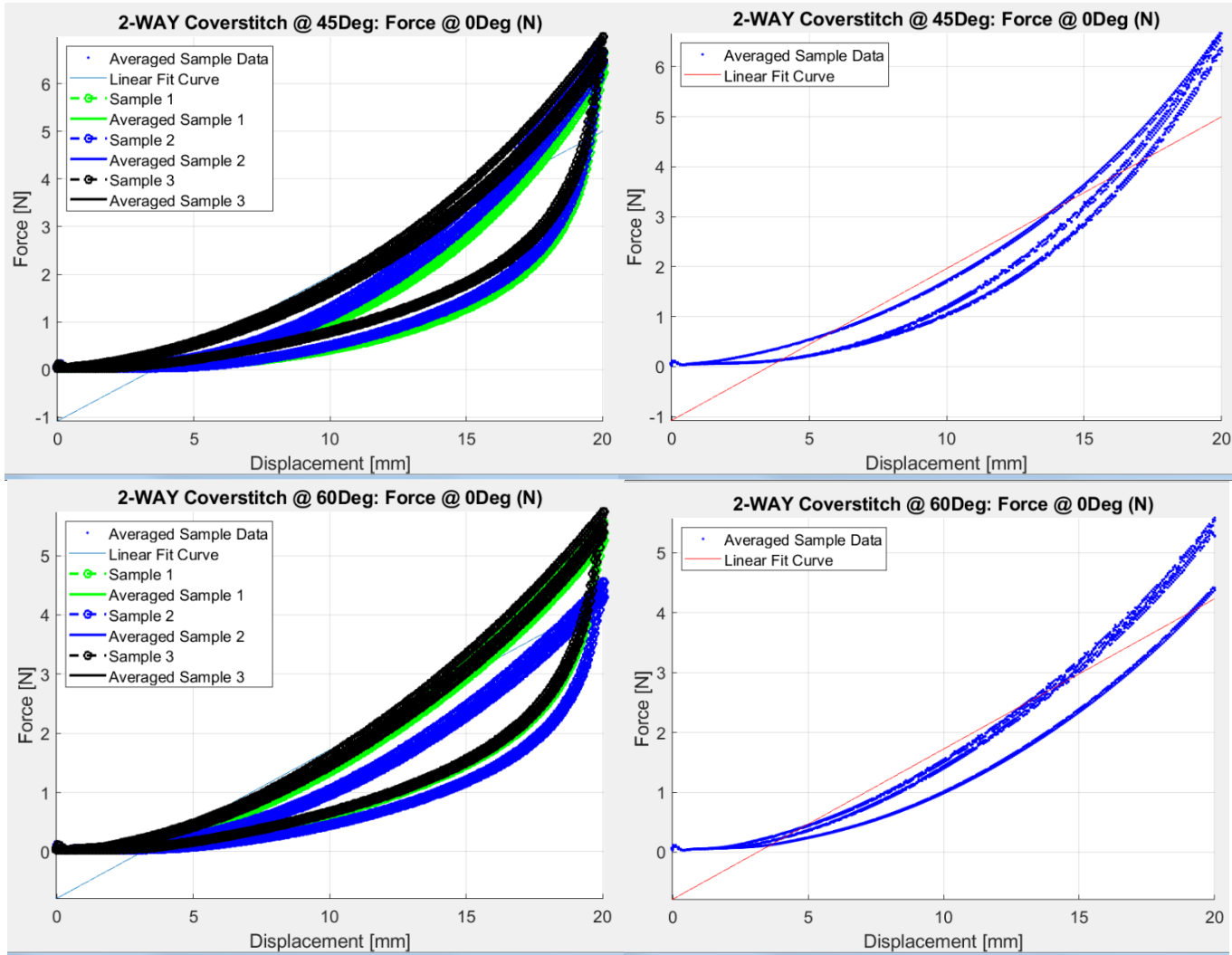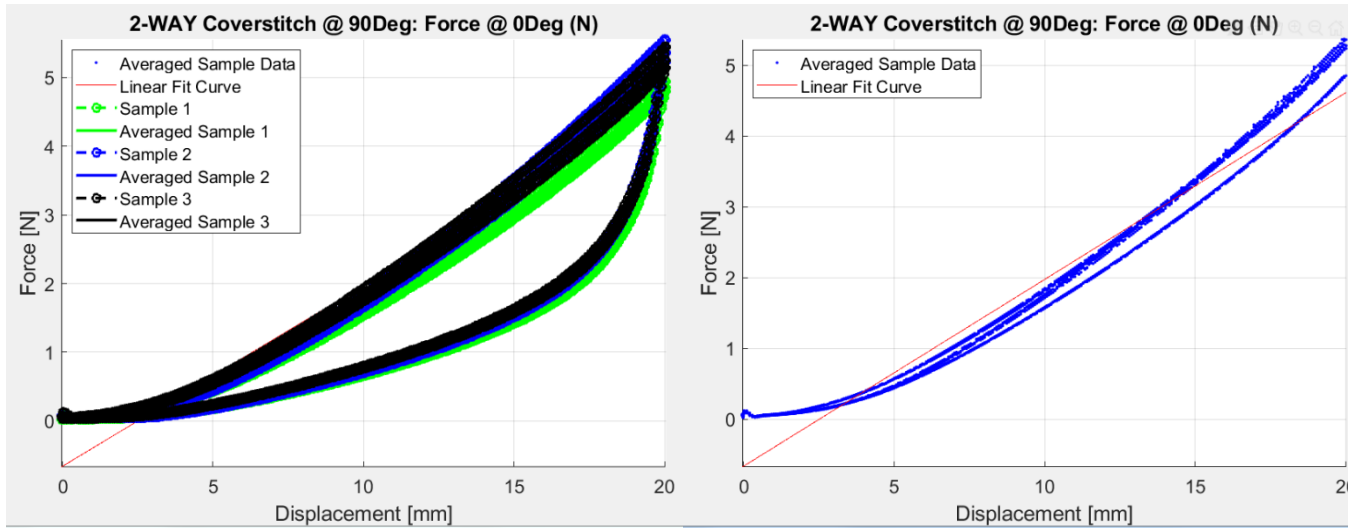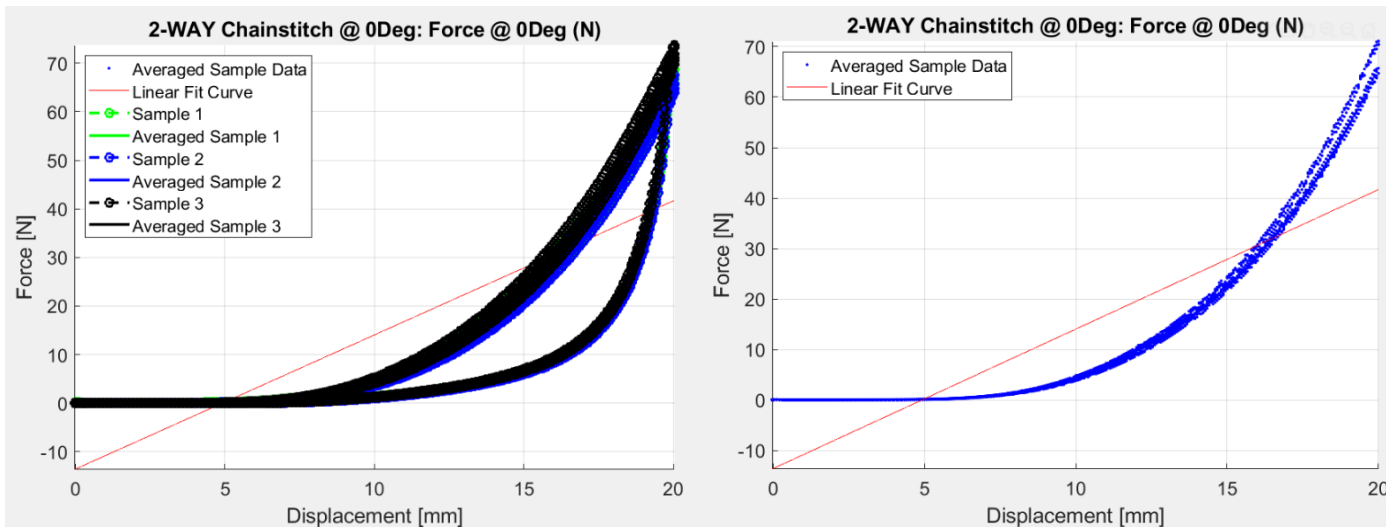
Figures B1-B10. <u>2-way Fabric</u> Force (Displacement) Graphs at Force Directions 0°, 30°, 45°, 60°, and 90°
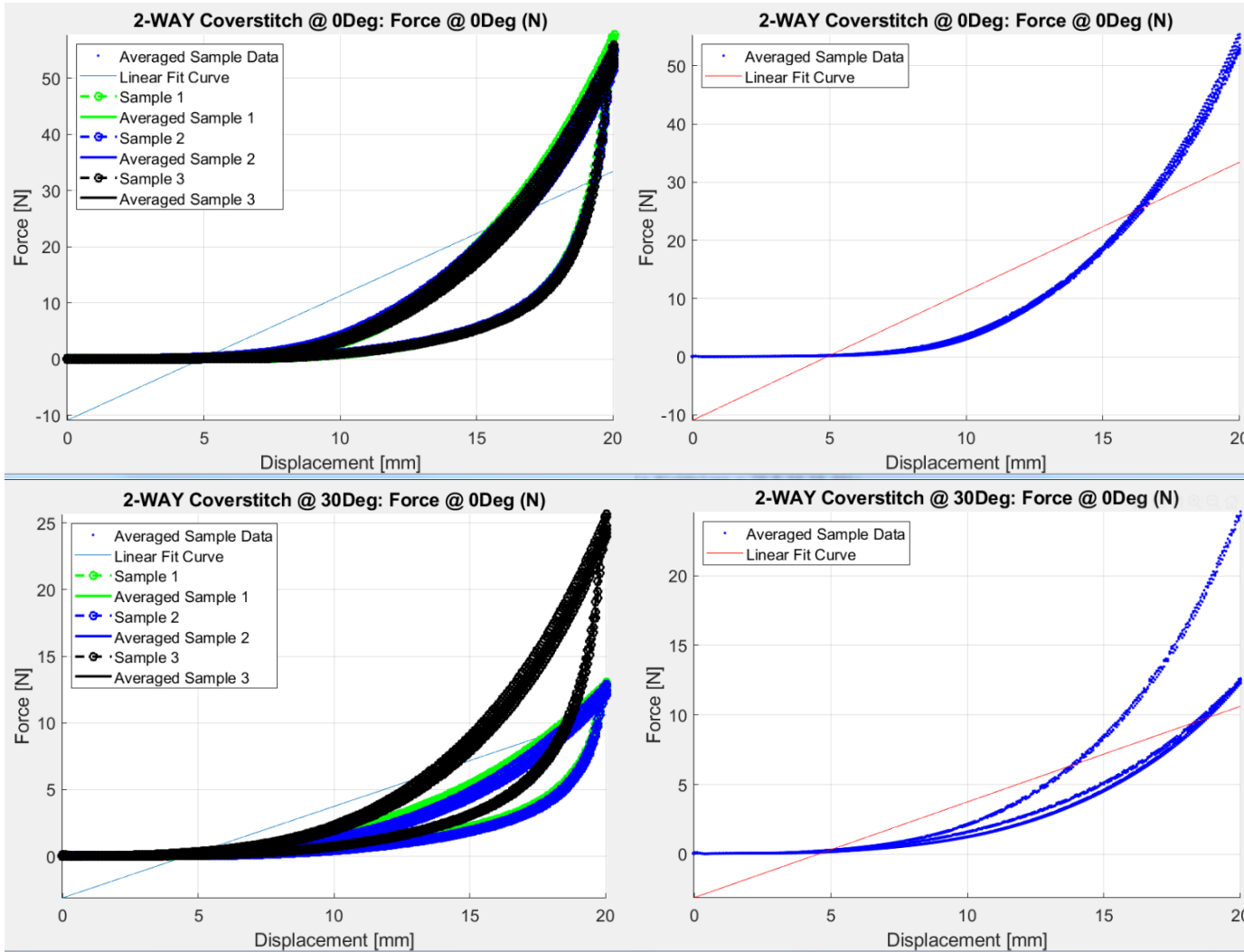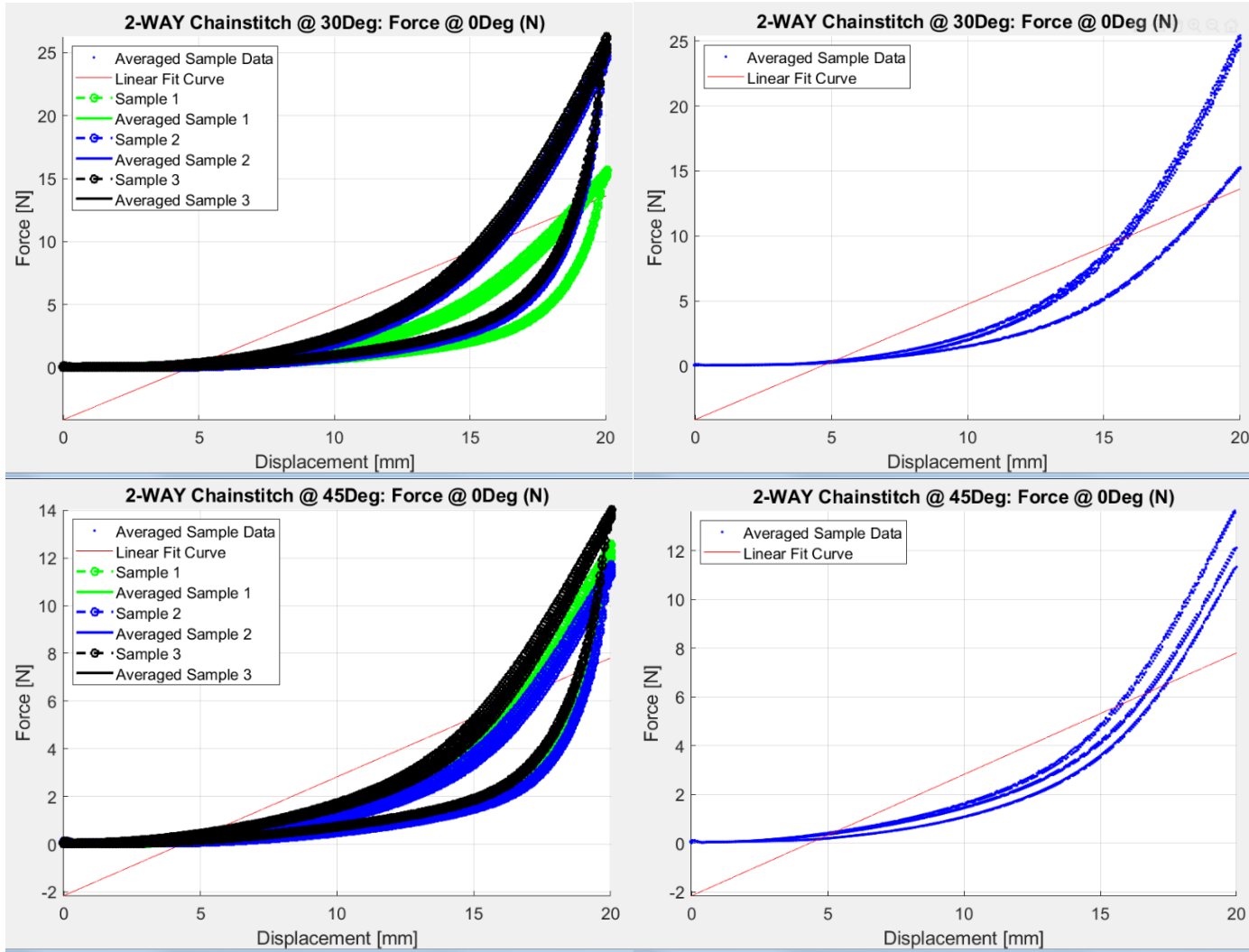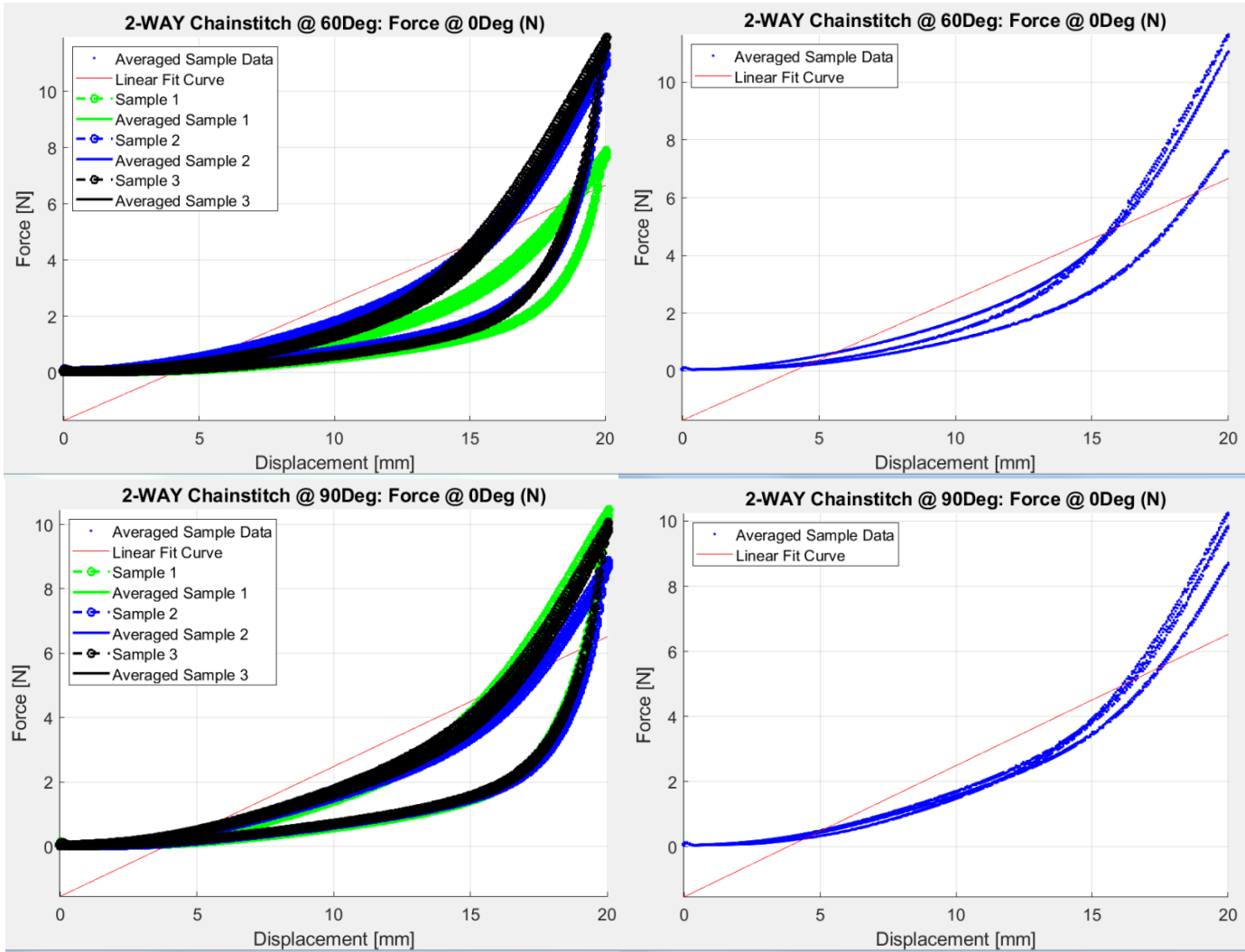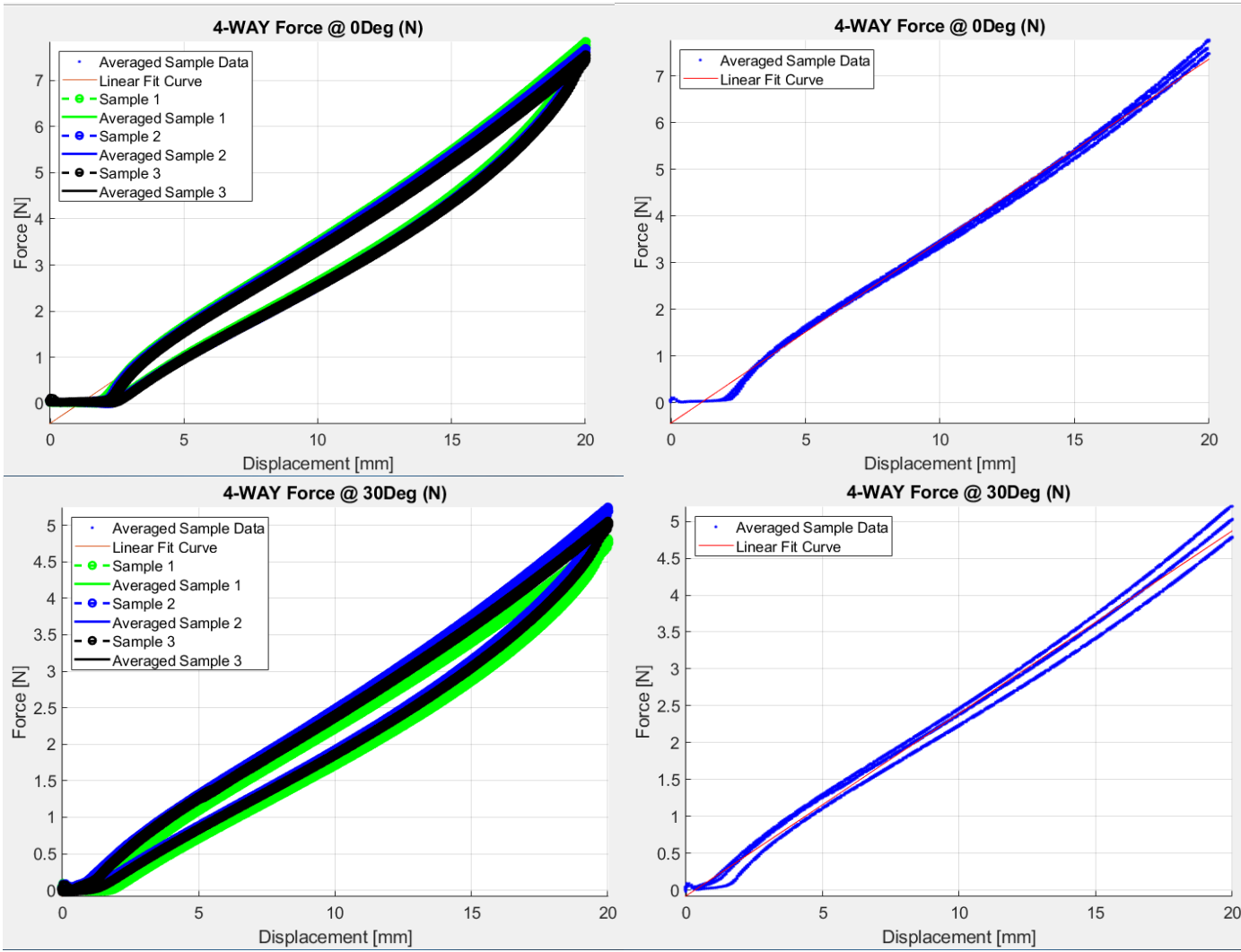
Figures B11-B20. <u>2-way Knit + Coverstitch</u> **Sensor Force (Displacement) Graphs at Force Directions 0°, 30°, 45°, 60°, and 90°**
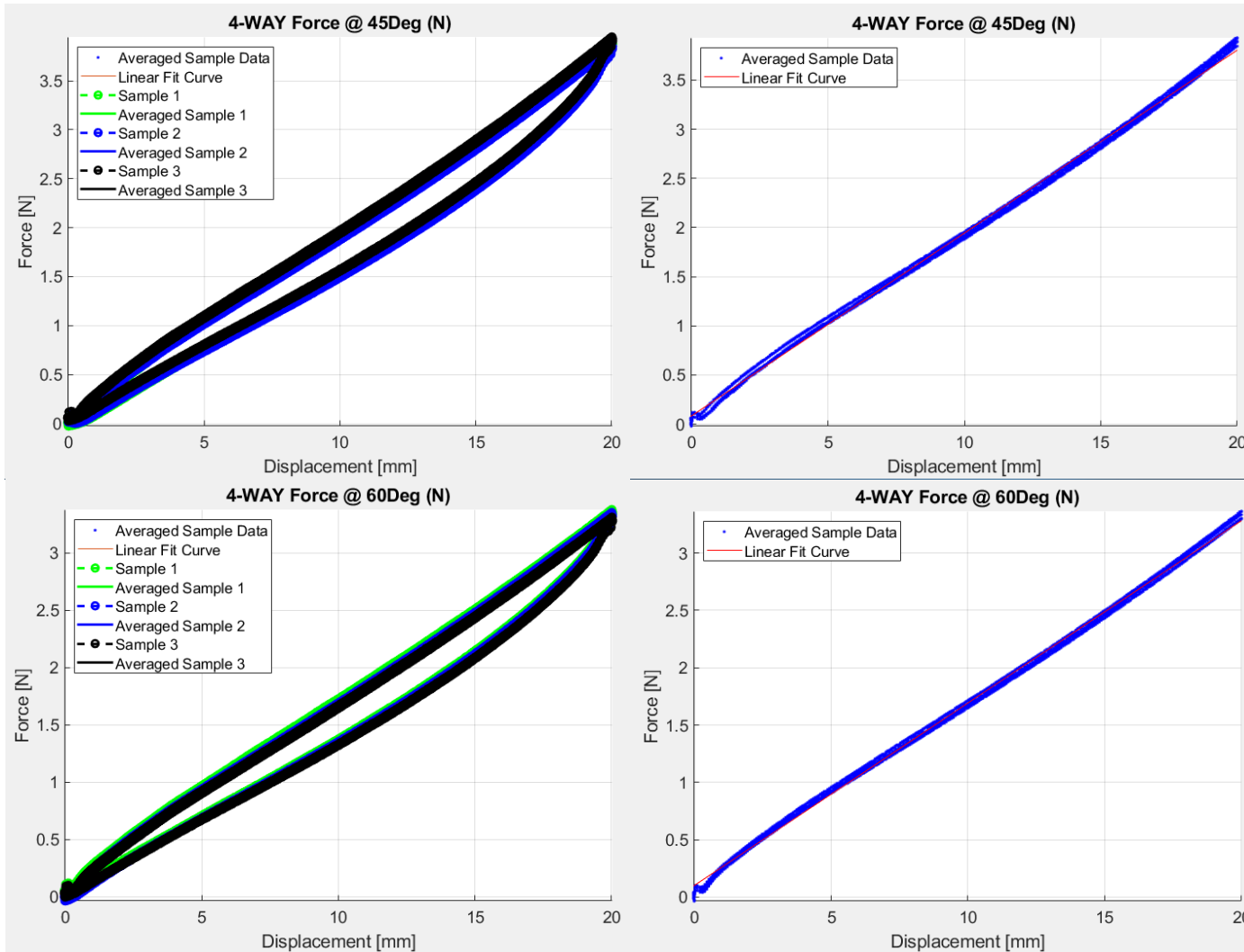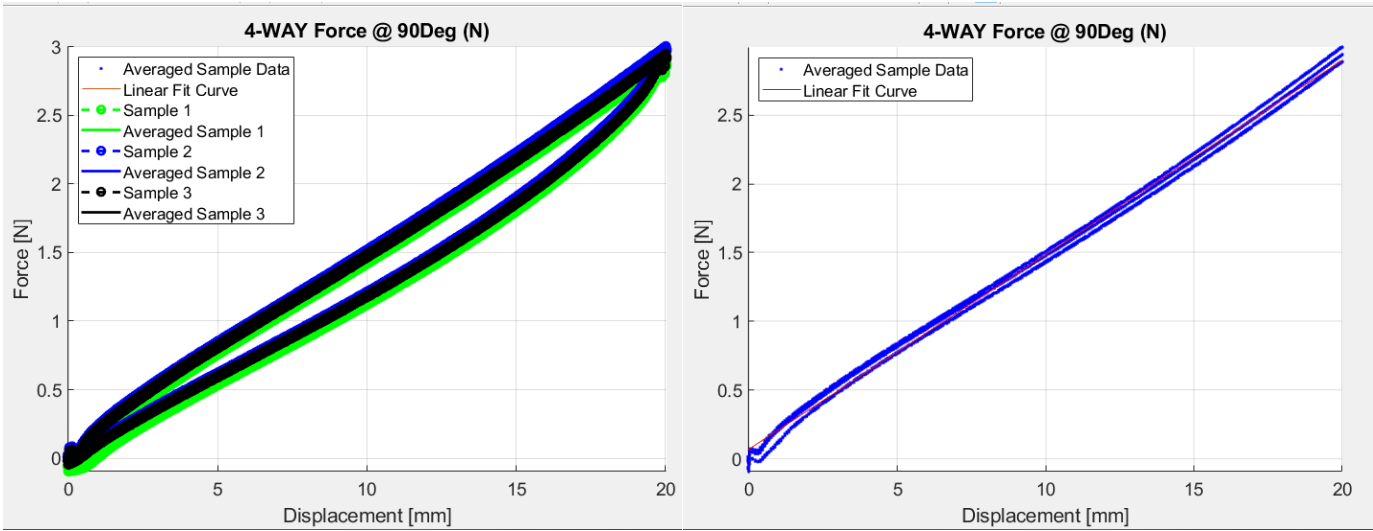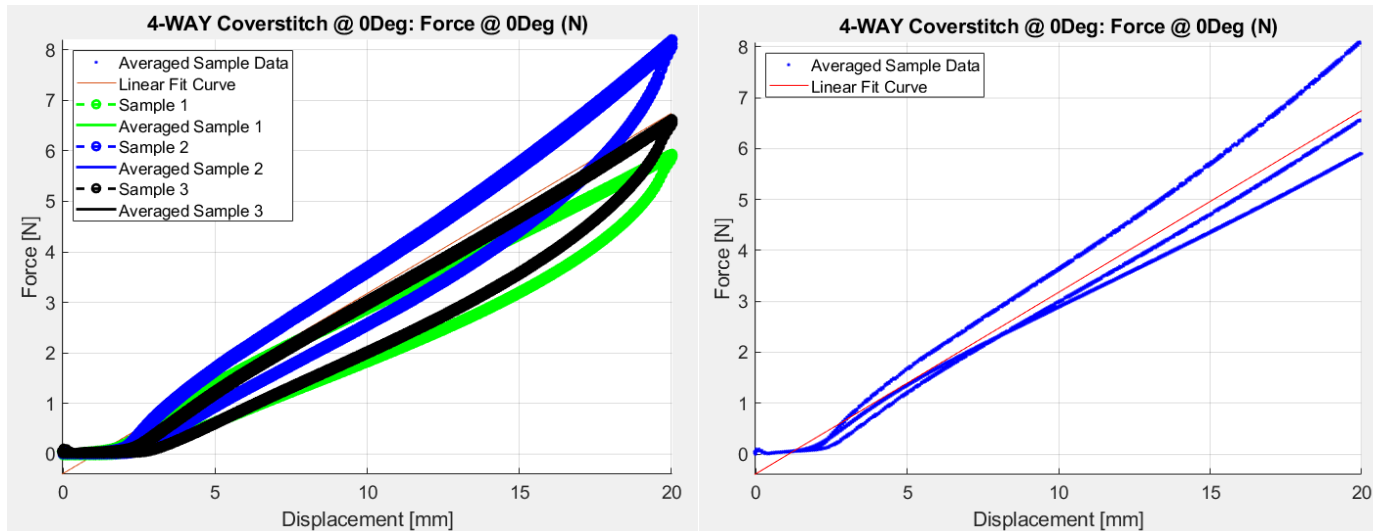
Figures B21-B30. <u>2-way Knit + Chainstitch</u> Sensor Force (Displacement) Graphs at Force Directions 0°, 30°, 45°, 60°, and 90°

4-WAY Force @ 0Deg (N)

4-WAY Force @ 0Deg (N)

4-WAY Force @ 30Deg (N)

4-WAY Force @ 30Deg (N)

4-WAY Force @ 45Deg (N)

4-WAY Force @ 45Deg (N)

4-WAY Force @ 60Deg (N)
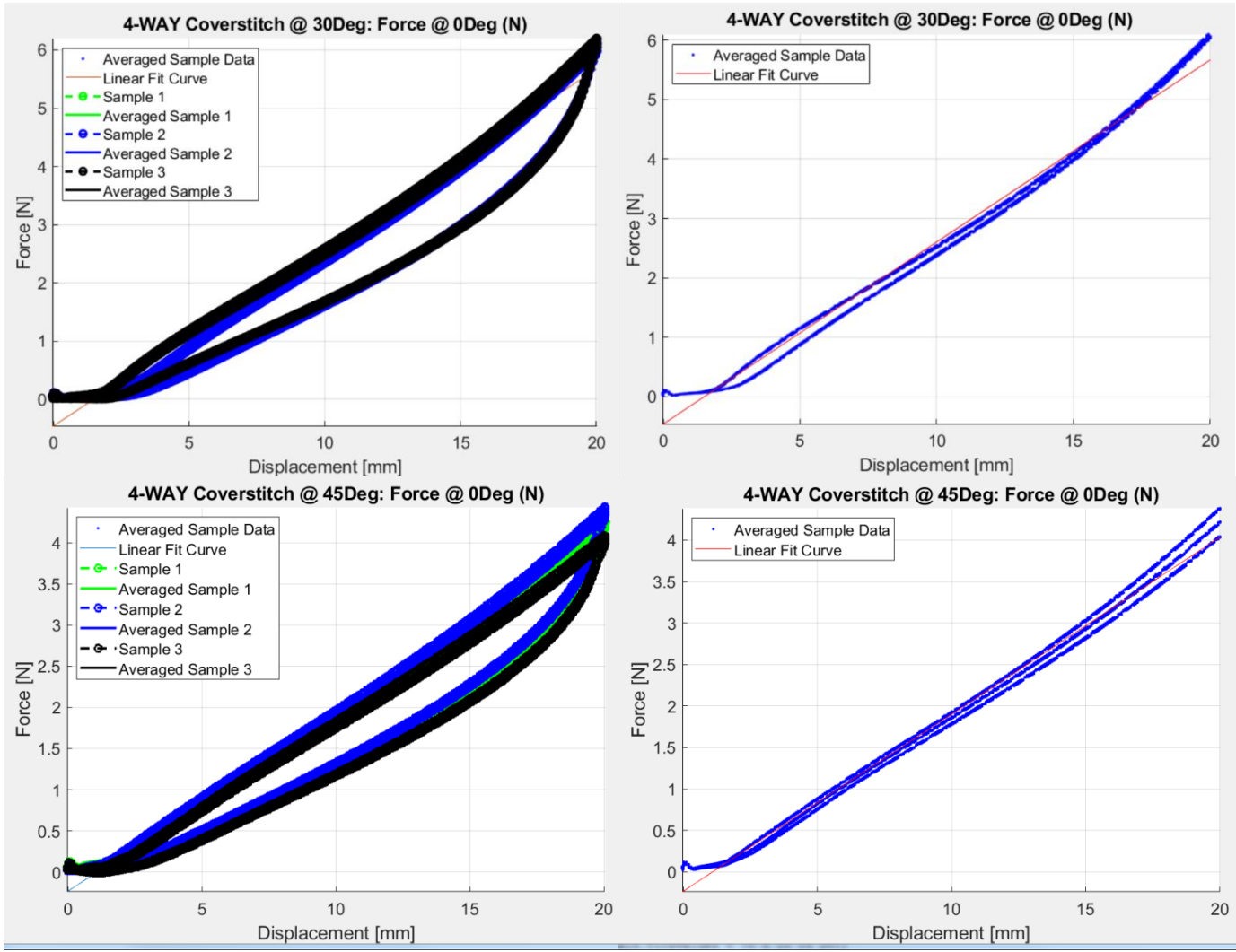
4-WAY Force @ 60Deg (N)

Figures B31-B40. <u>4-way Fabric</u> Force (Displacement) Graphs at Force Directions 0°, 30°, 45°, 60°, and 90°

114

4-WAY Coverstitch @ 30Deg: Force @ 0Deg (N)

4-WAY Coverstitch @ 30Deg: Force @ 0Deg (N)

4-WAY Coverstitch @ 45Deg: Force @ 0Deg (N)

4-WAY Coverstitch @ 45Deg: Force @ 0Deg (N)

Figures B41-B50. <u>4-way Knit + Coverstitch</u> **Sensor Force (Displacement) Graphs at Force Directions 0°, 30°, 45°, 60°, and 90°**

118

Figures B51-B60. <u>4-way Knit + Chainstitch</u> Sensor Force (Displacement) Graphs at Force Directions 0°, 30°, 45°, 60°, and 90°
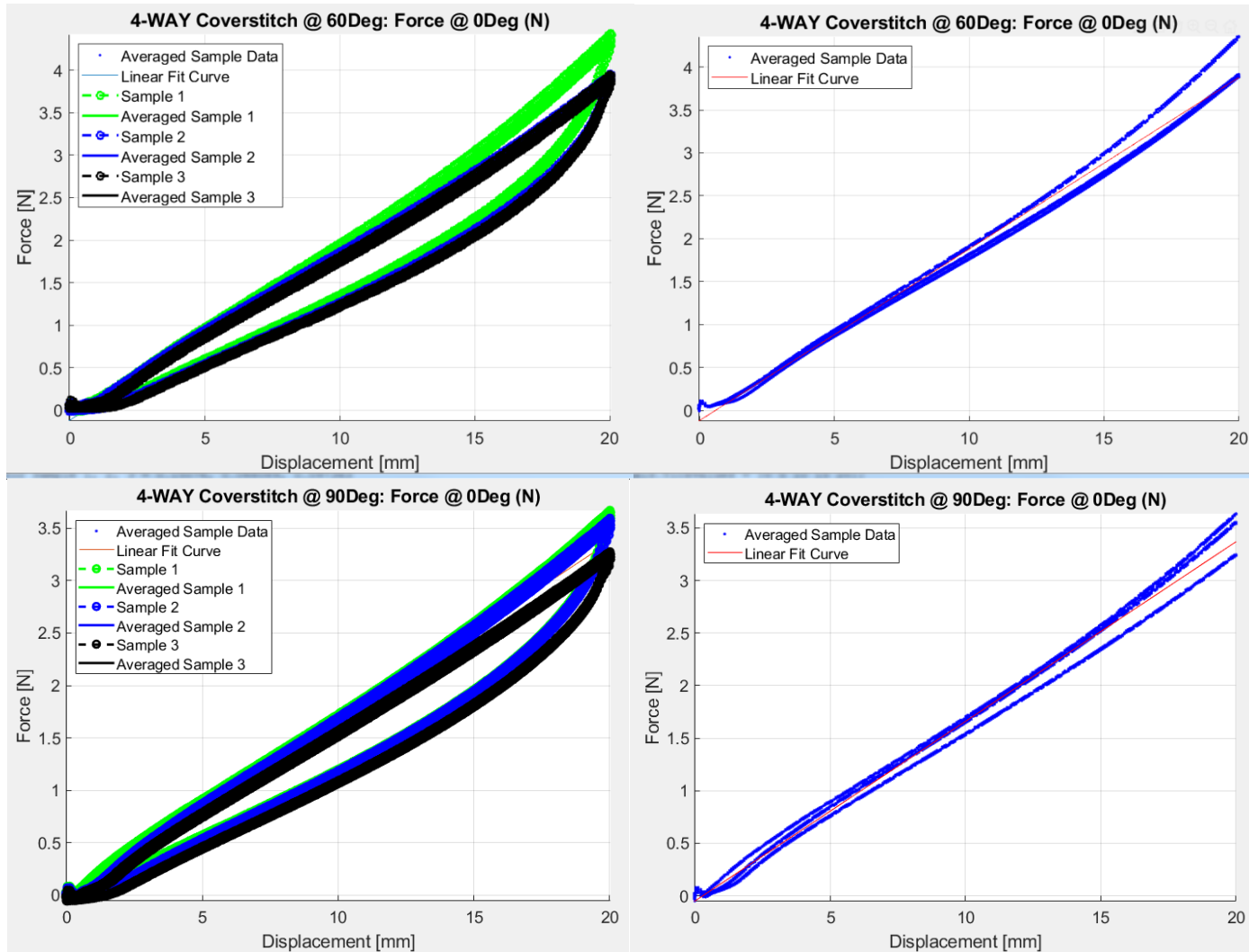
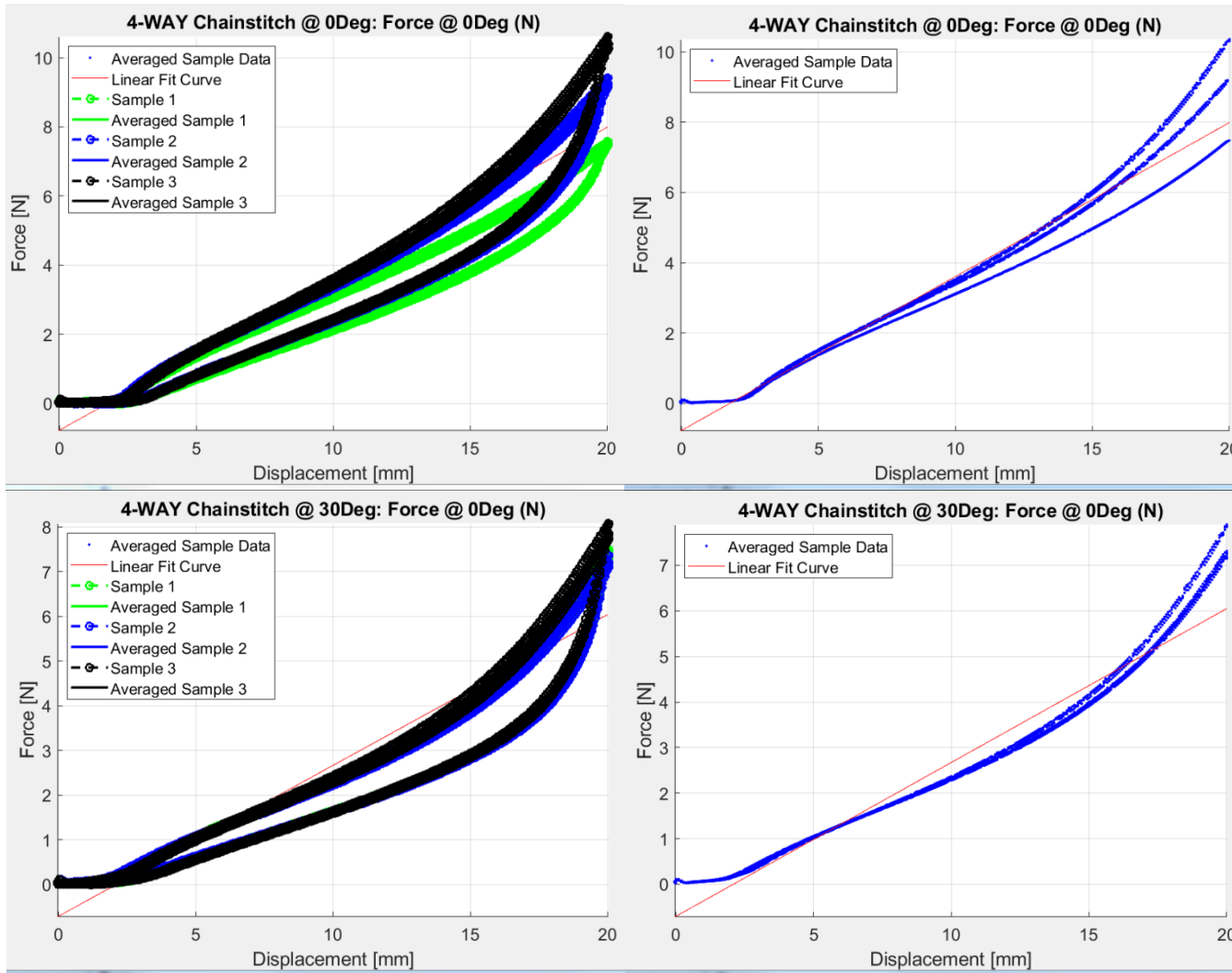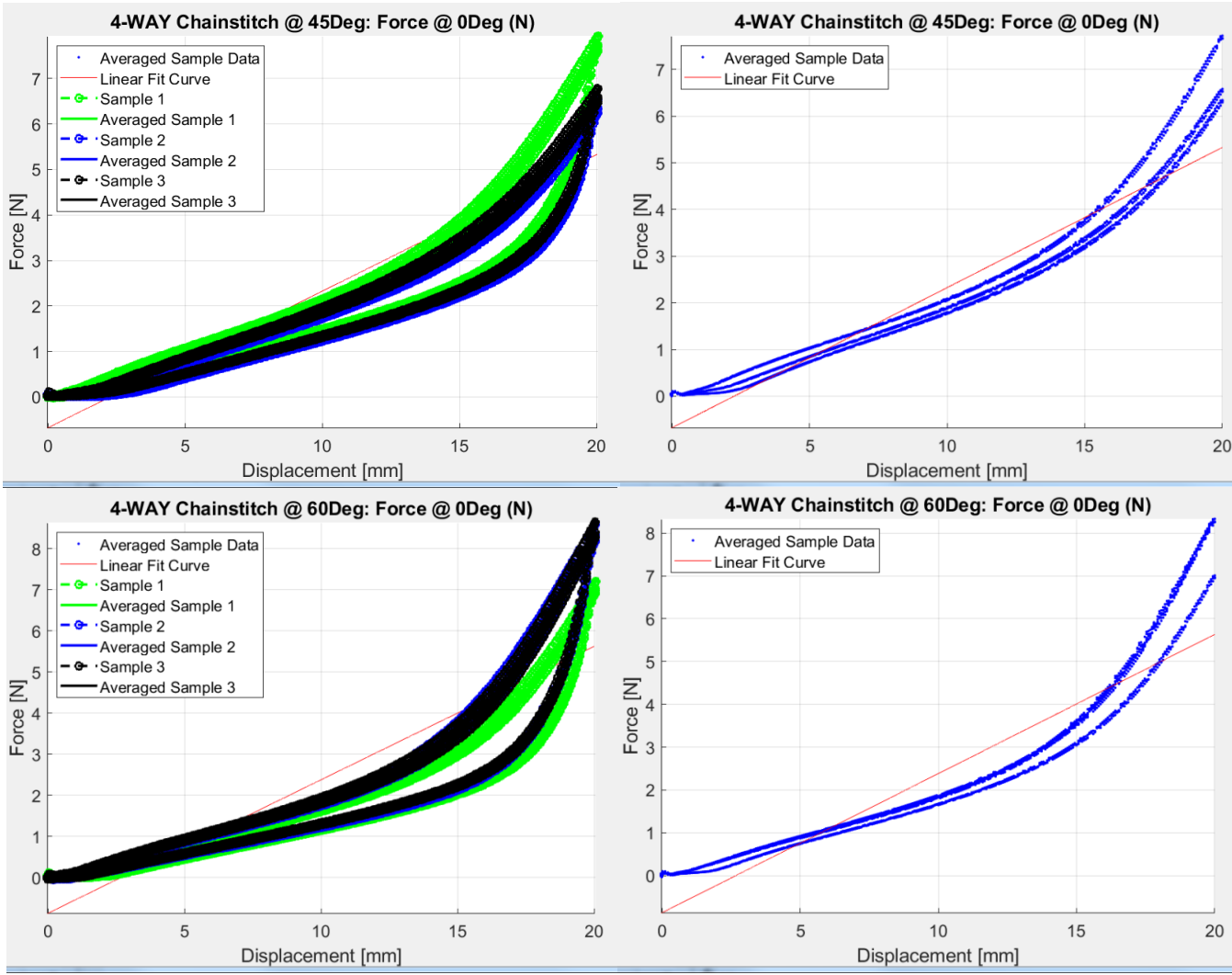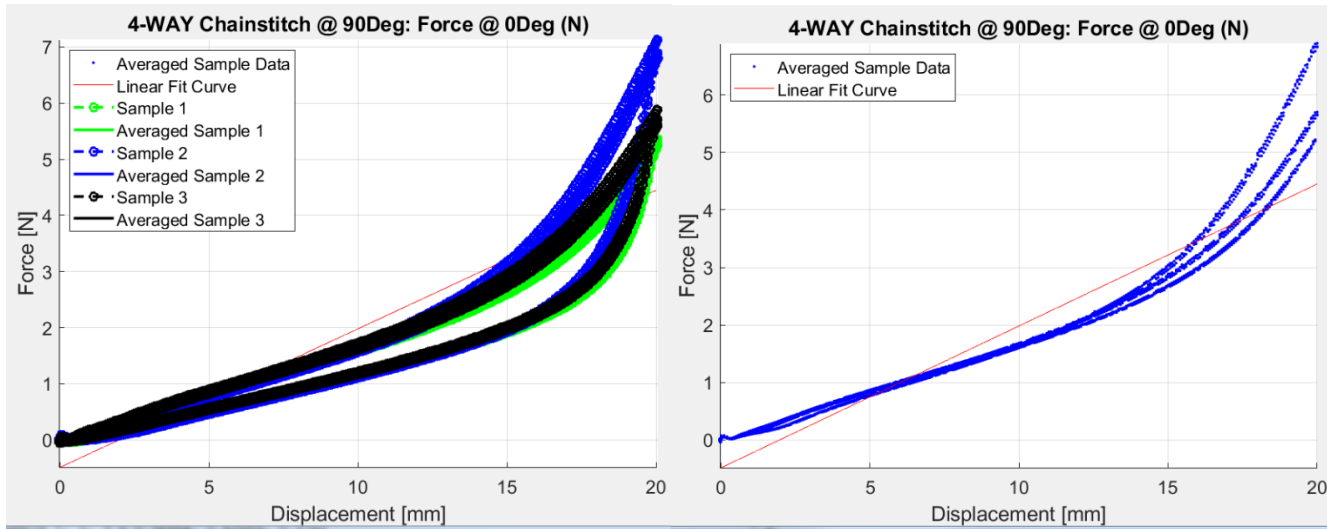The linear fit is given by the form: y=mx+b where y=Force, x=displacement, so that: F=md+b. These linear regressions were calculated using Matlab, and shown for all sample groups in Table B1. The linear fit slope values, linearity fit R^2 and RMSE are summarized in Table B2. Then the linear fit moduli were converted into elastic moduli using a sensor geometry factor to calculate Stress(Strain) values, in the form $\sigma = E\varepsilon + b$. These values are shown similarly in Table B3.

Table B1. Linear Fit Equations of the form F(d)=md+b for RQ1 Results

Sample Group		Linear Fit Equation for Force(Displacement)
4-way knit Fabric-Only	0°	y = 0.38945*x + -0.43197
	30°	y = 0.24751*x + -0.079269
	45°	y = 0.18595*x + 0.084602
	60°	y = 0.15901*x + 0.10183
	90°	y = 0.14131*x + 0.070423
2-way knit Fabric-Only	0°	y = 3.611*x + -16.4641
	30°	y = 0.7783*x + -3.3121
	45°	y = 0.33381*x + -1.1057
	60°	y = 0.22242*x + -0.53047
	90°	y = 0.22094*x + -0.40976
4-way knit Coverstitch	0°	y = 0.35644*x + -0.38603
	30°	y = 0.30655*x + -0.46069
	45°	y = 0.21335*x + -0.23309
	60°	y = 0.19968*x + -0.11568
	90°	y = 0.17083*x + -0.047297
4-way knit Chainstitch	0°	y = 0.43795*x + -0.77388
	30°	y = 0.33782*x + -0.7081
	45°	y = 0.30043*x + -0.67871
	60°	y = 0.32498*x + -0.86783
	90°	y = 0.24693*x + -0.48792
2-way knit Coverstitch	0°	y = 2.2158*x + -10.8789
	30°	y = 0.68688*x + -3.1204
	45°	y = 0.30374*x + -1.0751
	60°	y = 0.25104*x + -0.78751
	90°	y = 0.26377*x + -0.66204
2-way knit Chainstitch	0°	y = 2.7625*x + -13.5772
	30°	y = 0.8872*x + -4.1328
	45°	y = 0.49787*x + -2.1527
	60°	y = 0.41825*x + -1.7034
	90°	y = 0.40327*x + -1.546

Table B2. Force(displacement) slope m(N/mm) and linear fit characteristics

Sample Group	Calculations	Degree from 0°				
		0°	**30°**	**45°**	**60°**	**90°**
4-way knit Coverstitch	m(0°)	0.35644	0.30655	0.21335	0.19968	0.17083
	% of m(0°)	100%	86%	60%	56%	48%
	Fit Line R^2	0.95217	0.99079	0.99318	0.99102	0.99124
	Avg Fit Line RMSE	0.43338	0.169646667	0.10091	0.104737333	0.089331667
	% of fabric only	**92%**	**124%**	**115%**	**126%**	**121%**
4-way knit Chainstitch	m(0°)	0.43795	0.33782	0.30043	0.32498	0.24693
	% of m(0°)	100%	77%	69%	74%	56%
	Fit Line R^2	0.95852	0.95408	0.91688	0.86942	0.90181
	Avg Fit Line RMSE	0.515006667	0.42854	0.516703333	0.729453333	0.457643333
	% of fabric only	**112%**	**136%**	**162%**	**204%**	**175%**
2-way knit Coverstitch	m(0°)	2.2158	0.68688	0.30374	0.25104	0.26377
	% of m(0°)	100%	31%	14%	11%	12%
	Fit Line R^2	0.76489	0.68238	0.88316	0.90794	0.96393
	Avg Fit Line RMSE	7.130833333	2.552766667	0.639606667	0.4614	0.295803333
	% of fabric only	**61%**	**88%**	**91%**	**113%**	**119%**
2-way knit Chainstitch	m(0°)	2.7625	0.8872	0.49787	0.41825	0.40327
	% of m(0°)	100%	32%	18%	15%	15%
	Fit Line R^2	0.75997	0.72083	0.76754	0.76525	0.83567
	Avg Fit Line RMSE	9.009	3.1943	1.586933333	1.34	1.033636667
	% of fabric only	**77%**	**114%**	**149%**	**188%**	**183%**
Color guide:		*+/- 0-20%*	*+/- 21-40%*	*+/- 41-61%*	*+/- 61-80%*	*+/- 81-100%*

Table B3. Stress(strain) slope E(Pa) and linear fit characteristics

Sample Group	Calculations	Degree from 0°				
		0°	30°	45°	60°	90°
4-way knit Coverstitch	E(0°)	0.0071288	0.006131	0.004267	0.0039936	0.0034166
	% of E(0°)	100%	86%	60%	56%	48%
	Fit Line R^2	0.95	0.99	0.99	0.99	0.99
	Avg Fit Line RMSE	0.0087	0.0034	0.0020	0.0021	0.0018
	% of fabric only	**92%**	**124%**	**115%**	**126%**	**121%**
4-way knit Chainstitch	E(0°)	0.008759	0.0067564	0.0060086	0.0064996	0.0049386
	% of E(0°)	100%	77%	69%	74%	56%
	Fit Line R^2	0.96	0.95	0.92	0.87	0.90
	Avg Fit Line RMSE	0.010	0.0086	0.010	0.015	0.0092
	% of fabric only	**112%**	**136%**	**162%**	**204%**	**175%**
2-way knit Coverstitch	E(0°)	0.044316	0.0137376	0.0060748	0.0050208	0.0052754
	% of E(0°)	100%	31%	14%	11%	12%
	Fit Line R^2	0.76	0.68	0.88	0.91	0.96
	Avg Fit Line RMSE	0.14	0.051	0.013	0.0092	0.0059
	% of fabric only	**61%**	**88%**	**91%**	**113%**	**119%**
2-way knit Chainstitch	E(0°)	0.05525	0.017744	0.0099574	0.008365	0.0080654
	% of E(0°)	100%	32%	18%	15%	15%
	Fit Line R^2	0.76	0.72	0.77	0.77	0.84
	Avg Fit Line RMSE	0.18	0.064	0.032	0.027	0.021
	% of fabric only	**77%**	**114%**	**149%**	**188%**	**183%**
Color guide:		+/- 0-20%	+/- 21-40%	+/- 41-61%	+/- 61-80%	+/- 81-100%

Appendix C: Sensor Performance with Inline Forces

Three graphs per test condition were generated: the resistance change from nominal for the full elongation and relaxation cycle (Fig C1, Left), the resistance change from nominal for only the smoothed average elongation portion of the cycle (Fig C1, Center), and the normalized resistance change over the normalized displacement/strain (Fig C1, Right). To provide all the permutations of the graphs created for each of the test conditions during this portion of the study would be excessive for this document, so only one graph per sample group is given. This was chosen to be the normalized resistance per normalized displacement, which is thought to be the most generalizable for future work. If there is interest to view the other graphs, please contact the author.

The graphs are grouped as the 2-way coverstitch sensors stitched at 0°-90° on the knit (Figs C2-C6), then the 2-way Chainstitch sensors (Figs C7-C11), then the 4-way coverstitch sensors (Figs C12-C16), and finally the 4-way Chainstitch sensors (Figs C17-C21). The stitch angles in the figure titles refer to the angle from 0° (stiffest direction/lengthwise/wale knit direction) that the stitched sensor was sewn onto the knit fabric. This section only shows the setup of the force pulled in the same direction as the sensor (so the force angle with respect to the sensor is always 0Deg).
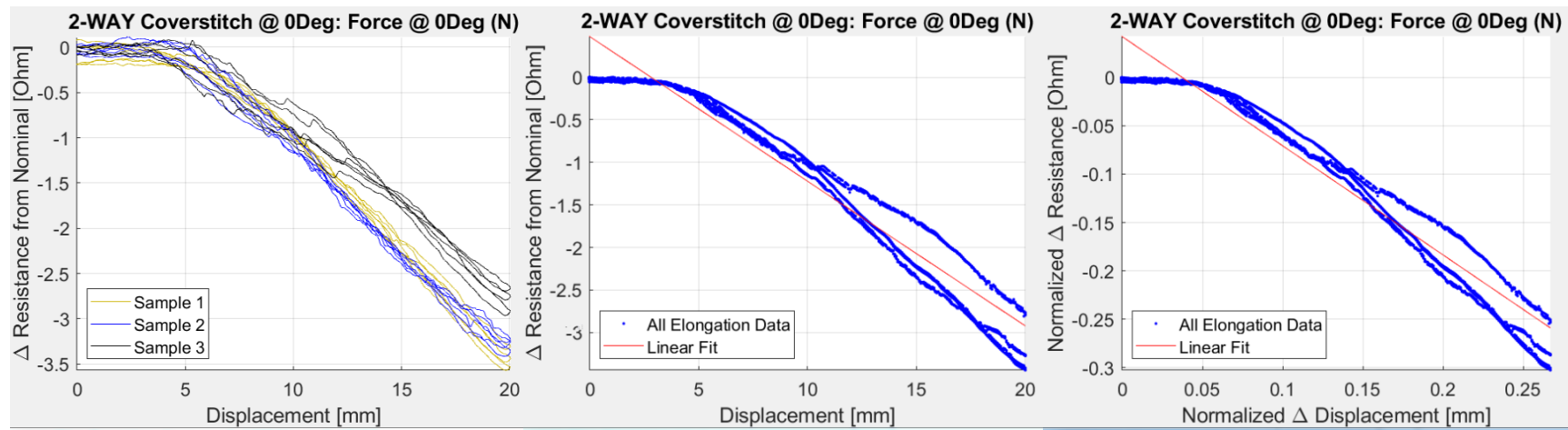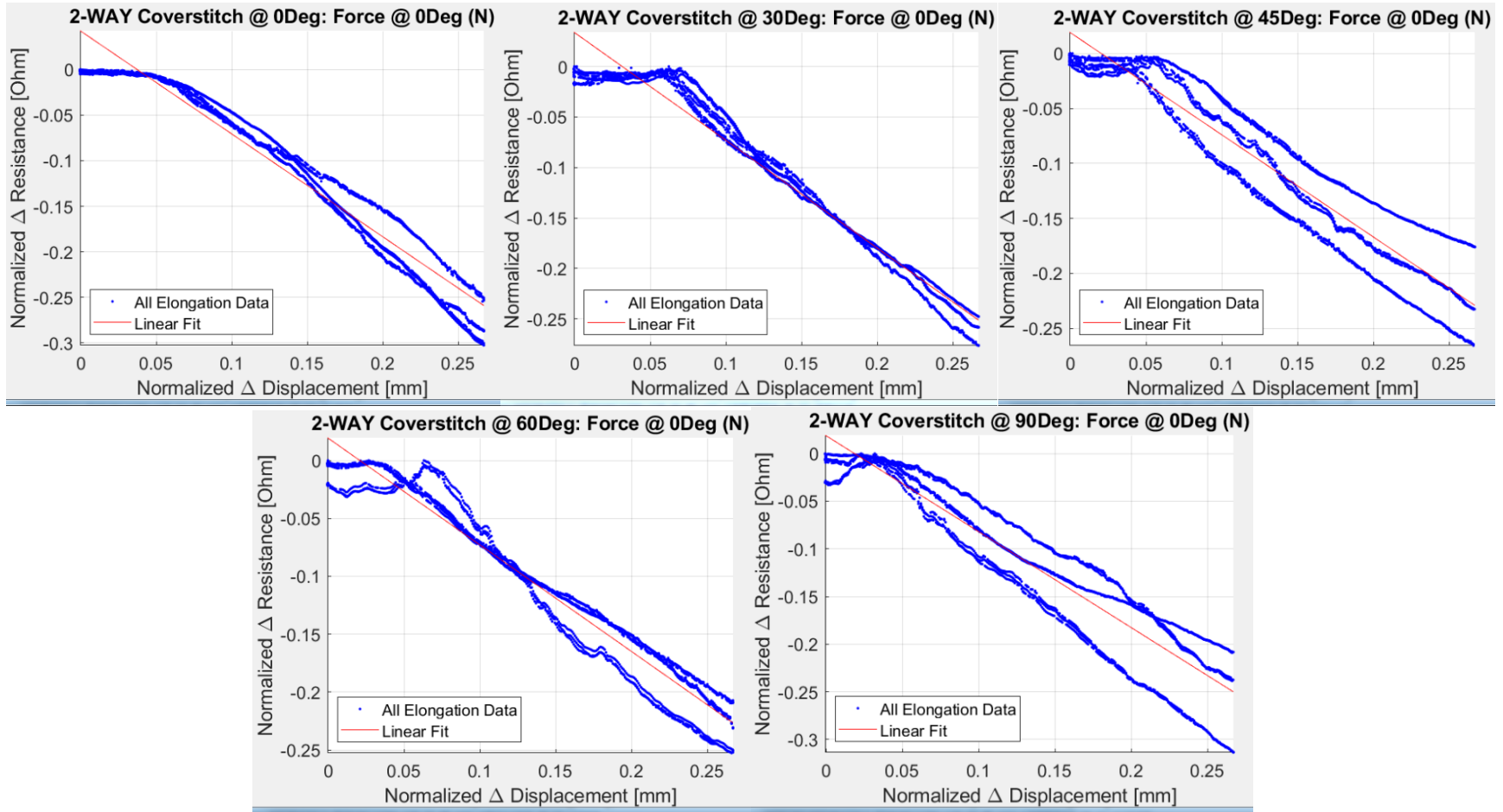

Figure C1: Graphs generated for sensor performance analysis: (Left) Resistance Change vs Displacement for the entire stretch/relaxation cycle (Center) Resistance Change vs Displacement for only the elongation (Right) Normalized Resistance over Strain
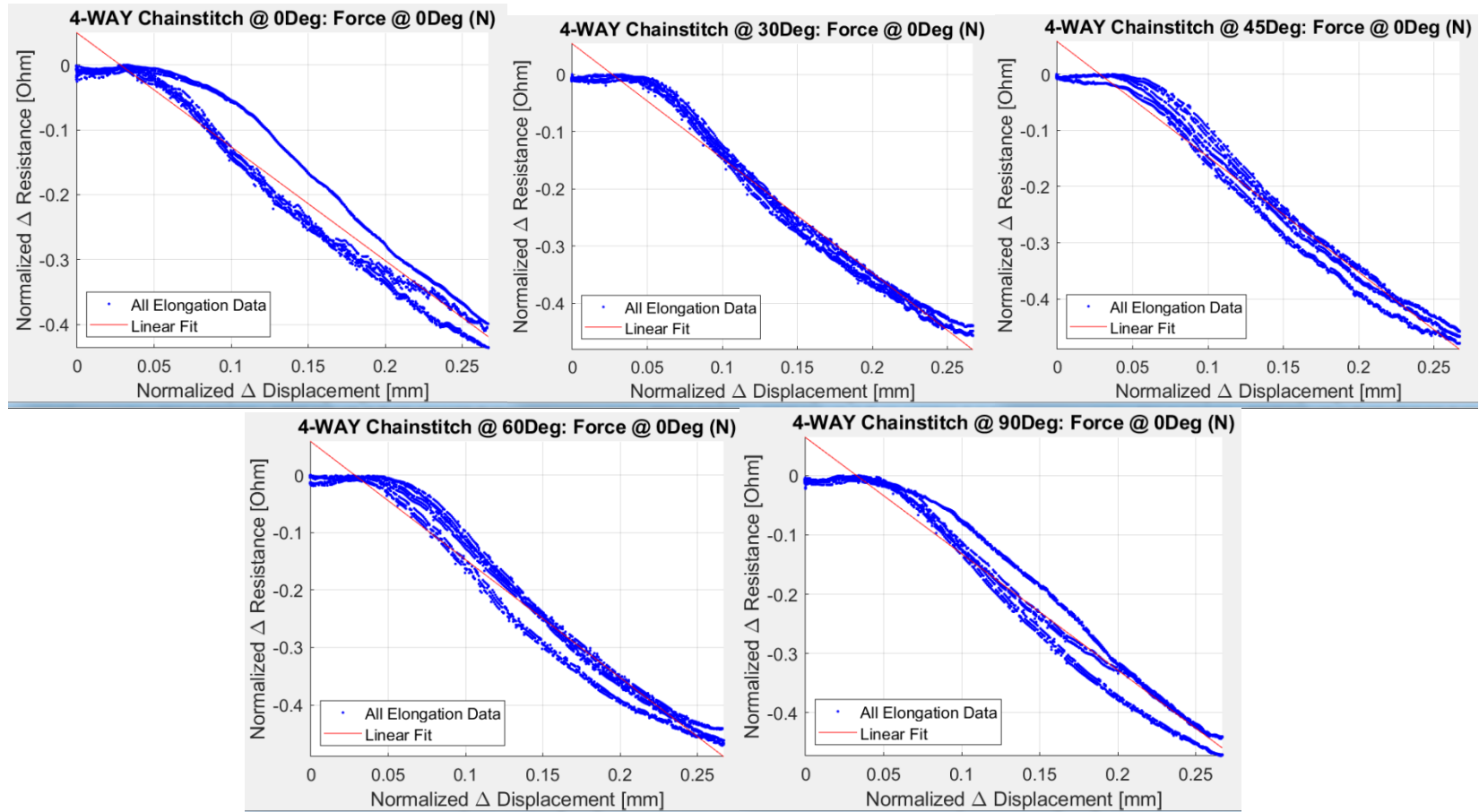
Figures C2-C6. Normalized Resistance vs Strain Graphs for <u>2-way Knit + Coverstitch</u> Sensors sewn at 0°, 30°, 45°, 60°, and 90°
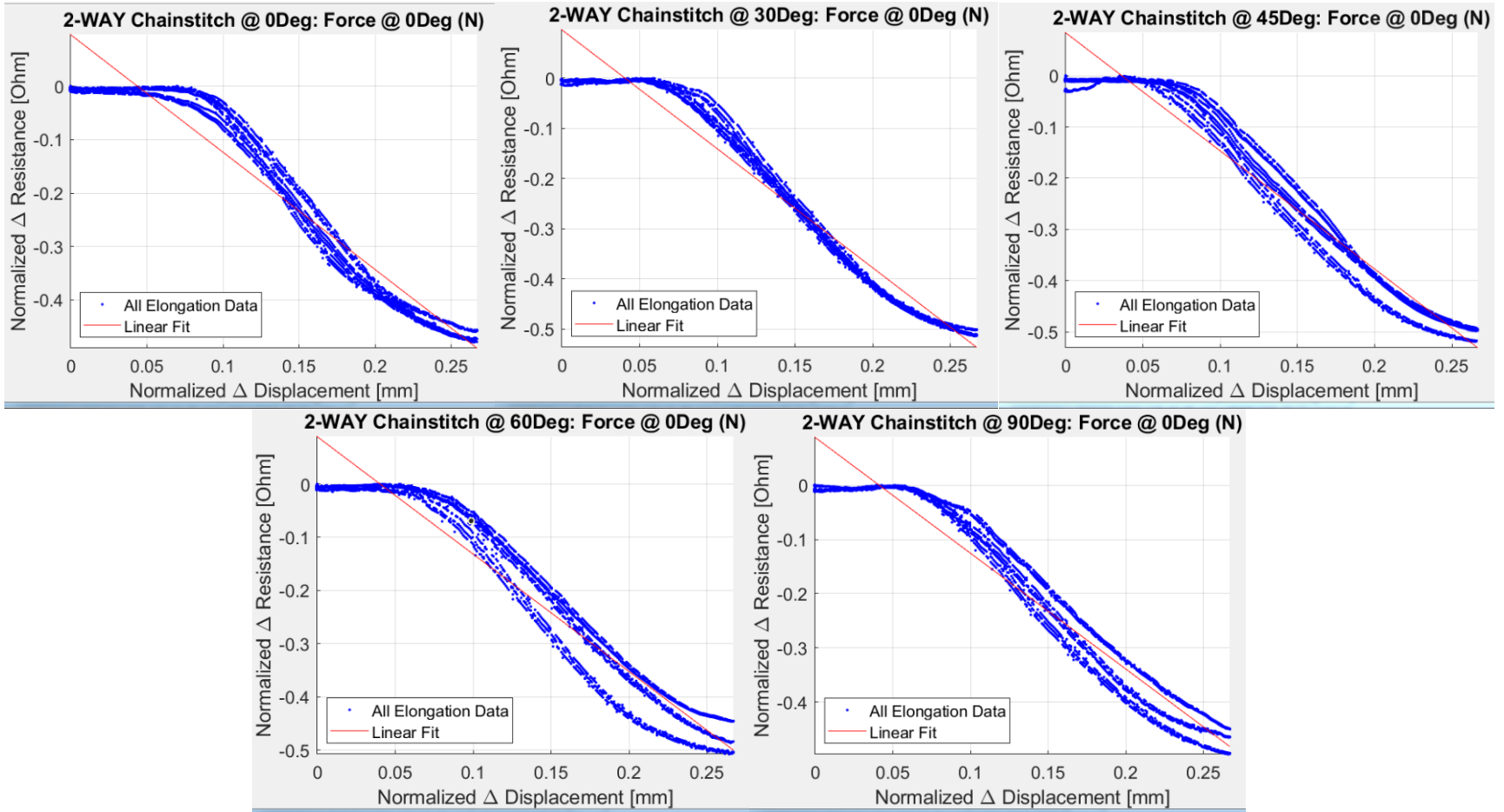
Figures C7-C11. Normalized Resistance vs Strain Graphs for <u>2-way Knit + Chainstitch</u> Sensors sewn at 0°, 30°, 45°, 60°, and 90° stitch angles with respect to the knits lengthwise/wales direction
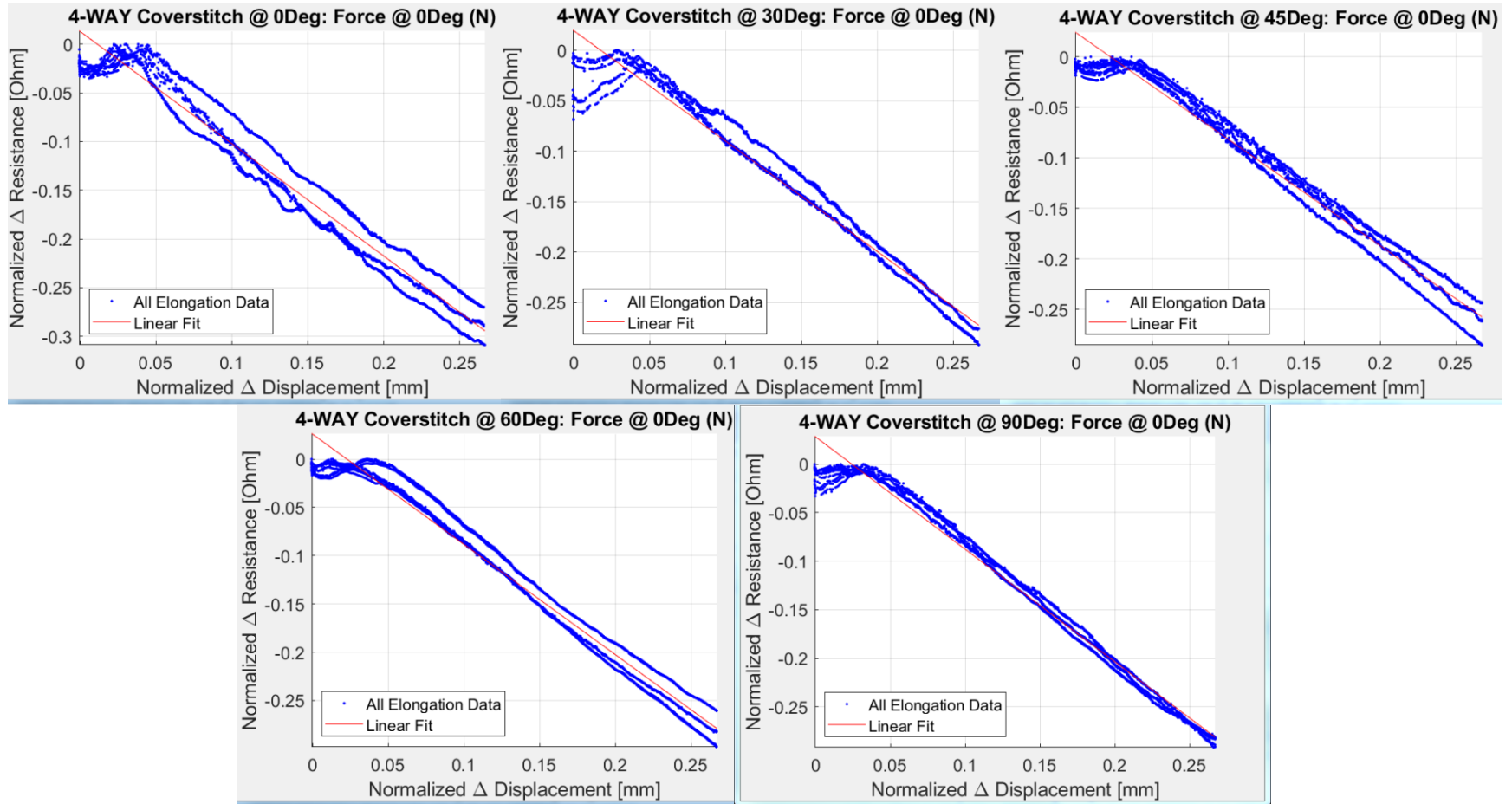
Figures C12-C16. Normalized Resistance vs Strain Graphs for <u>4-way Knit + Coverstitch</u> Sensors sewn at 0°, 30°, 45°, 60°, and 90° stitch angles with respect to the knits lengthwise/wales direction

Figures C17-C21. Normalized Resistance vs Strain Graphs for <u>4-way Knit + Chainstitch</u> Sensors sewn at 0°, 30°, 45°, 60°, and 90° stitch angles with respect to the knits lengthwise/wales direction

The linear fit equations for these graphs, Normalized Resistance = f(Normalized Displacement), are summarized in Table C1.

Table C1. Linear Fit Equation of the form: y=mx+b, where y=Normalized Resistance, x=Normalized Displacement (strain)

Sample Group	Stitch Angle	Force Applied Inline with Stitch Axis
4-way knit Coverstitch	0°	y = -1.1538*x + 0.01322
	30°	y = -1.0946*x + 0.019513
	45°	y = -1.0544*x + 0.023937
	60°	y = -1.143*x + 0.026043
	90°	y = -1.1601*x + 0.028263
4-way knit Chainstitch	0°	y = -1.7554*x + 0.049172
	30°	y = -2.0033*x + 0.053435
	45°	y = -2.0526*x + 0.057926
	60°	y = -2.0567*x + 0.058566
	90°	y = -1.9624*x + 0.06425
2-way knit Coverstitch	0°	y = -1.1293*x + 0.042199
	30°	y = -1.0672*x + 0.033552
	45°	y = -0.93021*x + 0.018963
	60°	y = -0.92177*x + 0.019321
	90°	y = -1.0085*x + 0.018919
2-way knit Chainstitch	0°	y = -2.1973*x + 0.096272
	30°	y = -2.3718*x + 0.096449
	45°	y = -2.3064*x + 0.083889
	60°	y = -2.2067*x + 0.088966
	90°	y = -2.1375*x + 0.088103

Appendix D: Sensor Performance with Offset Forces

The sample groups are organized first by sensor placement (the angle it was sewn into the fabric), then by knit type and stitch geometry. It was organized this way to view how sensor placement may affect the sensor's performance at responding to offset forces. The results for the 0° stitched angle sample groups for both knit types and sensor geometries are presented in the thesis document (Table 11), but also presented here for completeness (Table D1), along with the remainder of the stitch angle groups: 30° (Table D2), 45° (Table D3), 60° (Table D4), and 90° (Table D5).

Table D1. Gauge Factor, Linearity and Error Values for the Stitched Angle 0° sample groups, for Force Direction Angle: 0°-90°

Sample Group	Calculations	Force Direction (Degree from Stitch Axis)				
		0°	30°	45°	60°	90°
4-way knit Coverstitch 0°	GF	-1.1538	-0.71597	-0.49399	-0.089615	-0.70656
	% of GF(0°)	100%	62%	43%	8%	61%
	Fit Line R^2	0.956	0.958	0.851	0.685	0.866
	Fit Line Avg RMSE (Ω)	0.018	0.011	0.015	0.014	0.021
	Hysteresis Error (Ω)	0.81	0.35	0.63	0.55	0.50
4-way knit Chainstitch 0°	GF	-1.7554	-0.78811	-0.23292	-0.080503	-0.22008
	% of GF(0°)	100%	45%	13%	5%	13%
	Fit Line R^2	0.945	0.774	0.640	0.662	0.595
	Fit Line Avg RMSE (Ω)	0.032	0.031	0.013	0.004	0.013
	Hysteresis Error (Ω)	1.29	0.46	0.16	0.14	0.16
2-way knit Coverstitch 0°	GF	-1.1293	-0.80841	-0.73199	-0.76455	-0.91222
	% of GF(0°)	100%	72%	65%	68%	81%
	Fit Line R^2	0.949	0.973	0.915	0.953	0.948
	Fit Line Avg RMSE (Ω)	0.020	0.010	0.017	0.013	0.017
	Hysteresis Error (Ω)	0.28	0.30	0.24	0.24	0.47
2-way knit Chainstitch 0°	GF	-2.1973	-1.025	0.019658	-0.016448	-0.024615
	% of GF(0°)	100%	47%	-1%	1%	1%
	Fit Line R^2	0.933	0.810	0.142	0.035	0.076
	Fit Line Avg RMSE (Ω)	0.046	0.038	0.004	0.006	0.007
	Hysteresis Error (Ω)	1.62	0.39	0.10	0.11	0.14
% of GF(0°) Color guide:		0-10%	11-20%	21-40%	41-60%	61-100%

Table D2. Gauge Factor, Linearity and Error Values for the Stitched Angle 30° sample groups, for Force Direction Angle: 0°-90°

Sample Group	Calculations	Force Direction (Degree from Stitch Axis)				
		0°	30°	45°	60°	90°
4-way knit Coverstitch 30°	GF	-1.0946	-0.6801	-0.4981	-0.54821	-0.68969
	% of GF(0°)	100%	62%	46%	50%	63%
	Fit Line R^2	0.966	0.866	0.727	0.934	0.896
	Fit Line Avg RMSE (Ω)	0.015	0.020	0.022	0.011	0.017
	Hysteresis Error (Ω)	0.46	0.25	0.36	0.45	0.28
4-way knit Chainstitch 30°	GF	-2.0033	-1.4659	-0.67142	-0.30334	-0.13559
	% of GF(0°)	100%	73%	34%	15%	7%
	Fit Line R^2	0.977	0.977	0.920	0.950	0.705
	Fit Line Avg RMSE (Ω)	0.024	0.017	0.016	0.011	0.007
	Hysteresis Error (Ω)	1.64	0.92	0.32	0.12	0.13
2-way knit Coverstitch 30°	GF	-1.0672	-0.89907	-0.71471	-0.70667	-0.94836
	% of GF(0°)	100%	84%	67%	66%	89%
	Fit Line R^2	0.964	0.952	0.911	0.896	0.986
	Fit Line Avg RMSE (Ω)	0.016	0.015	0.017	0.019	0.009
	Hysteresis Error (Ω)	0.43	0.31	0.29	0.32	0.50
2-way knit Chainstitch 30°	GF	-2.3718	-1.8578	-0.84607	-0.082691	-0.58647
	% of GF(0°)	100%	78%	36%	3%	25%
	Fit Line R^2	0.954	0.944	0.900	0.672	0.836
	Fit Line Avg RMSE (Ω)	0.040	0.034	0.021	0.004	0.020
	Hysteresis Error (Ω)	1.84	1.21	0.79	0.10	0.29
% of GF(0°) Color guide:		0-10%	11-20%	21-40%	41-60%	61-100%

Table D3. Gauge Factor, Linearity and Error Values for the Stitched Angle 45° sample groups, for Force Direction Angle: 0°-90°

| Sample Group	Calculations	Force Direction (Degree from Stitch Axis)				
		0°	30°	45°	60°	90°
4-way knit Coverstitch 45°	GF	-1.0544	-0.83621	-0.5947	-0.54466	-0.55551
	% of GF(0°)	100%	79%	56%	52%	53%
	Fit Line R²	0.973	0.964	0.945	0.968	0.950
	Fit Line Avg RMSE (Ω)	0.013	0.012	0.011	0.008	0.010
	Hysteresis Error (Ω)	0.36	0.31	0.36	0.47	0.28
4-way knit Chainstitch 45°	GF	-2.0526	-1.501	-0.57711	-0.18911	-0.21722
	% of GF(0°)	100%	73%	28%	9%	11%
	Fit Line R²	0.973	0.960	0.924	0.921	0.878
	Fit Line Avg RMSE (Ω)	0.026	0.024	0.013	0.004	0.006
	Hysteresis Error (Ω)	1.51	0.86	0.22	0.10	0.16
2-way knit Coverstitch 45°	GF	-0.93021	-0.85151	-0.68566	-0.76769	-0.90801
	% of GF(0°)	100%	92%	74%	83%	98%
	Fit Line R²	0.887	0.930	0.891	0.916	0.850
	Fit Line Avg RMSE (Ω)	0.024	0.018	0.019	0.018	0.028
	Hysteresis Error (Ω)	0.52	0.31	0.34	0.38	0.53
2-way knit Chainstitch 45°	GF	-2.3064	-1.6553	-0.43243	-0.14931	-0.81941
	% of GF(0°)	100%	72%	19%	6%	36%
	Fit Line R²	0.948	0.948	0.905	0.641	0.866
	Fit Line Avg RMSE (Ω)	0.041	0.029	0.021	0.011	0.025
	Hysteresis Error (Ω)	1.73	1.10	0.30	0.13	0.38
% of GF(0°) Color guide:		0-10%	11-20%	21-40%	41-60%	61-100%

Table D4. Gauge Factor, Linearity and Error Values for the Stitched Angle 60° sample groups, for Force Direction Angle: 0°-90°

Sample Group	Calculations	Force Direction (Degree from Stitch Axis)				
		0°	30°	45°	60°	90°
4-way knit Coverstitch 60°	GF	-1.143	-0.86337	-0.63305	-0.57436	-0.60921
	% of GF(0°)	100%	76%	55%	50%	53%
	Fit Line R²	0.976	0.987	0.965	0.962	0.963
	Fit Line Avg RMSE (Ω)	0.013	0.008	0.009	0.009	0.009
	Hysteresis Error (Ω)	0.29	0.29	0.43	0.43	0.23
4-way knit Chainstitch 60°	GF	-2.0567	-1.3337	-0.64921	-0.19339	-0.13488
	% of GF(0°)	100%	65%	32%	9%	7%
	Fit Line R²	0.969	0.891	0.905	0.783	0.633
	Fit Line Avg RMSE (Ω)	0.028	0.035	0.016	0.007	0.007
	Hysteresis Error (Ω)	1.35	0.65	0.20	0.12	0.13
2-way knit Coverstitch 60°	GF	-0.92177	-0.78347	-0.71639	-0.81569	-1.0269
	% of GF(0°)	100%	85%	78%	88%	111%
	Fit Line R²	0.951	0.951	0.917	0.883	0.845
	Fit Line Avg RMSE (Ω)	0.015	0.014	0.017	0.022	0.032
	Hysteresis Error (Ω)	0.44	0.45	0.41	0.36	0.74
2-way knit Chainstitch 60°	GF	-2.2067	-1.5778	-0.37818	-0.07245	-0.7569
	% of GF(0°)	100%	72%	17%	3%	34%
	Fit Line R²	0.934	0.909	0.371	0.417	0.832
	Fit Line Avg RMSE (Ω)	0.045	0.038	0.034	0.006	0.026
	Hysteresis Error (Ω)	1.65	0.86	0.21	0.09	0.35
% of GF(0°) Color guide:		0-10%	11-20%	21-40%	41-60%	61-100%

Table D5. Gauge Factor, Linearity and Error Values for the Stitched Angle 90° sample groups, for Force Direction Angle: 0°-90°

Sample Group	Calculations	Force Direction (Degree from Stitch Axis)				
		0°	30°	45°	60°	90°
4-way knit Coverstitch 90°	GF	-1.1601	-0.94217	-0.74592	-0.61632	-0.64227
	% of GF(0°)	100%	81%	64%	53%	55%
	Fit Line R²	0.983	0.939	0.979	0.918	0.902
	Fit Line Avg RMSE (Ω)	0.011	0.018	0.013	0.014	0.016
	Hysteresis Error (Ω)	0.35	0.36	0.44	0.44	0.26
4-way knit Chainstitch 90°	GF	-1.9624	-1.3346	-0.72945	-0.2066	-0.1607
	% of GF(0°)	100%	68%	37%	11%	8%
	Fit Line R²	0.960	0.823	0.776	0.847	0.529
	Fit Line Avg RMSE (Ω)	0.030	0.046	0.029	0.007	0.011
	Hysteresis Error (Ω)	1.49	0.81	0.30	0.12	0.16
2-way knit Coverstitch 90°	GF	-1.0085	-0.77428	-0.79663	-1.0056	-1.2591
	% of GF(0°)	100%	77%	79%	100%	125%
	Fit Line R²	0.879	0.805	0.926	0.941	0.764
	Fit Line Avg RMSE (Ω)	0.028	0.029	0.017	0.019	0.051
	Hysteresis Error (Ω)	0.44	0.41	0.36	0.30	0.83
2-way knit Chainstitch 90°	GF	-2.1375	-1.6898	-0.94156	-0.28301	-0.74615
	% of GF(0°)	100%	79%	44%	13%	35%
	Fit Line R²	0.941	0.916	0.876	0.785	0.829
	Fit Line Avg RMSE (Ω)	0.041	0.040	0.027	0.011	0.026
	Hysteresis Error (Ω)	1.17	0.81	0.52	0.16	0.33
% of GF(0°) Color guide:		0-10%	11-20%	21-40%	41-60%	61-100%

In this part of the study, three graphs per test condition were generated similarly to previous (see Appendix C). To provide all the permutations of the graphs created for each of the test conditions during this portion of the study would be excessive, so only one graph per sample group is given. This was chosen to be the normalized resistance per normalized displacement for the elongation direction only, which is thought to be the most generalizable for future work. If there is interest to view the other graphs, please contact the author.
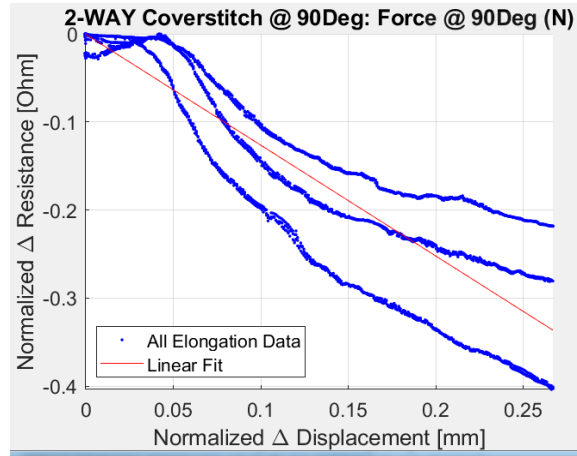
The graphs are grouped as the 2-way coverstitch sensors stitched at 0°-90° on the knit (D1-D25), then the 2-way Chainstitch sensors (D26-D50), then the 4-way coverstitch sensors (D51-D75), and finally the 4-way Chainstitch sensors (D76-D100).
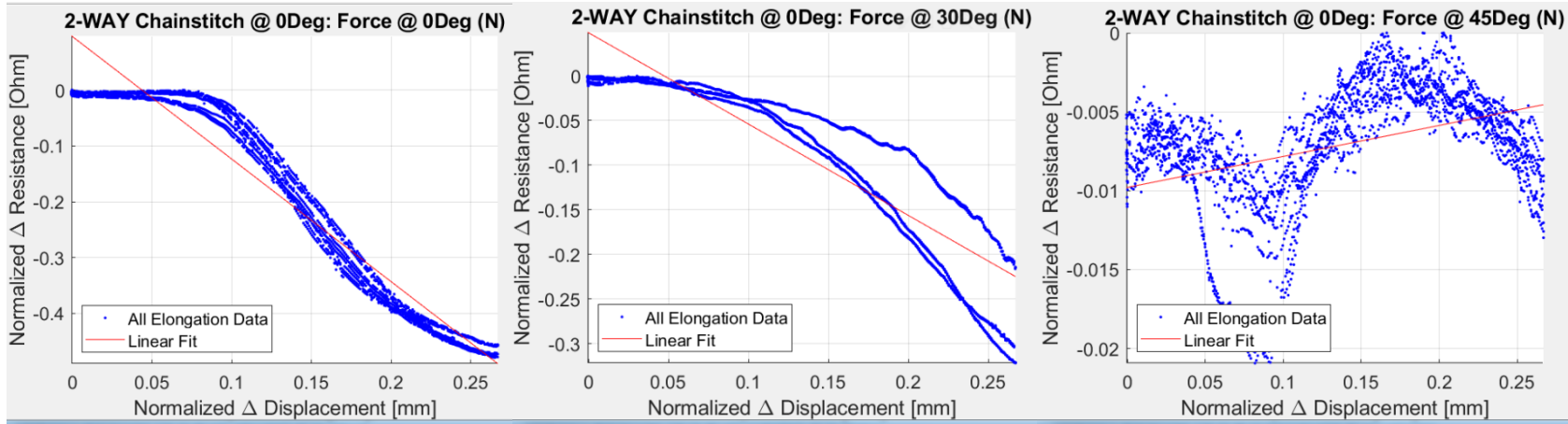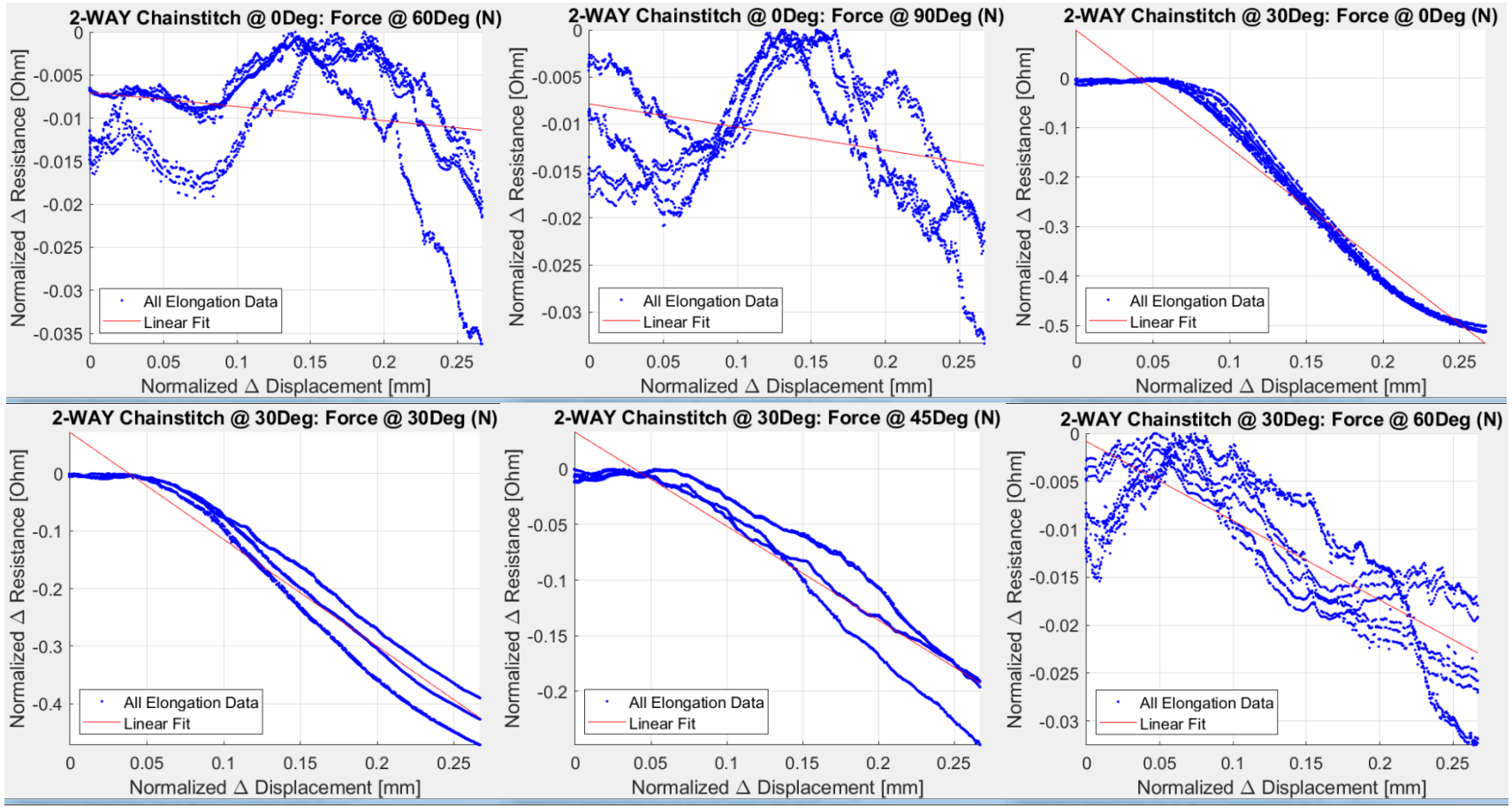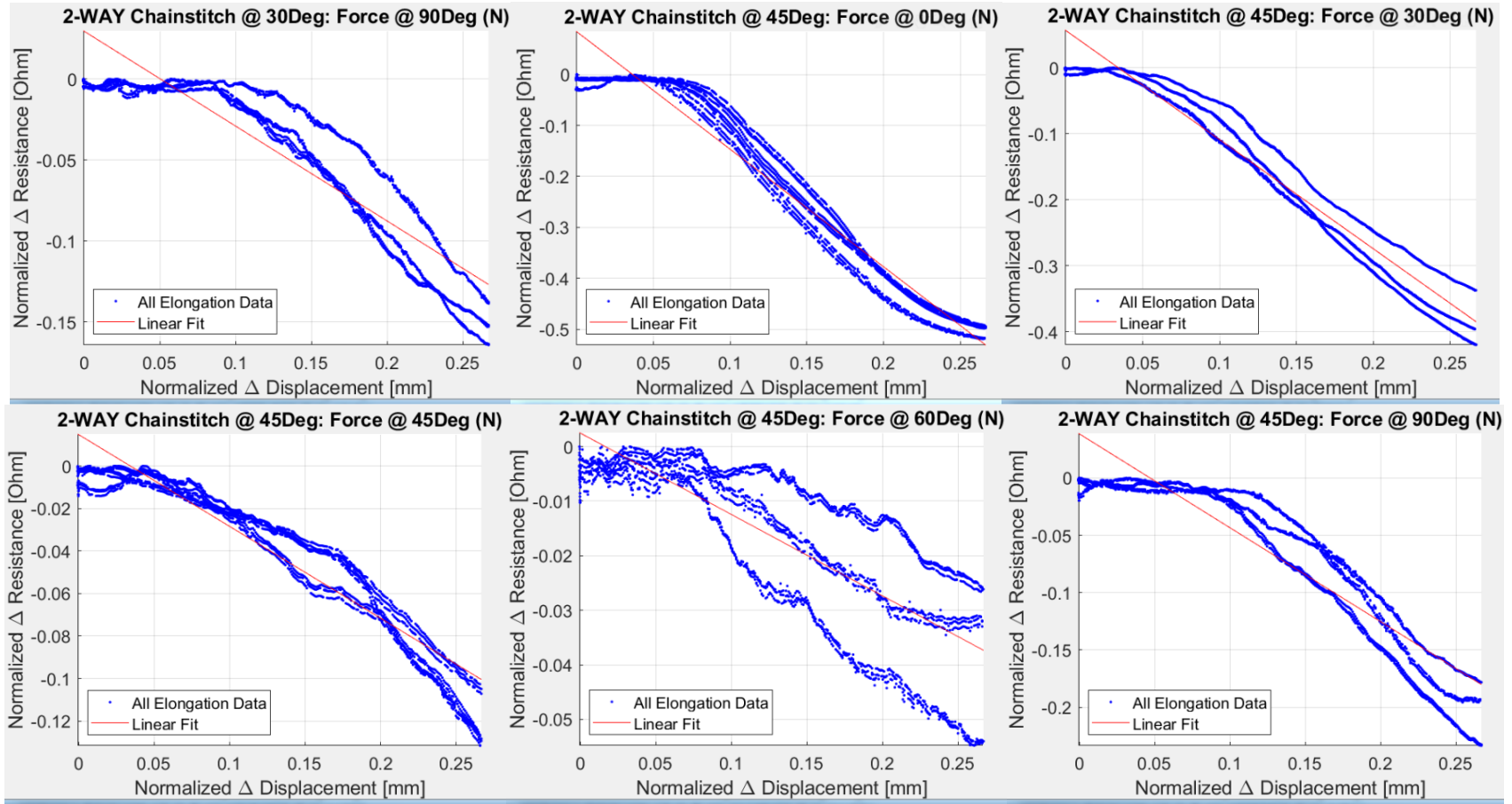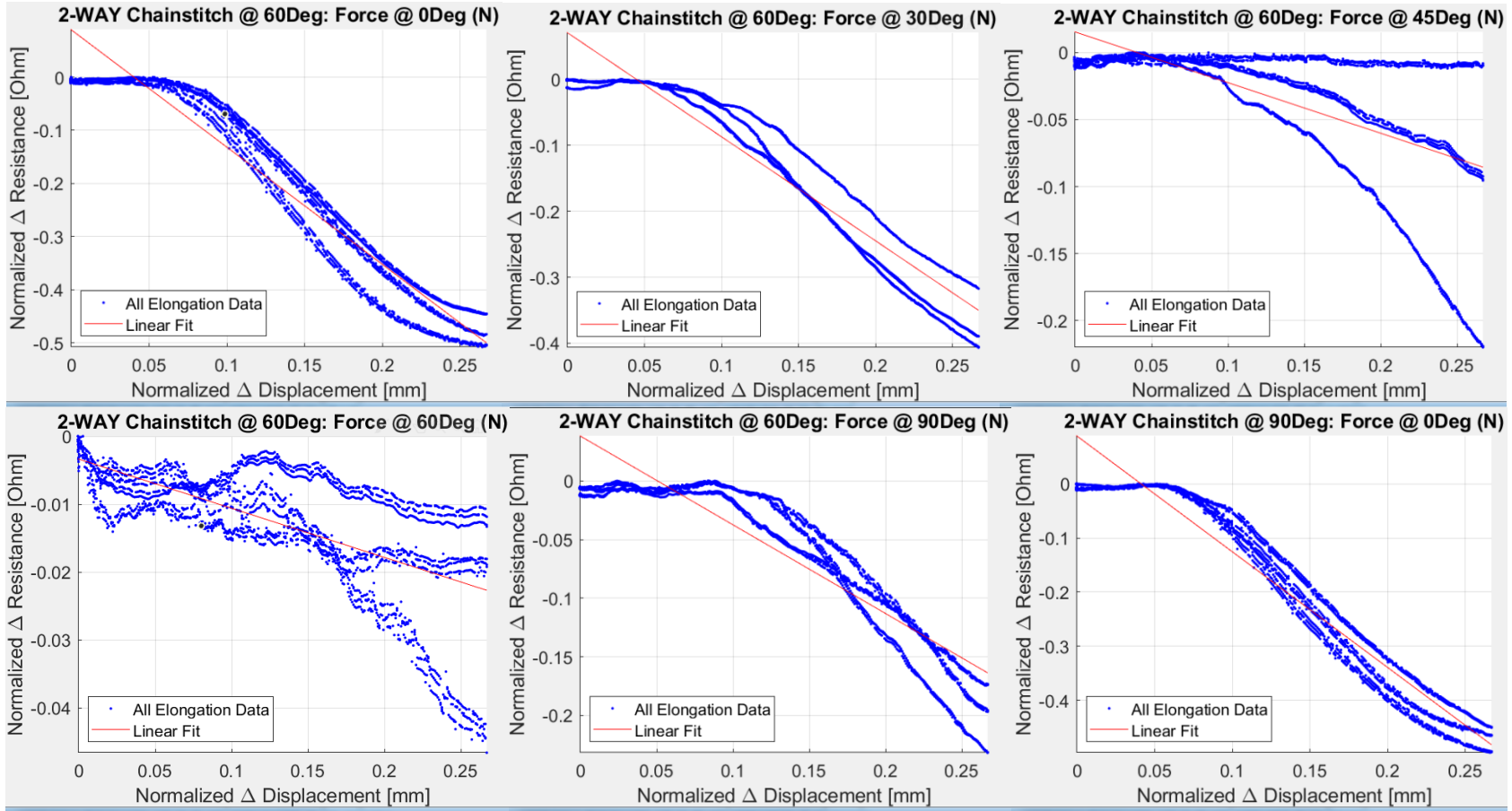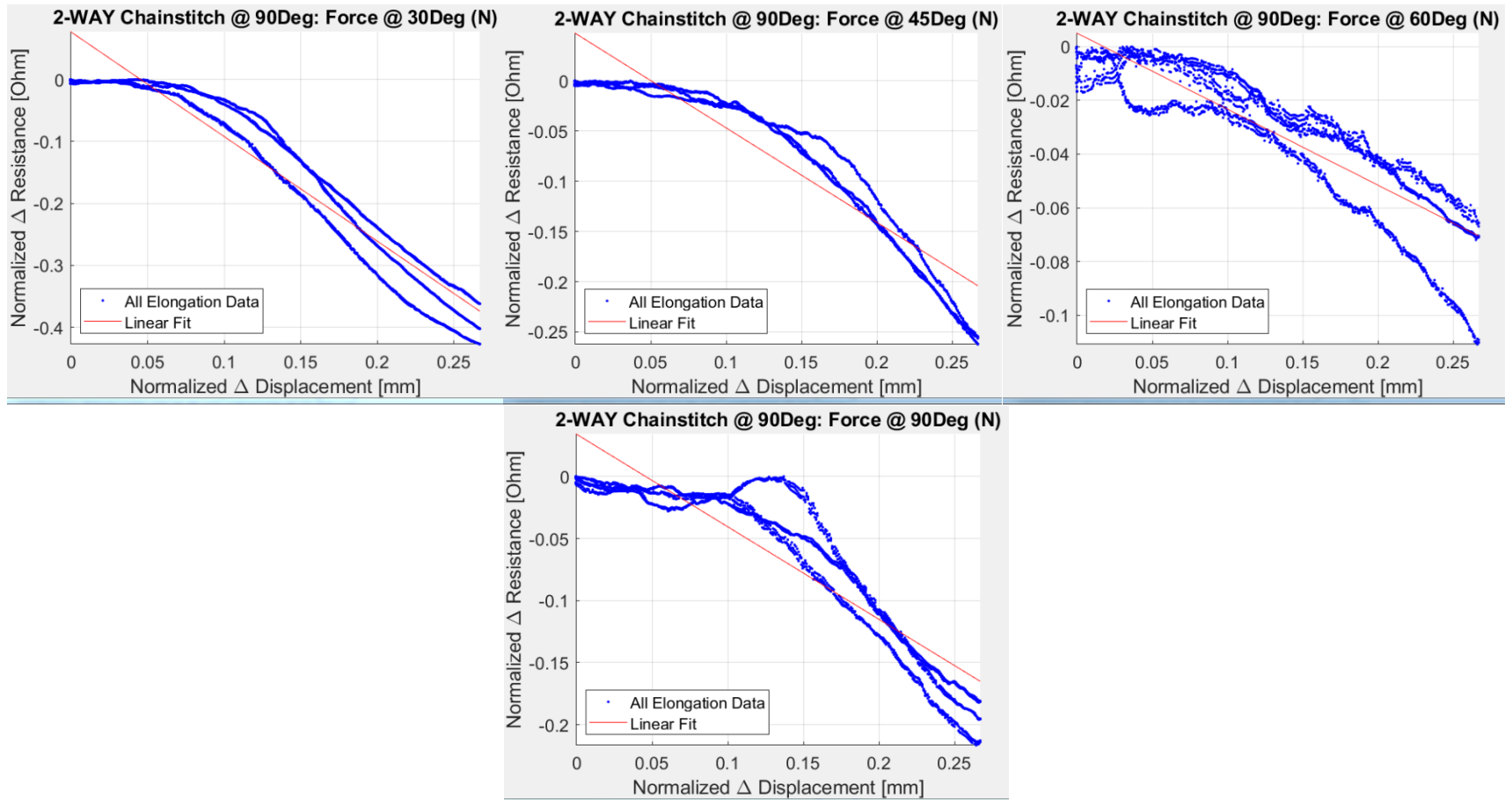
135

137

138
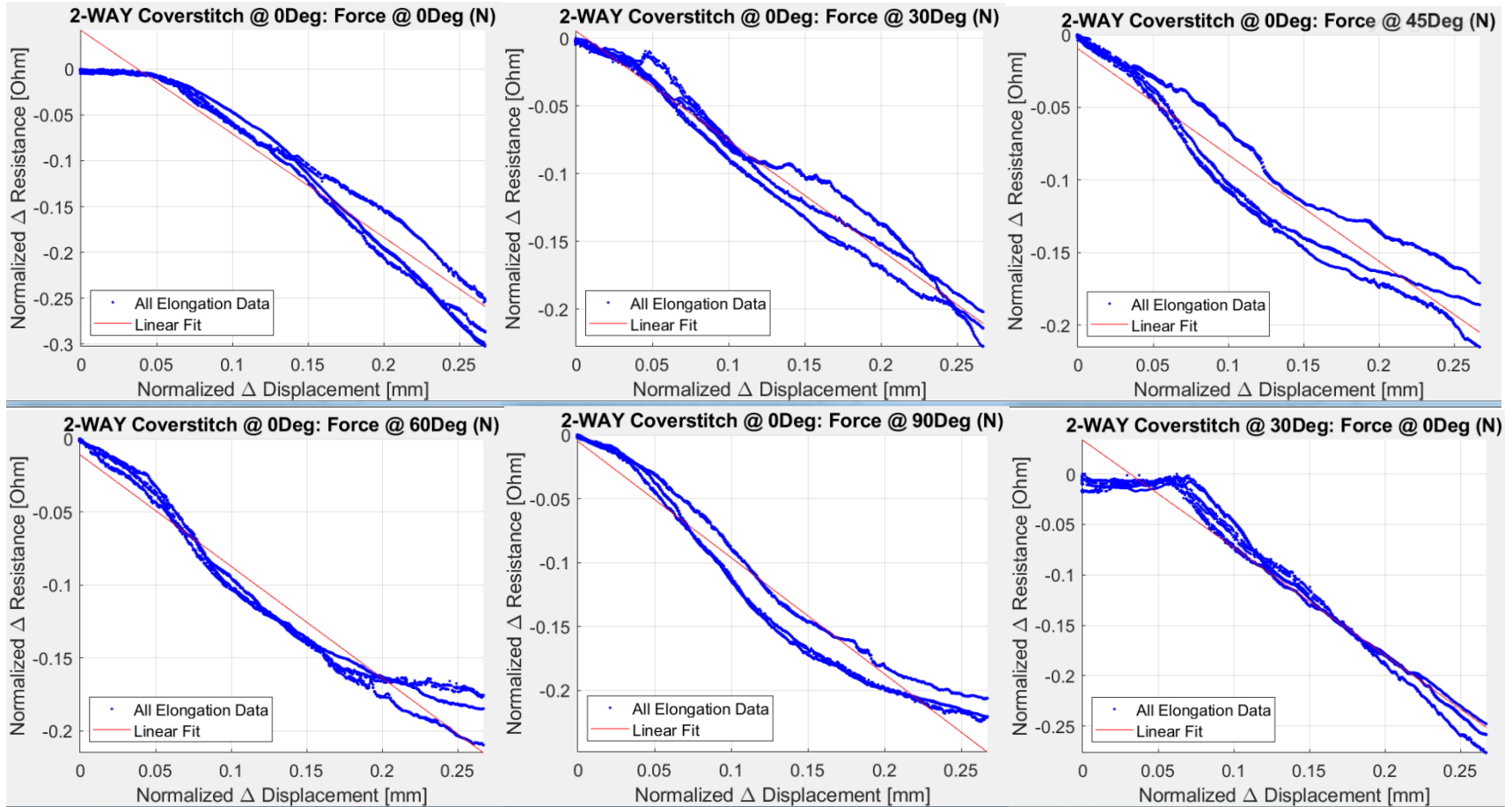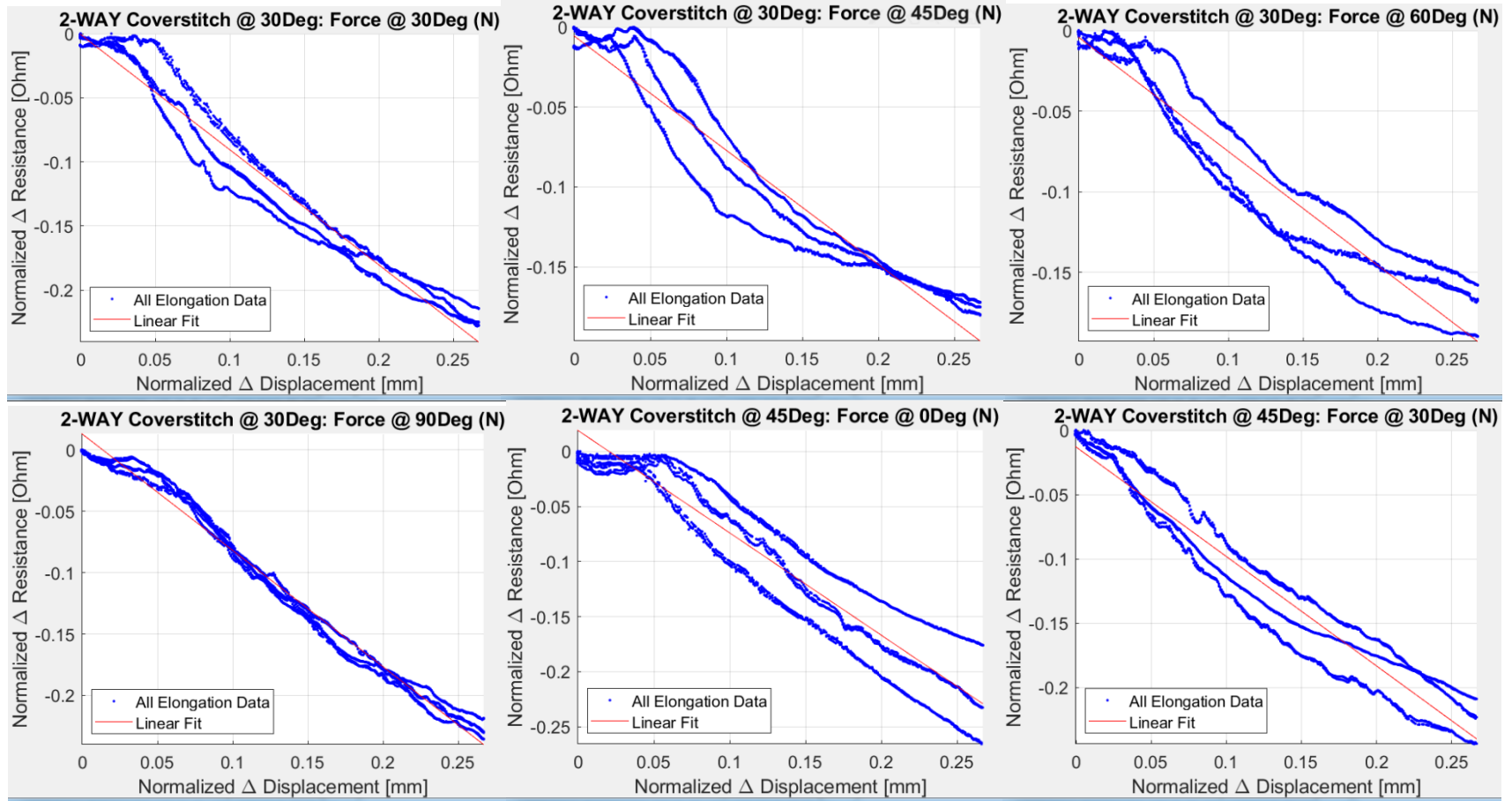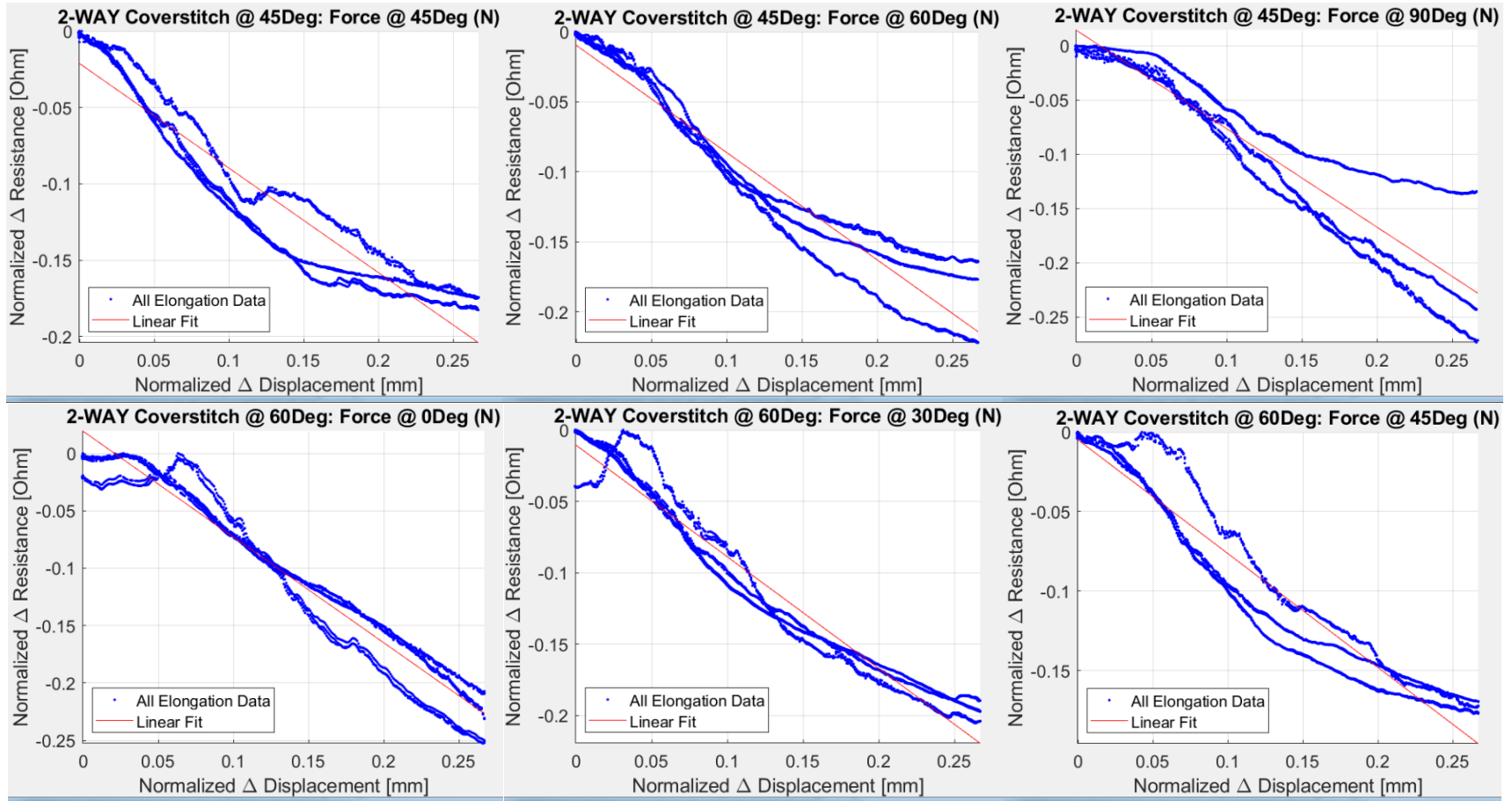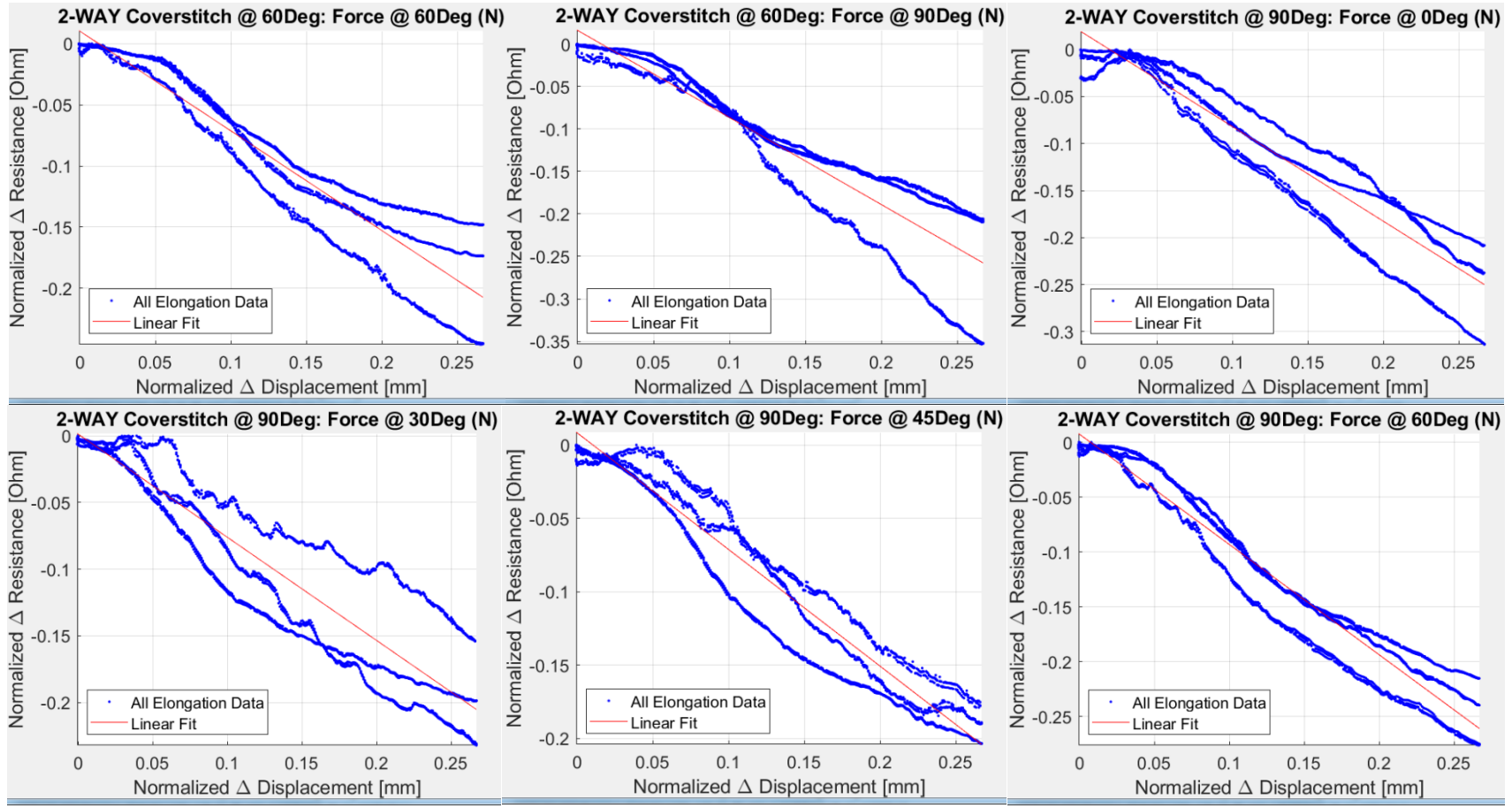
Figures D1-D25. Normalized Resistance vs Strain Graphs for <u>2-way Knit + Coverstitch Sensors</u> sewn at 0°, 30°, 45°, 60°, and 90° stitch angles with respect to the knits lengthwise/wales direction, with applied force at 0°, 30°, 45°, 60°, and 90° with respect to the sensor axis

140

2-WAY Chainstitch @ 30Deg: Force @ 90Deg (N)

2-WAY Chainstitch @ 45Deg: Force @ 0Deg (N)

2-WAY Chainstitch @ 45Deg: Force @ 30Deg (N)

2-WAY Chainstitch @ 45Deg: Force @ 45Deg (N)

2-WAY Chainstitch @ 45Deg: Force @ 60Deg (N)

2-WAY Chainstitch @ 45Deg: Force @ 90Deg (N)

2-WAY Chainstitch @ 60Deg: Force @ 0Deg (N)

2-WAY Chainstitch @ 60Deg: Force @ 30Deg (N)

2-WAY Chainstitch @ 60Deg: Force @ 45Deg (N)

2-WAY Chainstitch @ 60Deg: Force @ 60Deg (N)

2-WAY Chainstitch @ 60Deg: Force @ 90Deg (N)

2-WAY Chainstitch @ 90Deg: Force @ 0Deg (N)

Figures D26-D50. Normalized Resistance vs Strain Graphs for <u>2-way Knit + Chainstitch Sensors</u> sewn at 0°, 30°, 45°, 60°, and 90° stitch angles with respect to the knits lengthwise/wales direction, with applied force at 0°, 30°, 45°, 60°, and 90° with respect to the sensor axis
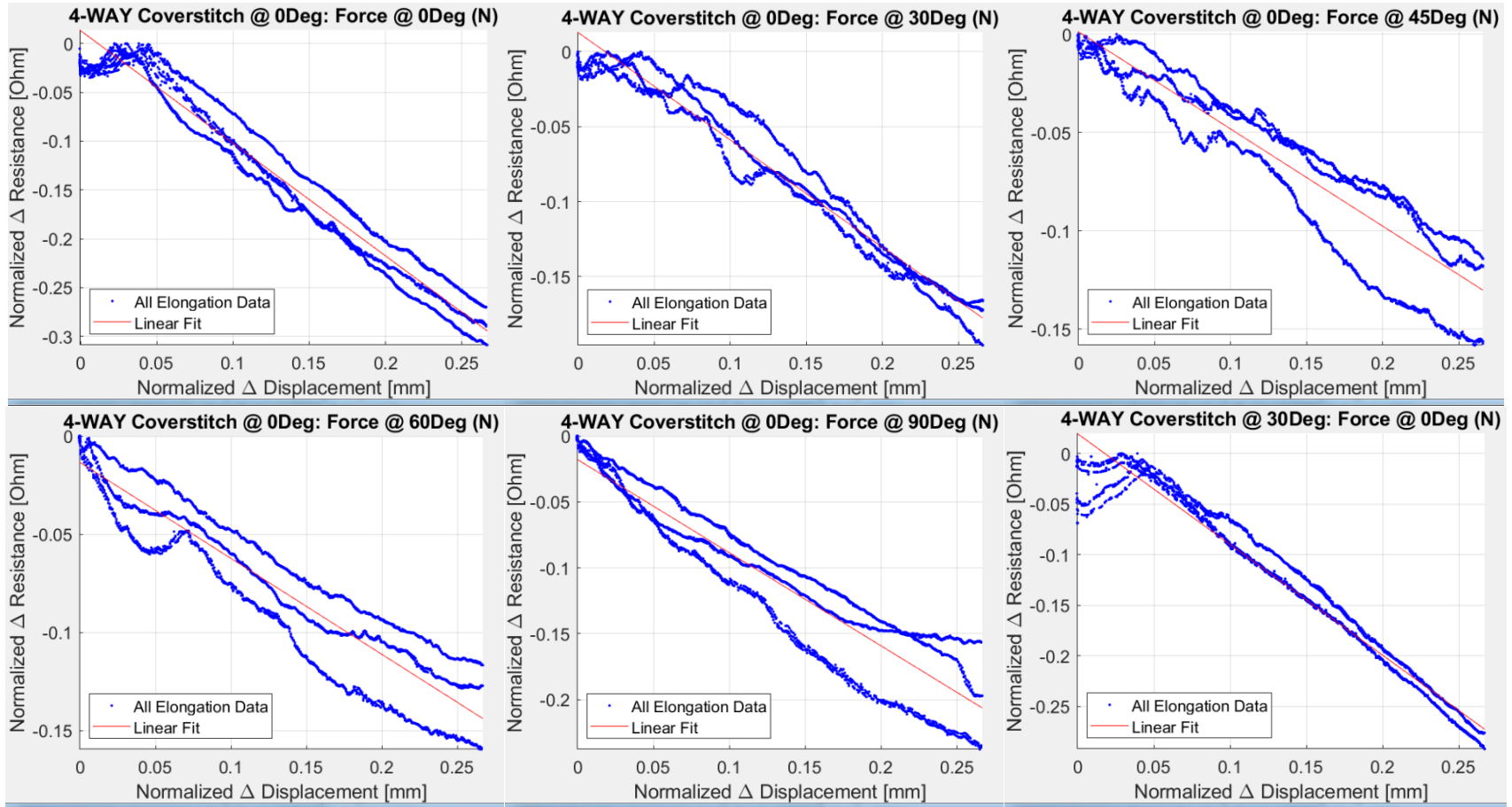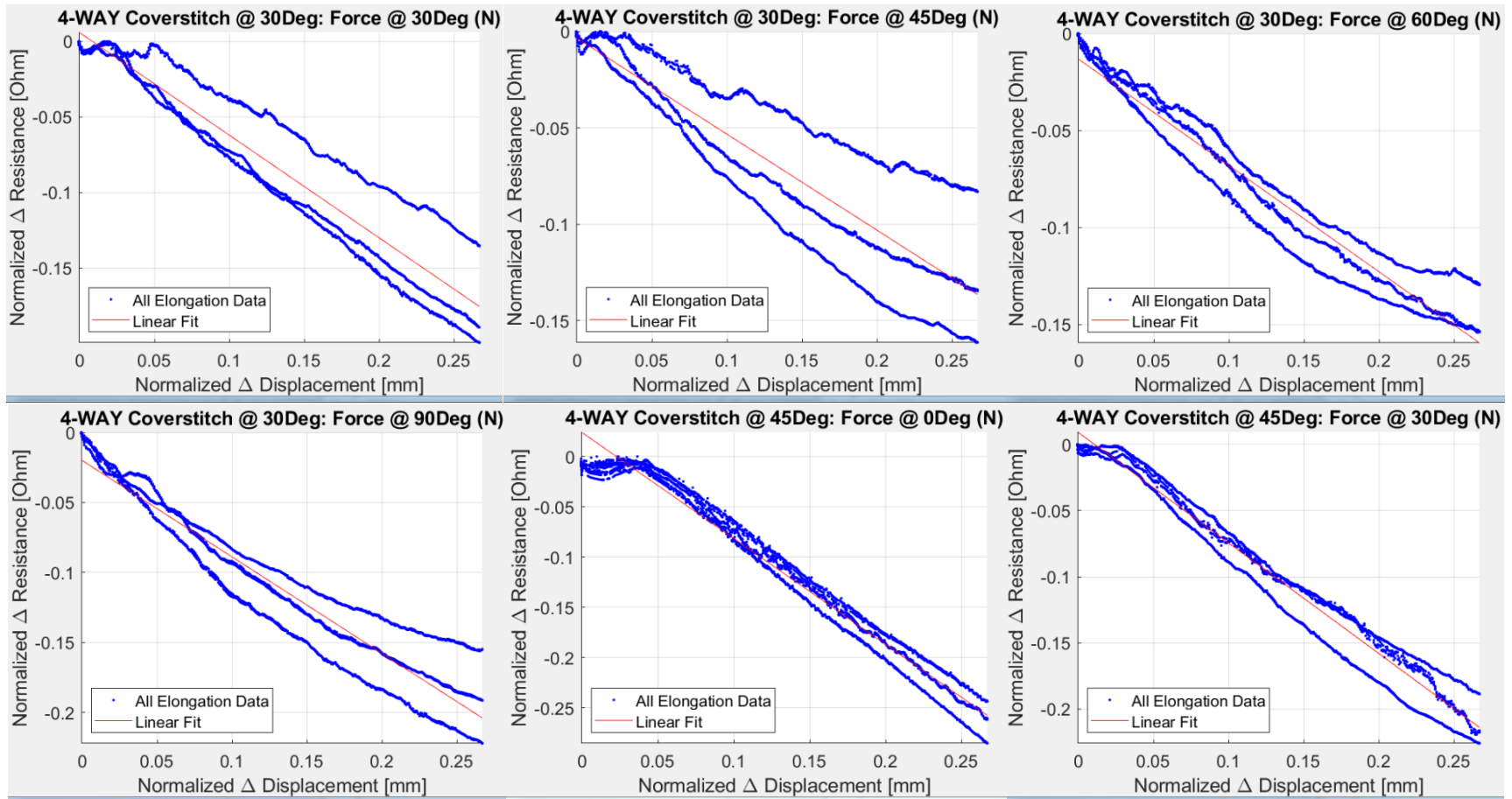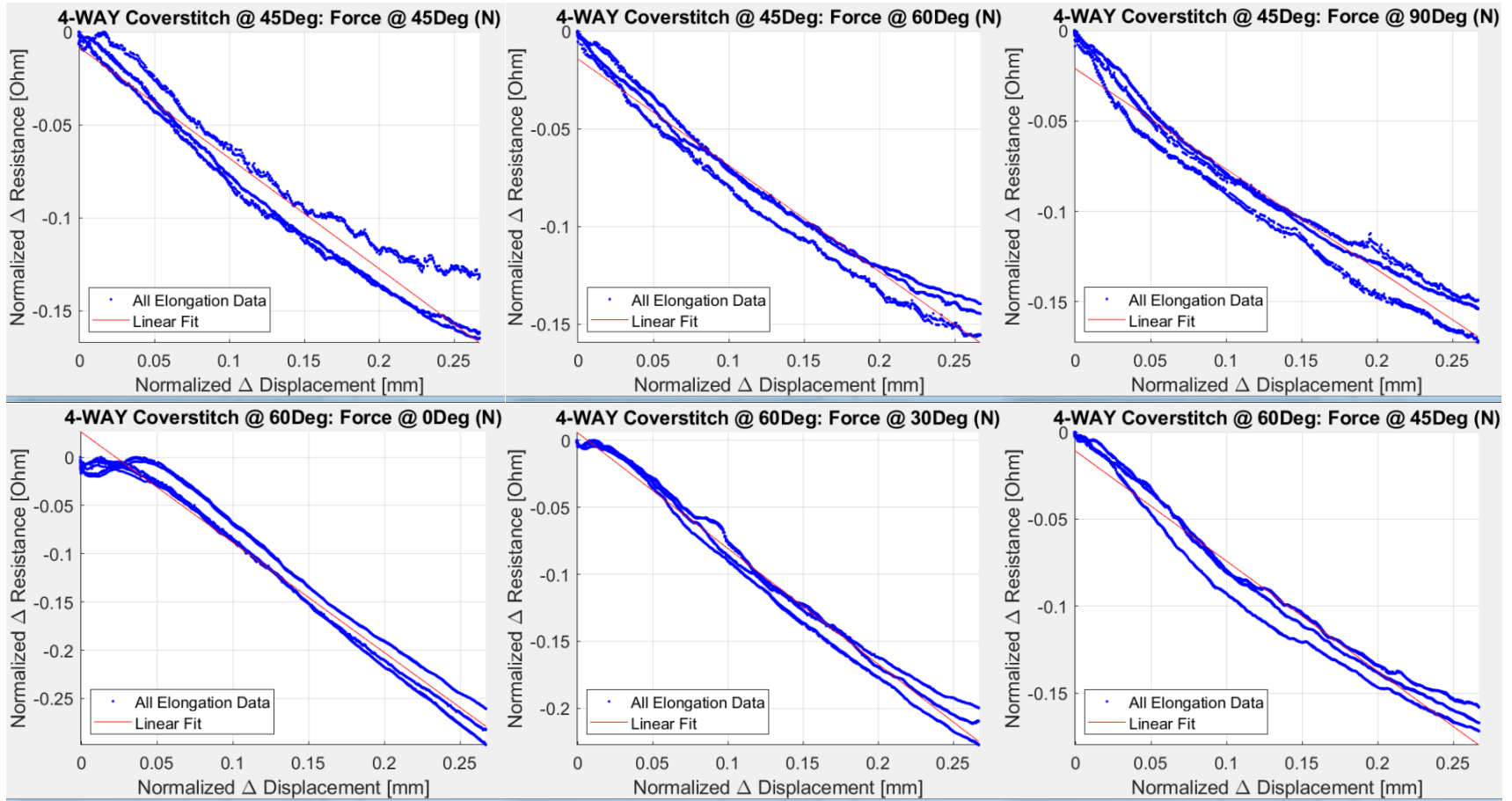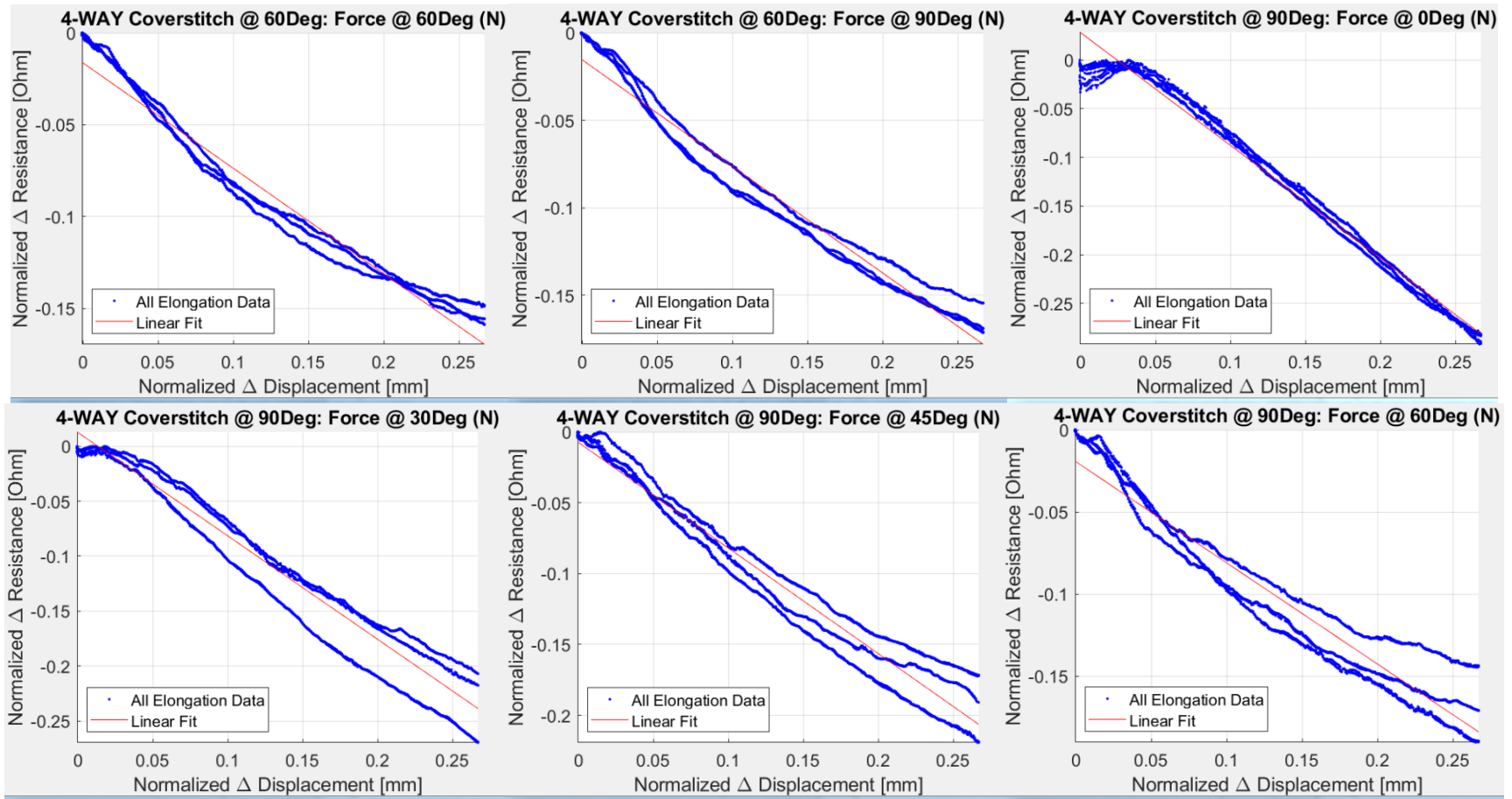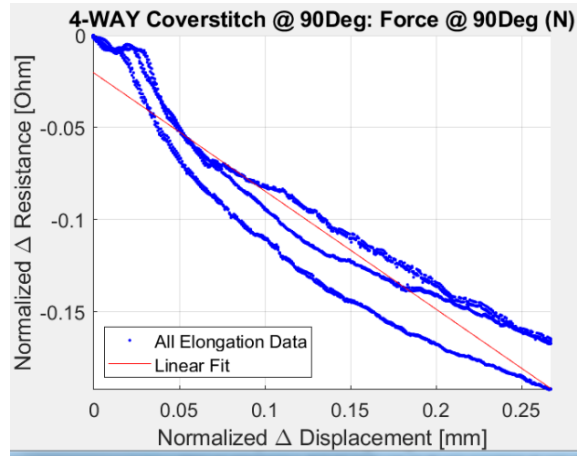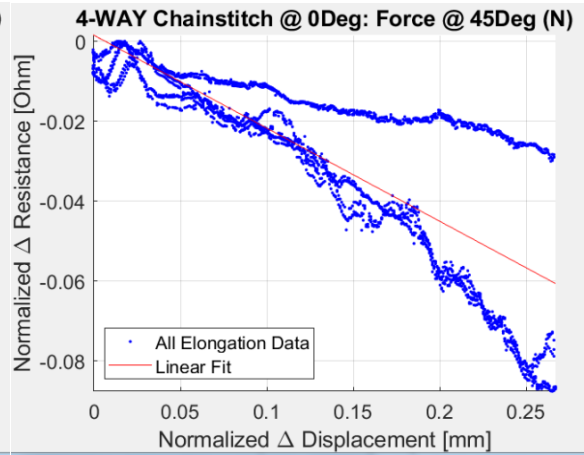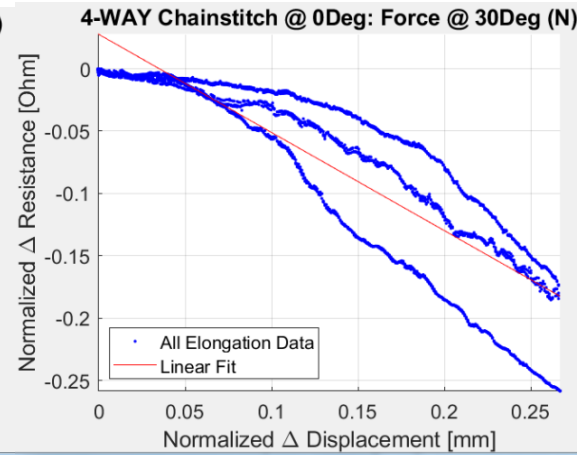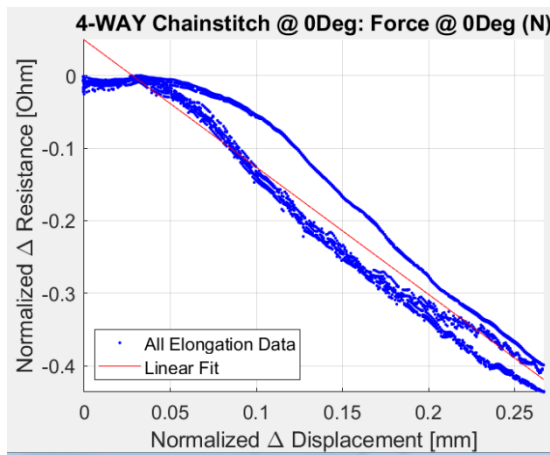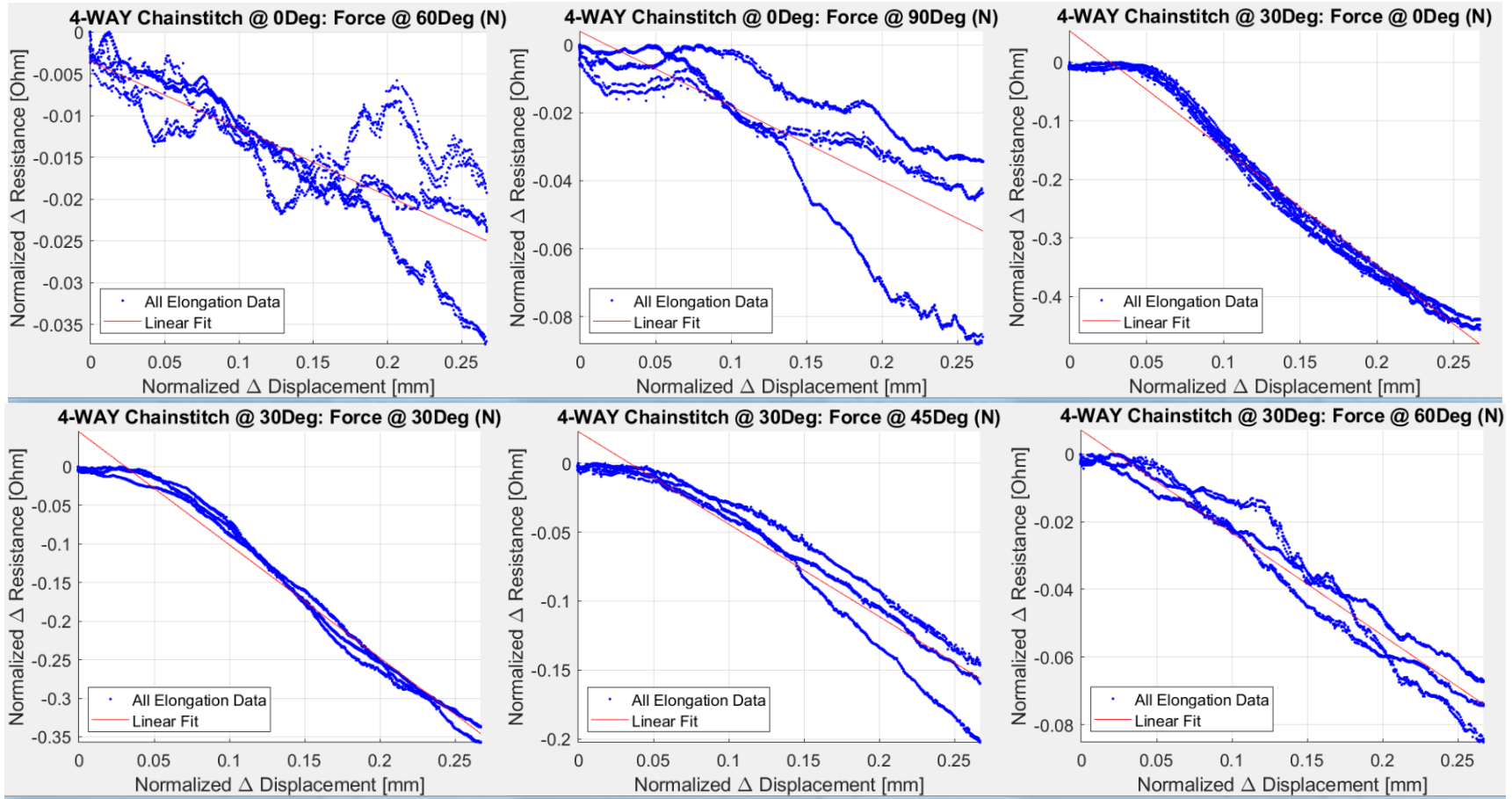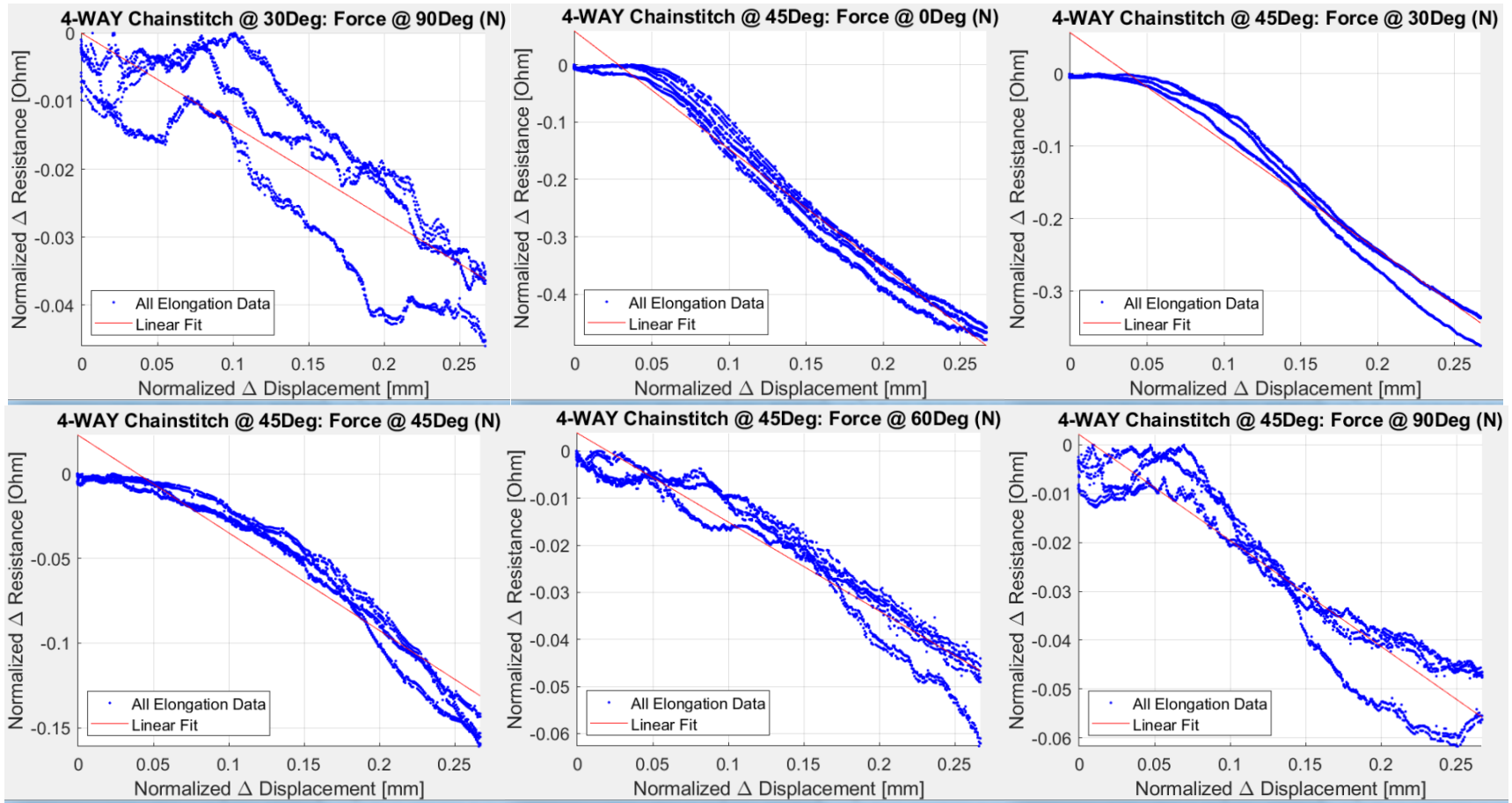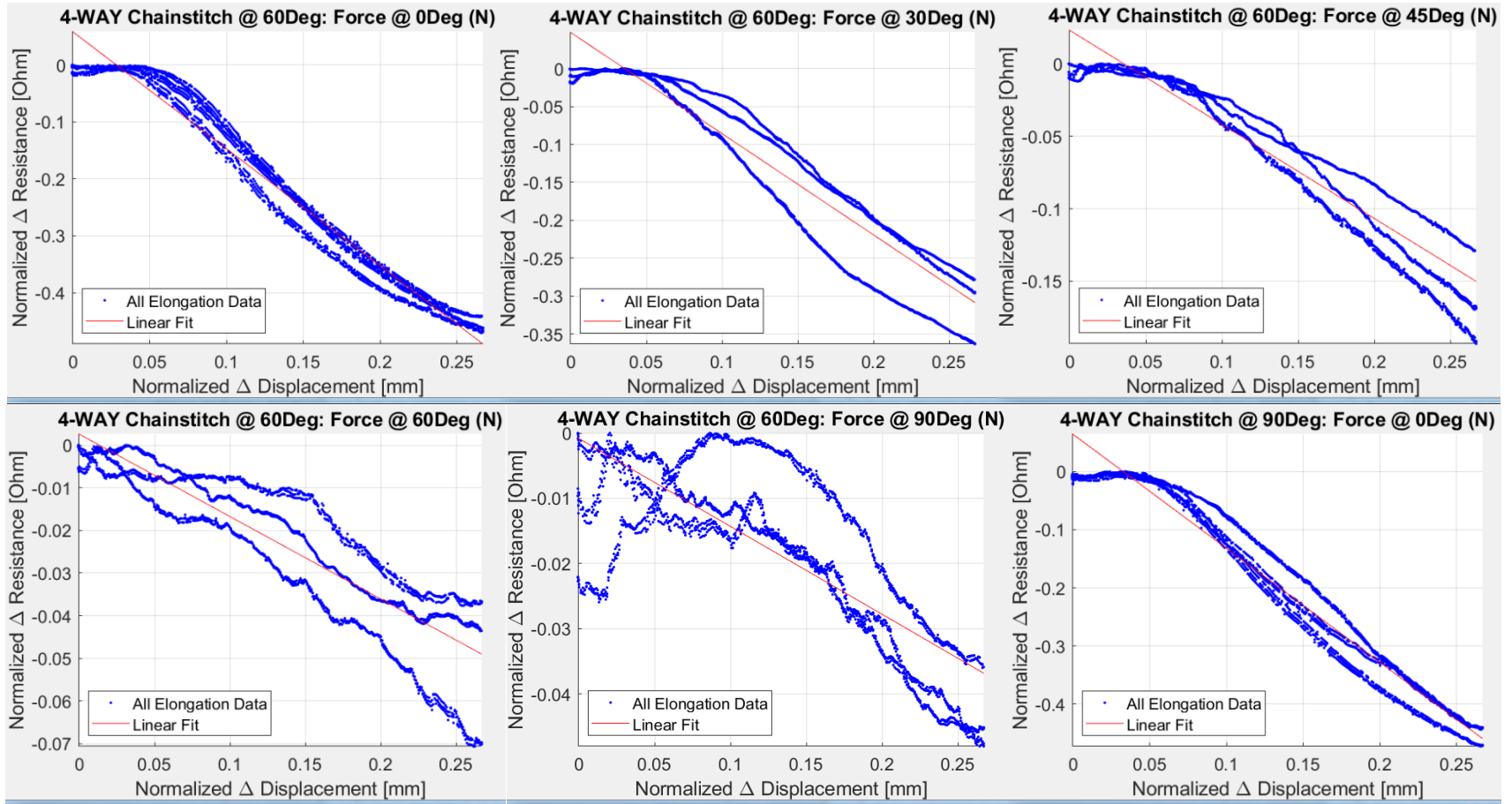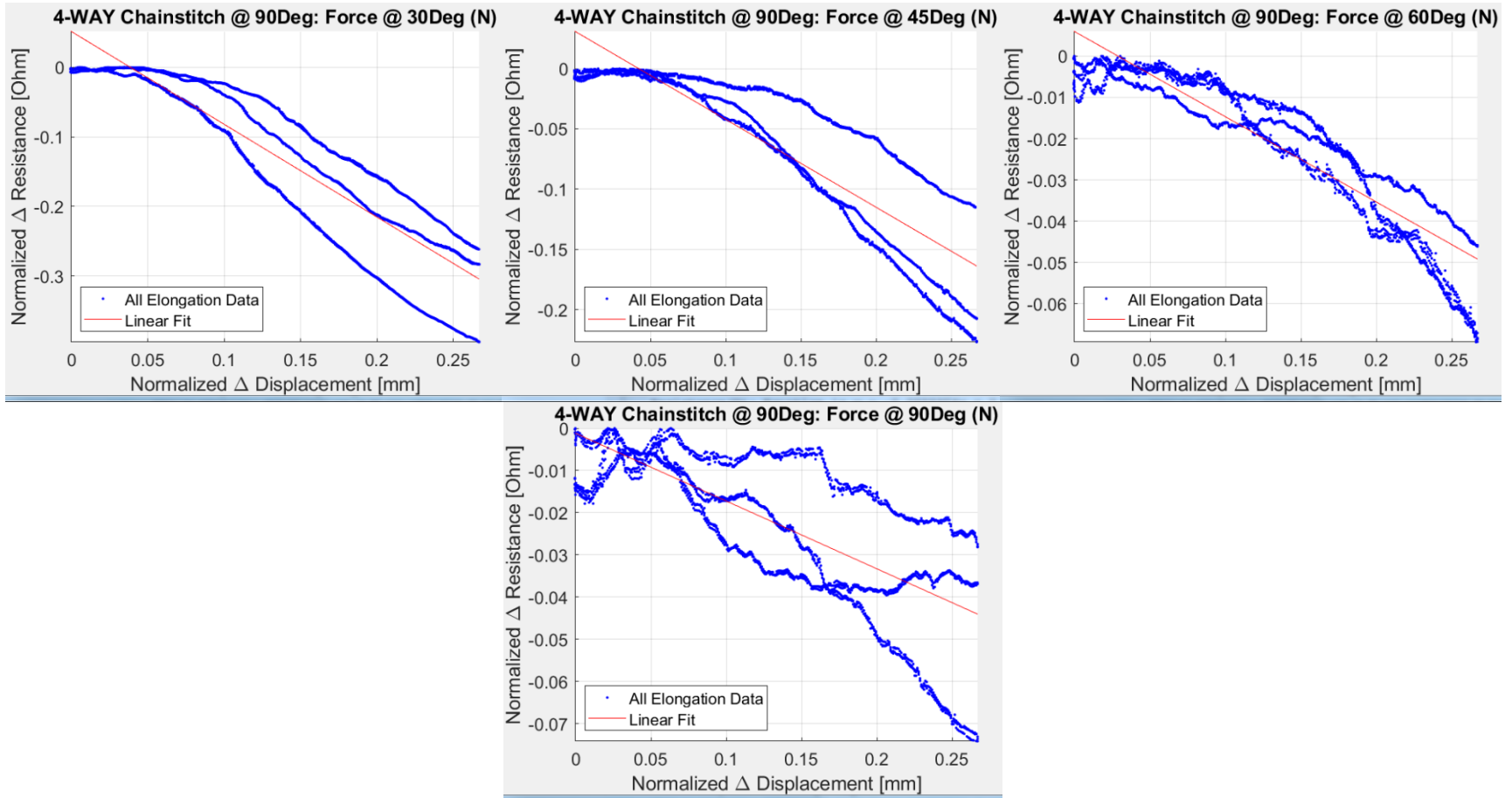
Figures D51-D75. Normalized Resistance vs Strain Graphs for 4-way Knit + Coverstitch Sensors sewn at 0°, 30°, 45°, 60°, and 90° stitch angles with respect to the knits lengthwise/wales direction, with applied force at 0°, 30°, 45°, 60°, and 90° with respect to the sensor axis

150

4-WAY Chainstitch @ 60Deg: Force @ 0Deg (N)

4-WAY Chainstitch @ 60Deg: Force @ 30Deg (N)

4-WAY Chainstitch @ 60Deg: Force @ 45Deg (N)

4-WAY Chainstitch @ 60Deg: Force @ 60Deg (N)

4-WAY Chainstitch @ 60Deg: Force @ 90Deg (N)

4-WAY Chainstitch @ 90Deg: Force @ 0Deg (N)

Figures D75-D100. Normalized Resistance vs Strain Graphs for 4-way Knit + Chainstitch Sensors sewn at 0°, 30°, 45°, 60°, and 90° stitch angles with respect to the knits lengthwise/wales direction, with applied force at 0°, 30°, 45°, 60°, and 90° with respect to the sensor axis

The linear fit equations for these graphs are summarized first for the 2-way sensors in Table D6, then the 4-way sensors in Table D7.

Table D6. Linear Fit Equation: y=mx+b, where y=Normalized Resistance, x=Normalized Displacement (strain) for 2-way Sensors

Sample Group	Stitch Angle	Force Direction (Degree from Stitch Axis)				
		0°	30°	45°	60°	90°
2-way knit Coverstitch	0°	y = -1.1293*x + 0.042199	y = -0.80841*x + 0.0050019	y = -0.73199*x + -0.0096154	y = -0.76455*x + -0.010972	y = -0.91222*x + -0.0050763
	30°	y = -1.0672*x + 0.033552	y = -0.89907*x + -0.00071633	y = -0.71471*x + -0.0056954	y = -0.70667*x + -0.0043855	y = -0.94836*x + 0.012938
	45°	y = -0.93021*x + 0.018963	y = -0.85151*x + -0.012991	y = -0.68566*x + -0.02119	y = -0.76769*x + -0.0095231	y = -0.90801*x + 0.014363
	60°	y = -0.92177*x + 0.019321	y = -0.78347*x + -0.010558	y = -0.71639*x + -0.0048136	y = -0.81569*x + 0.010303	y = -1.0269*x + 0.016336
	90°	y = -1.0085*x + 0.018919	y = -0.77428*x + 0.0013645	y = -0.79663*x + 0.0084115	y = -1.0056*x + 0.0074304	y = -1.2591*x + -0.00057347
2-way knit Chainstitch	0°	y = -2.1973*x + 0.096272	y = -1.025*x + 0.048639	y = 0.019658*x + -0.0097949	y = -0.016448*x + -0.0070179	y = -0.024615*x + -0.0078804
	30°	y = -2.3718*x + 0.096449	y = -1.8578*x + 0.071164	y = -0.84607*x + 0.033114	y = -0.082691*x + -0.00084082	y = -0.58647*x + 0.029554
	45°	y = -2.3064*x + 0.083889	y = -1.6553*x + 0.056685	y = -0.43243*x + 0.01486	y = -0.14931*x + 0.0024925	y = -0.81941*x + 0.038504
	60°	y = -2.2067*x + 0.088966	y = -1.5778*x + 0.070663	y = -0.37818*x + 0.015345	y = -0.07245*x + -0.0033611	y = -0.7569*x + 0.038252
	90°	y = -2.1375*x + 0.088103	y = -1.6898*x + 0.07676	y = -0.94156*x + 0.047206	y = -0.28301*x + 0.0050005	y = -0.74615*x + 0.034044

Table D7. Linear Fit Equation: y=mx+b, where y=Normalized Resistance, x=Normalized Displacement (strain) for 4-way Sensors

Sample Group	Stitch Angle	Force Direction (Degree from Stitch Axis)				
		0°	**30°**	**45°**	**60°**	**90°**
4-way knit Coverstitch	**0°**	y = -1.1538*x + 0.01322	y = -0.71597*x + 0.012754	y = -0.49399*x + 0.001218	y = -0.48903*x + -0.013421	y = -0.70656*x + -0.017876
	30°	y = -1.0946*x + 0.019513	y = -0.6801*x + 0.0058824	y = -0.4981*x + -0.0035003	y = -0.54821*x + -0.013274	y = -0.68969*x + -0.019895
	45°	y = -1.0544*x + 0.023937	y = -0.83621*x + 0.0091474	y = -0.5947*x + -0.0084945	y = -0.54466*x + -0.014319	y = -0.55551*x + -0.021117
	60°	y = -1.143*x + 0.026043	y = -0.86337*x + 0.005575	y = -0.63305*x + -0.010826	y = -0.57426*x + -0.016278	y = -0.60921*x + -0.015433
	90°	y = -1.1601*x + 0.028263	y = -0.94217*x + 0.012655	y = -0.74592*x + -0.0073789	y = -0.61632*x + -0.019364	y = -0.64227*x + -0.020328
4-way knit Chainstitch	**0°**	y = -1.7554*x + 0.049172	y = -0.78811*x + 0.027639	y = -0.23292*x + 0.0015204	y = -0.080503*x + -0.0035315	y = -0.22008*x + 0.0039176
	30°	y = -2.0033*x + 0.053435	y = -1.4659*x + 0.045454	y = -0.67142*x + 0.023015	y = -0.30334*x + 0.0070178	y = -0.13559*x + -3.1117e-05
	45°	y = -2.0526*x + 0.057926	y = -1.501*x + 0.056646	y = -0.57711*x + 0.022804	y = -0.18911*x + 0.0038229	y = -0.21722*x + 0.0021268
	60°	y = -2.0567*x + 0.058566	y = -1.3337*x + 0.047449	y = -0.64921*x + 0.023073	y = -0.19339*x + 0.0025891	y = -0.13488*x + -0.00082684
	90°	y = -1.9624*x + 0.06425	y = -1.3346*x + 0.051429	y = -0.72945*x + 0.030814	y = -0.2066*x + 0.0059581	y = -0.1607*x + -0.0011762

Appendix E: Stitched Strain Sensor Rosette

Additional graphs for studying relationships and correlations between the measured variables are shown in Figures E1-E3.
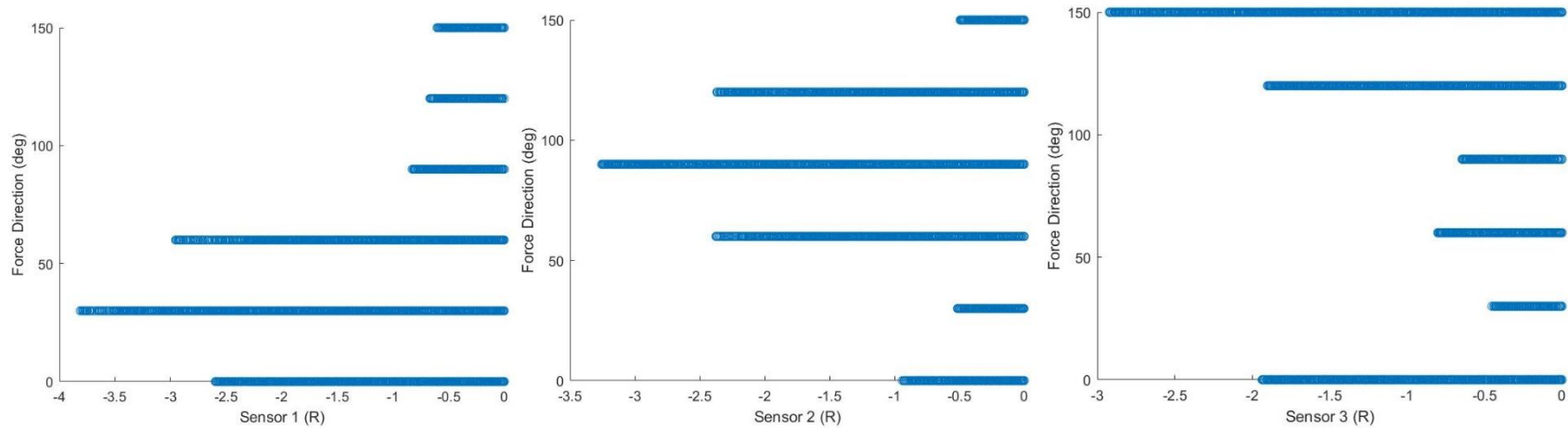
Figures E1-E3. Relationship of Force Direction for each Sensor